THE UNIVERSITY *of* LIVERPOOL

Remote Monitoring of Power System Conductor Voltages

A Thesis submitted in accordance with the requirements of the University of Liverpool for the degree of Doctor in Philosophy by Carl Andrew Gerrard

December 1996

Abstract

Conventional methods of measuring high voltages on power systems require a physical connection to the high voltage source. To prevent discharges the measurement devices must contain large insulators and are large and expensive. Consequently power system voltages are measured at relatively few points restricting the operators ability to measure system behaviour.

An instrumentation system has been developed that monitors the voltages on the exposed conductors of a three phase power system without any physical connection to the high voltage system.

By investigating the relationship between the electric field around the power system and the conductor voltages it was shown that, at sets of carefully selected positions, the pattern of changes in the electric field is unique for any set of changes in the conductor voltages. This was found to be true for a wide range of power system configurations investigated. This unique relationship indicated that measurements of the electric field could be used to determine changes in the conductor voltages.

An array of electric field sensors was developed to measure the electric field below a power system. Electronic processing instrumentation was constructed to process, in real time, the field measurements to determine the changes in conductor voltages and other information about the power system.

Investigation showed that if the geometry and voltage of a power system are reduced by the same factor the fields at equivalent points in the scaled and full sized systems are identical. In laboratory tests with a scale model of a power system, results using the instrumentation system were compared with those from a conventional voltage monitoring system. Over a wide range of normal and abnormal operating conditions results using both systems were in good agreement. Both systems were then installed in an operating 275kV substation on the UK national grid. Again the results of both systems agreed.

The investigations have shown that it is possible to monitor the voltages on individual conductors of a high voltage system without making any physical connection to them.

Acknowledgements

I would like to express my thanks to my supervisor Dr. J.R. Gibson for his interest, enthusiasm and guidance throughout the course of this work. Thanks are also due to Prof. G.R. Jones for his encouragement and many useful discussions.

The skills of the technical staff in the Department of Electrical Engineering and Electronics are gratefully acknowledged, thanks are due to Messrs A. Edwards, K. Graham, T. Heywood, G. Kings, I. Kelly, J. Humphries, R. Smith, P. Storey and the late Mr. J. Roberts.

Thanks is also due to my fellow research students within the laboratory, in particular Messrs J. Cosgrave, L. Isaac, G. Li, T. Singh, C. Yakum and Dr. S. Ahmed for their support and encouragement.

The power system investigations would not have been possible without the co-operation of the National Grid Company and I am indebted to Mr D. Molineux and his colleagues for providing access to the substation

This work was financed by the Engineering and Physical Sciences Research Council and Cookson Group PLC. The financial support of Cookson, and in particular the encouragement, support and enthusiasm of Dr. D. Simkin is gratefully acknowledged.

Mostly however I wish to thank my family and friends for their continuous interest, encouragement, support and understanding which has been invaluable throughout this work.

Contents

1. Introduction

Operators of high voltage electrical transmission and distribution systems measure voltages for both metering and protection purposes. The measurement instruments are connected directly to the high voltage system and require large amounts of insulation; for this reason they are generally large and expensive. Thus, although modern power systems are large distributed networks, voltages are usually measured at a limited number of positions.

Although most high voltage measurements are made for the purposes of metering and protection these, together with other measurements, can indicate the condition of the power system plant.

1.1 Monitoring

A requirement of electrical power transmission and distribution industries in developed countries is to provide a very reliable high quality supply. Reliability is the provision of an uninterrupted supply to customers, it is usually measured in terms of the mean frequency of interruptions and their mean duration. Quality is defined in terms of the stability of the voltage and the frequency, absence of both harmonic content and transient changes in voltage.

Modern power systems are very reliable, for most of their lifetime components operate normally and the quality of the supply remains within defined limits. However abnormal operation can result in a poor quality of supply and, if undetected, deterioration of the plant increasing the probability of future failure.

To detect abnormal operation it is necessary to monitor both the condition of the plant and the quality of the supply. Monitoring may include making regular measurements of operating parameters of a system and checking that these values are within specified limits. However another form of monitoring is to detect changes in a parameter as a function of time, rather than measure its exact value. Such changes may indicate faults.

For a power system some of the important parameters indicating behaviour are the voltages on the conductors. As systems generally operate at an approximately constant voltage it is often sufficient to measure changes from nominal operating voltages. Previous workers have used voltage changes to infer information about the condition of power system plant, for example **Ohnishi *et al*(1994)**, and the quality of supply, for example **Ruitz *et al*(1995)**.

Monitoring of power system voltages, as part of an overall program to detect problems, offers the possibilities of improved supply reliability, lower emergency repair costs and higher supply quality. However the insulation costs of connecting apparatus directly to high voltage systems has limited the development of power system monitoring techniques, particularly those requiring voltage measurements.

The present study led to the development of an instrumentation system which monitors the voltages on the exposed conductors of a three phase power system without any physical connection to the conductors. There are no high voltage insulation costs and the system can safely be installed while the power system is operating.

1.2 Principle of a Non Contact Monitoring System

To develop a voltage monitoring system that does not make a direct electrical connection to the high voltage source, some quantity affected by the high voltage must be measured and the voltage derived from the results. As the voltages on the conductors of a power system produce electric fields, the field distribution contains information about the conductor voltages.

The relationship between electric field and power system voltage was investigated for a wide range of power system geometries and operating conditions. For all the geometries investigated it was shown that it was always possible to find a set of locations such that the changes in field at all locations is unique for a given set of changes in conductor voltages.

The monitoring system developed measured the electric field distribution produced by the power system and derived information about the conductor voltages from the measurements.

1.3 Development and Evaluation of a Non Contact System

An array of electric field sensors with processing instrumentation, the *non contact system*, was developed to measure the electric field at eight locations. The system processed the sensor signals in real time and determined the changes in individual conductor voltages and other information about power system conditions.

Investigations showed that if the dimensions and voltages on the power system are scaled by the same factor then the fields at equivalent points in the scaled and full sized systems are identical. A scale model of a power system was constructed in the laboratory. It was operated for extended periods and the monitoring system behaviour examined. Tests were also performed with artificially created abnormal operating conditions on the conductors. A conventional method of measuring and recording the conductor voltages was used to confirm that the non contact system produced results correctly reproducing changes in all conductor voltages.

After the laboratory investigations, both systems were installed in an operating 275kV substation on the UK national grid. Again the agreement between the systems was within the limits of accuracy of the instrumentation.

2. High Voltage Measurements

Many techniques have been developed to measure high voltages on power systems and in research laboratories, no single technique is perfect and each is suited to a particular application. In addition to the conventional techniques in common use there have been many attempts to develop alternative measuring systems.

2.1 Conventional Techniques

Many high voltage measurement methods are adaptations of low voltage measurement techniques; the high voltage is converted, by a known fixed factor, to a voltage or current which is measured with a conventional instrument. An ideal measuring system must maintain a constant factor between the high voltage and the measured quantity for all operating conditions; ideal behaviour is rarely achieved. Conventional techniques require that a connection must be made to both the source under test and the ground. A full description of the techniques is given in the standard texts on the subject; for example **Naidu & Kamaraju(1982)**, **Kuffel & Zaengl(1984)** and **Wildi(1981)**

2.1.1 Resistive Devices

By applying the high voltage, V_{HT}, across a large resistance, R, figure 2.1a, a current flows and is measured by the meter, M. This current is proportional to the voltage and the meter may be calibrated in volts. Although simple the method is limited by

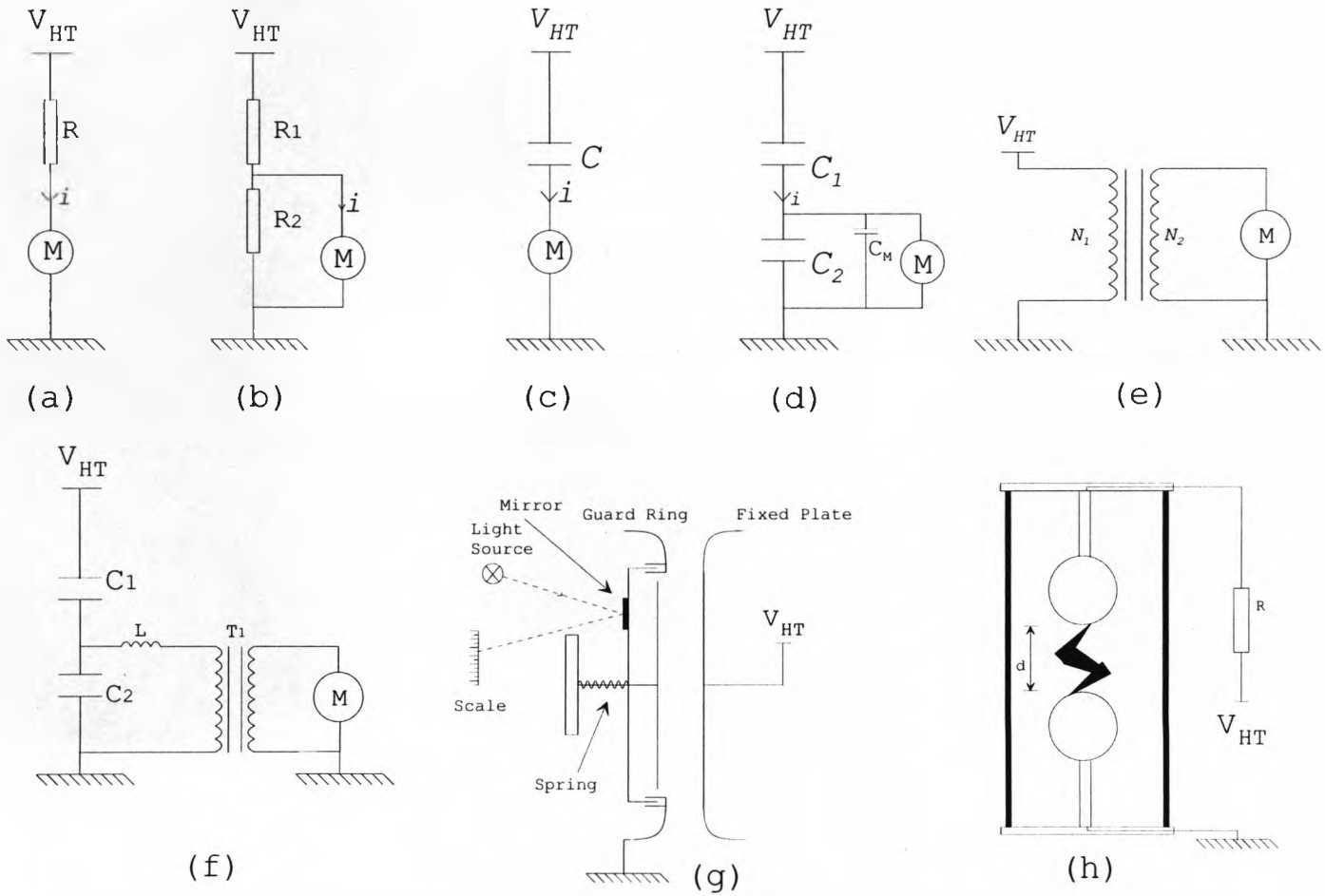

Figure 2.1 Conventional Methods of Measuring High Voltages on Power Systems and in Research Laboratories

the availability of high value resistors with suitable temperature coefficients. All resistors have a temperature coefficient, typical values are 10^{-4} K^{-1} for carbon resistors and 10^{-6} K^{-1} for wire wound ones. As current flows through the resistor power is dissipated as heat, the temperature of the resistor increases, the resistance increases and hence the ratio $I:V_{HT}$ of the device changes.

This problem may be reduced by using the highest value of R possible, this reduces the current flow and heating effect. Unfortunately this solution may not be pursued indefinitely as the insulation supporting the resistor has a finite resistance and current will also flow through it. Insulation resistance is largely determined by surface conditions which vary with deposits on the surface; surface resistance changes with humidity and other environmental conditions. For an accurate instrument it is necessary to ensure that the majority of the current flows through the resistor. The value of the resistance should thus be many orders of magnitude less than the nominal resistance of the insulating structure, **Kuffel & Zangel(1984)** state that the maximum resistor value should not exceed 100MΩ .

An alternative to the single resistor arrangement of figure 2.1a is to use two resistors in the divider arrangement of figure 2.1b. If the current drawn by the meter, M, is small the heating effects in both resistors will be similar and the effect of temperature variations will be minimised.

The physical size of the resistor(s) is also important as the high voltage produces an electric field around the resistor, if this field exceeds the breakdown voltage of the resistor material or the surrounding medium a 'flash over' will occur. To limit the

resistor material or the surrounding medium a 'flash over' will occur. To limit the magnitude of these fields high voltage resistors have large dimensions and are commonly constructed of chains of smaller resistive elements to limit the field across each one, **Kuffel & Abdullah(1970)**. At voltages above 1kV the distributed (or "stray") capacitance between points on the resistor chain and ground must also be considered. For steady, dc, conditions these capacitances have no effect, but for an ac or transient excitation the capacitances result in a ratio between input and output voltage that changes with frequency. Also very sudden changes in the input voltage can result in uneven voltage distributions along the divider resulting in a flash over. For these reasons resistive devices are generally used for dc measurements only, commercial instruments measuring up to 500kV have been reported, **Naidu & Kamaraju(1982)**.

2.1.2 Capacitive Devices

For measurement of high ac voltages capacitive voltage to current (V/I) converters and capacitive dividers can be used. Figure 2.1c shows a series capacitor-microammeter device. The relationship between the current, I, and the high voltage, V_{HT} is given by

$$I = j\omega C V_{HT} \qquad [2.1]$$

where ω is the angular frequency of the voltage. The meter, M, usually measures the rms value of the current and, for a sinusoidal excitation of fixed frequency, the device may be calibrated; if the frequency changes the ratio I : V_{HT} of the device will also change. If the voltage contains harmonics the ratio will differ for each one producing

an error in the indicated rms value. For example a fifth harmonic content of 1% results in an error of 5% in the measured voltage.

As with resistive devices two capacitors may be used to form a divider, figure 2.1d. The relationship between the measured voltage, V_m , and the high voltage, V_{HT} is

$$V_m = \left(\frac{C_1}{C_1 + C_2 + C_m} \right) V_{HT} \qquad [2.2]$$

This relationship assumes that no current is drawn by the instrument measuring V_m and that its response is frequency independent. Modern electronic devices may have input impedances exceeding $10^{12}\Omega$ and meet this assumption. As with the resistive divider stray capacitances exist between the terminals and ground. Provided the value of these capacitances is small when compared with the capacitances of the divider their influence on the response of the device is negligible. Much work has been performed to improve the response of capacitive dividers, particularly for measurement of transient voltages; for example **Blalock *et al*(1970)**, and **Feser *et al*(1988)**.

2.1.3 Voltage Transformers

The voltage transformer in figure 2.1e may be designed for the measurement of any ac voltage, the relationship between the measured voltage V_m and the high voltage V_{HT} is

$$V_m = \left(\frac{N_2}{N_1} \right) V_{HT} \qquad [2.3]$$

N_2 is the number of turns on the secondary (low voltage) winding and N_1 the number of turns on the primary (high voltage) winding. By selecting $N_1 >> N_2$ the secondary voltage may be measured with conventional instrumentation. The distributed capacitance between the windings can result in a high potential developing between the secondary winding and earth. To prevent this one terminal of both windings is always connected to ground. The bandwidth of a transformer is of the order of a few thousand Hertz and magnetic saturation of the core limits the dynamic range of the system.

Practical use of the voltage measurement transformer is limited to voltages below 100kV, **Naidu & Kamaraju(1982)**. At higher voltages the amount of insulation between the two windings and the number of turns required on the primary winding result in a large physical size and hence cost.

2.1.4 Capacitive Voltage Transformers

Capacitive dividers may be constructed for high voltages, but are unable to connect to a low impedance load. Voltage transformers can drive a low impedance load but are large and costly for voltages above 100kV. The best features of each device are combined in the capacitive voltage transformer of figure 2.1f.

The capacitive divider is used to reduce the high voltage to a few tens of thousands of volts (commonly known as the intermediate voltage), this allows a transformer of moderate size and cost to be built and a low impedance load connected to the device. The primary winding of the transformer is a low impedance load and may not be

directly connected to the capacitive divider. The inductor, L, is added to bring the circuit of C_2, L and T_1 into resonance and reduce the loading on the divider at the frequency of operation.

Capacitor voltage transformers work well at their designed operating frequency and are commonly used for metering purposes. However if the frequency changes the response of the device changes; **Lythall(1972)** states "they [capacitive voltage transformers] are renowned for their unfaithful representation of the waveform under fault conditions", standards for voltage transformers and capacitive voltage transformers are given by **BSI(1993)**.

2.1.5 Electrostatic Voltmeters

The electric fields produced by high voltages may be used to exert forces on charged objects, this concept is used in the electrostatic voltmeter of figure 2.1g. The device consists of two plates, one fixed and other attached to the spring. The force between the fixed and moving plate, F, is

$$F = \left(\frac{A\varepsilon_o\varepsilon_r}{2d^2} \right) V_{HT}{}^2 \qquad [2.4]$$

Where ε_r is the permittivity of the medium between the plates, ε_o is the permittivity of free space, A is the area of the plates and d is the separation between them. The right hand plate is fixed and the left hand plate is connected to a mounting via a spring resulting in a displacement proportional to the force between the plates. A light beam and mirror are used to amplify the movement of the plate and project it onto a scale calibrated in volts. The principle advantage of the electrostatic voltmeter is its high

input resistance, limited only by the insulation resistance of the structure supporting the plates. This is primarily a research instrument and is not used in commercial power systems, commercial devices have been manufactured measuring up to 600 kV with an accuracy of 0.1%, **Naidu & Kamaraju(1982)**.

2.1.6 Sphere Gaps

The sphere gap of figure 2.1h is often used as a reference for calibrating other devices. The unknown high voltage is applied across the spheres and the distance, *d*, is decreased until the air between the spheres breaks down. The resistor, R, is used to limit the current flowing to prevent damage to the spheres and the high voltage system. The breakdown field of air is a function of temperature, humidity and pressure, for accurate measurements it is necessary to correct for these factors. Tables of these factors and breakdown voltages for different sphere and distance combinations are specified by an international standard, **IEC(1960)**. Sphere gaps are not able to produce an instantaneous voltage measurement and are usually used for calibration and research purposes only.

2.2 Optical Sensing

Commercial production of optical fibres in the late 1970's lead to the development of a large number of sensors for measuring voltage, current and temperature on power systems. Optical fibres allow the transmission of optical energy over a flexible dielectric (insulating) filament and provide a convenient method of transmitting signals from a high voltage to ground and vice versa. **Moghisi(1989)** and **Pilling(1992)** have reviewed many of the techniques developed.

As with conventional techniques, the presence of a physical connection between the high voltage system and earth provides a potential discharge path. Surface tracking on the fibre can result in it forming the path of a "flash over"; to guard against this insulators must be fitted to the fibre, which increases size and cost. Insulators have been successfully used to pass communications optical fibres between ground and 132kV power systems, **FOCAS(1993).**

Optical sensors are usually installed on the high voltage line and the processing instrumentation placed at ground potential. The removal of a ground connection reduces insulation problems but also removes the ground reference, consequently most developments of optical systems have been for current measurement. Two categories may be used to classify sensors; active and passive. Active (also known as hybrid) sensors contain conventional electronics and sensors, the value of the measurand is transmitted to ground through an optical fibre. Passive sensors use physical phenomena influenced by electric or magnetic fields to modulate an applied light signal.

2.2.1 Hybrid Optical Sensors

Hybrid optical sensors require a source of electrical power to supply the electronics in the sensor, for short term testing batteries have been used, **Feser *et al*(1988)**. Any device attached to a high voltage power system must have a high reliability and be maintenance free, battery powering is thus not possible. Two long term methods of powering the sensor have been reported, **Moulton(1965)** describes a line powered current sensor, the line passes through a coil in the sensor, as current flows through

the line a secondary current is induced in the coil which is used to power the sensor electronics. Although simple in operation and efficient, line powering is not attractive to the power utilities as it is not fail-safe, no signal from a sensor may be due either to no current flowing in the line, which is still at high voltage, or due to sensor failure.

An alternative to powering the sensor electronics from the line current, first reported by **Caspers & Neuman(1980)**, is to use an optical energisation scheme, optical energy is transmitted to the sensor through an optical fibre, photo-diodes convert this to electrical energy which is used to power the sensor electronics. Optical energisation offers the advantage that the sensor operates with zero line current.

Pilling(1992) reports an optical hybrid voltage and current sensor using a capacitive divider to determine voltage. A distributed capacitance exists between the conductor and the internal electronics, a second capacitance exists between the case of the sensor and the ground. A conventional capacitor was connected between these two points and a signal proportional to line voltage developed across it. A current transformer was used to provide a signal proportional to the line current, both signals were encoded using pulse width modulation and transmitted to a receiver at ground potential using two optical fibres. As the distributed capacitance was determined by the environment in which the sensor was installed, it had to be calibrated for the installation.

Optical energisation was first reported seventeen years ago, development of hybrid sensors has been limited by the availability of efficient converters for the optical power supply. In more recent work, **Tardy & Derossis(1995)**, used a dedicated

power supply. In more recent work, **Tardy & Derossis(1995)**, used a dedicated optical to electrical power converter in a hybrid current sensor. A semiconductor laser is used to supply optical energy to the system, lengths of optical fibre of up to 1000m between the receiver and sensor element have been reported.

2.2.2 Passive Sensors

Anisotropic optical materials exist in which the refractive index in one plane is determined by an applied electric or magnetic field. If a polarised light beam is passed through the material the plane of polarisation will rotate as the refractive index changes. Of particular interest to voltage measurement are the Pockels and Kerr effects, in which the rotation is proportional to electric field for Pockels materials and the square of the field for Kerr materials. A full description of these phenomena is given by **Banjaree & Poon(1991)**.

For practical use in a power system the optical material or element must be positioned so an applied high voltage generates a known field across it, this may be accomplished by placing the sensor between points connected to the high voltage and ground. Installation in this location requires insulation both between the sensor and the ground and between the sensor and the instrumentation. In laboratories where line of sight operation is possible lasers are used to address the element from a distance, in a power system this is generally not possible and optical fibres are used.

The relationship between the field and refractive index of Pockel and Kerr Materials is a function of temperature, thus the response of any sensor manufactured from them is

also a function of temperature. As power systems operate over a large temperature range, **Wildi(1981),** this feature is undesirable. Examination of the literature reveals many papers on laboratory implementation of Pockels cells, **Ballik & Liuc(1983)** and **Hertz(1985)** are typical examples, no reference has been found to their successful implementation on commercial power systems.

2.2.3 Other Optical Sensors

In the last twenty years several other optical sensors to measure voltages on high voltage power systems have been reported;

Train & Dube(1983) describe a method for measuring the voltage across a high voltage dc insulator chain using a modified electrostatic voltmeter. Two spheres were connected to the top and bottom of an insulator element, one sphere was fixed and the other allowed to move on a torsion device. The potential difference across the sensor resulted in an electric field forcing the spheres apart, a laser measurement system was used to measure the sphere displacement and the voltage calculated.

Another system using a suspension insulator has been reported, **SIBRE(1984),** which uses the capacitance between the pin and cap of an insulator in a power line insulator string to develop a voltage proportional to the line voltage. An electronic circuit embedded within the insulator encoded this information and transmitted it to ground potential using an optical fibre. No information is available on how the device was powered or its effect on the integrity of the insulator string.

2.3 Other Systems

All voltage measuring apparatus requires a site at which to install it, this requirement has lead to voltages commonly being measured at the same location as protective switchgear. **Tokoro *et al*(1982)** report a capacitive divider for attachment to gas insulated switchgear (GIS). A hemispherical conducting probe surrounded by an insulating flange was attached to a port on the GIS, a distributed capacitance exists between the probe and the busbar, a second capacitor was connected between the outside of the probe and ground forming the lower arm of a capacitive divider. A conventional electronic system was used to produce a signal proportional to line voltage. The system was installed in three phase GIS, to limit the interactions of the phases on the sensors screens were fitted within the enclosure. From the results reported the authors conclude the system is suitable for use on live power systems, however no record of its commercial implementation has been found, **Hall(1993)** indicates this is due to the reluctance of the power industry to make any modifications to GIS enclosures that may compromise their integrity.

Nitech(1987) describe a monitoring system, called a 'Power-Donut', for direct attachment to overhead lines. The device was connected to an overhead line, was powered by the line current and recorded line current and voltage. A UHF radio link was used to transmit the recorded values to a receiver at ground potential where system voltage, current and temperature were logged at regular intervals. The device was intended for use in power system planning - the donuts were designed to be installed and removed under live line conditions using an insulating 'hot stick'. For commercial reasons the exact methods of operation of the device is not known,

Carter(1994) indicates the voltage response of the device changed as vehicles passed under the donut, from this it may be inferred that the device used a distributed capacitor divider.

Feldman *et al*(1992) reports the development of an instrument to estimate the potential of a high voltage dc line without a direct electrical contact to either the high voltage line or to ground. Of the literature examined this reference is unique as it is the first recorded instance of a voltage monitoring system with no physical contact to the high voltage system. An electric field sensor was suspended on an insulating pole and inserted into the field of the conductors. The line potential was changed by the author and the sensor output recorded, these measurements were used to calibrate the sensor output. The incident field on the sensor is also a function of the sensor position within the field distribution, as the pole was held out from a tower by two linesmen it was not possible to hold it steady and small variations in position occurred. The author used analytical modelling techniques to select areas, called sweet-spots, where the field changed little with position, hence changes in the position of the sensor would cause a minimum change in the output of the system. By placing a calibrated sensor in a sweet-spot the line potential was successfully estimated to an accuracy of ±10% over a range of 0 to 500kV.

2.4 Classification of Existing Systems

All high voltage measurement systems; actual, experimental and proposed consist of four components. The high voltage system, ground reference, sensor and

instrumentation. The relative position of each of these components may be used to classify the system into one of three categories.

Full contact systems

The sensor is connected to both the high voltage system and to the ground reference, the instrumentation is at ground potential; this category includes all conventional systems, section 2.1. The connection to the ground reference allows voltage measurements to be made with high accuracy, however the full potential is applied across the sensor and insulation is necessary to prevent breakdowns. As the voltage to be measured increases the physical size, amount of insulation and cost of the device also increases. This *insulation burden* has limited the development of many full contact systems.

No Electrical Contact

The sensor is physically connected to the high voltage line but is electrically isolated from both the ground and from the instrumentation, this category includes optical sensors and devices such as the Nitech power donut. The absence of the ground reference limits the accuracy with which voltage measurements may be made but reduces considerably the insulation burden described above. Development of hybrid voltage sensors has been limited by the absence of a ground reference and a suitable power supply. Development of passive sensors has been limited by the temperature coefficient of the materials used.

Non Contact Systems

No physical contact is made to the high voltage system, the instrumentation is at ground potential and the sensor may be at ground potential or at the potential of the location at which it is placed. This category includes **Feldman *et al*(1992)**'s work on voltage estimation. The absence of a connection to the high voltage line limits the accuracy with which measurements may be made. The principle advantage of these systems is that the insulation burden of all other methods is removed completely, this can result in a smaller and potentially cheaper system.

2.5 Summary

High voltages have been measured for many years, some methods pre-date the development of the power transmission and distribution industries. Different methods have been developed to meet the differing needs of the of the power industry and the research community. These conventional methods require large amounts of insulation to ensure safe operation and are usually large and costly.

Many researchers have reported new techniques to measure power system voltages, however the power industry does not use these devices in large numbers.

3. Voltage Monitoring

In general increasing the absolute accuracy required when making a measurement requires that more interfering effects must be controlled and increases the cost of performing the measurement. High absolute accuracy is not always necessary; in many applications measurements may be made to a relatively low accuracy but high resolution and the results processed to determine how the system or process measured changes with time. The technique of deriving information on a system by measuring parameters of the system as a function of time and processing the results to derive information on deviations from 'normal' operating conditions is called *monitoring*.

3.1 Monitoring

Neale(1987), discussing trends in monitoring of process plant, describes the objectives of owning process plant as its safe and profitable operation. The profitability of the process is determined by running costs of the plant and the quality of the product. Monitoring may be used to determine information on the state of the apparatus performing the process without interrupting the process, *Condition Monitoring*, or determine the quality of the product and provide feedback to improve it, *Quality Monitoring*.

3.1.1 Condition Monitoring

Maintenance of plant in any industry or service may be classified into three categories; reactive maintenance, scheduled maintenance and predictive maintenance. Reactive

maintenance is performed after a failure. Usually failure results in the process stopping and may cause additional damage to the apparatus; both loss of production and damage incur high costs in many cases. Scheduled maintenance involves regularly inspecting the apparatus and replacing components before failure occurs. Replacement is performed either when the component is detected as worn or at specified intervals determined from the component lifetime predictions. This procedure requires that the process is stopped, the plant examined and specified components replaced, usually before the end of their useful life. The cost of scheduled maintenance is the loss of production time and the cost of replacing components before the end of their useful life. The probability of a failure occurring is inversely related to the frequency of scheduled maintenance, thus the industry must maintain a balance between reactive and scheduled maintenance to minimise maintenance costs.

Predictive maintenance techniques (PMT) attempt to reduce the frequency of scheduled maintenance by detecting possible failures in advance. Scheduled maintenance intervals exist but plant is only stopped at the maintenance time if the PMT methods suggest that a failure will occur before the next scheduled maintenance period. Implementation of preventative maintenance programmes requires condition monitoring of the plant.

Steed(1995), describing the monitoring of transformer oil quality, lists the benefits of PMT , also known as "health checks" as : "reduced maintenance costs, reduction of the probability of destructive failure, identification of the root cause of failures and

the ability to operate plant to the end of its useful life, replacing it just before failure." PMT has been applied in a wide range of production industries, for example **Rice & Wu(1993)** monitored the acoustic emissions from a machine tool to detect the imminent failure of the cutting tool; a similar technique has been used by civil engineers to predict the failure of reinforced concrete structures, **Buchanan *et al*(1994).**

A number of techniques have been devised for use in the power supply industry, although none have been widely adopted. **Ohnishi *et al*(1994)**, describe a system that detected insulation failures in underground cables by measuring high frequency earth currents. **Cosgrave *et al*(1994)** report a system to detect partial discharges within gas insulated switchgear (GIS) by monitoring acoustical emissions. **Blatt(1991)** describes a non contact current monitoring system for high voltage switchyards which used a number of magnetic field monitoring coils to detect the fields caused by fault currents. **Lewis(1994)** describes the use of an optical sensor to monitor the operation of a transformer tap-changer, the motion of the changer was compared with normal values and discrepancies noted.

3.1.2 Quality Monitoring

Srinvasan & Jutras(1991) show how the quality of supply of an ac power system may be quantified by the stability of the voltage and frequency, the reliability of the supply, its' harmonic content and the incidence of transient voltage variations. On the U.K. national transmission system the maximum permitted variations of some of these parameters are defined by the system operator, **NGC(1992)**. **Barker *et al*(1994)**

show how events on the power system may be classified as 'slow', of more than one cycle duration, or 'fast', of less than one cycle duration. Table 3.1 shows possible events that may occur on a power system.

Event	Description	Possible Cause	Classification
Sag	Reduction in voltage for one or more cycles of fundamental frequency	Increase in load on System	Slow
Swell	Increase in voltage for one or more cycles of fundamental frequency	Decrease in load on System	Slow
Interruption	Loss of supply for one or more cycles of fundamental frequency	Fault in system causing disconnector to operate	Slow
Harmonics	Long term presence of voltages at frequencies other than the fundamental frequency	Non-linear loads on system	Slow
Phase Imbalance	Peak voltage on each of the three phases is not equal	Unbalanced loading of the three phases	Slow
Frequency Variation	Frequency of Voltage varies from specified Value (usually 50 or 60Hz)	Excess demand (low), system 'catch up' (high)	Slow
Transient	Very short duration deviations in the supply voltage from sinusoidal	Switching of loads onto or off the system, lighting strikes	Fast

Table 3.1 Possible Events That May Occur on a Power System

To maintain a high quality supply it is necessary for the supply company to monitor the voltage at strategic points in the transmission and distribution networks. One method of obtaining this information is to use conventional measurement techniques, section 2.1. **Ruitz *et al*(1995)** report the development of a power system quality monitoring system using a digital data acquisition and processing system. This recorded the outputs from three current and voltage transformers and calculated the magnitude, frequency and harmonic content of all signals, the system operated in real time. **Lickso *et al*(1992)** reports on the monitoring of domestic supplies, a digital voltage recorder was used to monitor the line to neutral voltage and indicate the

number of times the voltage exceeded normal operating limits. Both authors used conventional methods which required connections to the voltage sources. Insulation requirements of a direct electrical connection make these instruments relatively expensive for monitoring high voltage supplies. Therefore, although modern power systems are large distributed networks with large numbers of nodes, voltage and currents are usually only measured at a limited number of points.

3.2 Requirements of a Non Contact Monitoring System

The power generation, supply and distribution industries are continuously attempting to reduce costs, increase the quantity of power supplied and maintain a high quality supply. Monitoring both the quality of supply and the plant condition is recognised as one area requiring development that will assist in meeting these goals, **Jones(1994)**.

The current work is the development and evaluation of an instrumentation system that will provide some of the information required by systems monitoring power transmission and distribution networks at low cost. The instrumentation system continuously monitors the voltage on all the conductors of a three phase power system and detects, in real time, the events listed in table 3.1. No physical contact is made to the power system and all components of the instrument are sufficiently remote from the high voltage conductors to be put into place without de-energising the system. When compared to conventional (contact) high voltage measurement methods, the system is a low cost one.

3.3 Development of a Non Contact System

With no physical connection to the power system it was not possible to measure the conductor voltages directly, other parameters had to be measured and the voltages derived from the measurements. The effect of a conductor at high voltage at a distance from a surface at ground potential is to create an electric field. In free space around a power system the electric field is a function of the voltage on all exposed conductors. Therefore measurements of electric field should enable information on the conductor voltages to be derived.

To monitor individual conductor voltages of a system with several conductors by measuring the distant electric field it was necessary to determine the relationship between the electric field and the individual conductor voltages. The field distribution was examined to determine field measurement positions which allow derivation of the individual voltages. Once the number and position of the field measurements was determined electric field sensors and real time processing systems were developed to determine the change in individual conductor voltages from the field measurements.

4. Electric Field Generated by a Power System

4.1 Background

Computations and measurements of electric fields around power systems are performed for several reasons. These include ensuring that the field is limited to safe working levels when designing power system apparatus, determination of power system equivalent parameters, and investigating the effects of the field on personnel and apparatus in the surrounding area.

In a power system it is essential that the electric field within insulating components does not exceed the safe working limit of the material. The maximum field is determined by the maximum operating voltage and the geometry of the apparatus. As the maximum operating voltage is usually specified, the geometry must be designed to limit the electric field to safe levels; for example **Cui *et al*(1994)** report field calculations for the design of a high voltage transformer insulator.

For transmission line stability studies it is often necessary to know the inter-line capacitance per unit length of line, **Bergen(1986).** The charges on the lines may be determined from the electric field and, as the lines are operated at constant voltage, the capacitances may be determined, **Zaborsky & Rittenhouse(1954)**.

The increase of transmission voltages above 400kV in the late 1970's resulted in a large number of studies on the possible biological effects of exposure to power line fields. **Chartier *et al*(1985)** measured the field within high voltage switchyards and **Jacobs & Dietrich(1984)** calculated the electric field within a residential environment close to an

overhead transmission line. A review of such studies is given by **IEE(1991)**, many references contained conflicting information from differing sources and no conclusions were reached. **Deno & Zaffanella(1987)** calculated the voltages induced on objects such as vehicles placed in power system electric fields and the currents flowing to ground through them.

4.2 Form of a Three Phase Power System

All ac power systems consist of a number of conductors, each with a time varying voltage applied to it. A method commonly used for transmission and distribution systems is to use three conductors with a *three phase* excitation, **Say(1976)**. Figure 4.1a shows a two dimensional cross section of one common configuration, three circular section conductors above a ground plane. The conductors are shown in free space above an infinite extent ground plane, in some configurations the conductors may be surrounded by walls, figure 4.1b, or have a fourth conductor at 0V. If an origin is defined at ground level below the central conductor each conductor's geometry is defined by the co-ordinate location of its centre, (x_n,y_n), and its diameter, d_n. Vertical walls may be defined by the distance of the inner surface from the vertical co-ordinate axis their height and their thickness.

If dimensions in the cross section are small, compared to the distance over which the cross section remains constant, the two dimensional model may be used to determine the electric field around the power system. Selection of a two dimensional model has many advantages. When numerical methods, for example finite element techniques, are used computing time increases as the square of spatial resolution for two dimensional

models, and as the cube for three dimensional models. Analytical expressions for electric field may be derived for a two dimensional model, though generally not for a system with variation in the third dimension.

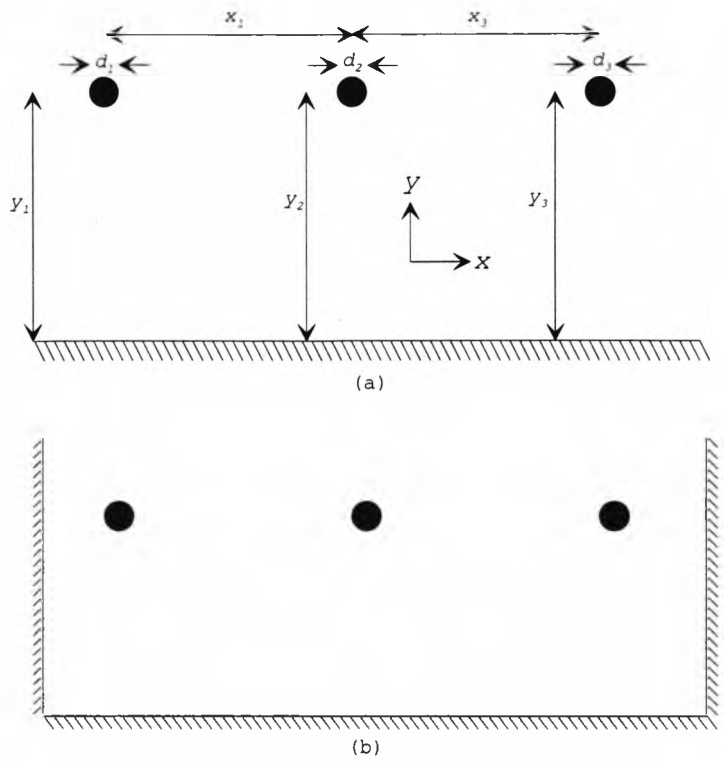

Figure 4.1 Power System Geometry

The instantaneous voltage on conductor n at time t, $V_n(t)$, is given by

$$V_n(t)=V_{pn}\sin\left(2\pi f_p t+\Phi_n\right) \qquad [4.1]$$

where f_p is the frequency of the power system, V_{pn} is the peak voltage of the conductor, under normal operating conditions V_{pn} is the same for all n. Sags and swells in the voltage of conductor n correspond to reductions and increases in V_{pn}. Φ_n is the phase angle of the voltage relative to a reference phase, for three phase excitation the values of Φ_n are 0, $-2\pi/3$ and $2\pi/3$.

4.3 General Form of the Electric Field Vector

Deno(1976) states that the electric field, $\vec{E}(t)$, at any point around a three phase power system is a time varying vector quantity. When the length of the conductors is much longer than dimensions in the cross section he states that the vector is in the plane of the cross section and may be described by

$$\vec{E}(t)=\hat{x}E_x \sin(2\pi f_p t+\Phi_x)+\hat{y}E_y \sin(2\pi f_p t+\Phi_y) \qquad [4.2]$$

$\hat{x}$ and $\hat{y}$ are unit vectors in the horizontal and vertical directions, E_x and E_y are the peak amplitudes of the field in each of these directions, and Φ_x and Φ_y are phase angles relative to the phase angle of the voltage on a reference conductor.

Four variables; *field variables*, E_x, E_y, Φ_x and Φ_y; are required to fully describe the electric field vector. From [4.2] it may be shown that the locus of the electric field vector rotates and describes an ellipse as a function of time, making one rotation for each complete voltage cycle, **Deno(1976)**.

4.4 Requirements of a Non Contact Voltage Monitoring System

At any point around a power system the electric field is a function of the voltages on all un-screened conductors, their co-ordinate locations and the system geometry. To develop a non contact monitoring system it is necessary to determine how the field variables change as conditions change on the power system, section 3.3. This requires the computation of $\vec{E}(t)$ for different power system operating conditions. Two techniques have been used to compute the electric field; one used a commercial finite element program, the other an analytical expression for the electric field.

4.5 Finite Element Solutions

4.5.1 The Finite Element Method

Finite element analysis (FEA) is a numerical method for the solution of differential equations, its first application to engineering applications is reported by **Turner *et al*(1956)**. **Segerland(1976)** describes the concept behind FEA as: "Any continuous quantity such as temperature, pressure and displacement can be approximated by a discrete model composed of a set of piecewise continuous functions defined over a finite number of subdomains".

Electric potential, and hence electric field, may be calculated by dividing the area over which it is to be calculated, *the domain*, into a large number of sub-domains known as *elements*. Two dimensional elements are usually triangular or quadrilateral in shape. The corners of the elements are connected at a grid of common points called *nodes*. The complete network of elements and nodes is known as a *mesh*. Derivation of the mesh is determined by the geometry and material properties of the system for which the field is being determined. Many commercial finite element programs generate the mesh automatically.

The potential of all nodes within conducting objects is fixed at the potential of the object, elsewhere the potentials at the nodes of an element are related by Poisson's equation. As all nodes are present in more than one element a set of simultaneous equations may be defined to describe the potential at each node. For reasonable spatial resolution the number of equations is large, solution is only possible using a

computer. Further details of algorithms for the efficient computation of the node potentials are given in the literature, for example **Silvester & Ferrari(1990)**.

4.5.2 Features of Finite Element Analysis

Finite element analysis allows electric potential to be calculated for systems with complicated geometry and differing material properties. The accuracy of the results depends on the number of mesh elements and the computational technique used to solve them.

The electric field within each element is found by numerically differentiating the potentials. It is not possible to calculate the field for a sinusoidal excitation, the field variables must be evaluated at several times in the sinusoidal cycle. At each point of interest the field variables are calculated by fitting equation [4.2] to the set of results.

Many researchers have written their own software to perform FE analysis; however writing of the code is a laborious task, and the resulting program is limited to a specific problem, for example **Yamashita *et al*(1988)**. A large number of commercial finite element programs exist, **Cabral(1993)**, and one such program has been used to analyse the field around a power system.

4.6 Analytical Solutions

Deno & Zafanella(1987) describe a method for calculating the electric field in two dimensions for any number, N_C, of conductors above an infinite extent earth plane provided the conductor length perpendicular to the two dimensional cross section is

much larger than any dimension in the cross section. The method assumes no free charge exists in the air and that the permittivity of air is equal to the permittivity of free space.

The n'th conductor is described by its co-ordinate location (x_n, y_n), diameter d_n, voltage, V_{pn}, and phase angle Φ_n. For analysis the voltage is written as a phasor $\tilde{V}_n$, where

$$\tilde{V}_n = V_{pn}\left[\sin(\Phi_n) + j\cos(\Phi_n)\right] \qquad [4.3]$$

By determining the capacitance between all pairs of conductors it is possible to replace each conductor by a phasor line charge, $\tilde{Q}_n = Q_{rn} + jQ_{in}$, and its image in the ground plane. The electric field produced by a line charge dipole can be derived, for example **Hayt(1989)**.

4.6.1 Determination of Line Charges

Each line charge is a function of the voltage, diameter and position of *all* conductors. For analysis of more than one conductor it is convenient to write the equations relating the conductor charges to the conductor voltages in matrix format. The conductor voltages are represented by the phasor matrix $[\tilde{V}]$, the line charges by phasor matrix $[\tilde{Q}]$ and the relationship between $[\tilde{V}]$ and $[\tilde{Q}]$ by

$$[C][\tilde{Q}] = [\tilde{V}] \qquad [4.4]$$

Matrix $[C]$, the *Maxwell Potential Coefficients*, is a square matrix with dimensions equal to N_C, its elements are, **Deno & Zafanella(1987)**,

$$C_{n_1 n_2} = \frac{1}{2\pi\varepsilon} \ln \sqrt{\frac{\left(x_{n_1} - x_{n_2}\right)^2 + \left(y_{n_1} + y_{n_2}\right)^2}{\left(x_{n_1} - x_{n_2}\right)^2 + \left(y_{n_1} - y_{n_2}\right)^2}} \qquad (n_1 \neq n_2) \quad [4.5]$$

$$C_{n_1 n_2} = \frac{1}{2\pi\varepsilon} \ln\left(\frac{4y_{n_1}}{d_{n_1}}\right) \qquad (n_1 = n_2) \quad [4.6]$$

where (n_1,n_2) is the position of the element in the matrix. Equation [4.4] may be solved for $[\tilde{Q}]$ using standard matrix manipulation techniques, for example **Kreyszig(1993)**.

4.6.2 Calculation of Electric Fields

Using phasor notation equation [4.2], the electric field at a point $P(x_P,y_P)$, may be written

$$\tilde{\vec{E}}_P = \tilde{E}_{xp}\,\hat{x} + \tilde{E}_{yp}\,\hat{y} \qquad [4.7]$$

where phasors $\tilde{E}_{xp}$ and $\tilde{E}_{yp}$ represent the phasors for the horizontal and vertical components of the electric field. The values of $\tilde{E}_{xp}$ and $\tilde{E}_{yp}$ due to one conductor n, $\tilde{E}_{xpn}$, $\tilde{E}_{ypn}$ are, **Deno & Zaffanella(1987)**,

$$\tilde{E}_{xpn} = \frac{(Q_{rn} + jQ_{in})(x_P - x_n)}{2\pi\varepsilon\left[(x_n - x_P)^2 + (y_n - y_P)^2\right]} - \frac{(Q_{rn} + jQ_{in})(x_P - x_n)}{2\pi\varepsilon\left[(x_n - x_P)^2 + (y_n + y_P)^2\right]} \qquad [4.8]$$

$$\tilde{E}_{ypn}(x_p, y_p) = \frac{(Q_{rn} + jQ_{in})(y_P - y_n)}{2\pi\varepsilon\left[(x_n - x_P)^2 (y_n - y_P)^2\right]} - \frac{(Q_{rn} + jQ_{in})(y_P - y_n)}{2\pi\varepsilon\left[(x_n - x_P)^2 (y_n + y_P)^2\right]} \quad [4.9]$$

For N_C conductors superposition may be used to add the field due to each line charge, therefore

$$\vec{\tilde{E}}_P = \left(\sum_{n=0}^{N_C-1} \tilde{E}_{xpn}\right)\hat{x} + \left(\sum_{n=0}^{N_C-1} \tilde{E}_{ypn}\right)\hat{y} \quad [4.10]$$

Equation [4.10] is of the form of equation [4.7] and fully describes the electric field at any point.

4.6.3 Features of the Analytical Method

The analytical method is limited to situations with simple geometry and with a constant permittivity. Conductors may be described at any location with any peak voltage, including zero. It is not possible to include conductors with no connection to a voltage source. As the conductors are replaced by line charges, the distribution of charge on the lines is ignored and results close to and within the conductor will be incorrect. However **Olsen(1994)** states "Results using this approximation are more often found to be useful than not". **Deno and Zafanella(1987)** used the analytical method to calculate the field under overhead lines, the results were compared to measured values and found to be in good agreement.

Conducting objects, at ground potential, with non circular geometry may be approximated by placing a number of zero volt conductors touching each other,

figure 4.2. The accuracy of the approximation is determined by the size of these conductors; the smaller the conductors the better the approximation. However the number of conductors in the model also increases and the effort necessary to solve the matrix equations increases.

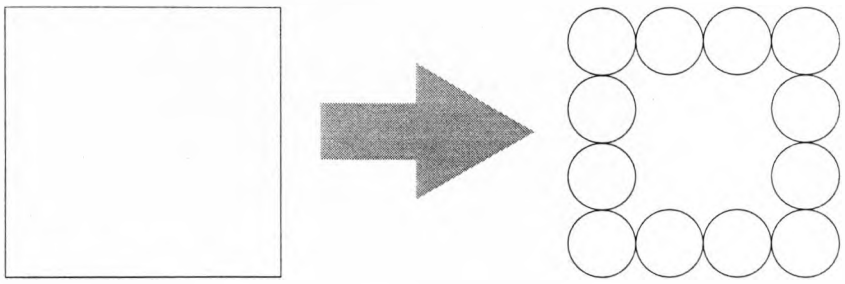

Figure 4.2 Approximation of Square Geometry by Circular Conductors

4.7 Scaling of the Power System Model

The analytical technique allows expressions to be derived for the electric field generated by a power system at any point in free space, therefore it can be used to examine the effect of scaling of the power system geometry. It was necessary to investigate the effects of scaling as, for laboratory investigations, it is frequently impossible to construct a full size model of a power system.

A conductor in the full sized system is centred at point (x_n, y_n) and has diameter d_n and a peak voltage V_{pn}. A conductor in the scale system is centred at (x_n^*, y_n^*), has diameter d_n^* and a peak voltage V_{pn}^*. The relationship between the geometry of the two systems is given by the scale factor, K where $x_n = Kx_n^*$, $y_n = Ky_n^*$ and $d_n = Kd_n^*$. Point $P(x_p, y_p)$ in the full sized system is equivalent to point $P^*(x_p^*, y_p^*)$ in the scaled system, where $x_p = Kx_p^*$, $y_p = Ky_p^*$.

For a single conductor [*C*] is reduced to one element and the equivalent line charge in the scaled system $\tilde{Q}^*$ is

$$\tilde{Q}^* = \frac{\tilde{V}_{P1}^*}{2\pi\varepsilon} \ln\left(\frac{4y_1^*}{d_1^*}\right) \qquad [4.11]$$

Substituting for y_1^* and d_1^* gives

$$\tilde{Q}^* = \frac{\tilde{V}_{P1}^*}{2\pi\varepsilon} \ln\left(\frac{4\,y_1/K}{d_1/K}\right) \qquad [4.12]$$

Comparing [4.11] and [4.12] shows that the equivalent line charge in the scaled system is determined by the scaled voltage $\tilde{V}_{P1}^*$ and not by the scaled dimensions.

Writing equation [4.8] in terms of the scaled parameters and substituting for x_p^*, x_n^*, y_p^* and y_p^* gives the horizontal component of the electric field in the scale model, $\tilde{E}_{xpn}^*$, as

$$\tilde{E}_{xp}^* = \frac{\left(Q_{rn}^* + jQ_{in}^*\right)\left(\frac{x_p}{K} - \frac{x_n}{K}\right)}{2\pi\varepsilon\left[\left(\frac{x_n}{K} - \frac{x_P}{K}\right)^2 + \left(\frac{y_n}{K} - \frac{y_p}{K}\right)^2\right]} - \frac{\left(Q_{rn}^* + jQ_{in}^*\right)\left(\frac{x_p}{K} - \frac{x_n}{K}\right)}{2\pi\varepsilon\left[\left(\frac{x_n}{K} - \frac{x_p}{K}\right)^2 + \left(\frac{y_n}{K} + \frac{y_p}{K}\right)^2\right]} \qquad [4.13]$$

[4.13] and [4.8] are identical if $\tilde{Q}_n = K\tilde{Q}_n^*$. This may be achieved by scaling the voltage, $\tilde{V}_n$, by the factor *K*. A similar analysis can be applied to equations [4.5] and [4.9] with identical results. Scaling the system geometry and voltage by the same

amount results in the absolute magnitudes and directions of the fields at equivalent points in the full sized and scale systems being identical.

4.8 Comparison of the Two Computational Methods

A computer program was written, the *analytical program*, to process a list of conductor diameters, voltages and co-ordinate locations using equations [4.4] to [4.9] to determine the field variables at any point or set of points.

Computer control routines were written to execute the finite element program four times corresponding to points in the power system voltage cycle as quasi-static cases. Further routines processed the four sets of results to determine the field variables.

For the two simple power system models shown in figure 4.1 both methods were used the compute the peak horizontal and vertical components of $\tilde{\tilde{E}}$ on a grid at 0.1m resolution between the limits $-10 \leq x_p \leq 10$m and $0 \leq y_p \leq 10$m. The differences in E_x and E_y between the two sets of results were evaluated.

4.8.1 Three Phases - Free Space Boundary

Table 4.1 shows the positions and excitations of the conductors for the power system geometry shown in figure 4.1a. Figures 4.3 and 4.4 show the amplitudes E_x and E_y determined by the FE program; figures 4.5 and 4.6 show the differences between the two computational techniques.

Conductor (n)	x_n(m)	y_n(m)	d_n(mm)	V_{pn}(kV)	Φ_n(degrees)
1 (Left)	-2	5	50	100	-120
2 (Centre)	0	5	50	100	0
3 (Right)	2	5	50	100	120

Table 4.1 Power System Parameters For the Free Space Boundary Model

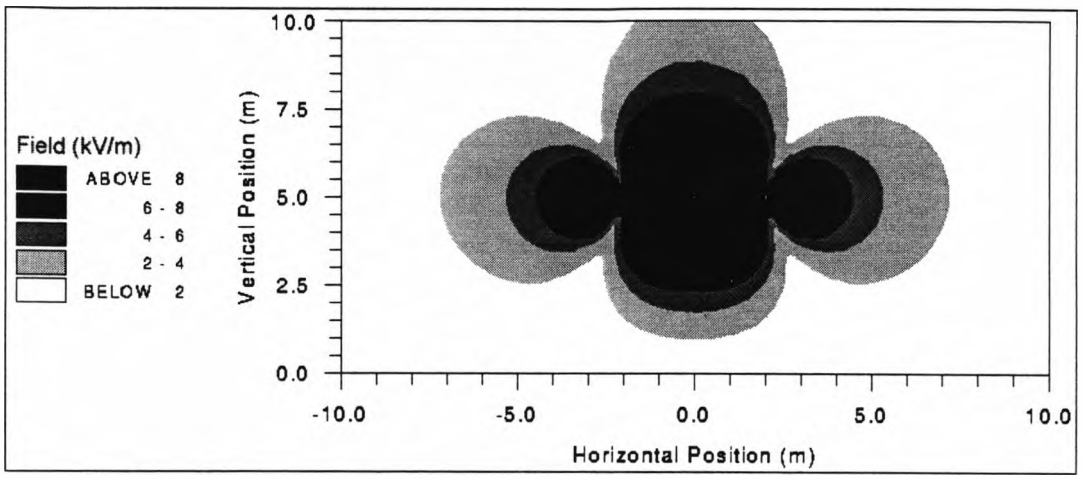

Figure 4.3 E_x Calculated by Finite Element Program for Power System in Figure 4.1a

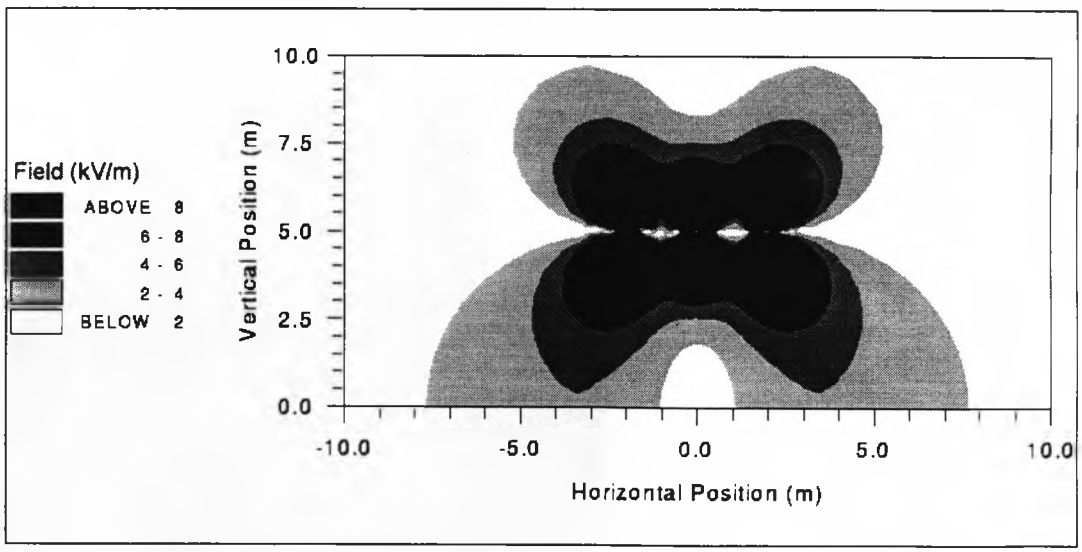

Figure 4.4 E_y Calculated by Finite Element Program for Power System in Figure 4.1a

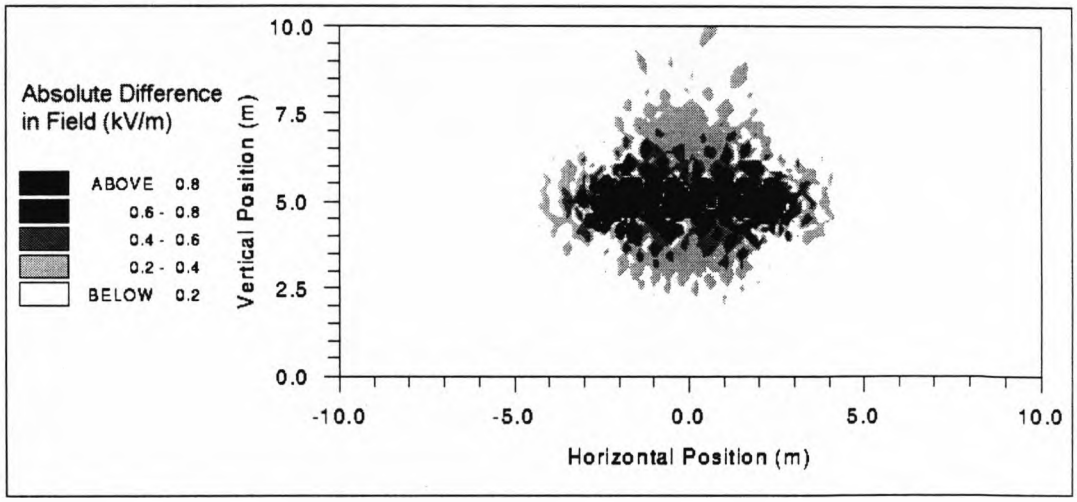

Figure 4.5 Differences in E_x for Power System in Figure 4.1 for Field Calculated by Finite Element Program and Analytical Program

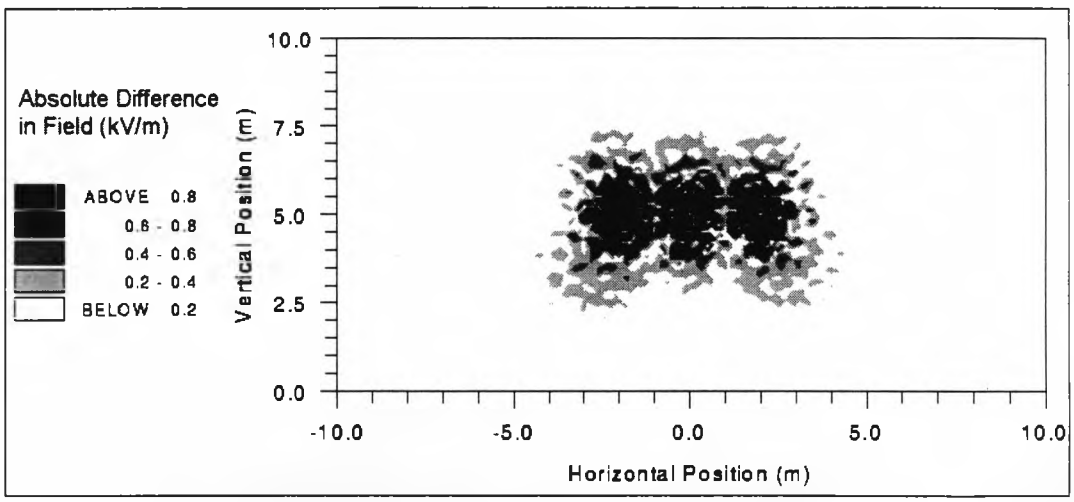

Figure 4.6 Differences in E_y for Power System in Figure 4.1 for Field Calculated by Finite Element Program and Analytical Program

Close to the conductors the differences are large because both methods are inaccurate. The representation of the conductors by line charges results in inaccuracies in the analytical program, while the conductor diameter is small relative to the size of the elements in the FE program causing it to be inaccurate.

Figure 4.7 shows E_y along a horizontal line at ground level, calculated by both methods and the percentage difference between them. Figure 4.8 shows the same

information at a height of 0.5m. The differences increase towards the boundaries of the FE mesh. By moving the boundaries to a greater distance it was shown that the differences arose because of the approximation used to model free space in the FE program

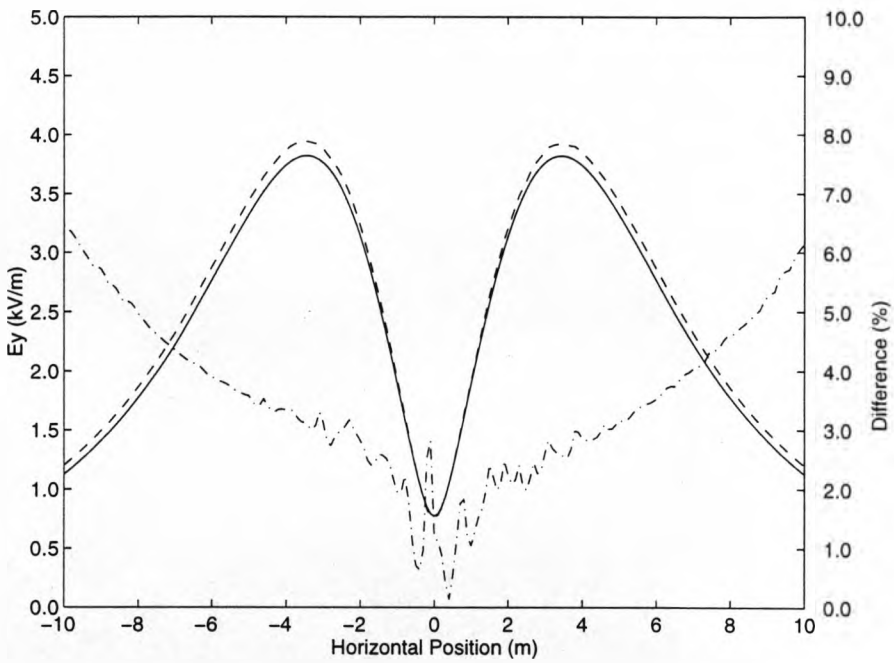

Figure 4.7 E_y at Ground Level for Power System in Figure 4.1
Solid Line = Analytical Program *Dashed Line* = FE Program
Dash / Dot Line = Percentage Difference

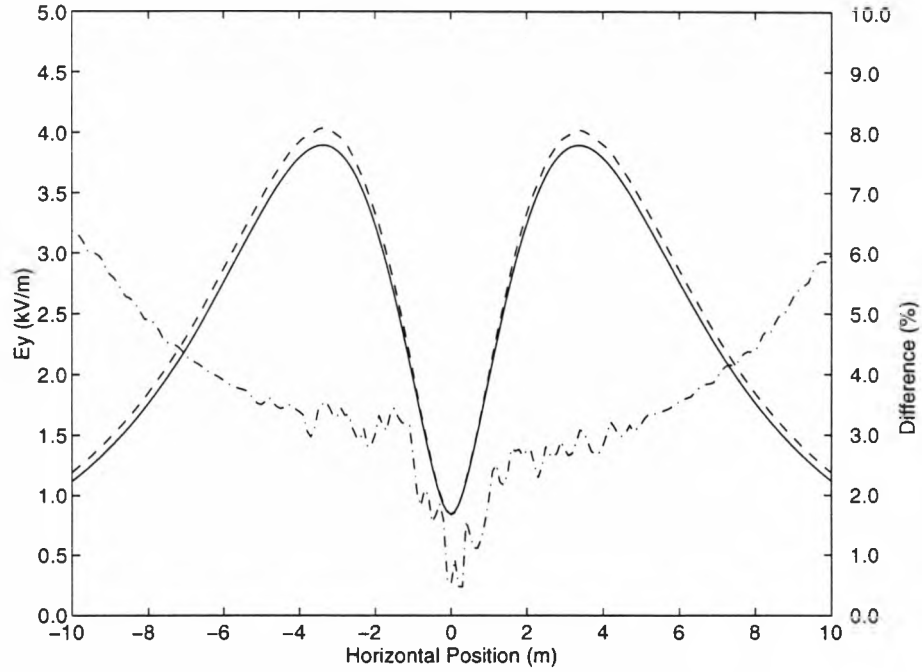

Figure 4.8 E_y at Height of 2m for Power System in Figure 4.1a
Solid Line = Analytical Program, *Dashed Line* = Finite Element Program
Dash/Dot Line = Percentage Difference

4.8.2 Vertical Walls Near the Conductors

Two vertical walls were added to the model of figure 4.1a forming that of figure 4.1b, the height of each wall was 11m and the distance between the wall and the outer conductors was set as 6m. In the analytical program the wall was represented by eleven conductors at zero volt potential with diameter 1m. They were positioned in a vertical stack centred 6.5m from the outer conductors. Contour plots, figure 4.9 and 4.10 show E_x and E_y calculated by the analytical model. Figures 4.11 and 4.12 show the difference between the two methods. As before the differences are large near to the conductors, there are also differences near the walls caused by modelling the rectangular wall using circular conductors.

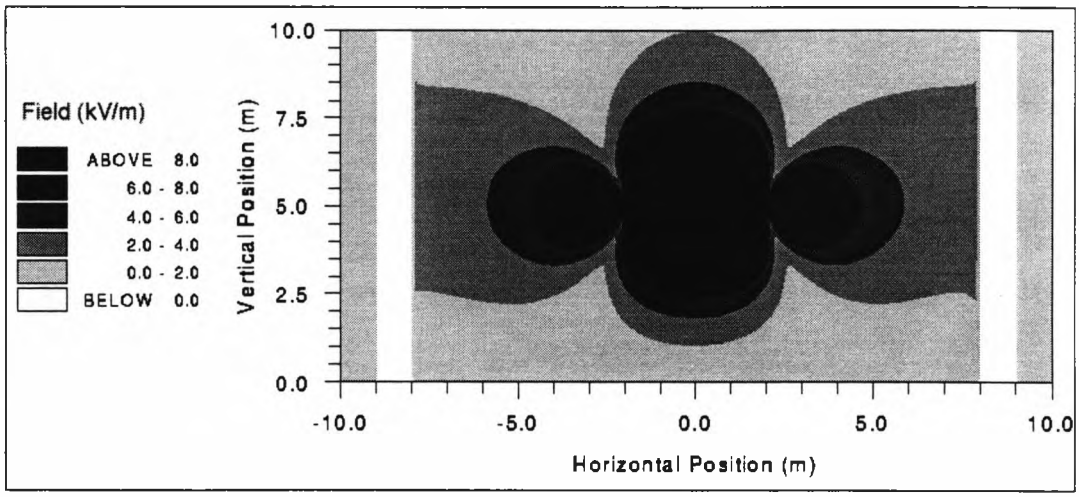

Figure 4.9 E_x for Power System in Figure 4.1b, Calculated by Analytical Program

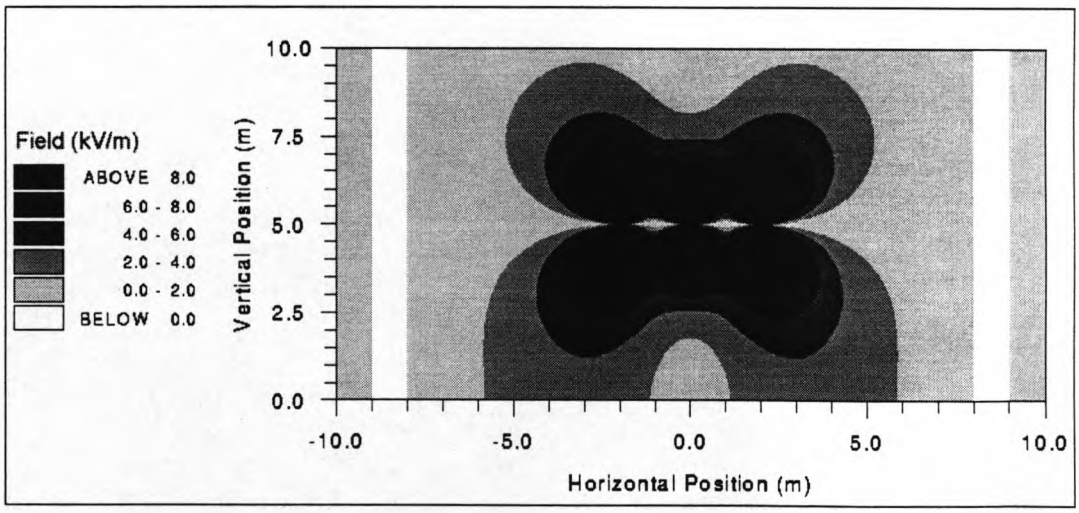

Figure 4.10 E_y for Power System in Figure 4.1b, Calculated by Analytical Program

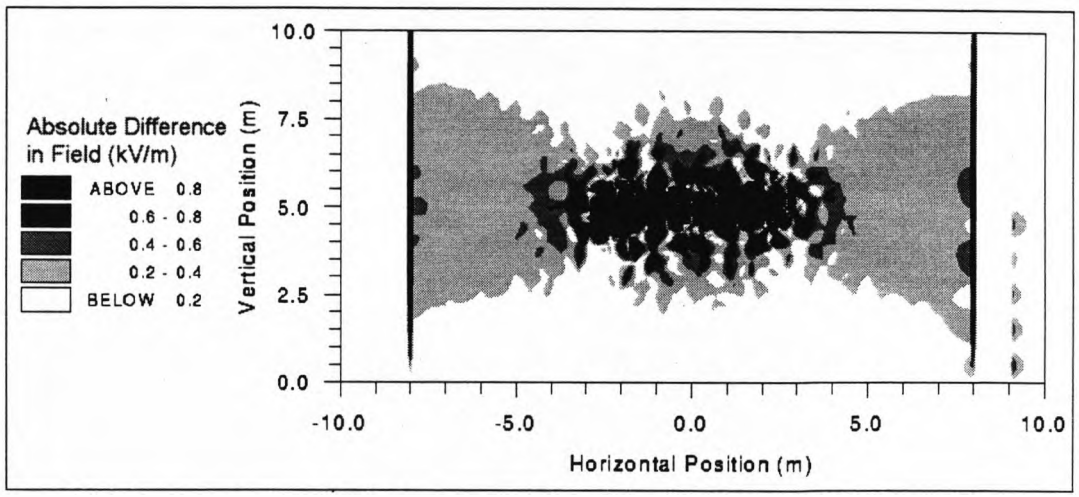

Figure 4.11 Difference in E_x for Power System in figure 4.1b, Calculated by Finite Element Program and Analytical Program

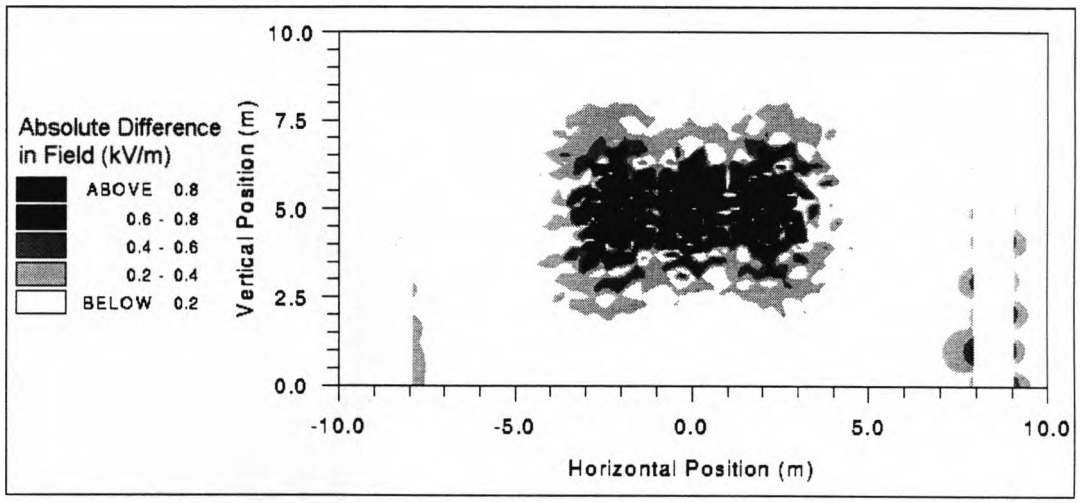

Figure 4.12 Difference in E_y for Power System in figure 4.1b, Calculated by Finite Element Program and Analytical Program

Figures 4.13 and 4.14 show E_y calculated by both methods along a horizontal line at ground level and at a height of 0.5m and the fractional difference between them. There are large errors close to the walls, because the modelling of the wall by a stack of cylinders is not exact.

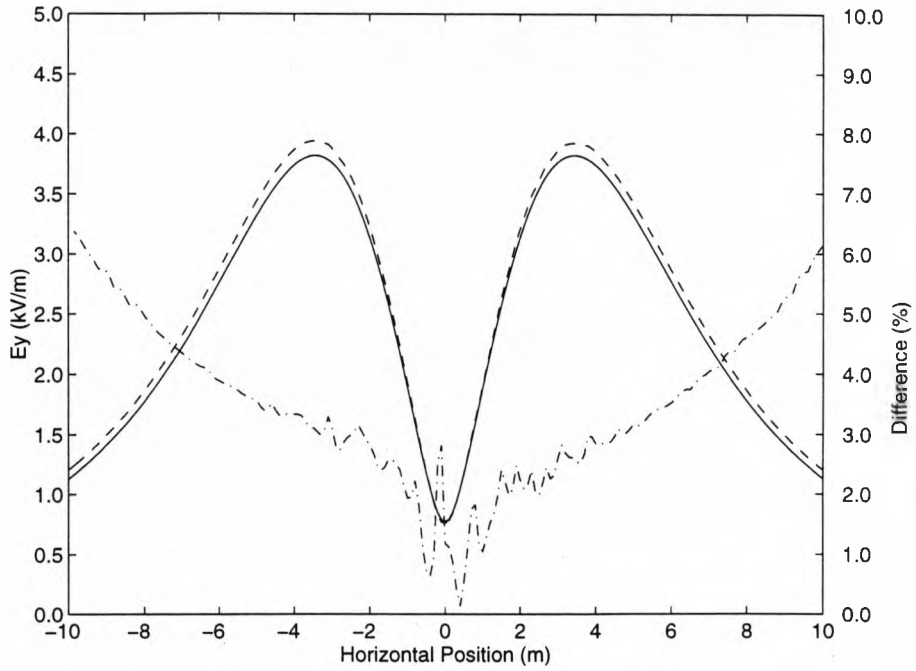

Figure 4.13 Differences in E_y at Ground Level for the Power System in Figure 4.1b, *Solid Line* = Finite Element Program, *Dashed Line* = Analytical Program, *Dash/Dot Line* = Percentage Difference

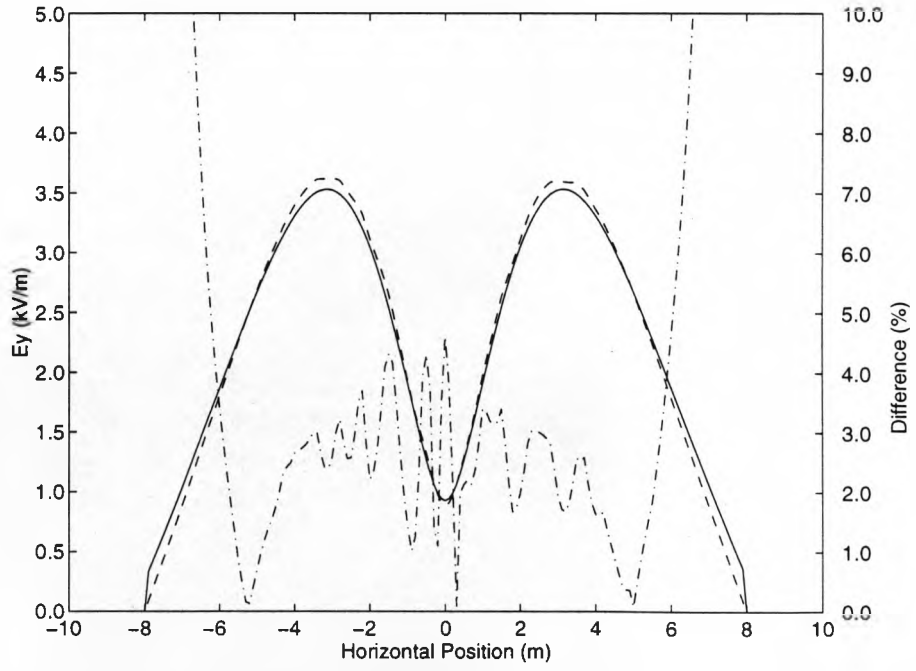

Figure 4.14 Differences in E_y at height of 0.5m for Power System in Figure 4.1b *Solid Line* = Finite Element Program *Dashed Line* = Analytical Program *Dash/Dot Line* = Percentage Difference

4.9 Selection of Computation Method

Section 3.3 indicates that, to develop a non contact monitoring system, it is necessary to determine how the electric field changes as conditions on the power system change. This requires that the field be computed for many different operating conditions.

At distances of more than 50 diameters from the conductors and distances over two metres from the walls of the model the differences between the two methods were small. Timing of the two computation methods indicates the analytical program was approximately 3000 times faster than the finite element program. **Deno & Zafanella(1987)** successfully used analytical methods to successfully model electric fields produced by overhead transmission lines. For these reasons the analytical program was selected as the tool to analyse the power system electric fields and results in regions where the calculations were inaccurate were not used.

4.10 Summary

The electric field around a power system was evaluated by two techniques, both are approximate, but except close to the conductors and earthed objects and at the boundaries of the finite element model, the differences between the two methods are small.

The large number of calculations to be performed when determining the influence of various power system parameters lead to the decision to use the analytical program for further analysis of the power system electric field. It was shown that if the

dimensions of the power system and voltage are scaled the field distribution will also scale, at equivalent points in the full sized and scale systems the field will be identical.

5. Theoretical Investigation of a Non Contact Monitoring System

To develop a system that monitors conductor voltages by measurement of the electric field produced, it was necessary to know the relationship between the electric field distribution around the power system and the conductor voltages on the power system, section 3.3. To minimise computation time investigations were restricted to power system geometries for which a two dimensional field, fully described by four field variables, section 4.3, was a good representation.

5.1 Investigation Method

Changes in any of the power system voltages change the field variables at all positions around the power system, in general the changes will not be uniform. The analytical program, section 4.8, was used to calculate the field variables at many positions for many combinations of power system parameters and to investigate the relationship between changes in the field variables and changes in the power system parameters.

The investigation was performed for many different power system configurations and similar conclusions were drawn in all cases. To allow comparison of many cases detailed results are presented for a system with three conductors above an infinite extent ground plane with the system geometry described by figure 4.1a and table 4.1.

Measurements of phase angles, Φ_x and Φ_y, would require more sophisticated instrumentation than a system to measure peak field amplitudes E_x and E_y. For this reason initial investigations were limited to examination of E_x and E_y, to determine if measurements of these would be sufficient to monitor conductor voltages.

The investigations examined the changes in the peak field amplitudes in all areas surrounding the power system when the conditions on the power system changed. Initially the peak field amplitudes produced under the normal operating conditions of the power system were calculated and stored for reference. A conductor voltage was changed by a small amount, (typically multiples of 0.1%), the field amplitudes recomputed and the changes from normal calculated. These changes were examined to discover if it was possible to determine the change in conductor voltages from measurements of changes in the field amplitudes. If such determination was possible the field amplitude(s) required and the location(s) at which they must be measured were also determined.

5.2 Effect of Voltage Changes on Peak Field Amplitudes

If the peak voltage on all conductors changes by the same factor the peak field amplitudes will also change by this factor at all locations. If the conductor voltages change by different factors the changes in the field are more complicated. Figure 5.1 shows the percentage change in peak field amplitude E_x for a 0.1% decrease in the left conductor peak voltage, V_{P1}. Figure 5.2 shows the percentage change in E_y for the same voltage change.

The 0.1% decrease in one conductor voltage results in an unbalanced power system, at some positions it causes decreases in the field while at others the field increases. At some points the magnitude of the changes is greater than 0.1%, at others it is less.

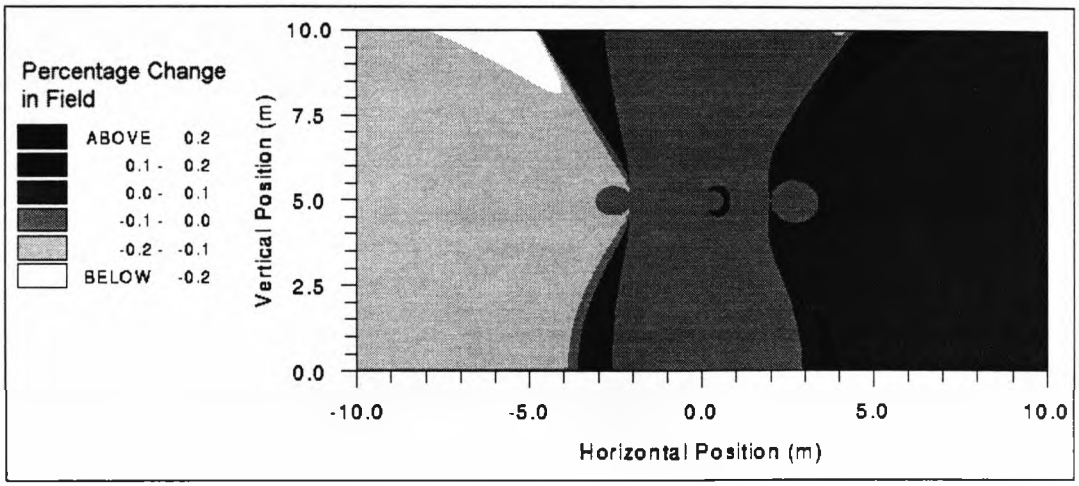

Figure 5.1 Percentage Change in E_x for 0.1% Decrease in Left Conductor Voltage

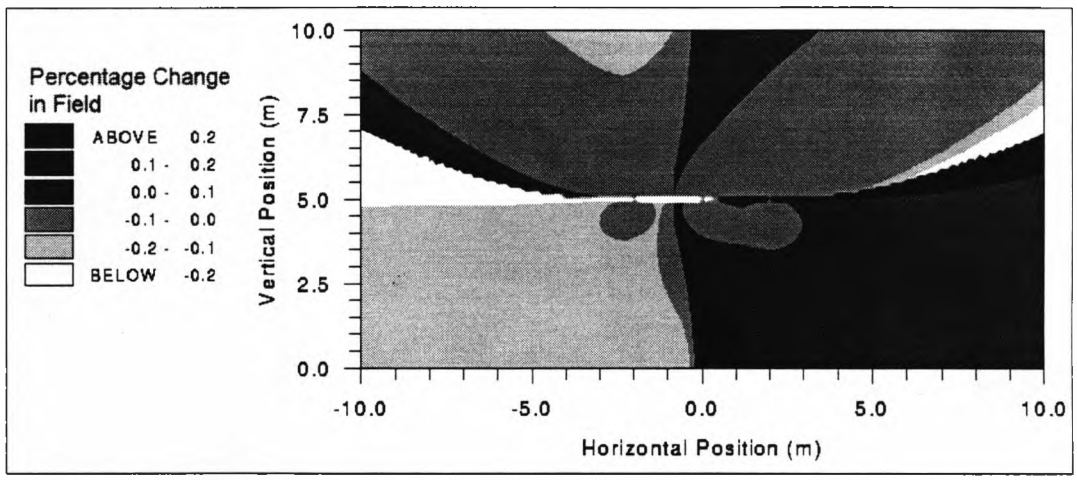

Figure 5.2 Percentage Change in E_y for 0.1% Decrease in Left Conductor Voltage

Table 5.1 shows the change in E_x at two points, P_1(-4m,2m), P_2(4m,0.5m) for three sets of changes in the conductor voltages. For sets *A* and *B* changes at P_1 are identical, for sets *B* and *C* the changes at P_2 are identical, to differentiate the three sets of voltage changes, the field changes at both points must be examined.

Further calculations showed that at a specific point the same change in E_x or E_y could be created by many different combinations of conductor voltage changes. To

differentiate changes in individual conductor voltages it is necessary to measure the peak field amplitudes at several locations.

Voltage Change Combination	Change in Conductor Voltage (%)			Change in E_x (%)	
	Left	Centre	Right	P_1	P_2
Set *A*	-0.9	-0.9	-0.9	-0.9	-0.9
Set *B*	-0.7	0.2	1.1	-0.9	0.7
Set *C*	0.7	0.7	0.7	0.7	0.7

Table 5.1 Changes in E_x For Two Combinations of Voltage Changes

Figure 5.3 shows the percentage change in E_x along a horizontal line orthogonal to the conductors, a *change profile*, at a height of 1m, for the three different combinations of conductor voltage changes shown in table 5.2. Figure 5.4 shows the E_y change profile for the same sets of voltage changes. In both cases the change profiles are different suggesting it is possible to differentiate between the three different voltage change combinations.

Voltage Change Combination	Line Type	Changes in Conductor Voltages (%)		
		Left	Centre	Right
Set 1	Solid	-0.5	+0.3	-0.1
Set 2	Dash/Dot	-1.0	+0.3	+0.9
Set 3	Dashed	+0.7	-0.3	+1.1

Table 5.2. Combinations of Conductor Voltage Changes for Figures 5.3 and 5.4

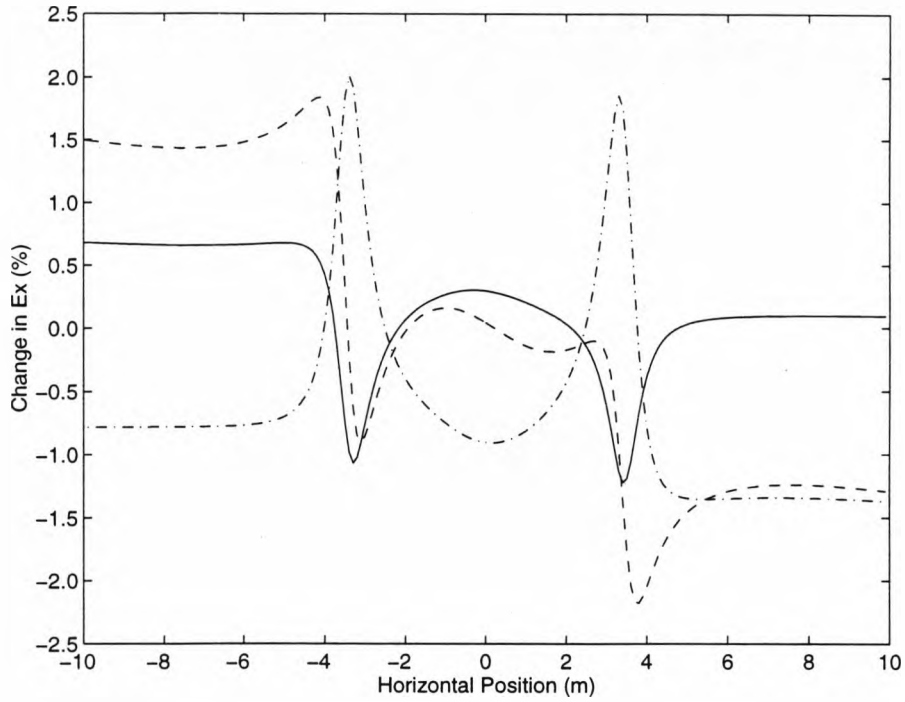

Figure 5.3 E_x Change profile at 1m, for Voltage Change Sets in Table 5.2
Solid Line = Set 1 *Dash/ Dot Line* = Set 2 *Dashed Line* = Set 3

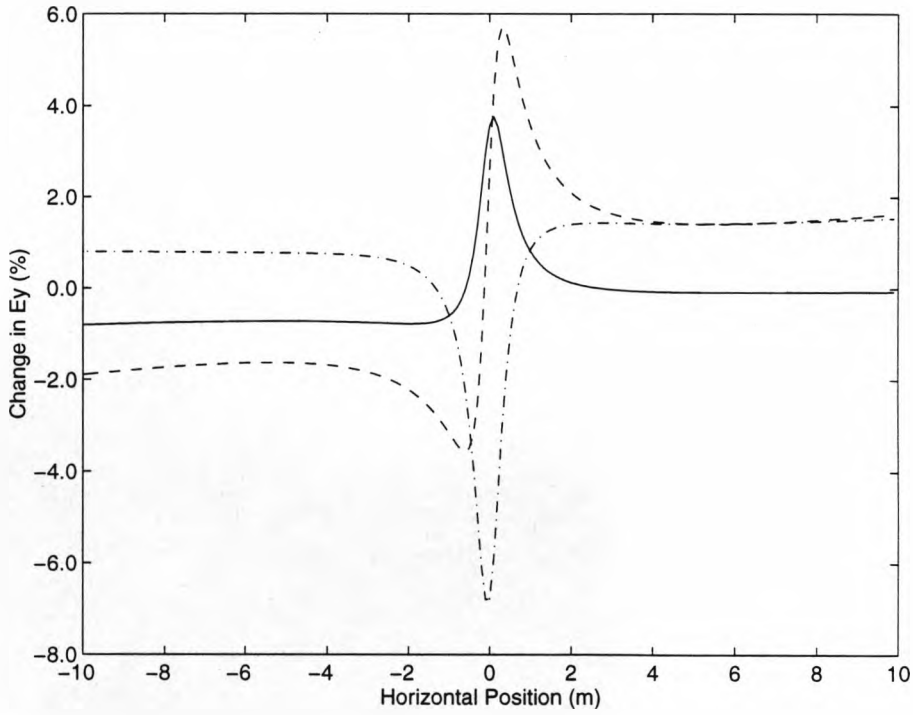

Figure 5.4 E_y Change Profile at 1m for Voltage Change Sets in Table 5.2
Solid Line = Set 1 *Dash/Dot Line* = Set 2 *Dashed Line* = Set 3

An extensive investigation indicated that changes in individual conductor voltages may be differentiated using a set of measurements of either E_x or E_y taken at a sufficient number of different positions. For example calculations were made for changes at 0.1% intervals in each conductor voltage over a range of ±2%. Using every possible combination of V_{P1}, V_{P2}, and V_{P3}, that is 68921 cases, the changes in E_y were calculated at eight locations in the ground plane. All 68921 sets of eight values were examined, no two sets were identical.

Further calculations were performed with different conductor diameters, different geometric configurations, with and without structures, such as surrounding walls in the vicinity of the conductors. For a given set of changes in the conductor voltages the change profiles were different for each geometric configuration. In all cases the magnitude of the field changes was similar and it was possible to find a set of locations at which the changes in the field amplitudes were unique for each set of voltage changes.

If changes in either E_x or E_y are measured at a number of carefully selected positions any set of measurements of changes corresponds to a unique set of changes in the conductor voltages. Therefore, provided that a method may be devised, the unique relationship between field changes and conductor voltage changes may be used to derive changes in conductor voltages from measurements of changes in field distribution. There is no obvious analytical method of relating measured change profiles to changes in conductor voltage. Consequently some form of search comparing measured change profiles with a database of pre-computed calculated ones covering all possible cases of interest will be required.

5.3 Selection of Sensor Positions

Figure 5.5 shows the absolute change in E_x for voltage change set 1, of table 5.2, calculated at heights of 0.1m, 1.25m and 2.5m. Figure 5.6 shows the absolute change in E_y at ground level, and heights of 1.25m and 2.5m for the same voltage change set. Figures 5.7 and 5.8 show the E_x and E_y change profiles for the same conditions.

The absolute change in the field is greater close to the conductors, however the percentage change increases as the distance from the conductors towards the ground plane increases. At the ground plane E_x is always zero, and percentage changes in E_y are high indicating that if E_y is measured the ground plane is a suitable place to mount the sensor elements. Further practical considerations in section 6.2.1 show that it is simpler to construct an electric field sensor that operates at the ground plane. It was decided to develop sensors to measure E_y and place them along a line orthogonal to the conductors at the ground plane.

At each sensor position the value of the change profile is a function only of the changes in the three conductor voltages, hence in theory if the field changes are measured at three points the changes in the three conductor voltages may be deduced.

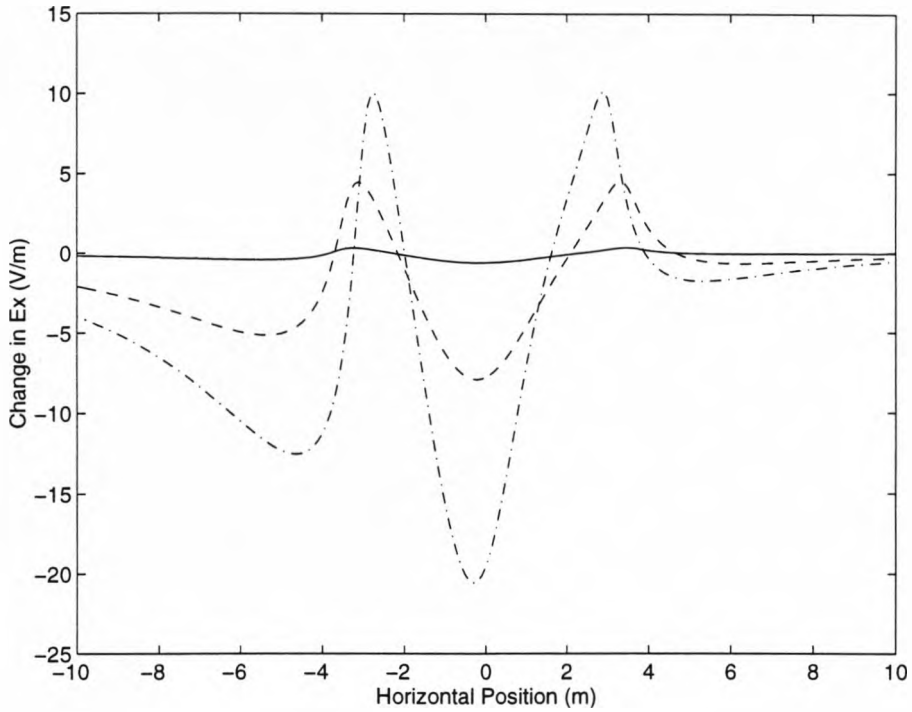

Figure 5.5 Absolute Change in E_x for Voltage Change Set 1 of Table 5.2
Solid Line = 0.10m *Dashed Line* = 1.25m *Dash/Dot Line* = 2.5m

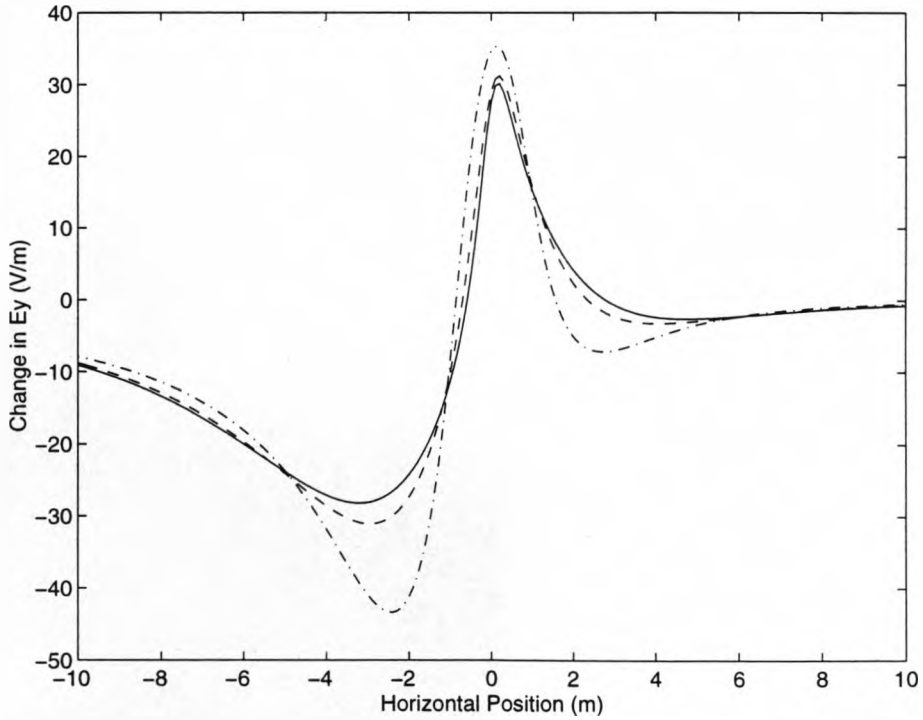

Figure 5.6 Absolute Change in E_y for Voltage Change Set 1 of Table 5.2
solid Line = 0.0m *Dashed Line* = 1.25m *Dash/Dot Line* = 2.50m

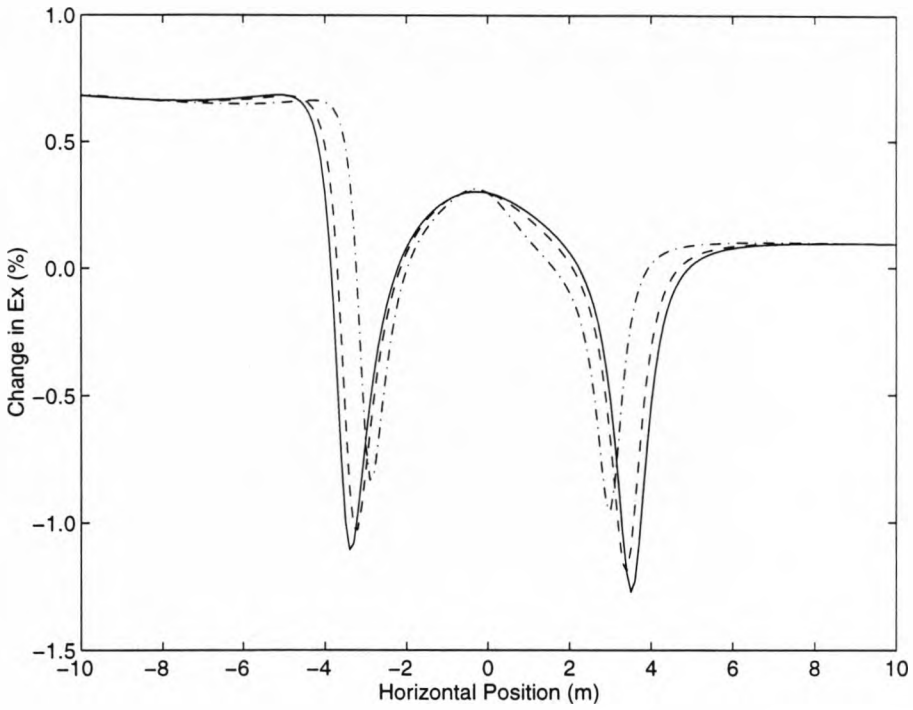

Figure 5.7 E_x change profile for Voltage Change Set 1 of Table 5.2
Solid Line = 0.1m *Dashed Line* = 1.25m *Dash/Dot Line* = 2.5m

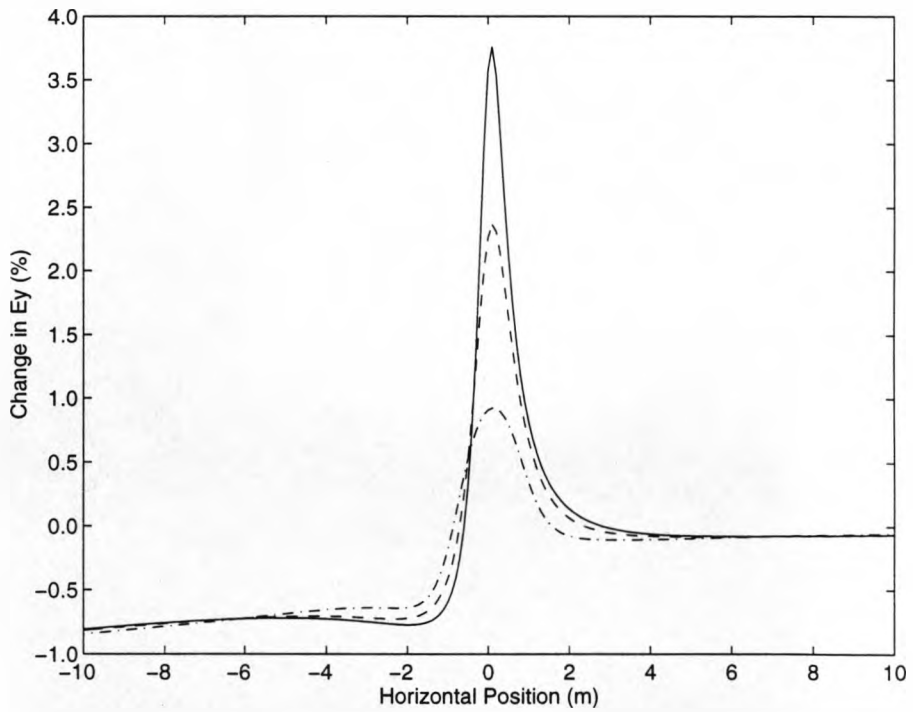

Figure 5.8 E_y change profile for Voltage Change Set 1 of Table 4.2
Solid Line = 0.0m *Dashed Line* = 1.25m *Dash/Dot Line* = 2.5m

In a real system noise will be present on the sensor signals. Provided there is no correlation between the noise on the sensors, additional sensors will enable the effects of the noise to be reduced. The number of sensors required will depend on the level of noise present and the accuracy to which the voltage changes are required.

Results of the form in figure 5.8 show that under certain conditions changes in the field distribution can occur over distances less than the conductor spacing, changes also extend beyond the total conductor spread. The spacing and spread of the sensors must be sufficient to detect these changes. If it is assumed that signals with low noise levels can be obtained then the change profile computations suggest that at least six sensors, spaced at about half the conductor separation, should be used.

5.4 Model Geometry Inaccuracies

The geometrical model of the power system used to calculate the database of change profiles searched, to determine the conductor voltages, usually includes approximations. For illustration a larger inaccuracy than would normally occur is examined. Figure 5.9 shows the ground level field distribution between the limits $-5 \leq x \leq 5$ m for the power system described in figure 4.1a and table 4.1 with, and without, walls at a distance of 7m from the central conductor.

Figure 5.10 shows the change profile for a 1% decrease in V_{P1} the left hand side conductor voltage for a power system with no walls, solid line, and change profiles for a 1% and 2% decrease in V_{P1} for a system with walls at 7m, (dashed and dash/dot lines respectively).

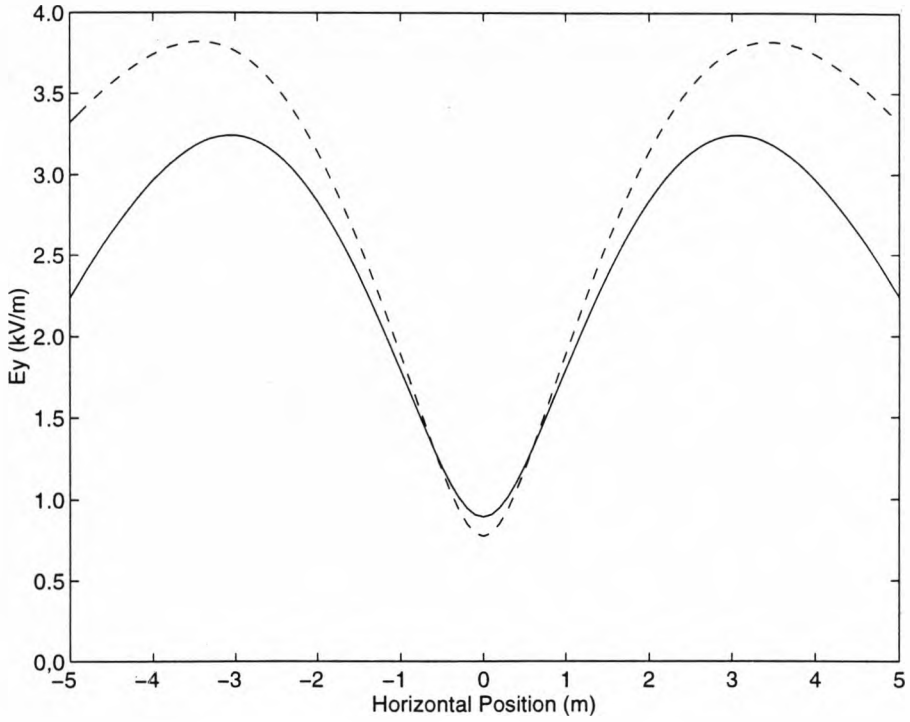

Figure 5.9 Field Distribution For Power System in Figure 4.1
(*Solid Line* = No Walls *Dashed Line* = Walls at 7m from conductors

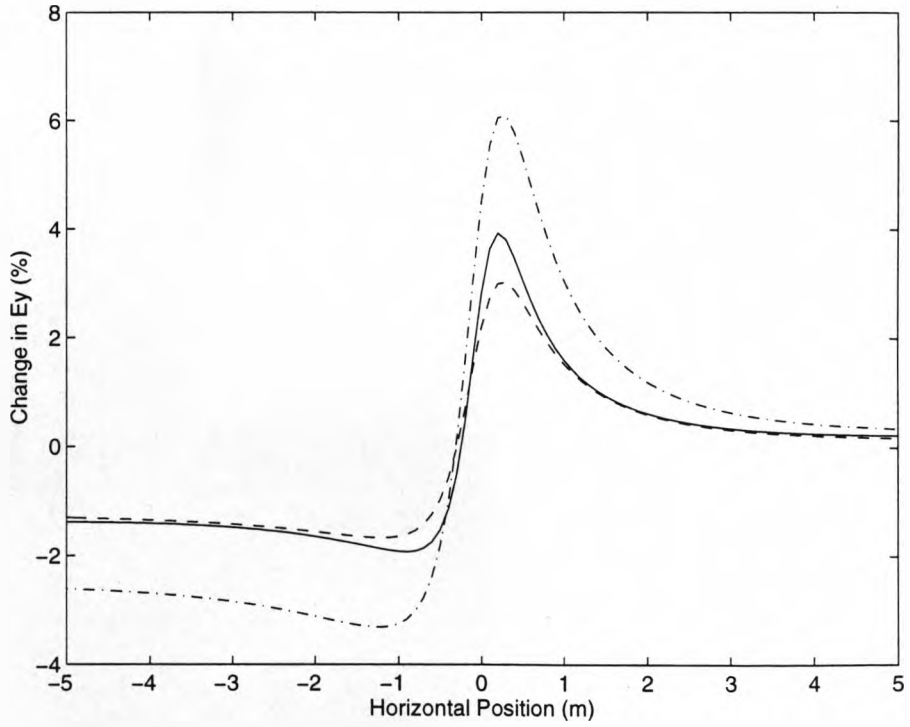

Figure 5.10 Change Profiles for Decrease in Left Conductor Voltage
(*Solid Line* = 1% No Walls *Dashed Line* = 1% Walls, *Dash/Dot Line* = 2%Walls)

The differences between the absolute field distributions are large, approximately 65% at the edge of the distribution, however the maximum difference between the 1% change profiles for the model with and without walls is approximately 20%, over a factor of three less than the change in the absolute field. The solid line is approximately one quarter of the way between the 1% (dashed) and 2% (dash/dot) lines. If the model of the system with no walls is used to determine the voltage change for the system with walls, a conductor voltage change of approximately 1.25% would be selected. The addition of walls is a large change, but only results in an error of 25% in the determined voltage change, and only 0.25% in the absolute conductor voltage.

A more realistic case is shown in figure 5.11, the ground level E_y distribution for the model in figure 4.1, (solid line), and for a model with a 1% error in the conductor heights ($y_n = 4.95$m), (dashed line). Figure 5.12 shows the change profiles, the solid line is for a 1% decrease in the left hand conductor voltage for the system with correct geometry. The dashed and dash/dot lines shows the change profile for 1% and 2% changes for the system with incorrect conductor height. A voltage change of 1.03% would have been selected. The 1% error in the measured height results in an error of only 0.3% in the voltage change or 0.03% in the absolute voltage.

5.5 Differentiation between Geometry and Voltage Changes

The previous calculations are for conductors at fixed positions, for flexible conductors the position of the conductor may change, and this movement will also create change profiles.

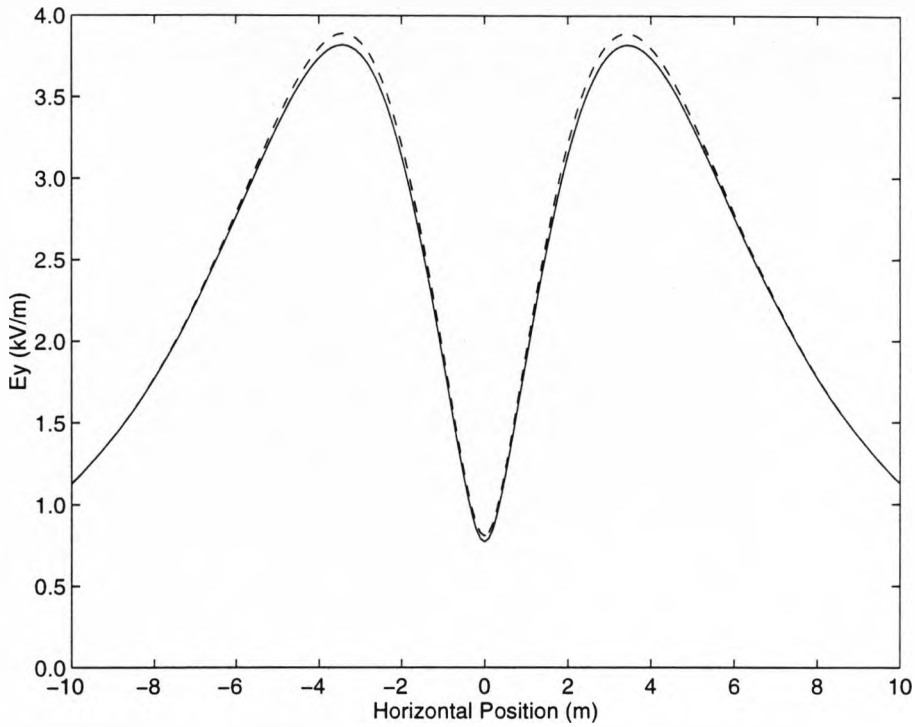

Figure 5.11 Field Distribution for Power System in Figure 4.1a
(*Solid Line* = Correct Geometry *Dashed Line* = 1% Error in Conductor Heights)

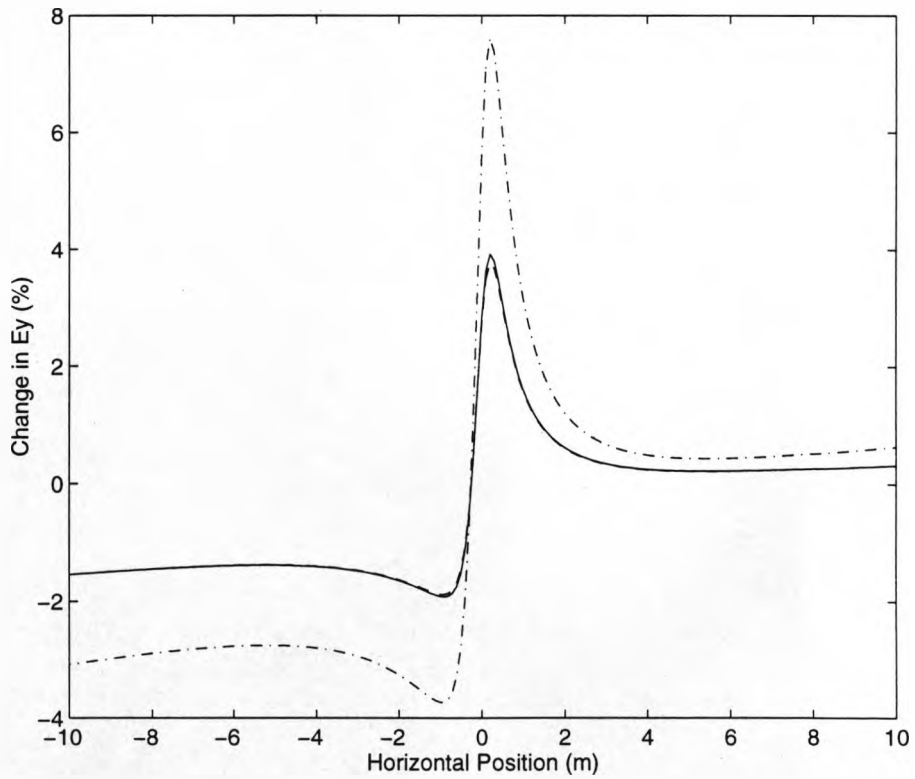

Figure 5.12 Change Profiles for Decrease in Centre Conductor Voltage
(*Solid Line* = 1%, Correct Height *Dashed Line* = 1% Incorrect Height)
(*Dash/Dot Line* = 2% Incorrect Height)

Figure 5.13 shows the change profiles for a 0.1% decrease in central conductor voltage, a 0.04% increase in height and the differences between them. The two results are not identical, but differences are very small indicating it is difficult to differentiate between changes in the two parameters. This result indicates that any monitoring system should be restricted to power systems with rigid conductors.

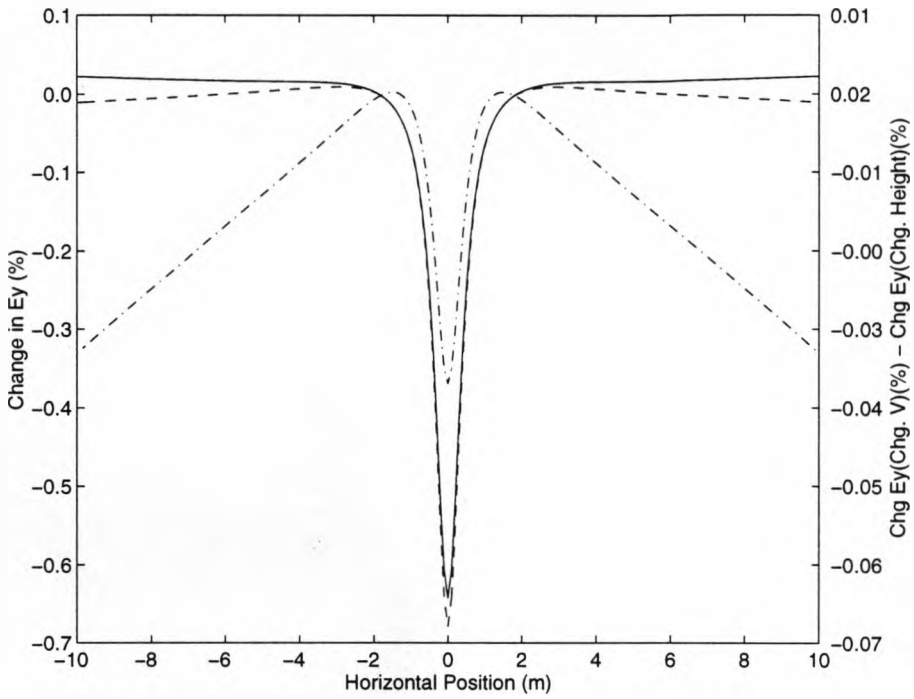

Figure 5.13 Change Profiles for Centre Conductor Changes
Solid Line = 0.1% Decrease Voltage *Dashed Line* = 0.004% Increase in Height
Dash/Dot Line = Difference Between Profiles

5.6 Summary

The relationship between the field variables around a power system and the conductor voltages has been investigated. The results indicated that changes in any power system parameter caused changes in the field variables at all locations around the power system. It was proposed that measurements of the change in ground level vertical electric field amplitude, E_y, at a number of positions along a line orthogonal to the conductors could be used to determine changes in individual conductor

voltages. Voltage change determination would be by searching a database of pre-calculated change profiles. The voltage measurements are insensitive to small errors in the geometry used to produce the pre-calculated values. It was shown that it is difficult to differentiate between changes in the conductor voltages and changes in the power system geometry, this limits the use of the monitoring system to power systems with fixed geometry (rigid conductors).

6. Electric Field Sensors

A monitoring system that measures electric fields requires sensors that produce signals related to the electric field. An ideal sensor is one that maintains a fixed linear relationship between the electrical field and the output signal under all operating conditions. An instrument that measures the field simultaneously at many points requires many sensor elements, for the instrument to be economically viable each element must be a low cost one.

6.1 Types of Sensor

Many electric field sensors, using a wide range of technologies, have been reported in the literature; **Bassen(1983)** has reviewed many of the systems developed. Sensors may be classified into two categories, *ground potential* or *space potential*. Ground potential sensors have an electrical connection to the ground plane, if they are mounted above the ground plane they cause considerable distortion of the field distribution. If they are mounted in the ground plane there is no field distortion but it is only possible to measure the normal component of the electric field. Space potential sensors have no connection to the ground plane and assume the potential of the point at which they are placed. As they are constructed of a different material to the surrounding medium the field will be distorted. However the distortion is limited to the area immediately around the sensor, provided the sensor dimensions are small relative to the dimensions of the power system creating the field.

6.2 Sensing Technologies

An electric field sensor requires that the electric field causes some change in the sensor that may be measured. Effects that have been used in sensors include measuring the displacement current that flows in a material placed in a field and measuring a change in a material's optical or mechanical properties.

6.2.1 Electrical Sensors

A displacement current will be induced in any material placed in an electric field. If the field changes the displacement current will change, causing a change in the charge on the surface of the material. If a circuit is formed between the surfaces a current flows that is proportional to the change in field.

Figure 6.1a shows a cross section of a small flat conducting plate, of area A, mounted in an infinite ground plane in a medium with relative permitivity ε_r. A capacitance, C_P, termed the *internal sensor capacitance* exists between the plate and the ground. The capacitance is increased by the connection of a capacitor, C_{Su}, between the plate and the ground plane. The value of C_P is determined by the geometry the sensor is installed in, as the total capacitance is equal to the sum of C_{Su} and C_P, its value will depend on the sensor installation geometry.

For a time varying field, $E(t) = E_M \sin(\omega t)$, the charge induced on the plate at time t, $Q(t)$, is given by:

$$Q(t) = \varepsilon_0 \varepsilon_r A E(t) \qquad [6.1]$$

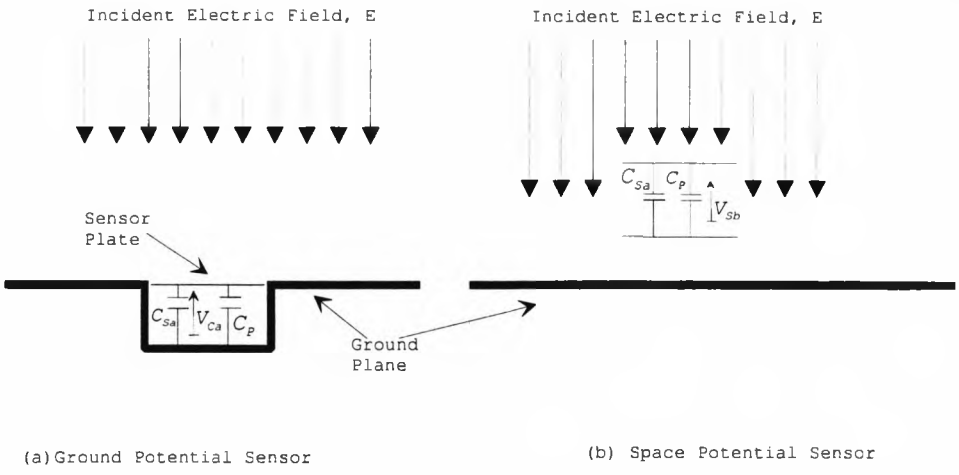

Figure 6.1 Ground Potential and Space Potential Electrical Field Sensors

As the field incident on the plate changes, the charge on the plate will change. If the medium is a perfect insulator, a current proportional to the rate of change of charge will flow through both C_P and C_{Sa} and a voltage, $V_{Ca}(t)$, will be developed across them. The relationship between the peak value V_{Ca} (t), V_{Ca} and the field amplitude, E_M, known as the sensor *sensitivity*, L, is given by

$$\frac{V_{Ca}}{E_M} = L = \left(\frac{\varepsilon_o \varepsilon_r A}{C_{Sa} + C_P} \right) \qquad [6.2]$$

Sensors of this type have been developed by **Davies & Turri(1990)** and **Collins & Meek(1965)**.

For constant fields, electrostatic cases, dE/dt is equal to zero. Ground potential sensors with integrating circuits have been used to measure high dc voltages, **Wolzak *et al*(1981)**, however 'drift' in the electronic circuitry limits their accuracy. An alternative method of measuring electrostatic fields is to mechanically modulate the field. A common technique is to use a rotating slotted disk or 'chopper', such devices

are commonly known as 'field mills' and are reported in the literature, for example by **Kirkpatric & Miyake(1932)** and **Sarma-Maruvada *et al*(1983)**.

Equation [6.2] was derived for a ground potential sensor, a similar analysis may be applied to space potential sensors consisting of two conducting plates connected by a capacitor, as shown in figure 6.1b. Changes in the incident field will cause a displacement current to flow between the plates resulting in a voltage across the capacitor, V_{Cb}. If field perturbation is to be limited to the area immediately around the sensor the voltage signal must be transmitted to the user, usually at ground potential, without an earth electrical connection to the sensor. **Deno & Zafanella (1987)** used a battery powered instrument to determine the rms value of the field and display it on a meter, the meter was read from a distance. **Feser & Pfaff(1984)** used a battery powered fibre optic link to transmit the voltage signal to ground potential.

6.2.2 Optical and Mechanical Techniques

There are many reports of sensors using electro-optic and electro-mechanical effects. Optical materials, termed Pockels and Kerr materials, exist in which the anisotropic refractive index is a function of the applied electric field. If a polarised light beam is passed through a Pockels material and an electric field is applied the plane of polarisation will rotate by an amount proportional to the field. **Shibata(1983)** states that, for an electric field, E, applied orthogonal to the axes of the material and the path of the light beam, the rotation of the plane of polarisation, Γ, is

$$\Gamma = \left(\frac{2\pi}{\lambda}\right) n^3 \gamma L E \qquad [6.3]$$

n is the refractive index of the material, γ is the Pockels coefficient of the material, λ is the wavelength of the beam and L is its path length through the material. In most implementations of the Pockels sensors, for example **Huang & Erickson(1989)**, optical fibres are used to supply randomly polarised light to the sensor. A polariser is used to convert this to a polarised beam that passes through the Pockels material, at the point the light exits the material a second polariser is used to convert the rotation modulated signal into an intensity modulated one that is transmitted to the user through a second optical fibre.

Materials exist, piezo electric materials, in which the mechanical properties of the material change when an electric field is applied. **Sollymar & Walsh(1993)** describe the relationship between the electric field, E, stress, T, and strain, S, in a piezo electric material as

$$T = cS - eE \qquad [6.4]$$

where c is the elastic coefficient and e the piezo electric coefficient. **Koo & Siegel(1982)** describe the development of a sensor using the piezo electric effect in strips of polyvinylidene floride (PVDF). Motion of the material is used to compress an optical fibre which is used as a strain gauge.

Sensors using the Pockels and piezo electric effects are constructed of all dielectric materials and require no connection to a reference potential. The perturbation of the field is limited to the area immediately around the sensor and they detect both static and time varying fields. Sensor bandwidth is limited by the opto-electronic sub

system used to convert the optical signals into electrical ones for Pockels and Kerr sensors and other mechanical properties of the piezo material for piezo sensors.

Both the Pockels and piezo electric coefficients vary with temperature, **Moghsi(1989)**. The measurement systems devised to date use amplitude modulation to transmit the signal to ground potential. The transmission characteristics of optical fibres are determined by the geometry of the path they take, mechanical motion can result in changes in the signal amplitude resulting in 'mechanical noise' added to the signal. **Leysop(1995)** states the cost of a Pockels sensor is £750. Whereas the materials required to construct an electrical sensor are readily available for approximately £1.

6.3 Sensor Design

Section 5.3 shows that for power system monitoring it is only necessary to monitor a single component of the electric field vector. Section 6.2 indicated that a ground potential electrical sensor is the most simple field sensor. The requirements of low cost multiple sensors led to a decision to develop this type of sensor, a complete device with necessary electronic components was called a *sensor element.*

Section 5.3 indicates that the maximum peak ground level field under the power system in figure 4.1 is of the order $10kVm^{-1}$ and the scaling results of section 4.7 indicate that similar amplitude fields will exist below the conductors of a scale laboratory system. **Deno(1976)** and **Wiggins *et al*(1989)** have both measured the

ground level field under power systems and have found typical peak values to be in the range $5kVm^{-1}$ to $10kVm^{-1}$. Most electronic instrumentation systems operate with a maximum input of a few volts and it was decided that the output of the sensor element should be 2.5V when the field is at its maximum ($10kVm^{-1}$). This required a sensor element sensitivity of 250×10^{-6} m. The output impedance of the sensor element had to be low enough to connect to standard instrumentation.

A lower frequency limit of 2 Hz was selected so that the sensor element could be used to measure sub-harmonics of the power system. Section 3.2 indicated that transients and harmonics of the fundamental frequency are features of the power system voltage, a minimum upper frequency limit of 3.5 kHz was selected to allow these to be detected. The limit of variations in the sensor element sensitivity due to changes in internal sensor capacitance C_P caused by changes in the installation geometry was set at 0.1%.

For a sensor in the ground plane underneath a power system the dimension of the sensor plate in the direction perpendicular to the conductor axes, the *width*, determines the spatial resolution of the field measurements. The signal from the sensor plate is some average of the incident field across the plate. Spatial changes in the field distribution that occur in a distance less than the sensor plate width can't be detected. For measurements under power systems of the form shown in section 4.1 and the scale model whose construction is described later, section 10.1.1, a maximum plate width of 20 mm was selected.

6.3.1 Sensor Design Calculations

The sensor plate and capacitor, figure 6.1a, can be represented as a either a Thévenin or Norton equivalent circuit. To determine how it may be interfaced to conventional instrumentation it is necessary to know both the magnitude and impedance of the source.

The internal sensor capacitance, C_P, is determined by the geometry, dielectric properties and installation position of the sensor. For a sensitivity that is independent of the sensor installation geometry it is necessary that $C_{Sa} >> C_P$ so that C_P may be neglected and the sensitivity, L, [6.2] becomes

$$L = \left(\frac{\varepsilon_o \varepsilon_r A}{C_{Sa}} \right) \qquad [6.5]$$

The minimum value of C_{Sa} is determined by the maximum value of C_P and the required accuracy of the sensor from

$$\frac{\Delta L}{L} = \frac{C_P(\max)}{C_{Sa}(\min)} \qquad [6.6]$$

where ΔL is the change in L caused by neglecting C_P. With the minimum value of C_{Sa} defined [6.5] may be used to define the maximum sensitivity per unit area (S/A)

An alternative analysis technique is to use a lumped constant method, the circuit is outlined in figure 6.2. For the ground potential sensor the capacitance C_{D1} represents the distributed capacitance between the high voltage source with peak voltage V_{HT} and the sensor, for the space potential sensor C_{D2} represents the capacitance between the high voltage source and the sensor and C_{D3} represents the capacitance between the

sensor and ground. Neglecting the internal sensor capacitance, C_P, the peak voltage developed across the ground potential sensor, V_{Sa}, is

$$V_{Sa} = \left(\frac{C_{D1}}{C_{D1} + C_{Sa}} \right) V_{HT} \qquad [6.7]$$

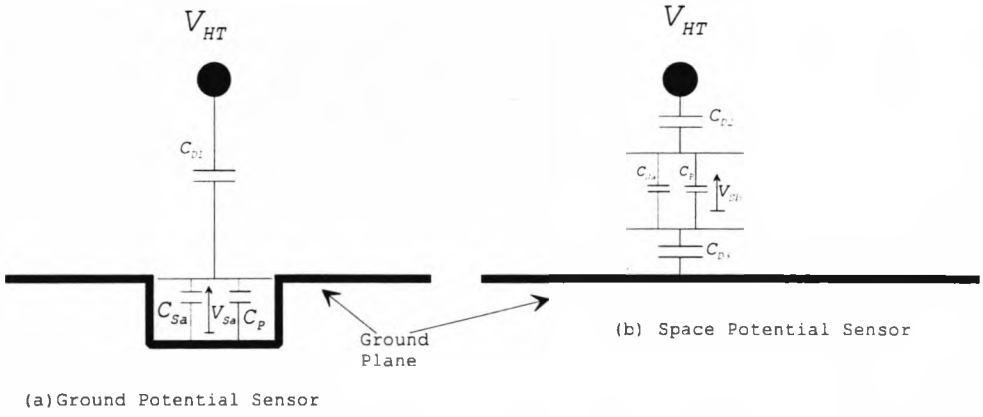

Figure 6.2 Lumped Constant Representation of Electrical Sensor

As the sensor voltage is required to be much less than the high voltage then $C_{Sa} >> C_{D1}$ and [6.7] may be written as

$$\frac{V_{Sa}}{V_{HT}} = \frac{C_{D1}}{C_{Sa}} \qquad [6.8]$$

At an angular frequency ω the source impedance of the sensor plate, Z_{source}, is

$$Z_{source} = \frac{1}{j\omega \left(C_{Sa} + C_{D1} \right)} \qquad [6.9]$$

Again $C_{Sa} >> C_{D1}$, equation [6.9] becomes

$$Z_{source} = \frac{1}{j\omega C_{Sa}} \qquad [6.10]$$

The sensor plate impedance is frequency dependent. Any instrument used to measure V_{Sa} will draw a current through Z_{source}, this causes a voltage drop and a frequency dependent voltage at the input to the instrument. For this reason it is necessary to design special instrumentation that draws a negligible current to measure the voltage from the plate source.

The maximum value of C_P is determined by the area, A, of the plates, and minimum distance between the sensor plate and the ground plane. For the sensor dimensions selected in 6.3 and the array housing dimensions of section 7.2. C_p may be calculated and is of the order of 20pF. Substituting the accuracy specified in 6.3, 0.1%, in [6.6], $C_{Sa}(min)$ is calculated as 20nF.

Substituting the required sensitivity of 250×10^{-6}m and the sensor width, 20mm, into equation [6.2] the sensor length required is 23m. This value is too large for use in a practical system, hence amplification of the signal from the sensor plate source is necessary.

6.3.2 Amplification - Input Bias Currents & Frequency Response

Figure 6.3a shows an operational amplifier in unity gain mode connected to the ground potential sensor. All operational amplifiers are imperfect and small bias currents, I_b, flow into or out of their input terminals. With only a capacitor connected to the input no dc path exists for these currents and, at turn on, the capacitor, C_{Sa}, is charged by the bias currents to the supply voltage of the amplifier and no signals may be measured. To avoid this effect a 'bleed' resistor, R_{Sa}, is connected across the

capacitor. I_b flows through R_{Sa} resulting in a constant dc offset voltage $V_{os} = I_b R_{s_a}$. Most operational amplifiers have a 'null' input that allows this offset to be removed.

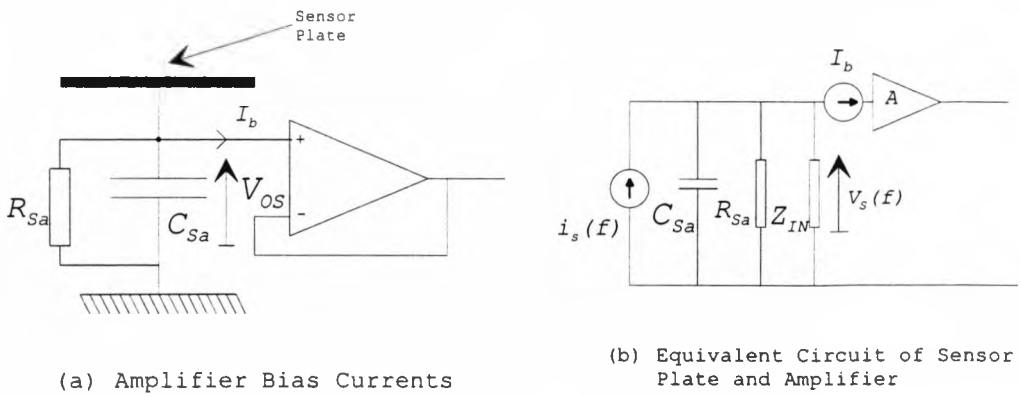

Figure 6.3 Effect of Bias Currents and Equivalent Circuit of Amplifier and Sensor Plate

Figure 6.3b is an equivalent circuit of the sensor and amplifier, the current flow produced by the electric field is represented by the current source, $i_S(f)$. The operational amplifier is represented as an ideal amplifier A with its source impedance shown as Z_{IN}. If the impedance of C_{Sa} is Z_C , the total impedance seen by the current source, Z_S is

$$Z_S = Z_C \| Z_{IN} \| R_{Sa} \qquad [6.11]$$

If the amplifier is selected so that that $Z_{IN} >> Z_C$ at frequencies of interest, and $Z_{IN} >> R_{Sa}$, the impedance may be written as

$$Z_S(f) = \frac{R_{Sa}}{1 + j\left(\frac{f}{f_C}\right)} \quad \text{where } f_C = \frac{1}{2\pi R_{Sa} C_{Sa}} \qquad [6.12]$$

The signal voltage developed at the input of the amplifier, $v_s(f)$, is determined by the product of the signal current, $i_S(f)$, and the impedance $Z_S(f)$. Figure 6.4 is a frequency response plot, showing, for a fixed amplitude electric field, $i_S(f)$, $Z_S(f)$,and $V_S(f)$ as

functions of frequency. The plot for $V_S(f)$is that of a second order function with low frequency roll-off. The corner frequency is determined by f_c, therefore, once the lowest frequency of interest has been specified, a limiting value for the product $R_{Sa}C_{Sa}$ can be determined. At frequencies above the corner frequency the sensor impedance is

$$Z_S = \frac{1}{j\omega C_{S_a}} \qquad [6.13]$$

Substituting $C_{Sa}(min)$ from 6.3.1 and the lower roll off frequency of 2Hz into [6.12] R_S must be greater than 3.9MΩ, a value of 4.7MΩ was selected. For a sensor element size that was practical to construct, the length of the sensor plate was selected as 50mm, these values give a lower corner frequency of 1.7 Hz, and a sensitivity of 442×10^{-9}m.

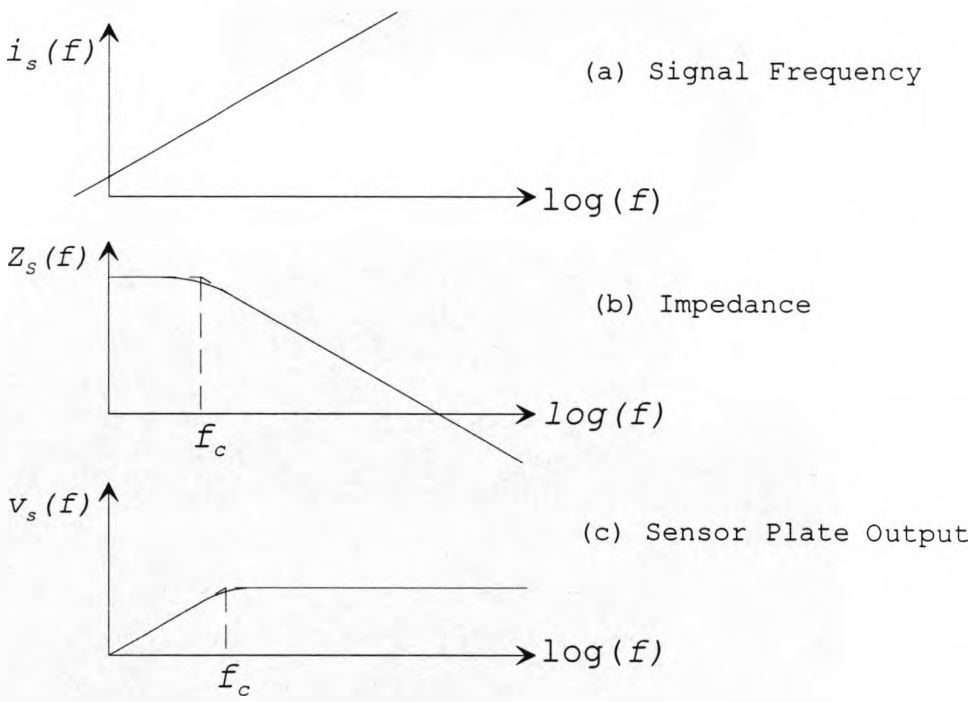

Figure 6.4 Frequency Response, $i_s(f)$, $Z_s(f)$, $V_s(f)$ for a Constant Amplitude Electric Field

6.3.3 Amplification & Noise

Addition of amplifiers in the signal path adds noise to the signal. **Carlson(1983)** shows how, for noise calculations, a real amplifier may be modelled as an ideal, noiseless, amplifier of gain, A, with a noise source, e, at the input. If it is necessary to use several stages of amplification, then for a cascade of N amplifiers with gains A_0 .. A_{N-1} and noise sources e_0 .. e_{N-1} the total amplification, A_{total}, is given by

$$A_{total} = \prod_{n=0}^{N-1} A_n \qquad [6.14]$$

At the output of the final amplifier the total noise added to the signal, e_{total}, by the amplifiers is

$$e_{total} = A_{total}\left[e_0 + \sum_{n=0}^{N-1}\left(\frac{e_{n+1}}{\prod_{k=0}^{n} A_k} \right) \right] \qquad [6.15]$$

Equation [6.15] indicates that noise in the first amplification stage, e_0, contributes the largest individual component of the noise added by amplification. To minimise e_{total} e_0, must be as small as practical and the gain of the first amplifier, A_0, as large as practical.

Electronic noise in operational amplifiers has an infinite frequency spectrum, the amount of noise added to the signal is determined by bandwidth of the operational amplifier and the bandwidth of the system the amplifier is used in. By reducing the bandwidth of the system at an early stage of the signal path the total noise is reduced. The sensor elements were exposed to all signals in the atmosphere, the greater the bandwidth of the sensor the greater the probability of picking up unwanted signals.

As gain-bandwidth products of common operational amplifiers are of the order 10^7, the bandwidth of the sensor element was frequency limited by low pass filtering of the signal from the sensor plate.

6.3.4 Electronic Construction

Figure 6.5a is a block diagram of the sensor element, the output of the $R_S C_{Sa}$ network was buffered by a high impedance operational amplifier, type OPA121, configured as a non inverting amplifier with a gain of 7.9 and a first order low pass response with a corner frequency of 8.5 kHz. The second stage of the sensor was a second order low pass filter with a gain of 1.56 and a corner frequency of 3.8 kHz. The final stage of the design was a non inverting amplifier with a gain that may be set to any value between 22 and 44. Appendix 4 contains a full circuit diagram of the sensor. For testing the gain of the third stage of the amplifier was set to 32.

6.4.5 Physical Construction

The sensor element was constructed using 2mm thick double sided circuit board, the sensor plate was formed using the upper surface conductor. The electronic components were mounted on the lower surface. A 0.5mm hole was drilled between the surfaces and a fine cable used to connect the upper plate to the electronic system. The dimensions of the completed sensor were 45×145 mm, the components mounted on the lower surface projected from the board by approximately 10 mm. Figure 6.5b illustrates the element construction.

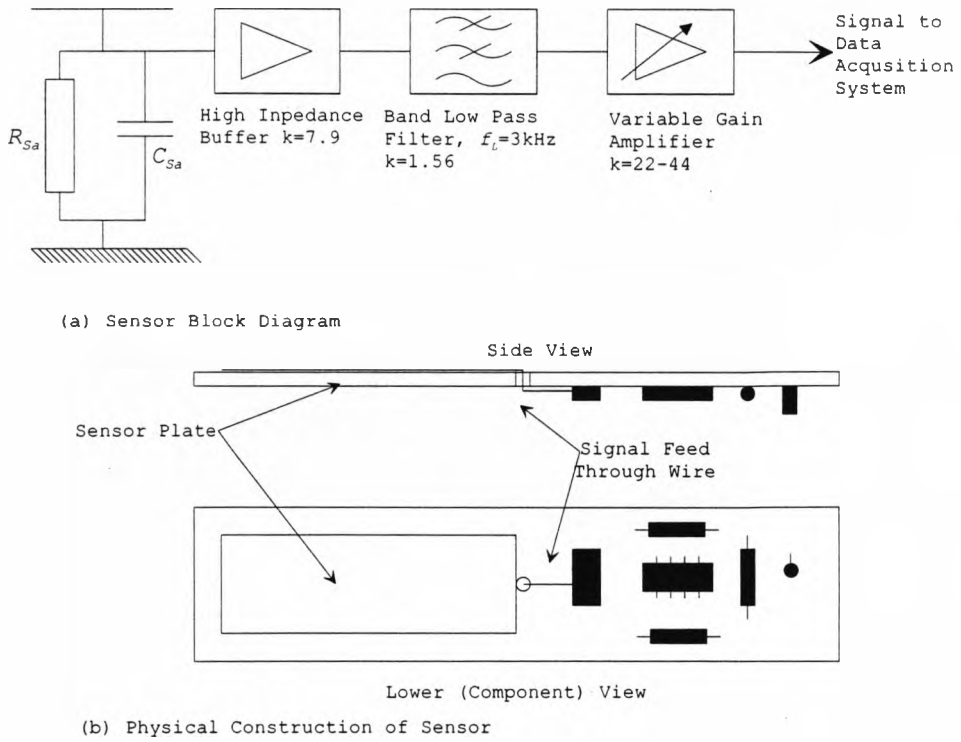

Figure 6.5 Block Diagram and Physical Construction of Sensor Element

6.4 Element Calibration & Testing

Calibration and testing of the sensor element required an alternating electric field of known, but variable, amplitude and frequency. A large parallel plate capacitor provides a region of uniform electric field whose amplitude and direction may be calculated from the plate separation and applied voltage. A parallel plate capacitor with plates 500 × 250mm, figure 6.6b, was constructed to test the element. A hole the size of the sensing plate was cut in the lower capacitor plate and the sensor was mounted behind it. The three different sets of insulating posts were constructed to give separations of 34, 45 and 78mm.

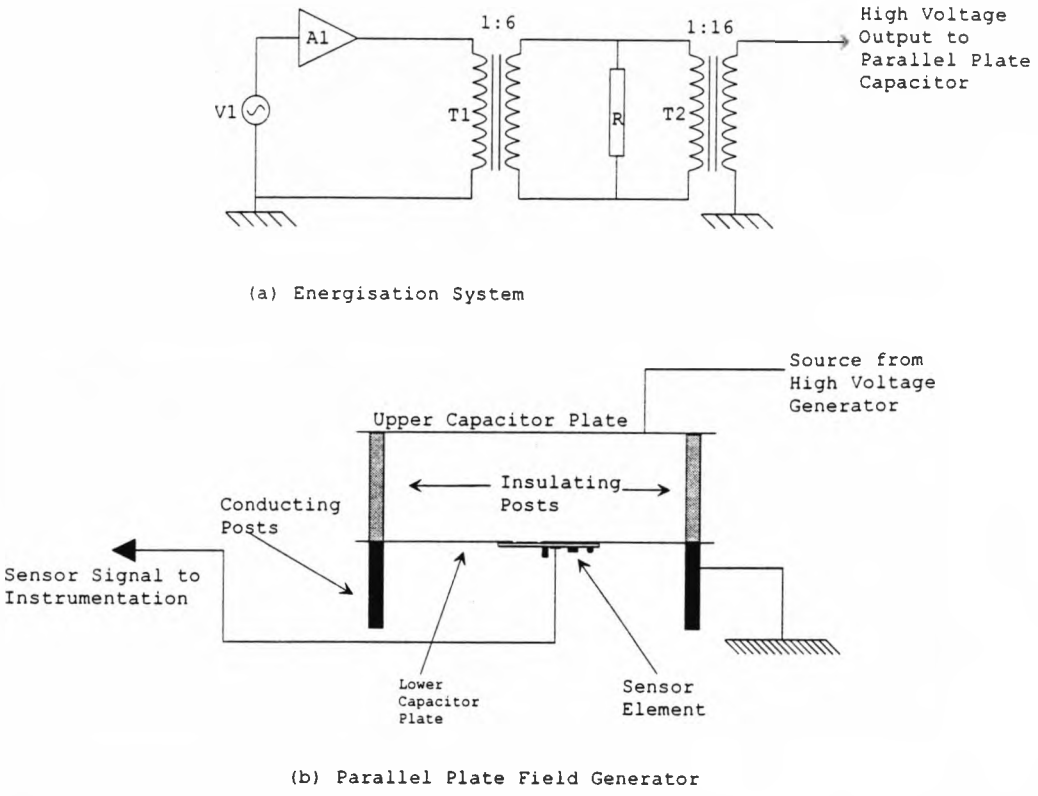

Figure 6.6 Testing of Sensor Element

To generate incident electric fields a variable frequency, variable amplitude high voltage supply was constructed (figure 6.6a). Signal generator V1 provided a variable frequency, variable amplitude output signal with a maximum amplitude of 2V. This signal was input to amplifier A1, a high power audio amplifier with a maximum output voltage of ±40V, capable of supplying a current of 2A when driving a resistive load. The amplifier output supplied the primary of T1 which has a 1:6 turns ratio. The secondary was connected to a restive load, *R*, which is "reflected" through the transformer to amplifier A1 and ensures that the power amplifier load was resistive with only a small reactive component. The signal produced across the resistive load was the input to transformer T2, a 1:16 step up transformer and the plates of the parallel plate capacitor were connected to the outputs of T2. Both

transformers were iron cored types designed primarily for 50Hz operation and limit the minimum and maximum operating frequencies of the test system. Direct measurement of the voltage on the capacitor plates using a high voltage CRO probe indicated that maximum fields of $30kVm^{-1}$ at frequencies between 2Hz and 10kHz could be created.

Limitations of the iron cored transformers made it difficult to maintain a constant plate voltage at all frequencies therefore both the plate voltage and the sensor output were measured, using a digital oscilloscope, as the signal generator frequency and voltage were varied. Figure 6.7 shows the voltage sensitivity of the sensor as a function of frequency for a plate separation of 78mm. The measured corner frequencies of the plot are 1.6Hz and 3.9kHz, they correspond to the design frequencies of 1.7 and 3.8 kHz.

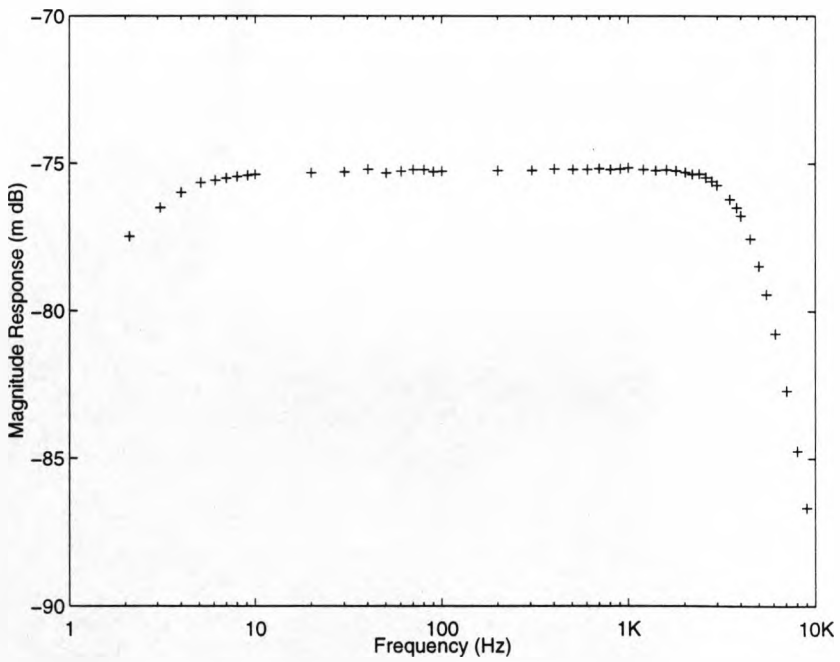

Figure 6.7 Frequency Response of Sensor Element, Plate Separation 78mm

For a constant field frequency of 50Hz the response and linearity of the sensor were measured using the three sets of insulating posts to confirm the relationship between the plate separation and the generated field. Figure 6.8 is the response of the sensor for a plate spacing of 45mm. Equation 6.2 indicates that the relationship between the sensor output voltage and applied field is of the form $V = kE$, where k is constant. Equations of the form $V = aE + b$ were fitted to the measured data such that the rms value of the sum of deviations between the fitted and measured was a minimum. Table 6.1 shows the results, S_a and S_b are the standard errors in a and b

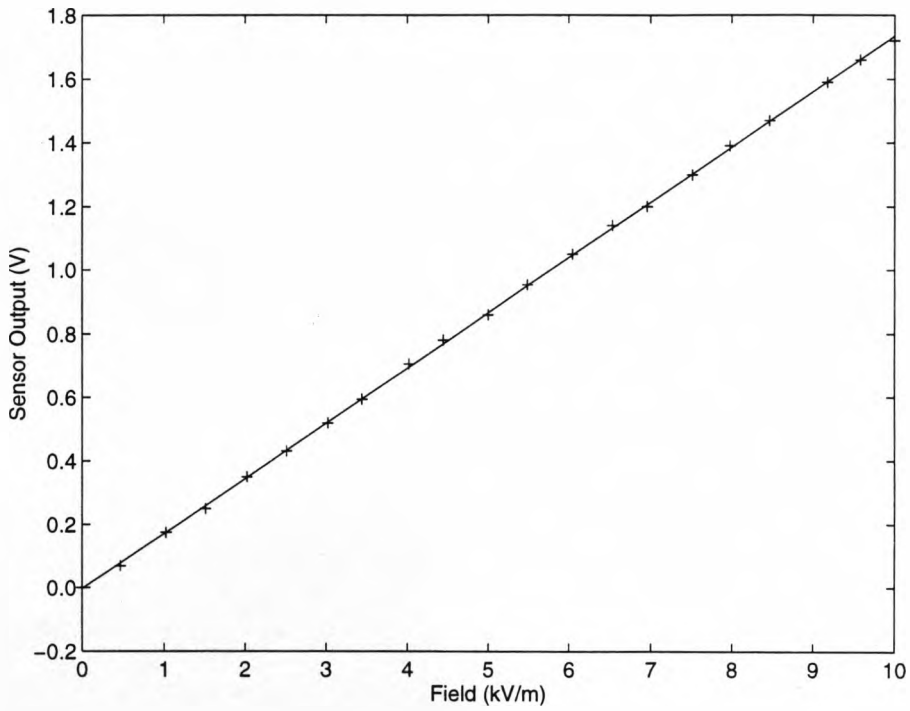

Figure 6.8 Response of Sensor Element at frequency of 50Hz, Plate Separation 45mm

Plate Spacing(mm)	$a(\times 10^{-6})$	$S_a(\times 10^{-6})$	$b(\times 10^{-3})$	$S_b(\times 10^{-3})$
34	174	±0.61	-3.20	±3.60
45	173	±0.49	-0.59	±2.85
78	172	±0.43	-0.10	±2.28

Table 6.1 Line Fitting to Sensor Test Data

In all cases the value of b was less than the standard error indicating that, within measurement accuracy, the sensor output is zero when no field is applied. The values for a agree within two standard errors. For the component values used, the plate source sensitivity before amplification was calculated as 442×10^{-9} m and the measurements were performed with the combined gain of the amplifications stages set to 395 ± 5, these values give a calculated element sensitivity of $174 \pm 2 \times10^{-6}$

6.6 Summary

Existing designs of electric field sensors were examined and, taking into consideration the results of the theoretical investigations in chapter 5, a decision was made to develop a ground potential electrical sensor as the sensor element for the required array. The sensor element developed provided a voltage output linearly related to the incident electric field over a specified frequency range. The response of the sensor agreed with theoretical values within measurement accuracy.

7. Signal Processing Hardware

Real time monitoring of a power system, by measurement of the electric field distribution using multiple sensor elements, required the development of electronic instrumentation. The complete non contact monitoring system developed had four distinct parts shown in the block diagram, figure 7.1; detailed circuit diagrams are in appendix 4.

7.1 Overall System Design

The electric field was detected by an array of sensor elements and the analogue signals produced were processed by a data acquisition system with digital outputs. Two separate digital processing systems, called 'fast' and 'slow', used these digital outputs to provide separate detection of the two classes of power system event defined in table 3.1. The data acquisition system ran continuously at a fixed sampling rate, 699Hz, and every set of samples was processed by both systems. The systems processed the signals at a rate greater than or equal to the rate at which they were acquired.

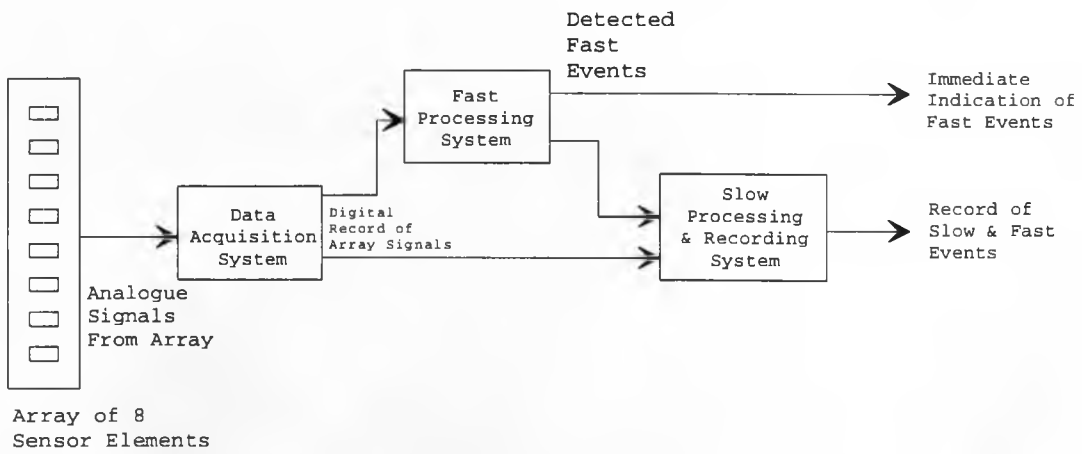

Figure 7.1 Block Diagram of Signal Processing Hardware

7.2 Electric Field Sensor Array

A single sensor element of the form described in chapter 6 produces a voltage proportional to the incident electric field. Simultaneous measurement of the electric field at a number of locations required an array of sensors. It was indicated, section 5.3, that to determine changes in the individual conductor voltages, the field should be measured at a minimum of six locations in the ground plane. Digital data acquisition systems operate more efficiently with a number of inputs equal to an integer power of two, thus it was decided to use eight sensor elements. For investigations using the scale model of the power system, section 10.1, an array housing, figure 7.2, was constructed. The housing held up to sixteen elements with centres spaced at 55mm intervals. Eight sensor elements and eight 'blanks' were installed in alternate positions in the housing. Power for each sensor element was supplied through a separate twisted pair cable from the data acquisition system's ±15V power supply. Individual coaxial cables connected the output of each sensor element to the data acquisition system, the dimensions of the complete array were 900mm × 170mm × 60mm.

7.3 Data Acquisition System

As the processing of the electric field signals was performed using digital systems the analogue signals from all the sensors in the array had to be simultaneously converted to a digital form. For a processing system with multiple inputs, called *channels*, an individual analogue to digital converter (ADC) may be used to convert the signal from each element. Alternatively separate analogue samples may be taken simultaneously for all the channels and stored, the sampled signals are converted in

sequence with a single ADC. Provided the product of the number of channels and simultaneous sample rate is less than the maximum ADC conversion rate the sequential technique is the lower cost method.

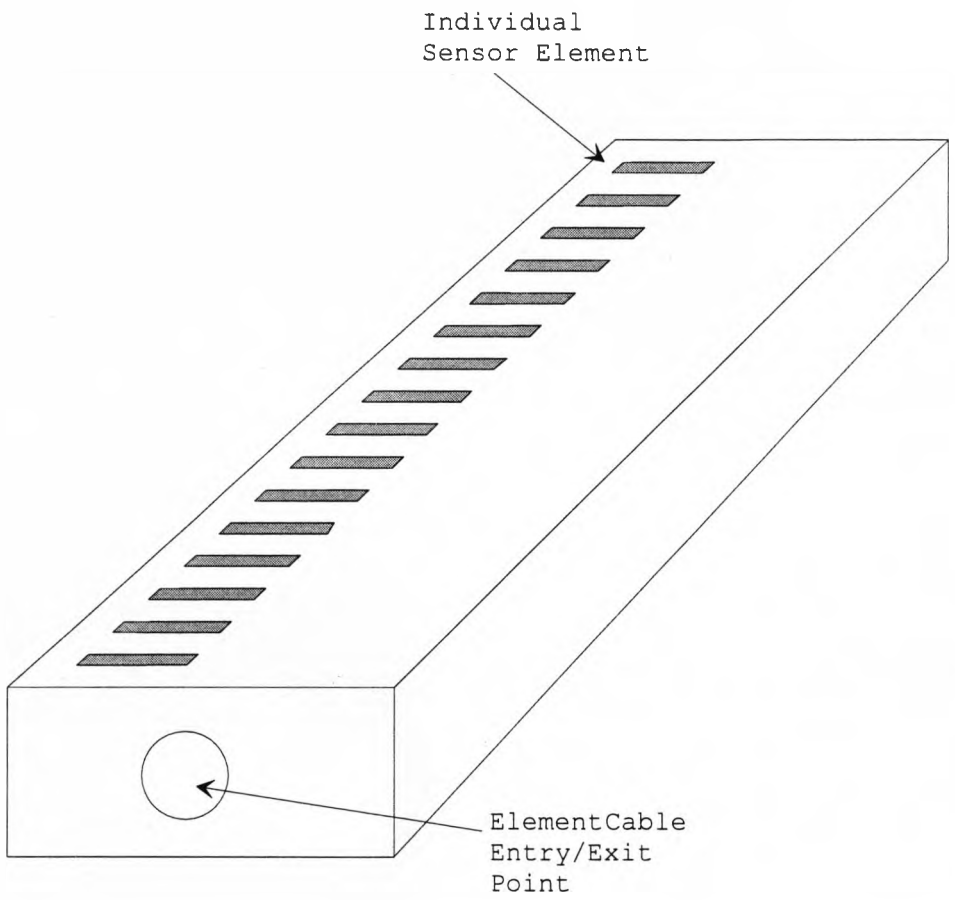

Figure 7.2 Electric Field Sensor Array For Use on Scale Model of Power System

Shannon(1949) indicates that the signal sample rate need not exceed the *Nyquist frequency,* twice the frequency of the highest signal component to be measured. As it was decided, section 3.3, that the system should only detect harmonics up to the 5th harmonic and should tolerate a frequency variation over the range 48 to 52 Hz a minimum sampling frequency of 520Hz was required. Examination of manufacturers' literature indicated that inexpensive ADC's with conversion frequencies above 100 kHz were readily available, therefore a single ADC system was selected.

7.3.1 Data Acquisition System Operation

Figure 7.3 is a block diagram of the data acquisition system. The eight bipolar signals from the sensor array were connected to separate sample and hold (S/H) gates with the gate sample control lines connected in parallel. When the hold input was momentarily pulsed the voltage on each channel at that instant was held and the S/H outputs formed an instantaneous 'snap-shot' of the signal from all eight sensor elements. The snap-shot existed until next time the hold input was pulsed.

The outputs of the sample and hold gates were connected to the inputs of an eight channel analogue multiplexer. The multiplexer control lines were driven so that each channel was selected for a fixed period once every snap-shot. The bipolar output of the multiplexer was converted to a unipolar signal by the level shifting circuit and ADC converted the unipolar signal to an equivalent digital value. The digital outputs from the ADC were connected in parallel to the data inputs of two dual port random access memories (DPRAMs) and copies of all snap-shots stored in both memories. The contents of the DPRAMs were read by the fast and slow processing systems. Timing and control signals for the complete data acquisition system were generated by state machines implemented in programmable logic.

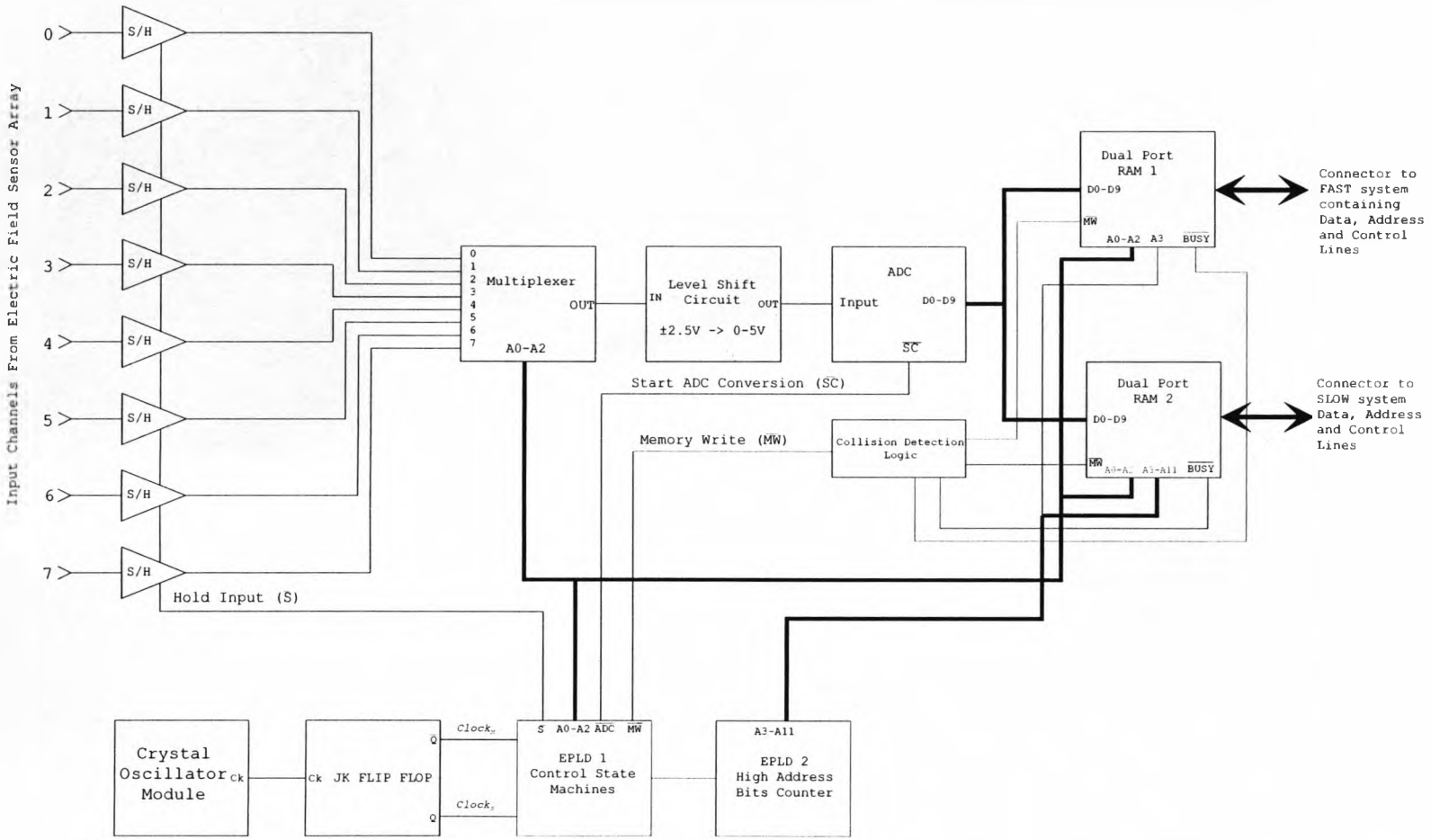

Figure 7.3 Data Acquisition System Block Diagram

7.3.2 Analogue Components

The sample and hold gates were supplied as quadruple devices with internal sample storage capacitors. When the digital control input was high the device was in transparent mode and the output signal was a replica of the input signal. When the control input went low the signal at that instant was held on the sample capacitor. The multiplexer was an eight channel device with three digital channel selection lines, the three bit binary code on the lines selected the input channel which was connected to the output.

The construction of both the multiplexer and S/H gates was such that small parasitic capacitances existed between the digital control inputs and the signal path. Changes in the control lines induced currents in the analogue circuits which appeared as 'ringing' at the outputs. For accurate analogue to digital conversion the ringing had to be allowed to decay after the digital inputs changed before the conversion was started. The manufacturer stated that the maximum duration of the S/H gate ring was 2μs. The duration of the multiplexer ring was not documented and was measured as 3.2μs.

The internal sample capacitor in the S/H gates was not perfect, while holding the sample the charge leaked, resulting in a drop in input voltage, known as *droop*. The maximum droop rate was specified as $20mVs^{-1}$; at a sampling frequency of 699 Hz the voltage dropped by 28μV between samples. The peak signal levels are 2.5V so the droop corresponded to an error of 1 part in 10^5 and was neglected.

The level shifting circuit added a fixed voltage of 2.5V to the ±2.5V bipolar signals from the sensor elements resulting in a 0 to +5V unipolar signal for conversion by the ADC. The ADC selected, type AD1061, is a ten bit 'half flash' converter. Conversion commenced on the falling edge of a digital control signal and the data on the outputs was valid after a maximum conversion time of 2.4μs. With the level shifting circuit the digital output was 0 for an input signal of -2.5V, 511 for a signal of 0V, and 1023 for a signal of +2.5V.

7.3.3 Digital Data Storage

The data acquisition system continuously sampled the signal from the sensor array, data had to be passed to the two processing systems without interrupting the sampling process. To simplify the interface and reduce the processing power required, the data acquisition system wrote the ADC values into two DPRAMs. A DPRAM is identical to normal RAM except that it has two sets of data and address lines, two ports, and may be simultaneously read or written using both ports in an asynchronous manner, the ports are referred to as *left* and *right*.

The two processing systems were connected separately to the left ports of each DPRAM, and the data acquisition system was connected in parallel to the right ports of both devices. The devices selected, type IDT7024, were 4K by 16 bit devices; the 10 bit ADC output was stored in one 16 bit location, thus up to 512 snap-shots of eight sensor outputs could be stored. The algorithms used for the processing of slow events used 'blocks' of snap-shot values, the whole 4K of the DPRAM connected to the slow system, called DP_S, was used. The fast system examined only the most

recent sample so the DPRAM connected to it, called DP_F, was configured as a 16 word by 16 bit device by connecting the upper eight address lines on both ports to +5V. Two snap-shots could be stored.

7.3.4 Digital Control and Timing Sub System

The timing signals necessary to control the data acquisition system were created by two interlocked state machines, called *master* and *slave*, and a synchronous counter. The system was implemented in two electrically programmable logic devices (EPLDs), called EPLD1 and EPLD2. Each EPLD contains 16 positive edge triggered bistables and a matrix that performs invert-AND-OR logic. EPLD1 was programmed with the master and slave state machines, the synchronous counter was implemented in EPLD2. Use of programmable logic allowed the design of the devices to be easily modified and resulted in only a small number of devices on the data acquisition board. On power up the devices used, type DC5060, reset all bistables to zero, this simplified the state machine design as it was not necessary to provide reset circuitry. States were allocated so that the bistable outputs directly provided the multiplexer channel select signals and three low address lines of the DPRAMs. The remaining (high) address lines to the DPRAM were provided by the synchronous counter.

The *master clock* for the data acquisition system was produced by a programmable crystal oscillator that provided a square wave output at 16 selectable frequencies between 55.9kHz and 14.3MHz. The master clock was divided by a positive edge

triggered JK flip flop to provide two anti-phase clock signals, $clock_M$ and $clock_S$ with the form shown in figure 7.5, at half the frequency of the crystal oscillator.

Figure 7.4 shows the state diagrams of the master and slave machines; they are interlocked by handshake lines **H** and **F**. The 24 state master machine was clocked by $clock_M$ and executed one complete cycle through all states for the conversion and storage of one snap-shot. For testing purposes a hold input MH was added to the design, the machine remained in state SM16 while MH was asserted. The states of the master machine corresponded to the execution of specific actions. In state SM17 the S/H gates were pulsed and the multiplexer was set to channel zero, in state SM18 the synchronous counter was incremented. States SM0 to SM15 caused the slave machine to execute a complete cycle eight times to convert all the channels. The slave machine was clocked by $clock_S$ and contains eight states. SS0 changed the multiplexer address, SS2 initiated the ADC conversion and SS7 wrote the result to the DPRAM, the remaining states were 'wait states' which provided a delay while the multiplexer ringing decayed and the ADC completed the conversion.

Figure 7.5 is a timing diagram for the conversion and storage of channel 0 and the start of channel 1. It shows the states of each machine, the handshake lines and the two clock signals. The total number of $clock_M$ cycles required for a complete cycle of the master machine is

$$Clock\ Cycles = (States\ in\ Slave) \times (No.\ Runs\ of\ Slave) + Other\ States\ in\ Master \qquad [7.1]$$

Substituting values into equation [7.1] indicates that 80 clock pulses were required for the sampling and conversion of one snap-shot. The frequency of the clock pulses

was half the master clock frequency, thus the rate all the channels were simultaneously sampled, the *sampling frequency,* was 1/160th of the master clock frequency.

The maximum possible sampling frequency was determined by the operating speed of the slowest component of the data acquisition system. The multiplexer required 3.2μs to settle after its address inputs changed and the slave machine allowed two clock periods for this. The minimum clock period to satisfy this requirement was 1.6μs, giving a maximum sampling frequency of 7.8kHz. A master clock frequency of 111.86 kHz was selected and the sampling frequency calculated as 698.9Hz, which was above the minimum (Nyquist) frequency required to meet the system specification in section 3.3. With this sampling frequency data in DPRAM DP_S was overwritten every 732ms. The data in DPRAM DP_F was overwritten every 2.86ms.

7.3.5 Address Conflicts

As the data acquisition system was continuously writing to the DPRAMs and the processing systems continuously reading them it was possible for the two systems to try and simultaneously access the same memory address. This is known as an *address conflict* and may have resulted in the processor reading incorrect data. The DPRAMs provide signals to indicate a conflict has occurred. For safety, logic on the data acquisition system board combines this signal with the write pulse from the data acquisition system. The data acquisition system write pulse was much longer than the read pulses from the processing systems, the additional logic inhibited the write pulse

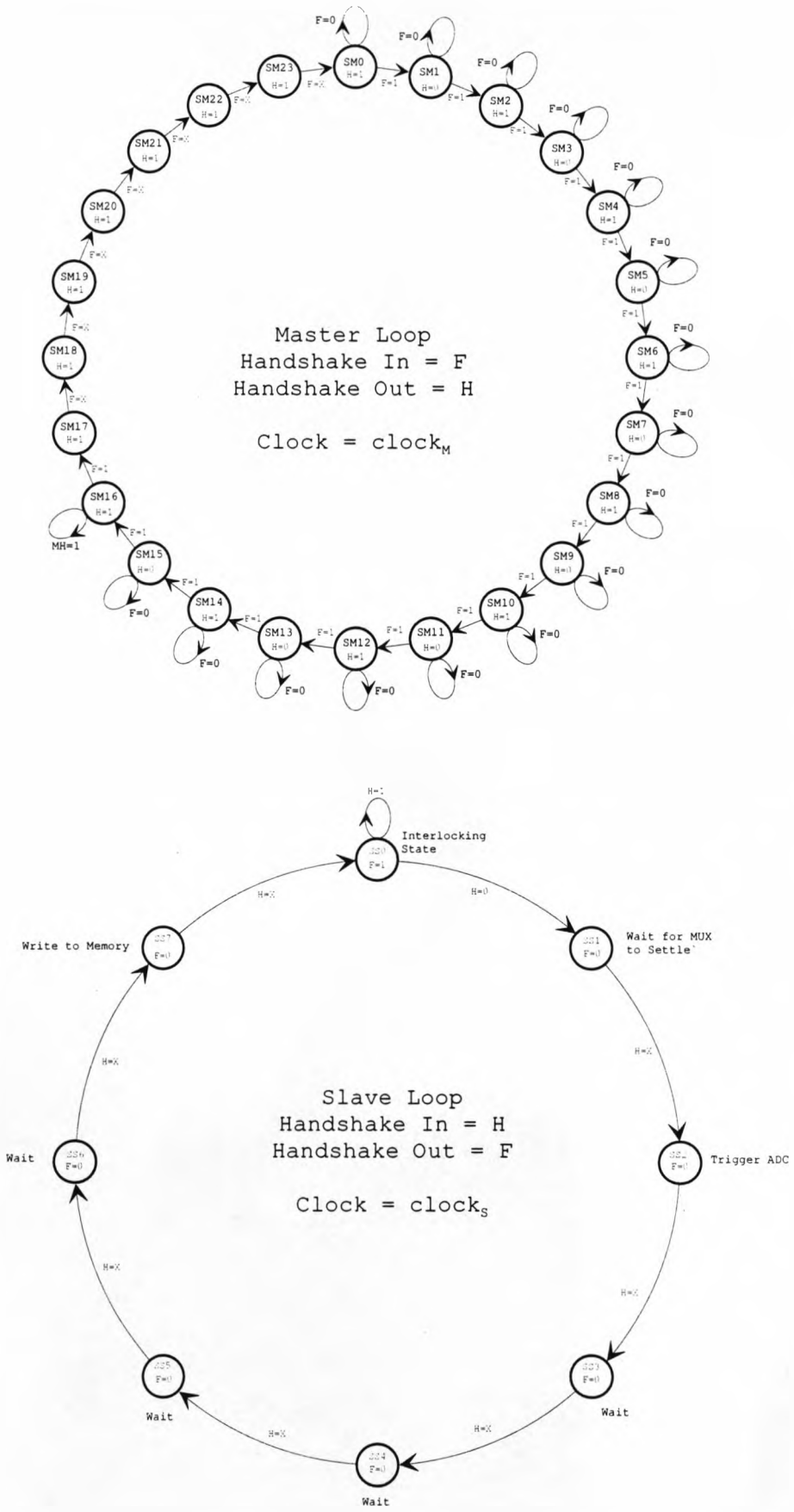

Figure 7.4 State Machine Diagrams for Data Acquisition System

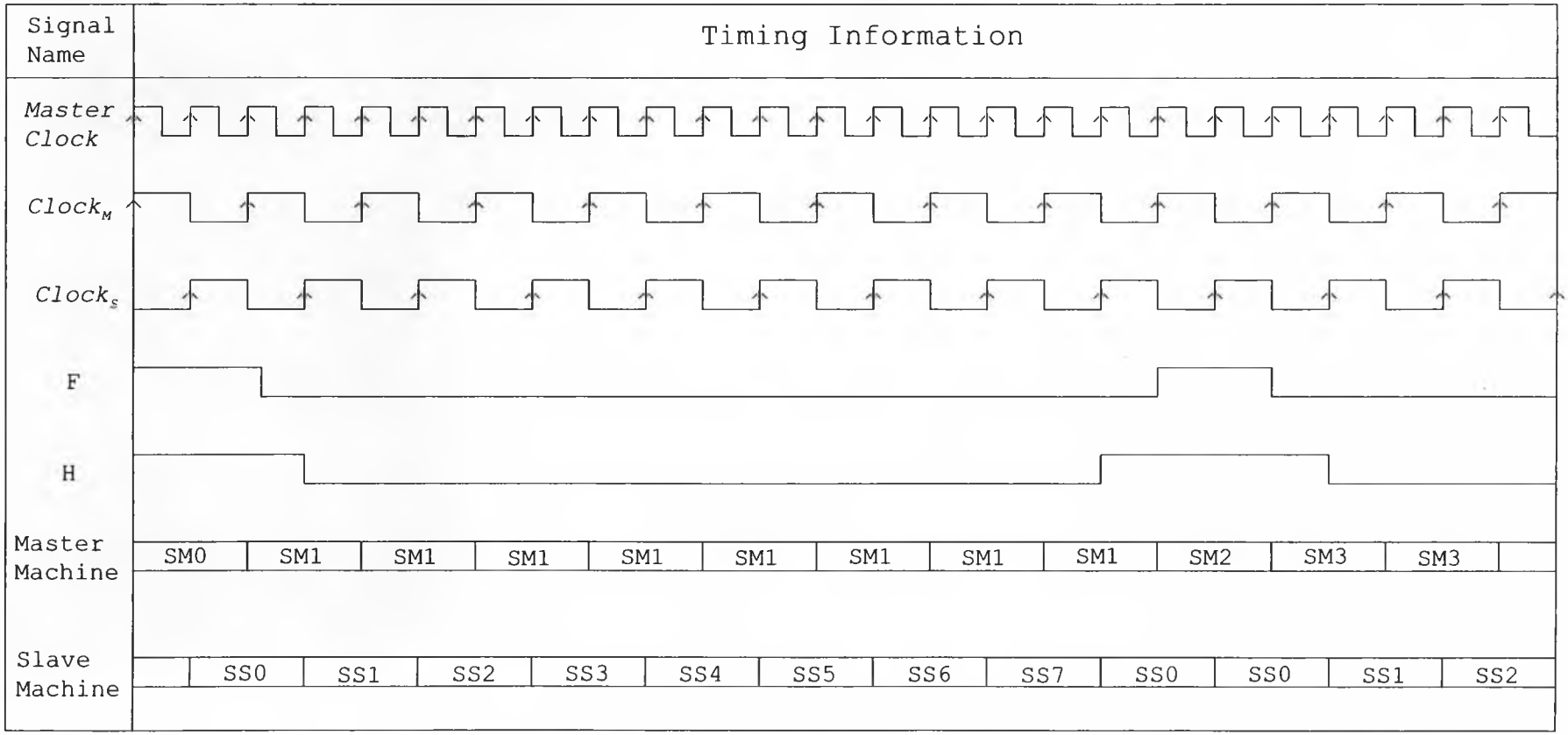

Figure 7.5 Timing Diagrams for Conversion of Channel 0 for State Machines in Figure 7.4

whilst the read was occurring. This resolved the conflict whilst allowing the data acquisition system to continue to sample at the required rate without loss of data.

Although conflicts could be detected it was preferable to prevent them occurring. The acquisition system wrote to all memory addresses in sequence at a fixed rate while the processing systems could select the address they read from. If the address currently being written to by the acquisition system was known to the processing system, the algorithm for reading the memory could be designed to avoid conflicts. To implement this the most significant address line used on the data acquisition side of each DPRAM was connected to an input port of the processing system connected to the other side, so the processor could determine if the data acquisition system was writing to the upper or lower half of the DPRAM.

7.3.6 Construction

The data acquisition system was constructed using wire wrap techniques with the analogue and digital sub systems on separate boards. The circuit layout and signal paths were designed to minimise the cross talk between the high speed digital signals and the analogue signals. Power to the system was supplied by a conventional laboratory supply with separate supply lines for the +5V logic and ±15V analogue supplies. Each sensor element was connected to the system with two 2 mm plugs for the power and a BNC connector for the signal. The data acquisition system was connected to the fast and slow processing systems using IDC connectors.

7.4 Slow Processing and Display System

The slow system performed relatively complex processing on 'blocks' of snap shots, and was also the recording and display system for both the fast and slow systems. During development of the system frequent changes were made to both the hardware and software. In order that these changes be made as quickly as possible a 90 MHz Pentium based personal computer (PC) was selected as the processor for the slow system.

Eggebrecht(1994) gives full maps for both IO and memory in a PC. IO space is limited to 512 bytes, thus the DPRAM was placed in the PC's memory map. A number of gaps exist in the map between 640KB and 1MB for features, such as the BASIC interpreter ROM, that are no longer used. For the slow system a vacant address at $A000 was selected as the base address for the DPRAM.

Figure 7.6 is a block diagram of the circuit constructed to interface the data acquisition system to the PC, a full circuit diagram is contained in appendix 4. A conventional 16 bit prototyping card was used to construct the interface, this was connected to the data acquisition system by a very short ribbon cable. The address lines from the PC bus were connected to the DPRAM through 74HCT244 unidirectional buffers. PC memory addresses refer to individual bytes and 16 bit transfers must occur on even address boundaries. For this reason A1 to A12 on the PC bus were connected to A0 to A11 on the DPRAM. A13 to A23 were decoded to provide a card select signal, $\overline{CRDS}$, this was combined with the memory read line, $\overline{MEMR}$, to provide a select signal to the DPRAM, $\overline{DPS}$. PC data lines D0 to D15

were buffered through 74HCT245 bi-directional buffers to allow both the reading and writing of data to the card. The buffered lines D0 to D9, D14 and D15 were connected to D0 to D9, D14 and D15 on the DPRAM. PC data lines D10 to D13 were connected to tri state buffer outputs enabled by $\overline{CRDS}$ signal and used as a simple four bit input port.

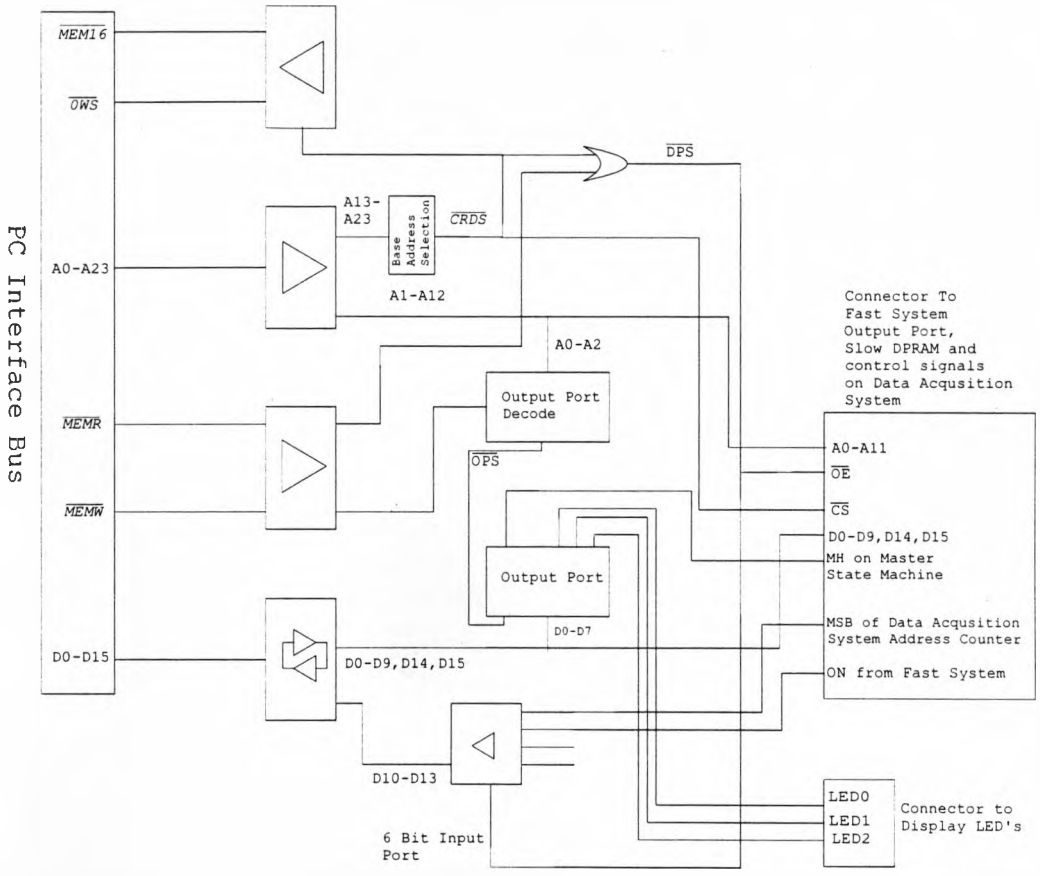

Figure 7.6 Slow Processing System Interface to PC

Inputs D10, D11 and D12 were used to read status information from the fast system. D14 was connected to the most significant bit of the data acquisition address counter to allow the program reading the data to prevent address conflicts as described in section 7.3.5. $\overline{CRDS}$ was combined with the memory write signal $\overline{MEMW}$ and address lines A1, A2, A3 to provide an enable line for a 74HCT573 latch used as an

eight bit output port. Bit 0 was connected to the hold control, MH, on the controller state machine, bits 2,4 and 6 were connected to LEDs mounted outside the PC.

7.5 Fast Processing System

The fast system processed individual snap-shots and indicated the occurrence of transients and other events of a short duration. When events were detected a digital output was immediately asserted, signals were also sent to the slow system DPRAM DP_S. When the slow system reads DP_S the number of transients occurring within the block of snap shots was recorded.

The data acquisition system continuously wrote the snap-shots to DPRAM, DP_F. The fast processor performed relatively simple processing on the snap-shot before the next one was written. For this reason a simple dedicated processor, 9.18MHz Zilog Z180 based microprocessor module, **Z World(1995)**, was selected. The module contains 128k of program and data RAM, power supply, serial port and monitor EPROM. Program code was developed on a conventional PC and downloaded through the serial port to the processor.

Six pre-decoded 'chip select' lines , $\overline{CS0}$ to $\overline{CS5}$ were provided on the module and six address lines A0 to A5, figure 7.7. $\overline{CS3}$ was used to select the input and output ports, $\overline{CS4}$ to select the DPRAM. Address lines A0 to A3 from the processor were connected to A0 to A3 on the DPRAM. An eight bit output port and two eight bit input ports were also constructed. Bit 0 on the input port was connected to the most significant bit of the data acquisition port on DP_F, this allowed the fast processor to

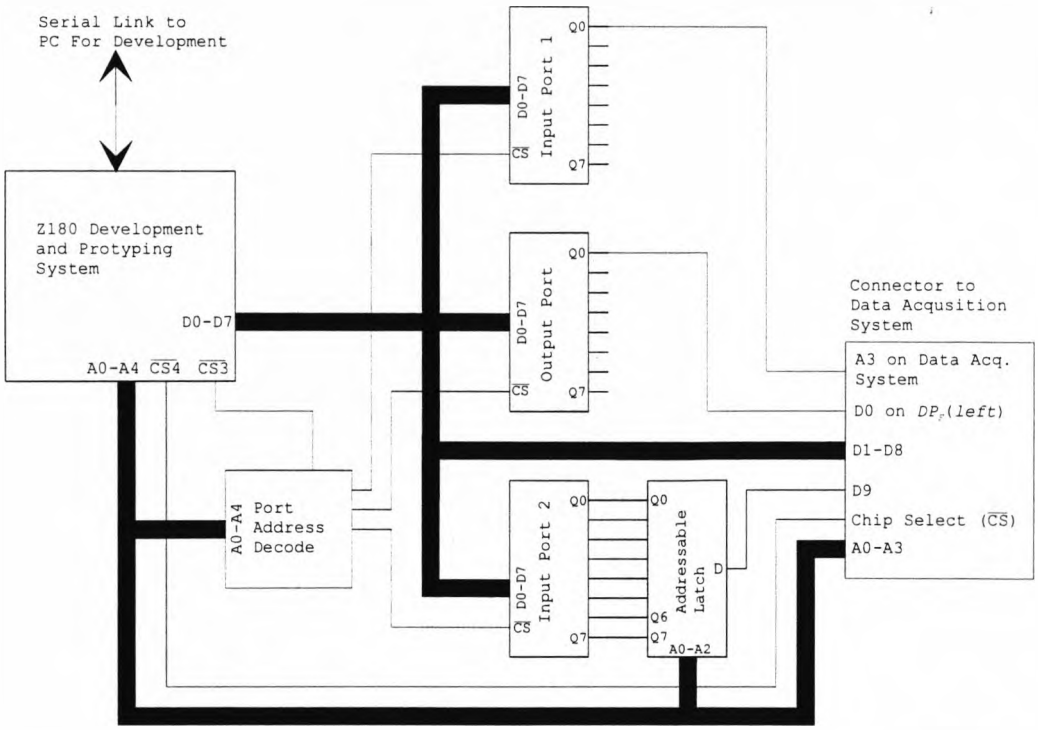

Figure 7.7 Block Diagram of Fast Processing (Transient Detection) System

determine which half of the memory was being written to. Bits 0 and 1 were the transient detected, TRAN, and system synchronised, SYNC, outputs of the fast system. The processor was an eight bit device, the data in the DPRAM was 10 bits, it was possible to access the DPRAM as two bytes, requiring 16 accesses per snap-shot, however this was a waste of processor resources as 75% of the upper byte was not used. An alternative method of reading the data in the DPRAM was designed. Calculations in section 9.1 indicated that nine significant bits were sufficient to detect transients. DPRAM lines D1 to D8 were connected to D0 to D7 on the fast processor system, D9 was connected to the data input of an eight bit addressable latch. The latch has one input bit, D, three address lines, A0-A2, eight output bits, Q0-Q7, and a latch enable signal $\overline{LE}$, when the $\overline{LE}$ input was taken low the value on

D was latched on the output, Q_n, corresponding to the binary value of A0-A2. The address lines were connected to the DPRAM address lines and $\overline{LE}$ was connected to the DPRAM chip select signal $\overline{CS4}$. When the lower eight bits of all eight snap-shot values were read the latch outputs held the 9th bit of each snap-shot. Input port two was used to read these as a single eight bit byte. Only nine processor reads (eight of the RAM and one of input port two) were required to read all the snap-shot values.

7.6 Data Transfer Between Systems

To transfer the electric field data between the data acquisition system and both processing systems, without interrupting the data acquisition system and avoiding address conflicts, required that the processing system reads from a different area of DPRAM to the one the data acquisition system was writing to.

For the slow system the snap-shots were written sequentially to blocks of eight memory addresses. The memory, DP_S, was divided into two halves, called *upper* and *lower* and the data in each one, 256 snap-shots, called a *data-set*. The MSB of the data acquisition system counter was monitored, this allowed the slow system to determine which half of the memory was being written to and to read from the other half. The time for a data-set to be written, T_{slow}, was 366ms. In this time the slow system transferred the data-set and processed it before the next data-set was written.

For the fast system the MSB of DP_F was monitored, this allowed the processor to determine if the upper or lower snap-shot was being written. A snap-shot was

written every 1.43ms, the fast system transferred and processed the snap-shot in this time before the next snap-shot was written.

The transient detected, TRAN, output of the fast system was connected to bit 15 on the left (input) side of slow system DPRAM, DP_S. Detected transients were written to bit 15 of DPRAM, this allowed the slow system to count the number of transients occurring in the data-set.

7.7 System Testing

Both systems were tested by applying known signals to the data acquisition system inputs and examining the data received by the processing systems. Both systems acquired data which correctly represented the input test signals.

8. Slow System Data Processing

When no transient events are occurring the voltage spectrum of each phase of a power system consists of a large component at the operating frequency, f_p, and a series of harmonic components at integer multiples of this frequency, figure 8.1. As the loads on the power system change the magnitude of each component changes, usually the duration of such changes is at least a few cycles at the operating frequency.

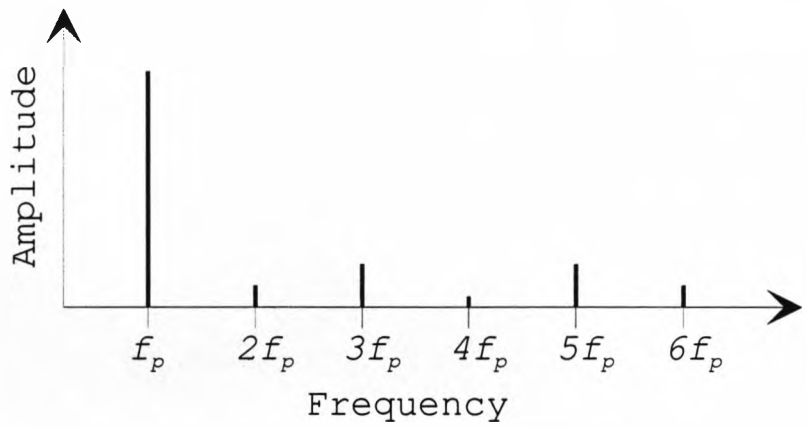

Figure 8.1 Typical Spectrum of Power System Voltage

By processing the electric field signals sampled and stored by the data acquisition system it is possible to produce a continuous record of the changes in the fundamental and harmonic components of the conductor voltages.

8.1 Overview of Operation

Each data-set of 256 samples from the eight electric field sensors produced by the data acquisition system was transferred from DPRAM, DP_S, to the slow processing system. The transfer and analysis tasks for one data-set were completed whilst the data acquisition system was reading the next data-set.

The analysis task was a complicated one as several interdependent tasks were performed. Additional complications in the software structure arose because it was necessary to apply a rolling average technique using the results of several data-sets. Averaging was required to reduce the noise in the signals from the electric field sensor elements.

The first step in the analysis of a data-set was the production of separate sets of numeric values which described the signal from each sensor element, *signal descriptors*. The signal descriptor for one sensor consisted of the frequency and magnitude of the fundamental component and the magnitudes of harmonics up to order five.

Long term averages of the amplitudes of the fundamental components were maintained for all sensors and it was assumed that these corresponded to the signals produced when the power system was operating normally. Rolling averages, taken over several data-sets, of all components of the signal descriptors were computed. The deviation between the fundamental component of each signal and its long term average was determined. The pattern of deviations obtained by examining all sensors was compared to a database of previously determined patterns. When a match was found the changes in voltage used to calculate the matching data base entry indicated the percentage difference between the present and normal value of the individual conductor voltages.

The final action by the system after analysing a data-set was to display and store, in the slow system memory, the changes in the individual conductor voltages and the average harmonic content of all the conductor voltages. The system also displayed and recorded the transients events reported by the fast system, chapter 9.

8.2 Derivation of Signal Descriptors

The 256 samples acquired for each sensor element were in the time domain, they were transformed into the frequency domain to compute the signal descriptors.

8.2.1 Fourier Analysis

A continuous time domain signal, $f(t)$, may be represented in the frequency domain by the Fourier transform, $F(\omega)$

$$F(\omega) = \int_{-\infty}^{+\infty} f(t)e^{-j\omega t}dt \qquad [8.1]$$

For a signal consisting of sample values in the time domain application of the discrete Fourier transform (DFT) produces a spectrum, at discrete frequencies in the frequency domain, by computing individual finite impulse response filters (FIRF) at the discrete frequencies. The spacing of the discrete frequencies Δf is determined by the sampling frequency, f_{sample}, and the number of frequencies at which the FIRF are computed, N_f.

$$\Delta f = \frac{f_{sample}}{N_f} \qquad [8.2]$$

For N_s time domain samples $x[0]$, $x[1]$.....$x[N_s - 1]$ the respose of a FIRF at a frequency $k\Delta f$ is

$$F(k\Delta f) = \sum_{n=0}^{N_s-1} x[n]\left[\cos\left(\frac{2\pi kn}{N_f}\right) + j\sin\left(\frac{2\pi kn}{N_f}\right)\right] \qquad [8.3]$$

where k is a positive integer, $0 \le k \le N_f - 1$. The cosine and sine terms in [8.3] are independent of the sample value, $x[n]$, they may be pre-calculated and stored. The terms are commonly known as *twiddle factors*, **Duhamel & Vetterli(1990)**, each sample in the data-set requires a different twiddle factor, thus N_S twiddle factors are required in a *twiddle factor set.*

To compute a complete frequency spectrum the FIRF must be computed at every discrete frequency, this requires a total number of operations proportional to the product N_sN_f. **Cooley & Tukey(1965)** reported an algorithm to reduce the number of operations to $N_f \log_2(N_S)$, DFT calculations that use this algorithm are commonly known as Fast Fourier Transforms (FFTs). When computing complete spectra the FFT algorithm requires fewer calculations than computation of all N_f frequency components using the DFT, equation [8.3], the factor by which the number of calculations are reduced, K, is

$$K = \frac{\log_2(N_S)}{N_S} \qquad [8.4]$$

For a power system with no transient events occurring the voltage spectrum contains only the fundamental and harmonics, figure 8.1. It is not necessary to compute the frequency spectrum at frequencies other than the fundamental and harmonics and it is more efficient to perform individual FIRFs, at the fundamental and harmonic frequencies, rather than a complete FFT.

8.2.2 Effect of a Finite Sample Length

Derivation of the DFT equation assumes the signal is of infinite duration in the time domain which is not possible. The effect of a finite duration may be calculated by multiplying the time domain signal by a rectangular *window*. For the slow system the length of the window was equal to the period required to obtain the data-set, T_{slow}.

Figure 8.2a shows a sinusoid of frequency f_X and infinite duration in the time and frequency domains, figure 8.2b is a similar representation of a rectangular pulse of width T_{slow}. Multiplication in the time domain corresponds to convolution in the frequency domain and the results for a windowed sine wave are shown in figure 8.2c. The single point frequency response, figure 8.2a, has been 'stretched' to a peak response and a 'ripple' has been added to the response. **Ramirez(1985)** states that the effect may be described by three parameters; the 3dB width of the peak, β, the ratio between the peak amplitude and the first side lobe, *L*, and the rate the ripple decreases or 'rolls off' as the frequency changes, *D*.

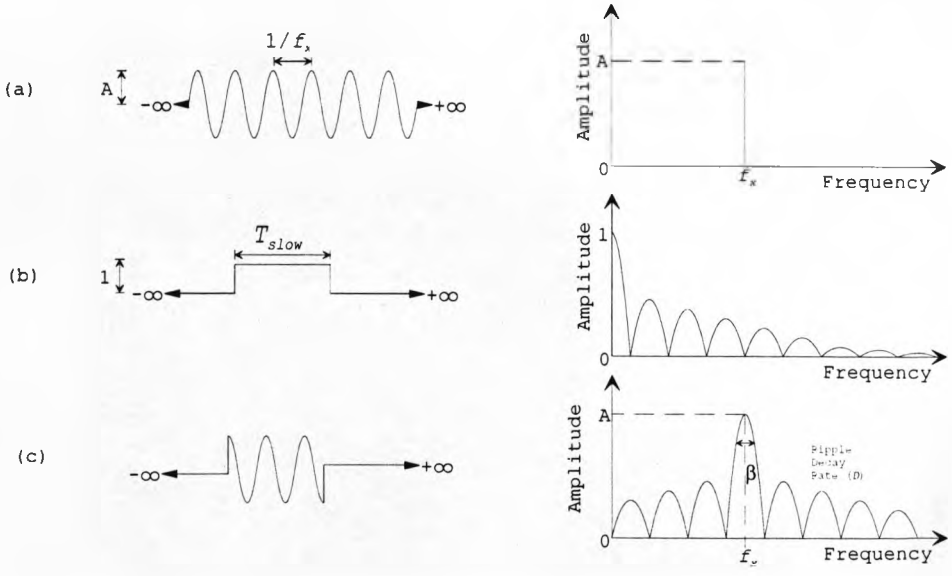

Figure 8.2 Windowing Effect of Finite Sample Length

The ripple is reflected about the dc axis and is superimposed on the original signal resulting in inaccuracies in the magnitude of the peak. The amount of reflected ripple is determined by the ripple roll-off rate, D, and the frequency of the signal. The ripple may be reduced by increasing the period of time the data-set covers, T_{slow}, or by using a non rectangular window.

For the slow system T_{slow} could have been increased by increasing the number of samples in the data-set, N_s, maintaining a fixed sampling frequency, or by reducing the sampling frequency, f_{sample}. The minimum value of f_{sample} was determined by the highest frequency of interest in the data-set and the corresponding Nyquist limit. Increasing the number of samples increased both the memory necessary to store them and the time necessary to calculate the FIRF's, the need to operate in real time and the speed of the processing system limited the maximum value of N_S.

Non rectangular windows may be used to reduce the ripple in the DFT. For N_s time domain samples $x[0]..x[N_s - 1]$ the windowed samples $x^*[n]$ may be calculated by multiplying each sample by a window value $w[n]$

$$x^*[n] = x[n] \times w[n] \qquad for\ 0 \le n \le N_s - 1 \qquad [8.5]$$

Table 8.1 shows the properties of a sinusoidal signal multiplied by the rectangular window and two other windows in common use.

By using a non rectangular window the ripple may be reduced, however this results in an increase in the width of the peak and attenuation of the signal. As the contribution of some samples to the result is reduced the effect of noise in the signal is increased.

Window	Rectangular	Cosine Squared	Hamming
Equation $w[n]$	$w[n]=1$ $0 \le n \le N_s-1$	$w[n] = (0.5(1-\cos(2\pi n/N))^2$ $0 \le n \le N_s-1$	$w[n] = 0.8 + 0.46(1-\cos(2\pi n/N_s)$ for $0 \le n \le N_s-1$
Amplitude	1.00	0.37	0.54
First Lobe (dB)	-13.20	-46.90	-41.9
Bandwidth	0.86β	1.79β	1.26β
Roll Off (dB/Oct)	6.00	18 (Beyond 5β)	30

Table 8.1 Windows in Common Use

8.2.3 Frequency Determination

The signals from the sensor elements contained a large component at the power system operating frequency, this frequency was one of the signal descriptors. A simple method of finding the frequency of a large component of a signal is to calculate FIRFs between limits f_{low}, f_{high} at intervals of Δf and examine the results, the frequency is that at which the FIRF is a maximum. This, *peak detection*, method of finding the frequency also gives the magnitude of the component. The number of FIRFs required, N_P, is

$$N_P = \frac{f_{high} - f_{low}}{\Delta f} \qquad [8.6]$$

The resolution of the measurement is Δf and the maximum accuracy is $\pm\Delta f/2$.

The effect of "peak stretching" by windowing is such that when a FIRF is performed at frequency f_x on a windowed sinusoidal signal of frequency f_y ($f_x \neq f_y$) the result is non-zero. This result may be used to find the frequency of a signal. Figure 8.3 shows the result of two FIRFs, $FIRF_L$, $FIRF_H$, at fixed frequencies f_{low} and f_{high}, applied to a windowed sinusoid of frequency f_i, where f_i is varied. At every frequency, except

$(f_{high} + f_{low})/2$, each DFT has a different response. Figure 8.4 shows the value $FIRF_H$ / $FIRF_L$ as a function of f_i over the range $f_{low} \leq f_i \leq f_{high}$; each value of the ratio corresponds to a unique signal frequency between the limits f_{low} and f_{high}.

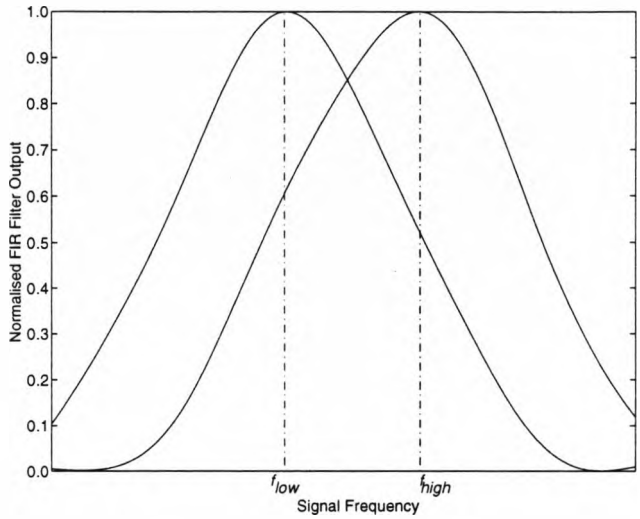

Figure 8.3 Response of Two FIRFs $FIRF_L$, $FIRF_H$ to an Input Signal of Variable Frequency

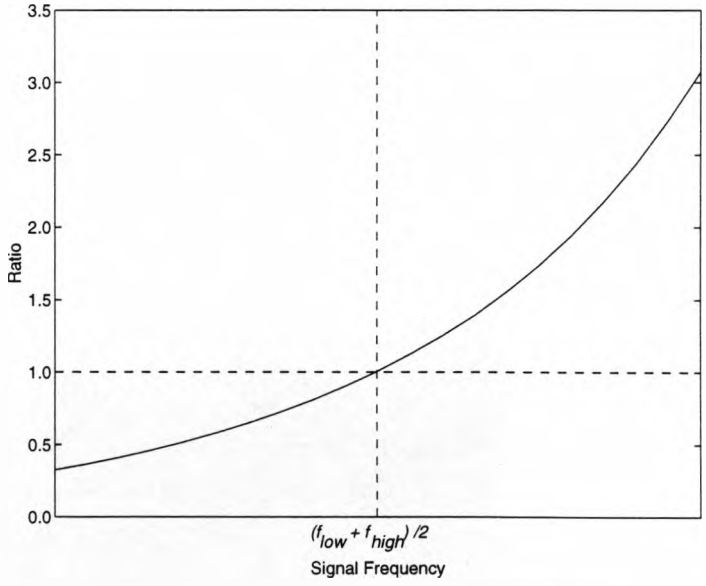

Figure 8.4 Ratio $FIRF_H/FIRF_L$ as Function of Input Frequency

By calculating the ratio at a number of frequencies between f_{low} and f_{high} a "look up" table of frequency values may be formed. To find the signal frequency only two

FIRFs need be calculated, their ratio computed and the frequency found from the table. The resolution of this, *ratio detection*, method is determined by the intervals used for f_i when computing the look up table, the magnitude of the component is not determined.

Once the fundamental frequency has been determined by either method, approximate frequencies of any harmonics may be found by multiplying the frequency by the harmonic number. If the resolution of the fundamental frequency measurement is Δf the resolution of the harmonic frequencies will be $q\Delta f$, where q is the harmonic number. To find the true frequency of the harmonic and its magnitude the maximum value of the spectrum within the range $\pm q\Delta f$ of the approximate value must be found.

The slow system had to store twiddle factors for all possible values of fundamental and harmonic frequencies, to measure harmonics up to order N_H the total number of twiddle factor sets to be stored, N_F, was

$$N_F = \sum_{q=1}^{q=N_H} q\left(\frac{f_{high}-f_{low}}{\Delta f}\right) \qquad [8.7]$$

8.3 Averaging

One signal descriptor was calculated for the signal from each sensor. Each data-set produced eight signal descriptors, a *descriptor-set*, Q. A "rolling average" technique was used to calculate an average of the components of N_A descriptor-sets and produce an average descriptor set for each data-set.

The principle of operation is shown in figure 8.5 for N_A =10. A circular buffer held the last N_A descriptor sets and a pointer indicated one location of the buffer. The totals for all components of each descriptor currently in the buffer were also held. When a new descriptor-set was calculated the components of the descriptor set at the pointer position were subtracted from the components of the sum, the new components were added in their places and the totals divided by N_A to find the average values. The new descriptor set was stored at the current pointer position and the pointer advanced to the next position in the buffer. After the first N_A data-sets the buffer was filled and a new "rolling" average descriptor set was calculated for each successive data-set.

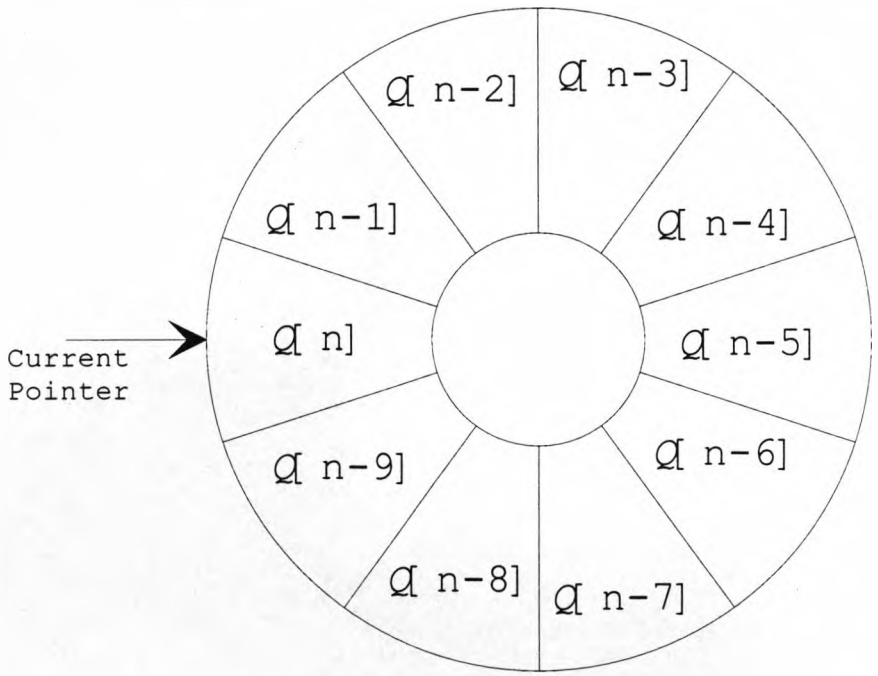

Figure 8.5 Operation of Circular Buffer

In addition to reducing noise the averaging process also reduced any signals, power system events, whose duration was less than the averaging period. For a change

D_{event} in the component of a signal descriptor of duration T_{event} the change in the component of the rolling average D_{avg} was

$$D_{avg} = D_{event}\left(\frac{T_{event}}{N_A T_{slow}}\right) \qquad [8.8]$$

As well as the rolling average the slow system required a long term average of the fundamental component of the magnitude to represent the signals to represent the signals produced during normal power system operation. As it was not necessary for this to be updated every data-set, a conventional sequential average was used, the rolling average descriptors of each data-set were added to a sum and the average was periodically calculated. This was suitable for a development system but a permanently installed system would require an alternative method using values established during installation and commissioning

8.4 Primary Voltage Variations

Comparison of the rolling averages of the fundamental component of all the signal descriptors with the long term average values produced a *change pattern*.

It was shown, section 5.3, that a unique set of changes in the conductor voltages produces a corresponding unique change in the ground level field distribution. For any set of conductor voltages which differ from the normal values the change in the signal from each sensor element, a *template*, may be calculated, provided that a method of determining ground level fields for all combinations of conductor voltages is available. By computing templates for many different combinations of conductor voltage variations a *template database* was created.

The change pattern may be compared to all the templates in the template database and the template most closely matching the change pattern determined, the change in voltages used to calculate the template will represent the changes in the component of the conductor voltages at the fundamental frequency, the change in the *primary voltages.*

8.4.1 Template Database Generation

The analytical program, section 4.6, was used to calculate and store the peak field at each sensor position for normal operation. The model peak conductor voltages in the analytical program were systematically varied and, for each combination of changes, the new peak field at each sensor position was calculated. The percentage change in the field, and hence in the sensor signal, corresponding to the voltage changes, was calculated and stored.

The number of templates in the database, N_T, was determined by the number of conductors, N_C, the range of voltage changes each conductor must be tracked over, ΔV_{low} to ΔV_{high}, and the voltage change resolution required, R_V

$$N_T = \left(\frac{\Delta V_{high} - \Delta V_{low} + R_V}{R_V} \right)^{N_C} \qquad [8.9]$$

8.4.2 Template Fitting

To determine the voltage changes in real time it was necessary to find the template that most closely matches the measured field changes as quickly as possible. A measure of the 'fit' between the template with values $t[0]..t[N_e\text{-}1]$ and the change

pattern $d[0]..d[N_e\text{-}1]$, where N_e is the number of sensor elements in the array, is the sum of the squares of the differences between them, S

$$S = \sum_{n=0}^{N_e-1} (d[n] - t[n])^2 \qquad [8.10]$$

If the measured changes are exactly equal to the template S will equal zero. For a given change pattern the closest matching template may be found by computing S for each template and selecting the template corresponding to the lowest value of S. For this *simple scan* the number of times S must be calculated is equal to the number of templates, N_T.

An alternative to the simple scan is to perform a *two stage scan*, the database is first scanned at a low resolution, R_L, and an approximate minima found, a scan at a fine resolution, R_V, may then be performed about the approximate minima to find the true minima. The total number of calculations of S required, N_2, is equal to the sum of the number of calculations in the low and high resolution scans

$$N_2 = \left(\frac{\Delta V_{high} - \Delta V_{low} + R_V}{R_L} \right)^{N_C} + \left(2\frac{R_L}{R_V} \right)^{N_C} \qquad [8.11]$$

For certain values of R_L/R_V $N_2 << N_T$, for example if ΔV_{high} = 2%, ΔV_{low} = -2%, R_V = 0.1% and R_L = 0.4% then N_T = 68921 and N_2 = 1589. For reliable results using the two stage scan the minima found by the low resolution scan must always lie within the range of the high resolution scan. Because real data contains random fluctuations the maximum value of R_L/R_V is limited.

8.5 Processing Decisions

The various methods of evaluating signal descriptors and deducing conductor voltages were investigated to determine which were best suited to the slow system. The optimum parameters for operation, the range of voltage and frequency resolutions to be tolerated and the maximum accuracy and resolution achievable were also determined.

8.5.1 Design Constraints

NGC(1992) state that under normal operating conditions the fundamental frequency of the UK power system will remain within the limits 49.5 to 50.5Hz. Under abnormal operating conditions the frequency limits are relaxed to 48Hz and 52Hz, therefore a frequency range (f_{low} to f_{high}) of 48Hz to 52Hz was selected for the slow system. Under normal operating conditions the laboratory supply voltage amplitude variations were expected to exceed those on a high voltage power system, direct monitoring showed that they remained within ±2% of the normal value. Limits ΔV_{high} and ΔV_{low}, of normal value +2% and -2% were selected as the voltage ranges for which the slow system was required to produce accurate results.

As the system was to work in real time, all calculations using one data-set had to be completed before the next data-set was available. The data-sets were produced by the data acquisition system at T_{slow} intervals, the time to process the data-set, the *processing time*, had to be less than this. The processing time was determined by; the choice of signal description technique, range of frequency and voltage variations to be tolerated by the system and the resolution of the final results.

The accuracy of all results was limited by noise on the original signals, the choice of; rolling average length, data window and template fitting routine used. These choices were a compromise between accuracy and processing time of the routines. The signal description and template fitting routines required memory to store twiddle factors and templates, *storage memory*. The number that may be stored and hence the resolution of the measurements was limited by the memory available.

8.5.2 Memory Limitations

The slow processing system had 16Mb of memory, this stored the monitored parameters, section 8.1, and also held the twiddle factors, templates, circular average buffer, other program data, and program code. 12Mb of the system memory was allocated to storing the results, 2Mb for storing the templates and 2Mb for the program code, twiddle factors, and remaining program data. Processing was performed using integer arithmetic wherever possible; two bytes of memory were required for each integer quantity stored, hence up to 125,000 templates could be held in the system memory allocated to template storage.

8.5.3 Frequency Determination

The frequency range for the fundamental component was specified in section 8.5.1, each set of twiddle factors required 256 complex values, each of four bytes thus 1024 bytes were required per twiddle factor set. Table 8.2 shows the amount of storage memory required for different frequency resolutions, Δf.

Frequency Resolution Δf, (Hz)	Storage Memory (kB)
0.4	150
0.2	300
0.1	600
0.05	1200

Table 8.2 Twiddle Factor Storage Memory for Different Frequency Resolutions $f_{low} = 48\text{Hz}, f_{high} = 52\text{Hz}$

To leave memory for other program data to be stored a frequency resolution of 0.1Hz was provisionally selected. The processing time of the full system, section 8.7, showed that real time operation was possible with this frequency resolution. The signals in the data-set are multiplied by a window. The choice of this window influences the results of the frequency determination routines.

A simulated data-set was generated representing signals at a frequency f_i, ($f_{low} \leq f_i \leq f_{high}$), with a small amount (10% of signal amplitude) of random noise added. Both frequency detection routines were used to determine the frequency, f_o, using three windows in each case. The routines were run 1000 times, f_i was compared with f_o and the number of cases where f_i matched f_o and was within one interval Δf either side of f_i were determined, if few results occurred within one Δf the number of results within $4\Delta f$ was also computed. Table 8.3 contains results for ratio detection and table 8.4 results for peak detection.

Window	Rectangular (none)			Cosine Squared		Hamming	
Signal Amplitude (% Full Scale)	Result Band (Hz)			Result Band (Hz)		Result Band (Hz)	
	Exact	±0.1	±0.4	Exact	±0.1	Exact	±0.1
100	27	28	136	998	1000	199	216
10	0	0	105	991	1000	161	209
1	0	0	0	316	693	9	22
0.1	0	0	0	98	142	0	0

Table 8.3 Investigation of Ratio Detection Routine, Number of Results Within Given Result Band 1000 Tests, f_{low} = 48Hz f_{high} = 52Hz

Window	Rectangular (none)			Cosine Squared		Hamming	
Signal Amplitude (% Full Scale)	Result Band (Hz)			Result Band (Hz)		Result Band (Hz)	
	Exact	±0.1	±0.4	Exact	±0.1	Exact	±0.1
100	1000	1000	1000	1000	1000	1000	1000
10	201	300	1000	1000	1000	591	1000
1	106	126	362	902	1000	96	105
0.1	0	0	0	100	512	10	29

Table 8.4 Investigation of Peak Detection Routine, Number of Results Within Given Result Band, 1000 Tests, f_{low}=48Hz f_{high}=52Hz

The cosine squared window most reliably predicted the frequency in the tests performed and was selected for use with both methods of frequency detection. The ratio detection routine was reliable when the signal was large and the window was non rectangular but performs poorly at small signal amplitudes, it is also many times faster than the peak detection routine (a factor of 20 times for Δf = 0.1Hz). For these reasons the ratio detection routine was selected to determine the fundamental frequency and the peak detection routine was selected for the harmonics which have smaller amplitudes.

8.5.4 Descriptor Averaging

Using the scale model of the power system described in section 9.1 a constant amplitude signal was applied to the conductors and a DFT algorithm used to determine the fundamental component of the signal. If the mean average of this for one channel is μ, the rms value of the noise on the channel, e_{rms}, is

$$e_{rms} = \sqrt{\sum_{n=0}^{N-1} (d[n] - \mu)^2} \qquad [8.13]$$

Table 8.5 shows the rms error measured on sensor element 0 for averaging different numbers of data-sets.

Number of Data-sets Averaged (N_A)	e_{rms} (% of signal)
1	1.57
5	1.12
10	1.00
20	0.95
40	0.92

Table 8.5 RMS Noise in Signal Description For Different Numbers of Data-sets Averaged

Examination of Table 8.5 indicated that the reduction in noise was not significant when N_A exceeded 10, therefore a value $N_A = 10$ was selected as a compromise between noise reduction, length of the circular buffer and reduction in sensitivity to short term changes. Equation [8.8] indicates power system events with a duration less than 3.6s will be attenuated.

8.5.5 Template Fitting

The scale model and conventional (contact) monitoring system, chapter 10, were used to investigate the accuracy and speed of the template fitting routines. The fundamental magnitude of each sensor and the conductor voltages were recorded for approximately four hours. The two template fitting routines, each at two resolutions, were applied to the recorded data to determine the changes in peak conductor voltages and determine the time taken to fit the templates. The voltage results were compared with directly measured results and the difference between the two calculated. Table 8.6 shows the time taken to fit a template to the change pattern and the rms differences between the measured and determined voltage changes.

Fitting Method	RMS Difference (%)	Processing Time (ms)
Simple R_V=0.2%	0.12	139
Simple R_V = 0.1%	0.09	1030
Two Stage R_L = 0.4% R_V = 0.1%	0.14	24
Two Stage R_L = 0.2% R_V =0.1%	0.14	138

Table 8.6 Comparison of Template Fitting Routines $\Delta V_{high} = 2\%$ $\Delta V_{low} = -2\%$

Each template contains eight values, one for each sensor element, these values require 16 bytes of storage memory. Table 8.7 shows the number of templates, calculated using equation [8.8], and storage memory necessary for the voltage range ±2% at different resolutions.

Resolution R_V (%)	No. Templates	Storage Memory (kB)
0.4	1331	21.2
0.2	9261	144.8
0.1	68921	1076.9

Table 8.7 Template Storage and Memory Requirements $\Delta V_{high} = 2\%$ $\Delta V_{low} = -2\%$

A voltage change resolution, R_V, of 0.1% was selected as giving the highest resolution for which the templates could be fitted into the allocated memory. The simple fitting algorithm gave the highest accuracy, however its processing time exceeded T_{slow} (366ms) preventing real time operation. The two stage fit was only slightly less accurate and was much faster, with processing time much less than T_{slow}; therefore this method was selected with $R_L = 0.4\%$, $R_V = 0.1\%$.

8.6 Processing System Software

Figure 8.6 is a flow chart of the slow processing system, a top-down processing philosophy was used to write the software, appendix 5 is a listing of the top level program with outline descriptions of the lower level subroutines called by it.

At power on the PC was configured to automatically start running the software, an initialisation command was sent to the fast system, the twiddle factors and templates were loaded into the system memory and other program data was initialised. When both the fast and slow processing systems were fully initialised the main loop of the software started.

At the start of the main loop the system waited for the data acquisition system to finish writing a data-set, as soon as it was complete the samples were transferred to the slow system and the signal descriptors calculated. The circular average was updated, the values added to the long term totals, and the differences between the long term average and the circular average used to calculate a change pattern. A two stage fit routine was used to find the change in the individual conductor primary voltage. The fast system was interrogated to determine if any transients had occurred in the data-set. The final action performed on each data-set was to store the values of the features of the power system monitored to the slow system memory and display them on a VDU.

8.6.1 Determination of Signal Descriptors

A cosine squared window was applied to the 256 samples from each sensor and the ratio detection routine used to find the frequency of the fundamental frequency, f_p, to a resolution, Δf, of 0.1Hz, a third DFT was performed at the fundamental frequency to find the magnitude of the fundamental component. The frequency of the harmonics was estimated by multiplying f_{fund} by the harmonic number, q, $(2 \leq q \leq 5)$ a peak detection routine was used over the frequency range $q(f_p - \Delta f)$ to $q(f_p + \Delta f)$ to find the harmonic frequency to a resolution R_f and determine the harmonic magnitude.

The analysis process was performed for all eight channels of the sensor array and a rolling average of the last 10 signal descriptors was used to create averaged descriptors. The time to produce an averaged set of signal descriptors was measured as 187ms.

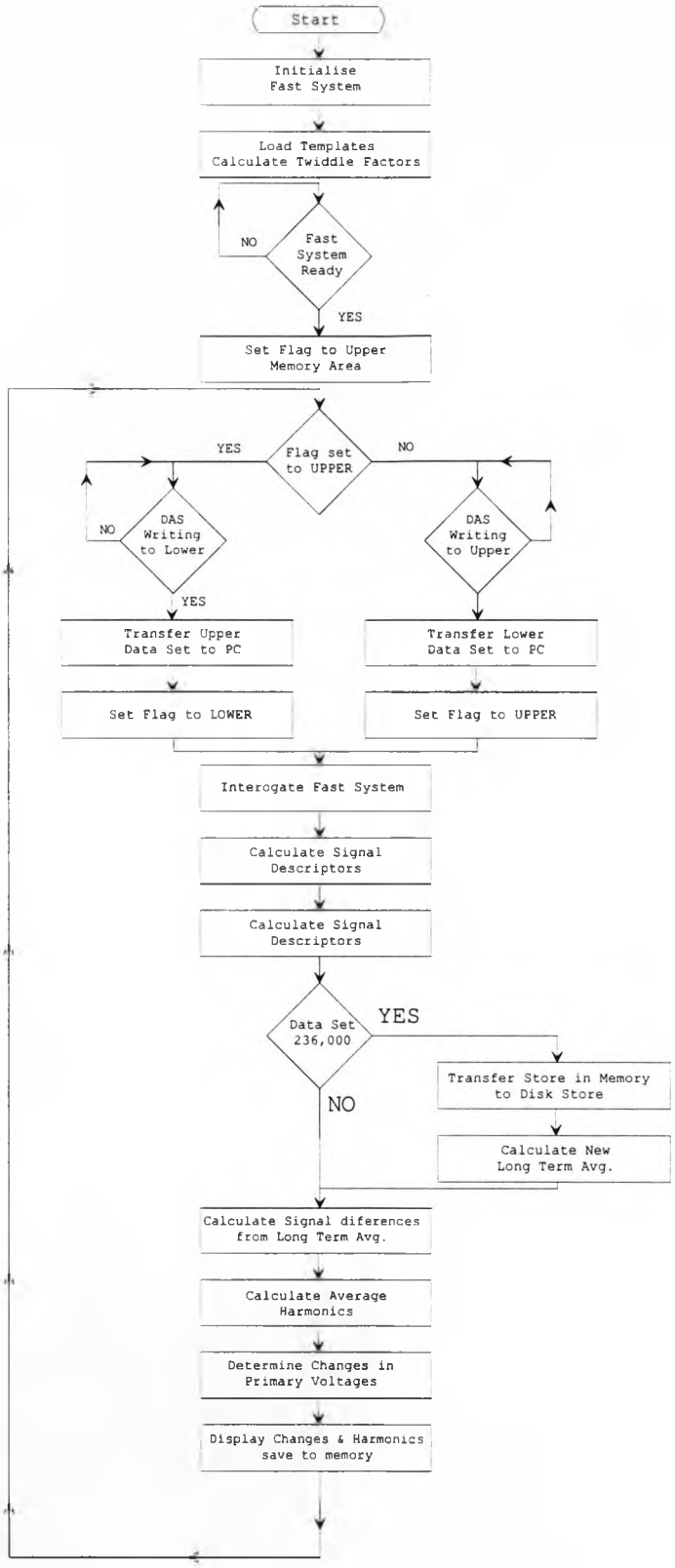

Figure 8.6 Flow Chart for Slow Processing System

8.6.2 Long Term Average & Voltage Change Determination

The long term average of the signal for each sensor was calculated by summing the fundamental component of the signal for 236,000 data-sets, these were obtained over a period of approximately 24 hours. The sum was divided by 236,000 and used as the long term average for the next 24 hours. For the first 24 hours an average of a stored set of descriptors was used. The time to divide the sum was measured as 120 μs.

The two stage template fitting routine with $R_L = 0.4\%$, $R_V = 0.1\%$ was used to determine the changes in conductor voltages. The time taken to fit the templates was measured as 27ms.

8.6.3 Display & Logging

The change in each conductor's primary voltage, the power system frequency and the average of the harmonic content as a percentage of the fundamental component on all the channels for each averaged averages descriptor sets, a *voltage summary*, was displayed to a VDU, figure 8.7 and saved to memory. For development of the system the descriptor-sets were also saved to memory, this allowed more detailed 'off line' processing than was possible in real time. The development system memory was volatile, in the event of loss of power to the system the stored signal descriptors and voltage summaries were lost. Every 24 hours the system stopped monitoring for approximately 5 seconds and transferred the voltage summaries and signal descriptors to a non volatile disk store.

```
19/06/96 14:27:22 DS No. : 9 Filename : c:\tmp\CLA010.BIN
No. Transients Detected : 0
          Fund      Fund      2nd       3rd       4th       5th
Chan      Freq      Mag       Mag       Mag       Mag       Mag
====      ====      ===       ===       ===       ===       ===
 0        499       23376     40        184       15        389
 1        499       23489     19        197       13        315
 2        499       20782     21        239       13        316
 3        499       9896      10        177       11        230
 4        499       6922      24        186       10        237
 5        499       13817     12        149       25        262
 6        499       19273     20        58        12        234
 7        499       19225     23        99        13        241

                        Percentage Harmonic * 1000
                        ==========================
   2nd                    3rd                 4th                 5th
  =====                  =====               =====               =====
  120                    917                 80                  1526

                    Changes in Conductor Voltages (% * 10)
                    ======================================
                  LHS                 CEN                 RHS
                  ===                 ===                 ===
                  -8                  -11                 -9
```

Figure 8.7 Display of Slow System Software Operating

8.7 Summary

The slow system software performed real time analysis of the data transferred to DPRAM DP_S by the data acquisition system. It determined the changes in primary voltages from nominal, for the individual conductors of the power system over a range ±2% with a resolution of 0.1%. The power system frequency was measured over a range 48Hz to 52Hz with a resolution 0.1Hz and the average harmonic content of the power system deduced.

This information was displayed to a VDU and saved to memory for later analysis. The total processing time per data-set was 215ms, this was less than the sample period, 366ms, ensuring that reliable real time operation is maintained with time available for future extensions.

9. Fast System Processing

Voltage transients on power systems, "*transients*", are short duration deviations from the normal sinusoidal conductor voltages, for example figure 9.1. Most transients are caused by lightning strikes, switching operations or faults and can cause damage to apparatus connected to the system. By detecting transient changes in the ground level electric field it is possible to detect and record transient changes in the power system voltages.

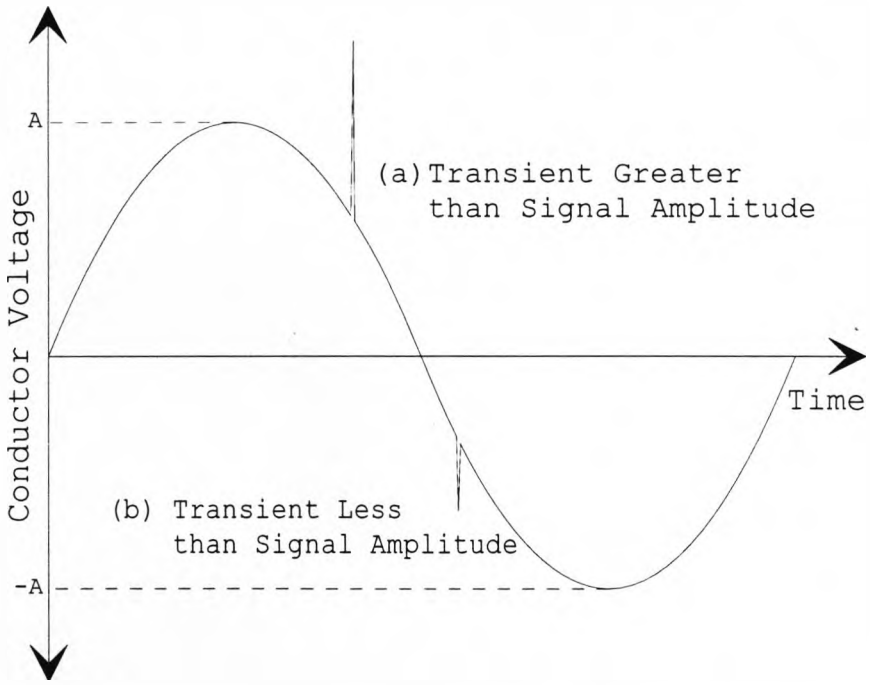

Figure 9.1 Voltage Transients

Very large transients may exceed the signal amplitude, figure 9.1a, and may be detected by a simple magnitude comparator. Smaller transients, figure 9.1b, require a more sophisticated detection technique.

Under normal operating conditions the signal from the electric field sensors was a sinusoid with an amplitude and frequency that varied slowly as loads on the power

system changed. As the form of the signal was known, a small number of the most recent samples were used to predict the value of the next sample. If a transient occurred the sample value differed significantly from the predicted one, hence transients were detected within one sample period of their occurrence.

9.1 Principle of Operation

The detection process was complicated as the prediction of the next sample value required information derived from several snap-shots before the current one. Some simplification was possible as transients on one conductor produced transient changes in the field at all sensor locations, hence transients could be detected by examination of the signal from only one sensor element.

Each snap shot of the instantaneous field on the eight sensors was transferred from DPRAM DP_F to the fast system. The sample for the single channel monitored was extracted and processed whilst the data acquisition system was writing the next snap shot. There were two processing operations; the first was comparison of the sample with an already existing prediction. If the sample and the prediction differ the signal had deviated from its normal form, if the difference exceeded a pre-set *threshold value* a digital output was asserted for the duration of the transient. The second process was inclusion of the sample in the record of recent values and prediction of the value of the next sample.

9.2 Requirements of Sample Prediction

If the harmonic components of the voltage signal are neglected the signal from each electric field sensor element, $V_S(t)$, is a sinewave of amplitude A_P at the power system operating frequency, f_p

$$V_S(t) = A_P \sin\left(2\pi f_p t\right) \qquad [9.1]$$

For each sensor element, the data stored in DPRAM DP_F by the data acquisition system was a series of signed nine bit integer values at T_{fast} intervals. The value, $V_s[n]$, of the n'th sample after the start of the signal, defined as the instant the signal crosses the zero volt axis was represented by the equation

$$V_S[n] = A\left(1 + \sin\left(2\pi f_p\left[nT_{fast} + T_{lag}\right]\right)\right) \qquad [9.2]$$

$A = 0$ for $A_P = 0$ and $A = 255$ for $A_P = A_M$, the amplitude of the largest signal to be measured. The quantitisation interval of $V_S[n]$, ΔA, was unity. T_{lag}, the *lag time*, was the time between the start of the signal, defined as the point the signal crosses the zero volt axis, and the first sample after the start, figure 9.2. A, f_p and T_{lag} are called the *characteristics* of the signal, if the current values of the characteristics and n held by the processor were correct, the fast system was said to be *synchronised*. When synchronised a digital output was asserted and equation [9.2] was used to predict the next sample value. The positive and negative half cycles of the signal were symmetrical about the zero volt axis, by considering only the magnitude of the signal identical processing may be performed for each half cycle reducing the complexity of the fast system software.

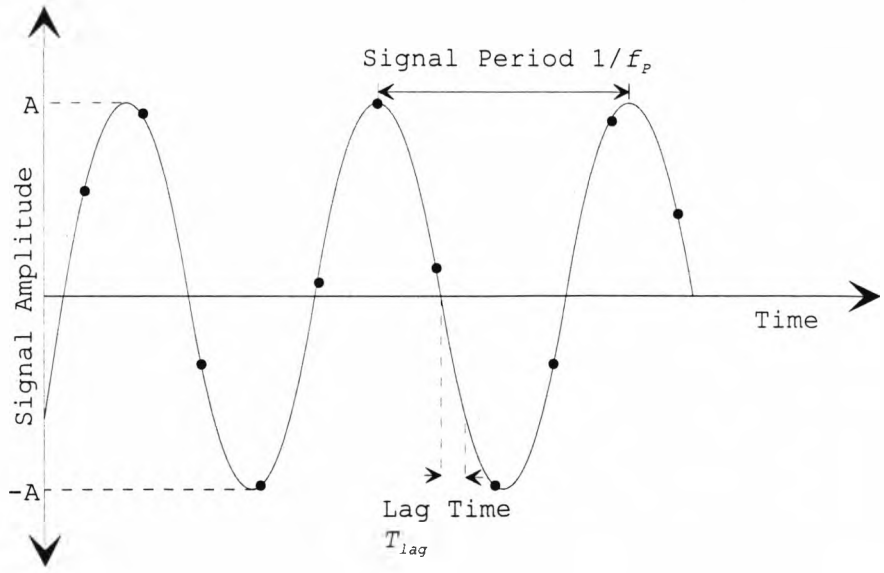

Figure 9.2 Characteristics of a Sampled Sinusoidal Signal

The amplitude and frequency of the signal slowly changed between the limits defined in section 8.5.1. As T_{fast} and f_p were not related the value of T_{lag} was different for each half cycle. To accurately predict the next sample value the fast system had to continuously measure the signal characteristics. Due to measurement resolutions differences existed between the actual values of the characteristics, and the computed values, A^*, f_p^*, T_{lag}^*, used to predict the sample value. These differences resulted in an uncertainty in the predicted sample value. The threshold value used to indicate the presence of a transient had to be greater than the maximum uncertainty.

9.3 Measuring Signal Characteristics

Both the amplitude and frequency of the power system change slowly compared with the period over which the measurements used for prediction were taken. That is, once current values had been determined only small changes occurred over a period of several cycles, therefore each signal characteristic was determined independently.

Because the three characteristics were regarded as independent variables the maximum uncertainty in the predicted value, U_T, was approximately equal to the sum of uncertainties caused by separate inaccuracies in each characteristic. For initial fast system development a threshold value of 5% of A was selected, the sum of all uncertainties had to be less than this value.

9.3.1 Amplitude Measurement

The measured amplitude of the signal, A^*, could be found by detecting the greatest sample value over half a cycle. Although simple the disadvantage with this, *peak amplitude detection*, method, is that the greatest sample value may not occur at the true peak amplitude of the signal, figure 9.2. Figure 9.3 shows a sampled signal and a set of predicted sample values with correct values of f_p^* and T_{lag}^*, $(f_p^* = f_p)$, $(T_{lag}^* = T_{lag})$, and an incorrect value of A^*, $(A^* \neq A)$. The maximum uncertainty in the predicted sample value due to amplitude differences, U_A, occurs at the peak value of the signal and, as a percentage of A, is

$$U_A = 100\left[1 - \sin\left(\frac{\pi}{2} + 2\pi T_{fast} f_p\right)\right] \qquad [9.3]$$

For a power system frequency, f_p, of 50Hz and sample frequency of 700Hz (T_{fast} = 1.43ms), equation [9.3] gives the maximum amplitude uncertainty as 10% of A.

An alternative method, for a signal with a constant frequency and slowly changing amplitude is to use the error between the predicted values and the sample values in a feedback loop, *loop amplitude detection*.

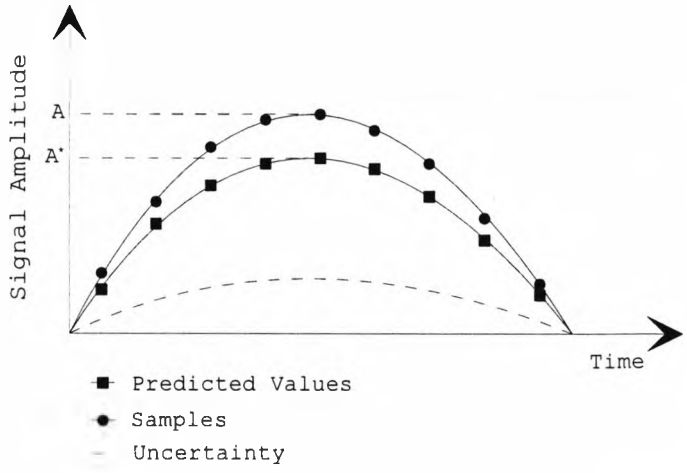

Figure 9.3 Uncertainty in Predicted Values Due to Magnitude Differences

If the measured magnitude is too small, as in figure 9.3, the predicted values will be too small and the errors between the predicted values and the samples will be negative, if the measured magnitude is too large the errors will be positive. If the magnitude errors are summed over half a cycle the result may be used to modify the value of A^* by the data quantitisation interval ΔA. The uncertainty in A is equal to ΔA, and U_A is

$$U_A = \frac{100\Delta A}{A} \qquad [9.4]$$

When the fast system started processing the magnitude of the signal was unknown and a number of half cycles had to be processed before a reliable value of A^* was found. If the initial value of A^* held by the fast system was A_I the initial time to find the signal amplitude T_A was

$$T_A = \frac{|A - A_I|}{2\Delta_A f_P} \qquad [9.5]$$

If $A_I = 0$ a maximum time, $A_M/(2\Delta A f_p)$, had to be allowed for the system to produce a reliable value of A.

For signals with values of A greater than 10 the uncertainty of the loop amplitude detection method was less than the peak amplitude detection method. As the sensor element gain was set to give signals with A much greater than 10, the loop amplitude detection method was selected. In general A was at least 100 so the maximum uncertainty due to magnitude differences was 1% of A.

9.3.2 Frequency Measurement

If the number of samples in N_C half cycles, N_S, is counted the measured frequency, f_p^*, is

$$f_P^* = \frac{2N_C}{N_S T_{fast}} \qquad [9.6]$$

The resolution of f_p^* is determined by the value of N_C. Figure 9.4 shows a signal with correct values of A^* and T_{lag}^* and a incorrect value of f_p^*, ($f_p^* \neq f_p$). The maximum uncertainty, U_f occurs at the end of the half cycle and, as a percentage of A, is

$$U_f = 100 \sin\left(\frac{f_{high}^2 T_{fast}}{f_p\left[N_C + 2 f_{high} T_{fast}\right]}\right) \qquad [9.7]$$

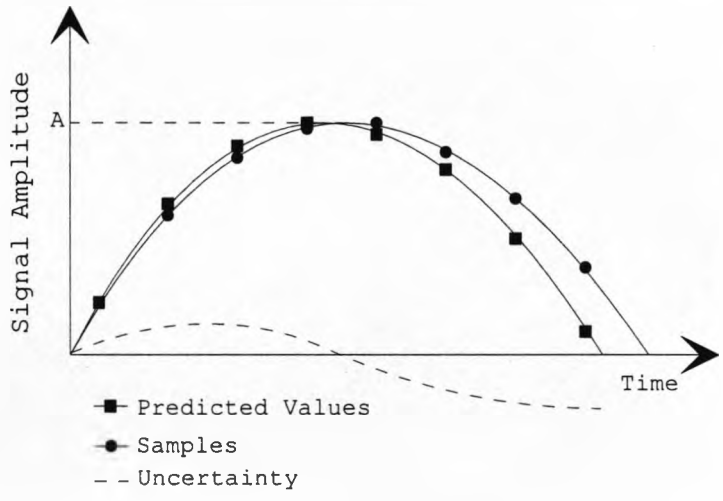

Figure 9.4 Uncertainties in Predicted Values Due to Frequency Differences.

Using a value of N_C other than one reduces the uncertainly in the measurements but complicates the processing necessary to measure the frequency as samples have to be counted over more than one half cycle. To calculate the frequency during each half cycle using a measurement made over N_C half cycles it was necessary to use a circular buffer technique, section 8.3. Increasing N_C also reduces the sensitivity of the system to changes in frequency of duration less then N_C half cycles.

The processing time to calculate the frequency was independent of the value of N_C. However at the start of the program N_C half cycles had to occur before a reliable frequency measurement was available. The time for this to happen, T_f was

$$T_f = \frac{N_C}{2f_p} \qquad [9.8]$$

For programming convenience N_C was usually an integer power of two. For evaluation on a digital processor the frequency range f_{low} to f_{high} was quantitised into N_f intervals. Table 9.1 shows U_f and N_f, for different numbers of zero crossings.

Number of Full 1/2 Cycles Counted N_C	Number of Discrete Frequencies N_f	Maximum Uncertainty U_f (%A)
8	6	2.9
16	10	1.4
32	18	0.8
64	36	0.4

Table 9.1 Properties of Frequency Measurement Routine
f_{high} = 52Hz, f_{low} = 48Hz

Uncertainty due to frequency differences, U_f, was set at 0.8% by selecting N_C = 32.

9.3.3 Lag Time Measurement

A zero crossing was detected by finding a pair of samples which include values either side of zero. T_{lag}^{*} may be approximated by interpolating between sample values, figure 9.5 shows the signal crossing zero and the use of interpolation to find the time of the zero crossing.

P and Q are the unsigned magnitudes of the samples before and after the zero crossing, if the signal between the samples is approximated to a straight line the measured lag time T_{lag}^{*} is given by

$$T_{lag}^{*} = \left(\frac{P}{P+Q}\right) T_{fast} \qquad [9.9]$$

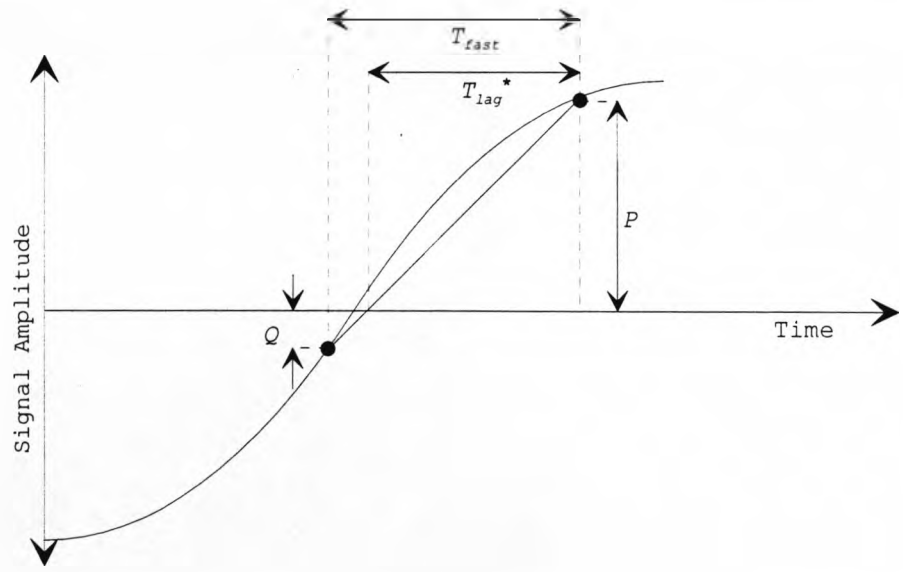

Figure 9.5 Measurement of T_{lag} by interpolation between sample points

For evaluation by a digital processor the sample period is divided into N_I intervals and the nearest interval to the zero crossing is determined. This quantitisation results in differences between the values T_{lag} and T_{lag}^{*}. Figure 9.6 shows a sampled signal and a set of predicted sample values with exact values of A^{*} and f_p^{*} and an incorrect value

of T_{lag}^{*}. The maximum uncertainty in the predicted values, U_{lag}, occurs at the beginning and end of the half cycle and, as a percentage of A, is

$$U_{lag} = 100 \sin\left(\frac{2\pi f_p T_{fast}}{N_I}\right) \qquad [9.10]$$

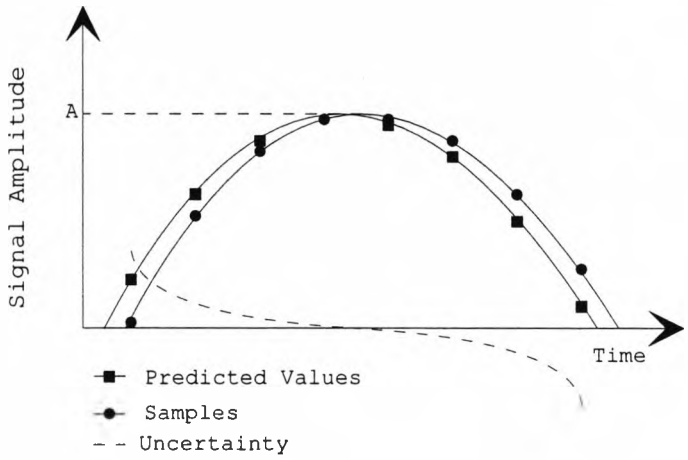

Figure 9.6 Uncertainties in Predicted Value due to Differences in Lag Time

For programming convenience N_I is usually an integer power of two, table 9.2 shows the maximum lag time uncertainty for different values of N_I.

The greater the number of intervals the lower the uncertainty, however the processing time to calculate T_{lag}^{*} increases as the number of intervals increases. A value of $N_I = 16$ intervals was selected, this gives an uncertainty due to lag time inaccuracies of 2.8%. Summing U_{lag}, U_f and U_A gives the maximum uncertainty in the predicted values, U_T, as 4.6 %.

Number of Intervals N_I	Maximum Uncertainty U_{lag} (%A)
8	5.6
16	2.8
32	1.4

Table 9.2 Performance of Lag Detection Routine

9.4 Predicted Value Storage

The predicted values were generated using equation [9.2], this contains a sine term and on the small processor used in the fast system it was not possible to calculate a trigonometric value in real time. Instead the sine terms were pre-calculated and stored for all combinations of values of T_{lag}^*, f_P^* and n. The total number of sine terms stored, N_P, was

$$N_P = N_s(max) \times N_f \times N_I \qquad [9.11]$$

$N_S(max)$ is the maximum number of sample values in a half cycle, determined by the longest signal period (lowest signal frequency, f_{low}) and the sample period T_{fast}

$$N_s(max) = \frac{1}{2T_{fast}f_{low}} \qquad [9.12]$$

As each sine value was stored as eight bits the total memory necessary to store them, was N_P bytes, for the values selected N_P = 2304.

9.5 System Operation

A top down programming philosophy was used to develop the fast system software, figure 9.7 is a flow chart of the system. All routines that run in real time were written in Z180 assembly language to minimise their processing time. A high level language ("C") was used to initialise the system and calculate the table of sine terms at the start of the program.

The fast system had to process every sample read from DP_F to detect transients, assert the digital output, TRAN, and store information for future sample prediction, *Single Sample Processing*. This processing of each sample had to be completed before the next one was written to DP_F. Once during each power system half cycle the signal characteristics had to be determined and, to complete sample processing before the next sample was written to DP_F, each individual characteristic was determined in a different sample period; processes performed once per half cycle were called *Half Cycle Tasks*.

Each half cycle contained either six, seven, or eight samples, depending on the values of f_p^* and T_{lag}^*, it was necessary to check for a zero crossing after any sample which might have been the last. If the correct values of the signal characteristics and n were not known the fast system was not synchronised and transient events were incorrectly indicated, this occurred when the system first starts or when the signal characteristics were changing rapidly. The synchronisation of the system was tested every half cycle and a digital output, SYNC, asserted to indicate synchronisation. Table 9.3 shows the timing of all events occurring in a half cycle

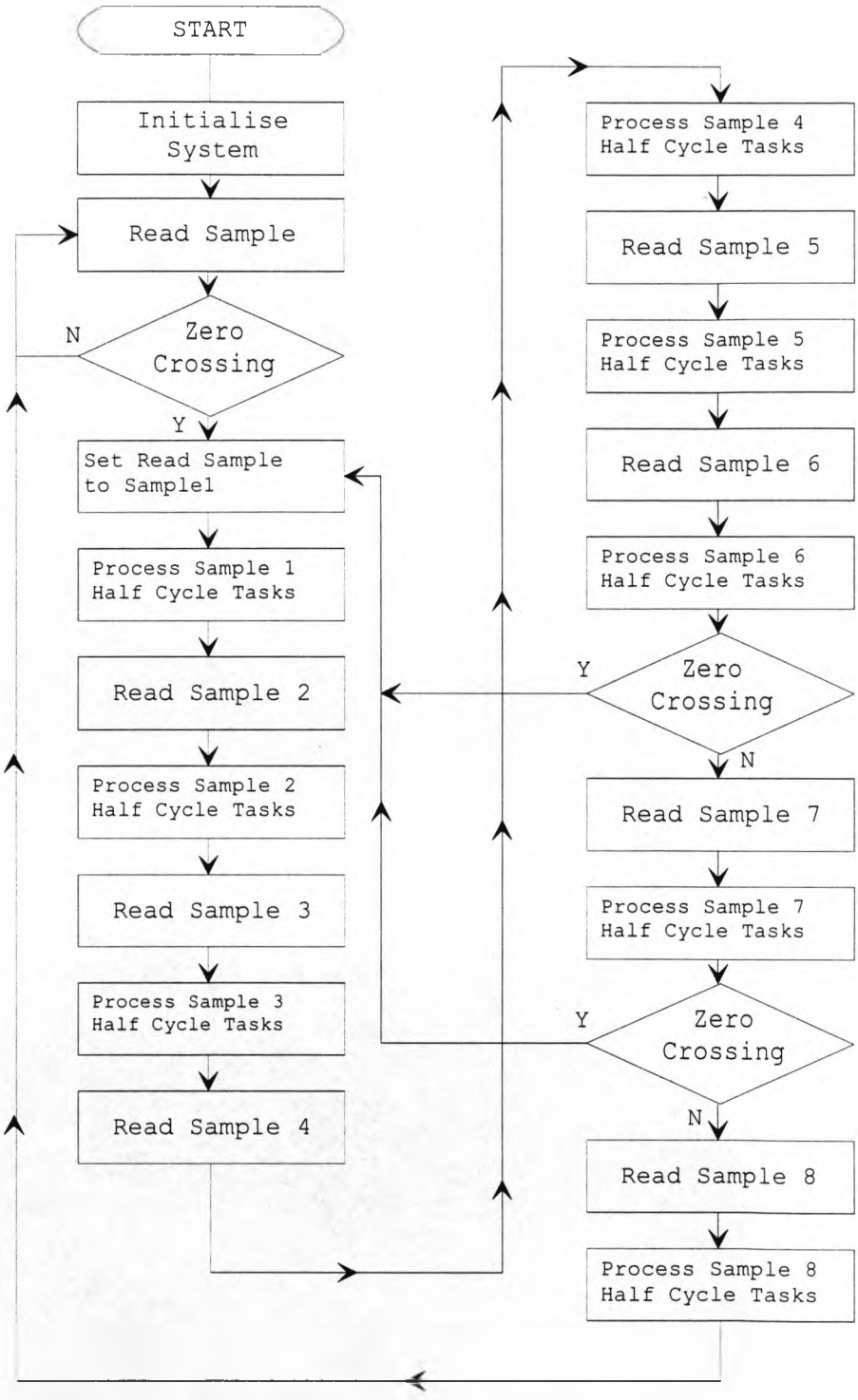

Figure 9.7 Fast System Flow Chart

Sample. Period	Sequence of Routines Called
1	Half Cycle Task - Calculate Lag Time, T_{lag}^* Single Sample Processing
2	Half Cycle Task - Calculate Frequency, f_p^* Single Sample Processing
3	Half Cycle Task - Calculate Amplitude, A^* Single Sample Processing
4	Half Cycle Task - Check Signal Stability Single Sample Processing
5	Single Sample Processing
6	Half Cycle Task - Check for Zero Crossing Single Sample Processing
7	Half Cycle Task - Check for Zero Crossing Single Sample Processing
8	Half Cycle Task - Check for Zero Crossing Single Sample Processing

Table 9.3 Events Performed during sample period

9.5.1 Communication Between Tasks

The single sample processing tasks required current values of the signal characteristics. The half cycle tasks required information, such as the number of samples between N_C zero crossings. The program held this data as a set of global variables, each task reads and modifies the variables as required. Table 9.4 lists the main variables, their functions and when they were used.

Variable Name	Description	Information
T_{lag}^*	Measured Lag Time	Read: Single Sample Processing Task Set: Half Cycle Task - Calculate Lag Time
A^*	Measured Amplitude	Read: Single Sample Processing Task Set: Half Cycle Task - Calculate Amplitude
f_p^*	Measured Frequency	Read: Single Sample Processing Task Set: Half Cycle Task - Calculate Frequency
SC^*	Sample Counter	Read: Half Cycle Task - Calculate Frequency Set: Incremented When Sample Read
SP^* / SN^*	Positive Sum / Negative Sum	Read: Half Cycle Task - Calculate Amplitude Set: Reset by Same Task
n	Half Cycle Counter	Read: Single Sample Events to Find Pred. Value Set: Half Cycle Event - Check for Zero Crossing
SYNC	Synchronisation Flag	Read:Single Sample Events Before TRAN asrtd. Set : Half Cycle Task - Check Stability
TRAN	Transient Flag	Read : (Output Ports) Set: Single Sample Events If Tran. Detected

Table 9.4 Variables Used to Communicate Between Tasks

9.5.2 Sample Processing Routine

The current values of T_{lag}^*, f_p^* and n were used to look up the sine term, this was multiplied by the current signal amplitude, A^*, to give the predicted value. The sample was read from DP_F and converted to an eight bit unsigned magnitude value, this was subtracted from the predicted value and the difference examined. If the difference was greater then the transient threshold the TRAN flag and output were asserted, positive differences less than the threshold were added to total SP^*, negative differences to total SN^*. The total processing time of sample events was measured as 186µs.

9.5.3 Lag Time Measurement

Equation [9.9] contains a division operation which required more processing time than was available in a sample period. A division free method of interpolating between zero crossing samples was developed, figure 9.8. The sample magnitudes before and after the zero crossing, P and Q were added to give a sixteen bit sum, S.

A decision selected the largest of P and Q which was shifted 4 bits left, this had the effect of multiplying the value by 16. The sum, S, was repeatedly subtracted from the shifted value until the result was less than or equal to zero. The number of subtractions was equal to the number of sixteenths of a sample period from the time of the largest sample and was called the *Lag Value, L.* T_{lag}^* was defined as the time to the sample after the zero crossing, if the sample before the crossing, P, was the larger it was necessary to subtract the number of subtractions from 15 to give the correct value of L. The processing time was measured as 380µs.

9.5.4 Frequency Measurement Routine

When the snap shot was transferred from the data acquisition system to the fast system the free running counter SC^* was incremented. A circular buffer held the values of the counter for each of the last 32 half cycles and a pointer indicated the current element of the buffer. Once each half cycle the value at the current buffer position was subtracted from the current counter value to give the number of sample periods measured in the N_C half cycles, the *period count*, the current counter value was written to the buffer and the pointer advanced to the next location. The value of f_p^* could be calculated using equation [9.6] but this was unnecessary as the period

count was used directly as an index into the sine function look up table. The processing time was measured as 100μs.

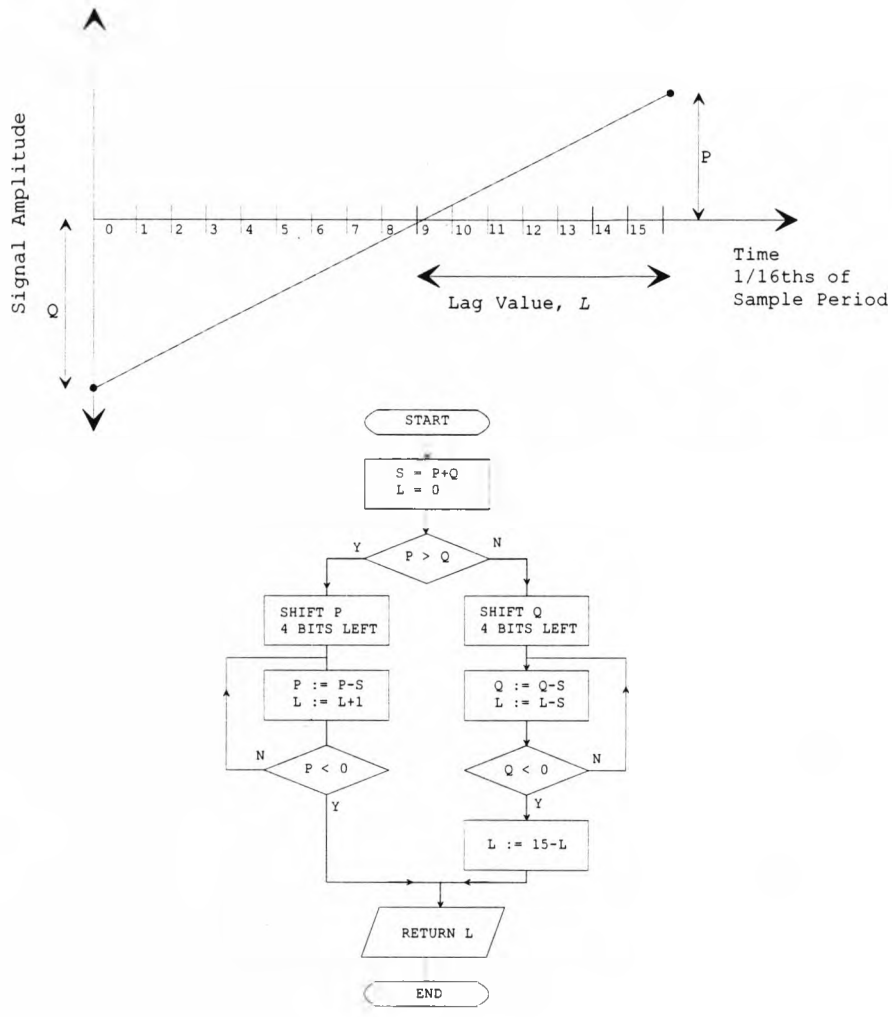

Figure 9.8 Operation of Routine to Interpolate T_{lag}^{*}

9.5.5 Amplitude Detection Routine

The value of the amplitude A^{*} was held as a global eight bit value. When the amplitude detection routine was called the totals SP^{*} and SN^{*} were compared, if SP^{*} was greater the amplitude, A^{*}, was decreased by one bit, if SN^{*} was the greater A^{*} was increased by one bit. At the end of the routine SP^{*} and SN^{*} were reset to zero, the routine processing time was measured as 35μs.

9.5.6 Stability Testing Routine

When the system was not synchronised the predicted values were incorrect and the TRAN output operated frequently. The SYNC output was also an input of the slow system DPRAM, section 7.3, to indicate that the fast system was synchronised, the slow system was programmed to records transients only if the fast system was synchronised.

To detect synchronisation four criteria must be satisfied; the system must have the correct values of A^*, $T_{lag}{}^*$ and $f_p{}^*$, and the values must not be changing rapidly. $f_p{}^*$ was considered synchronised if the period count had changed by less than two over the previous four cycles. If the values of NS^* and PS^* are less than the product of the number of samples and the threshold value A^* was considered synchronised. If the zero crossing occurs after samples six, seven or eight. $T_{lag}{}^*$ was considered synchronised, when all conditions are satisfied the SYNC output was asserted, otherwise the output was negated. The routine processing time was measured as 113μs.

9.6 Fast System Testing

The system was tested with synthetic signals to determine that it operated correctly before it was connected to the slow system. Both the detection of transients and the time to synchronise were investigated.

9.6.1 System Synchronisation

The signal generator was applied to channel 0 of the data acquisition system and f_p was set to 49.8 ± 0.05Hz using a digital CRO and the SYNC output of the system was monitored. The time between the program starting and the assertion of the SYNC output were measured for different signal amplitudes, figure 9.9. The initial flat period on the graph, of duration 354 ms is the time to determine the frequency of the signal, T_{freq}^*. During this period the predicted values were incorrect and the amplitude detection routine does not operate correctly. After this flat period the time to synchronise is determined by the time to find the amplitude of the signal. The gradient was measured as $0.51 Vs^{-1}$. Equations [9.5] and [9.8] indicate the flat period and gradient should be 357ms and $0.50 Vs^{-1}$ respectively.

9.6.2 Transient Detection

A signal generator was used to apply an approximate 50Hz signal to channel 0 on the data acquisition system and a small circuit constructed to generate voltage transients. Two digital CROs, both triggered by the fast system TRAN output, were used to monitor the input signal, sample clock and TRAN output. Figure 9.10 is an oscillogram showing the input signal with transient and the clock. The oscilloscope was triggered at the instant the transient was detected by the fast system, within one clock cycle of it occurring.

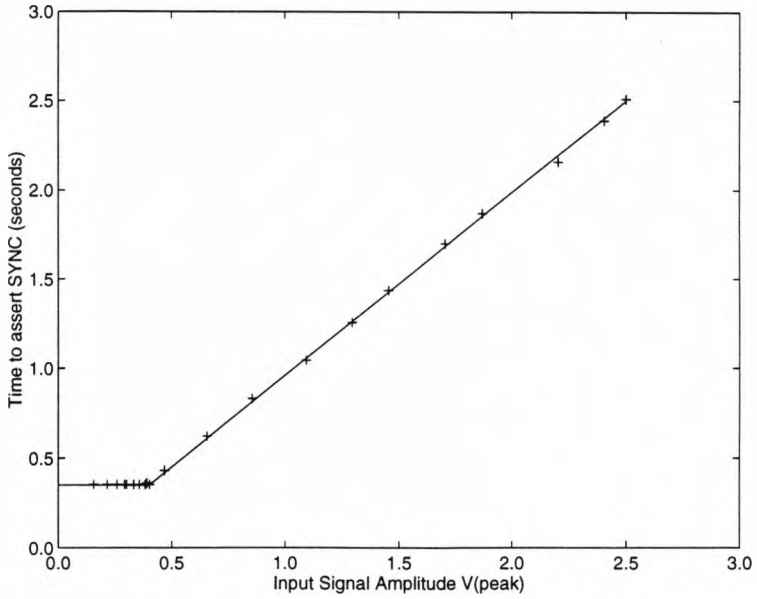

Figure 9.9 Time for Fast System to Synchronise for Different Signal Magnitudes

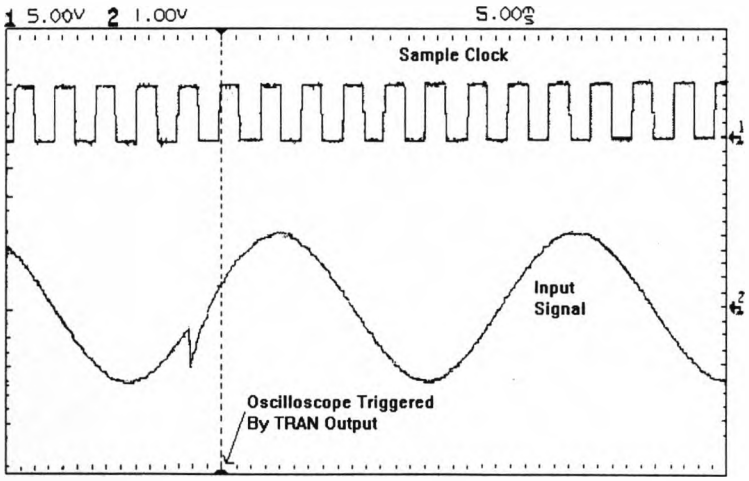

Figure 9.10 Oscillogram Showing Detection of Transient by Fast System
Timebase 1ms/mark Sample Clock 1V/mark Input Signal 1V/mark

9.7 Summary

The fast processing system detected transient changes in the signal from sensor element zero. The system tolerated slow changes in the amplitude and frequency of signal. Measurements confirmed that the total processing time was always much less

than the sample period, 1.43ms, the longest processing time occurs in sample period one and was 566µs.

10. Laboratory Investigations

Testing the non contact system required a power system on which all the abnormal operating conditions listed in table 3.1 could be created. Additionally a conventional method of measuring the voltage had to be provided to determine the accuracy of the non contact system.

On a modern well maintained power system faults and abnormal operation occur infrequently, it is not possible to artificially create these events as disruption will be transmitted to the users of the power system. However analysis, section 4.7, showed that if the geometry and voltage of the power system are scaled by the same factor, the field at equivalent points in the scaled and full sized systems will be identical.

A laboratory scale model of a power system was constructed and, as the system does not supply any users, circuits were constructed to produce abnormal operating conditions. The scale system voltage was relatively low and conventional high voltage resistive dividers were used to produce low voltage replicas of each conductor's voltage. A conventional voltage recording system, the *contact monitoring system*, was developed to monitor these voltages. Figure 10.1 is a block diagram of the laboratory experimental apparatus and its interconnection.

10.1 Laboratory Scale Power System

Figure 10.2 shows the scale system which, for safety reasons, was operated inside an earthed 'cage' with the energisation system interlocked to the cage door. The conductors and their supports were mounted on a table, the under side of the table

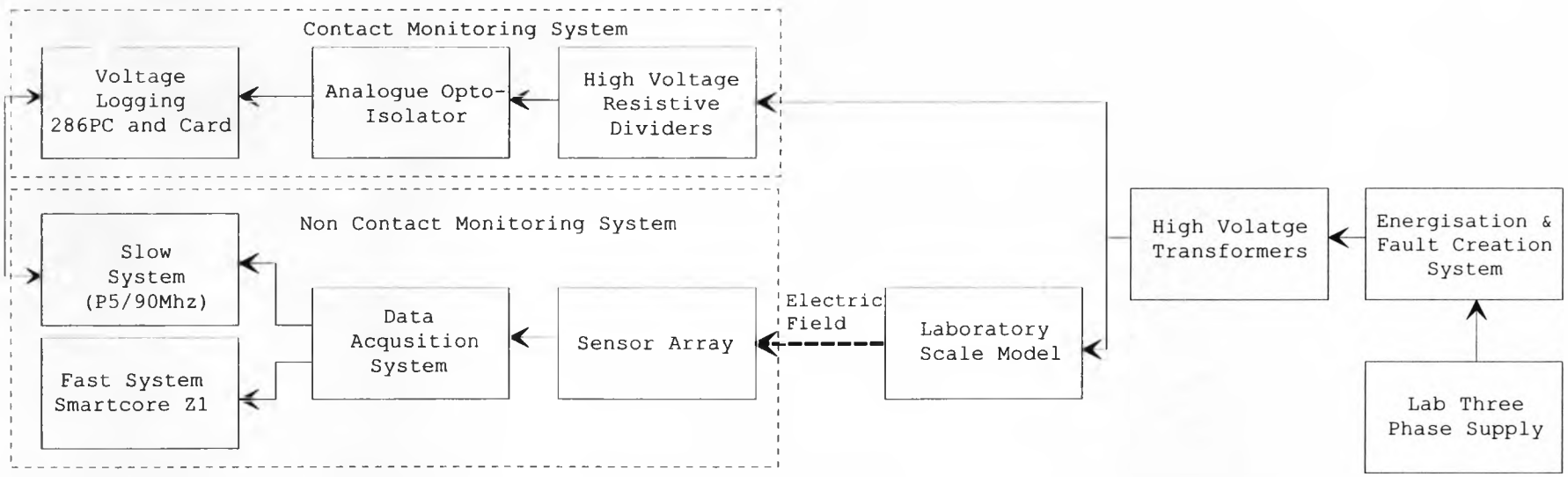

Figure 10.1 Block Diagram of Laboratory Experimental Apparatus

was used to mount the resistive dividers, and the energisation system was placed on the cage floor.

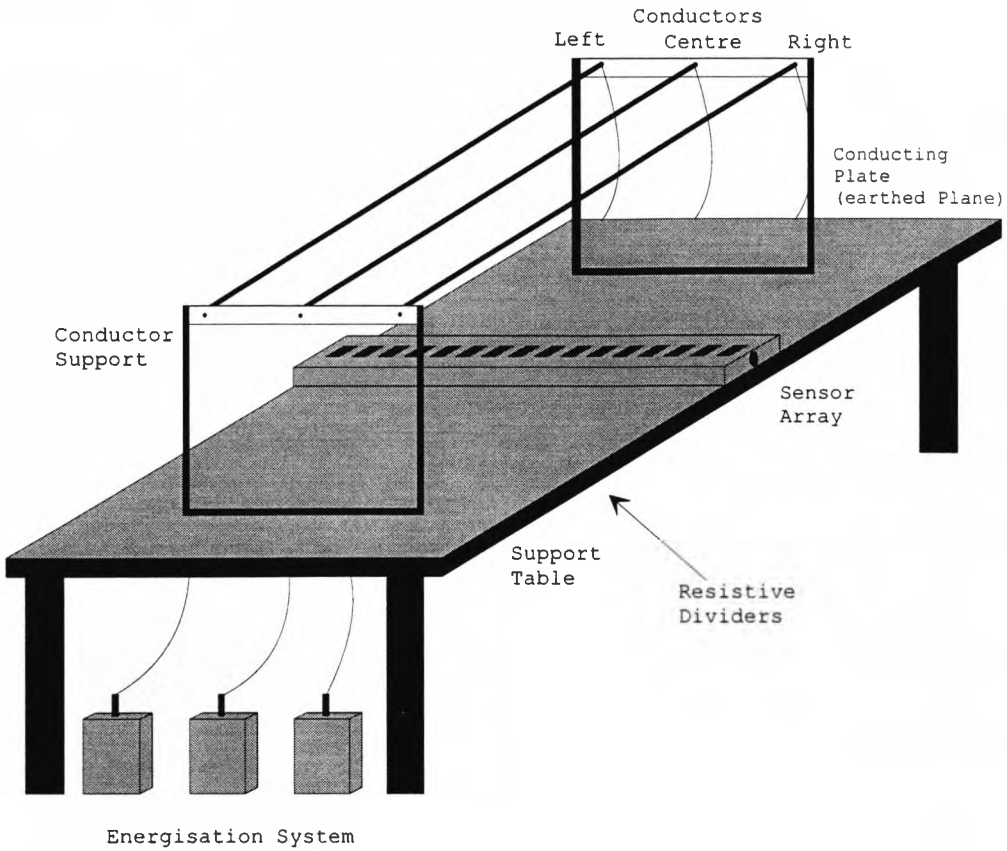

Figure 10.2 Diagram of Laboratory Scale Model and Cage

10.1.1 Physical Construction

Figure 10.3 is an end view of the scale system and the cage; the scale system dimensions were approximately one tenth of those of the power system described in section 4.1 and are listed in table 10.1.

The conductors were held in perspex insulators, supported by 25mm square steel tubes. To form the earth plane the table was covered with a 2mm aluminium plate, connected to the laboratory experimental earth. The sensor array, section 7.1, was mounted on the table, the centre of the first sensor element was 451mm to the left of

the centre conductor. Insulating conduit routed the outputs of the sensor elements to the non contact monitoring system positioned outside the cage.

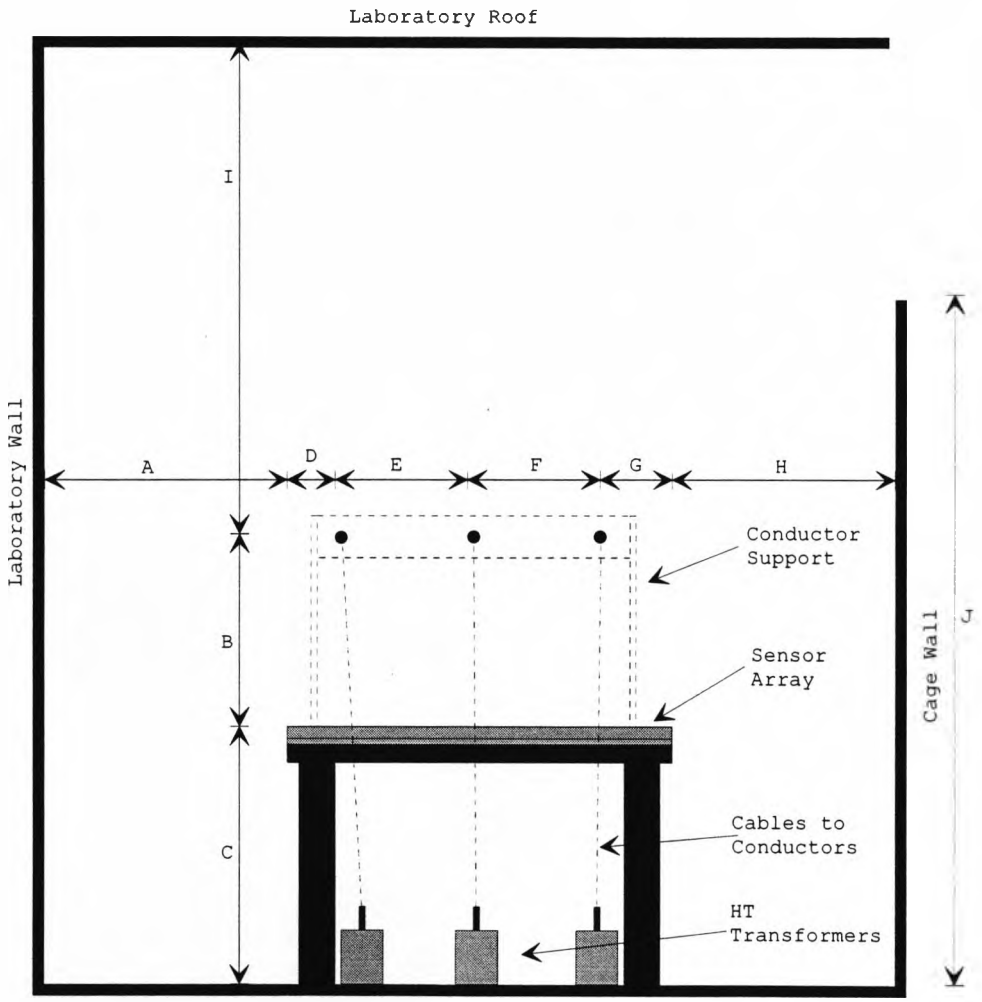

Figure 10.3 Dimensioned End View of Laboratory Scale Model and Cage

10.1.2 Laboratory System Energisation

Figure 10.4 is a circuit diagram of the conductor energisation system. The laboratory 415V three phase supply was connected through the cage safety interlock to a three phase variable auto transformer with the control located outside the cage.

Key	Description	Value(m)
A	Edge of Table to Left Hand (Lab) Wall	0.450
B	Conductor to Array	0.350
C	Array to Floor	1.100
D	Edge of Table to Left Conductor	0.250
E	Left to Centre Conductor	0.200
F	Centre to Right Conductor	0.200
G	Edge of Table to Right Conductor	0.250
H	Edge of Table to Right (Cage) Wall	1.180
I	Conductors to Lab Roof	6.800
J	Cage Wall Height	2.400
	Conductor Diameter	0.010
	Conductor Length	1.600

Table 10.1 Laboratory Scale Model Dimensions

The auto transformer outputs supplied three individual step up transformers with their outputs connected to the conductors. The maximum peak conductor voltage was 11kV but most investigations were performed at approximately 10kV. To prevent corona generation the high voltage terminals on the transformers and the conductors were encased in silicone rubber.

Direct modification of high voltages requires specialist high voltage equipment, for the scale model this was costly and impractical. As negligible current was drawn from the step up transformer outputs the ratio between the output and input voltages remained constant, therefore changes in the conductor voltages were produced by changing the input voltage to the transformers.

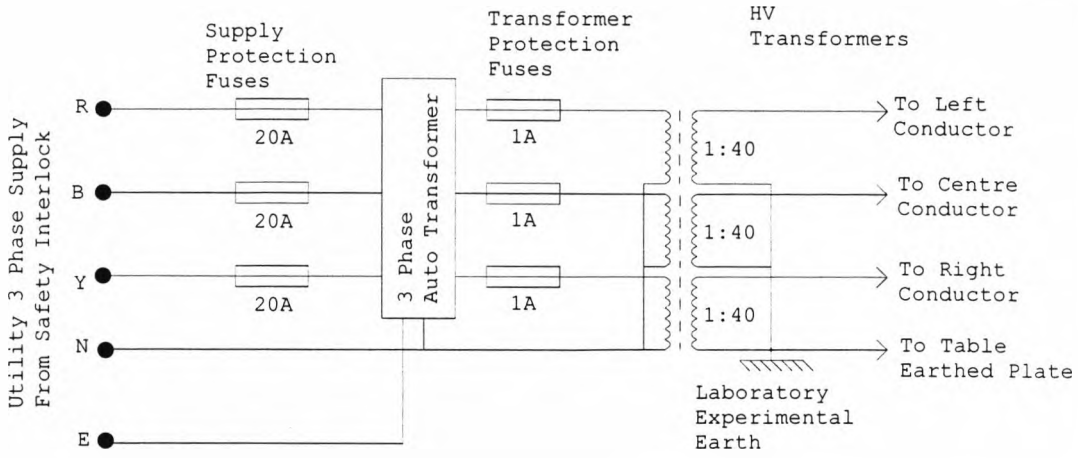

Figure 10.4 Energisation System for Laboratory Scale Model

Experimentation required both large voltage changes, up to 100% of the supply voltage, to simulate faults and small changes, less than 2%, to generate sags and swells. A different technique was used for each type of change.

Adjustment of the three phase auto transformer was used to produce large simultaneous changes in all conductor voltages. Large changes in individual conductor voltages were produced by incorporating one or more single phase, auto transformers, figure 10.5a.

It was not possible to accurately control the auto transformer to generate small changes in the conductor voltages (sags and swells). Instead the input voltage to the transformers was changed by loading the laboratory supply, using high power 20Ω resistive loads. Current drawn by the load lowered the voltage at the output of the auto transformer and hence the conductor voltages. 'Step' voltage changes were achieved by switching the load on and off, gradual changes in voltage were created by using an additional auto transformer to control the current drawn by the load,

figure 10.5b. Voltage swells were created by simultaneously loading all three phases then reducing the load on the phase that was to swell. Investigation showed that changes of up to ± 2% could be created in this manner.

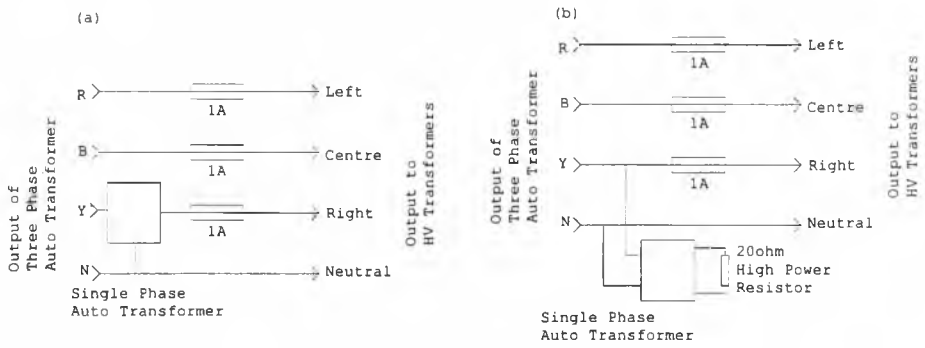

Figure 10.5 Example Energisation System to Generate Changes in Individual Conductor Voltages for Laboratory Scale Model

The supply used to energise the laboratory scale model also supplied other users within the building; as these local users loads varied the voltage within the laboratory, and hence the input to the step up transformers also varied. Changes in the supply voltage due to national load changes also occurred. Direct monitoring showed that the total change did not exceed ± 2% of the voltage's long term average value.

10.1.3 Laboratory System Contact Monitoring System

For comparison with the results of the non contact system the conductor voltages were directly measured. Each conductor was connected to ground through a resistive divider, the upper arm was constructed with 30×1MΩ 2W carbon film resistors connected in series and the lower arm consisted of 4×56 kΩ 0.5W carbon film resistors connected in parallel (combined resistance 14kΩ). These values resulted in a ratio of input to output voltage of $1 : 466\times10^{-6}$. Thus for a 10kV conductor voltage the output voltage of the divider was 4.66V. During operation temperature increases

in the 1MΩ and 56kΩ resistors never exceeded 4K and 0.5K respectively. The temperature coefficient of the 1MΩ resistors was 200ppmK^{-1}, and the 56kΩ 800ppmK^{-1}, these values gave a maximum error in the measured voltages of 0.03%, less than the design resolution of the non contact system. The resistors were mounted underneath the table on a 'bakelight' plate and, to prevent corona production, all high voltage connections and joints between resistors were surrounded with silicon rubber.

The output of the dividers was suitable for connection to conventional instrumentation, however failure of the dividers would have resulted in the 10kV conductor potential being applied to the instrument. To prevent this happening a three channel analogue optical isolator was developed.

Figure 10.6 is a block diagram of one channel of the analogue optical isolator, the voltage signal from each resistive divider was buffered by a high input impedance operational amplifier and used to modulate a voltage to frequency converter that controlled a light emitting diode, LED. The optical signal from the LED was transmitted by 100mm of optical fibre to a receiver where a photo diode, amplifier and frequency to voltage converter produced a replica of the input voltage signal. To maintain isolation between the two halves of the system, components on the driver side of the fibre were powered by a 12V 12Ah rechargeable battery, power for the receiver was derived from the laboratory supply. The transmitter required 250mA, allowing the system to operate for approximately 48 hours between battery recharges. The system had a dynamic range of -6V to 6V, controls to 'trim' the gain and offset of the circuit and a bandwidth of 4kHz, full circuit diagrams are contained in

appendix 4. The compete system was calibrated using an oscilloscope with a high voltage probe, the offset in the circuit was set to zero.

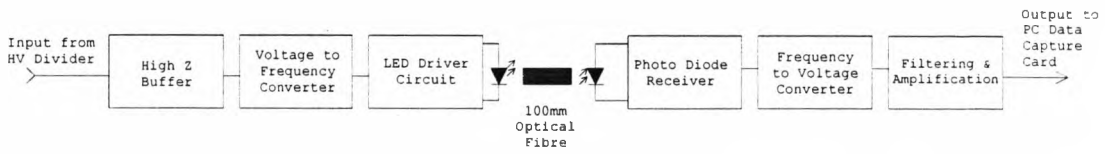

Figure 10.6 One Channel of Three Channel Analogue Opto Isolator

A commercial data acquisition card with eight analogue inputs and 24 digital inputs/outputs, Amplicon PC30-PGL, and an 80286 based personal computer were used to monitor the conductor voltages. The card was configured to simultaneously sample the three conductor voltages at a 700 Hz sampling frequency, approximately the same sampling frequency as the non contact system. To interlock the contact and non contact systems the most significant bit of the non contact system data acquisition system address counter was connected to a digital input on the acquisition card. This signal toggled each time a data-set was processed by the non contact system.

The data acquisition card and 80286 PC were not capable of simultaneously acquiring data and processing it. Voltage samples had to be acquired, stored and processed later. The 80286 also had limited storage memory, it was only large enough to store voltages sampled at 700Hz over a period of a few minutes. For long term (many days) monitoring the interlocking toggle signal from the non contact system was monitored. In the time the non contact system took to process two data-sets the contact system acquired one block of 256 voltage samples from each conductor. The acquisition was coincident with the time period during which the non contact system acquired the first of its two blocks. The contact system then processed the voltage

samples acquired to find the fundamental frequency and the primary voltage. These values were saved to the memory of the contact system, the changes in primary voltage from the long term mean was determined by later "off line" processing of the stored values.

For medium term (many hours) monitoring software was written to store the sets of 256 time domain voltage samples in the contact system memory at regular intervals. The harmonic content of the conductor voltages was determined by "off line" processing the voltage samples. The total number of sets of voltage samples that may be stored is limited by the available memory in the 80286.

For short term investigations, for example when testing the fast system, the outputs of the analogue opto isolator were monitored using two digital storage oscilloscopes.

10.2 Typical Results Output

Each time a data-set was processed by the non contact system a voltage summary was produced containing the percentage change from normal of the individual conductor primary voltages, the average amplitude of each harmonic as a percentage of the average of the three conductor primary voltages, the frequency of the power system; and the number of transients (section 8.6). At the sampling rate of 699Hz 236,250 voltage summaries were produced in a full day. It is not practicable to plot this number of values, the results shown are produced by plotting every tenth value of the particular quantity, that is results are plotted every 3.66 seconds.

Figures 10.7 and 10.8 show the changes in individual conductor primary voltages determined by both the non contact and contact systems. These are shown for a 24 hour period. Figures 10.9 and 10.10 show the average harmonic content, frequency and number of transients occurring over the same period determined using the non contact system only.

10.3 Tests Performed using the Laboratory System

A range of tests was performed using the scale model, tests were performed with both systems operating in real time; in addition the signal descriptors generated every time the non contact system analysed a data-set were stored to allow detailed examination of the system performance.

The individual conductor primary voltages were measured by the contact system for many days and each conductor's primary voltage was averaged over each twenty four hour period. The twenty four hour averages were examined to investigate the effect of using such averages as normal values in the non contact system processing.

The scale model was monitored for long periods, enabling the effects of local and national load changes to be observed. Changes in the individual conductor primary voltages were determined using both systems and the results compared to determine the extent to which they agreed.

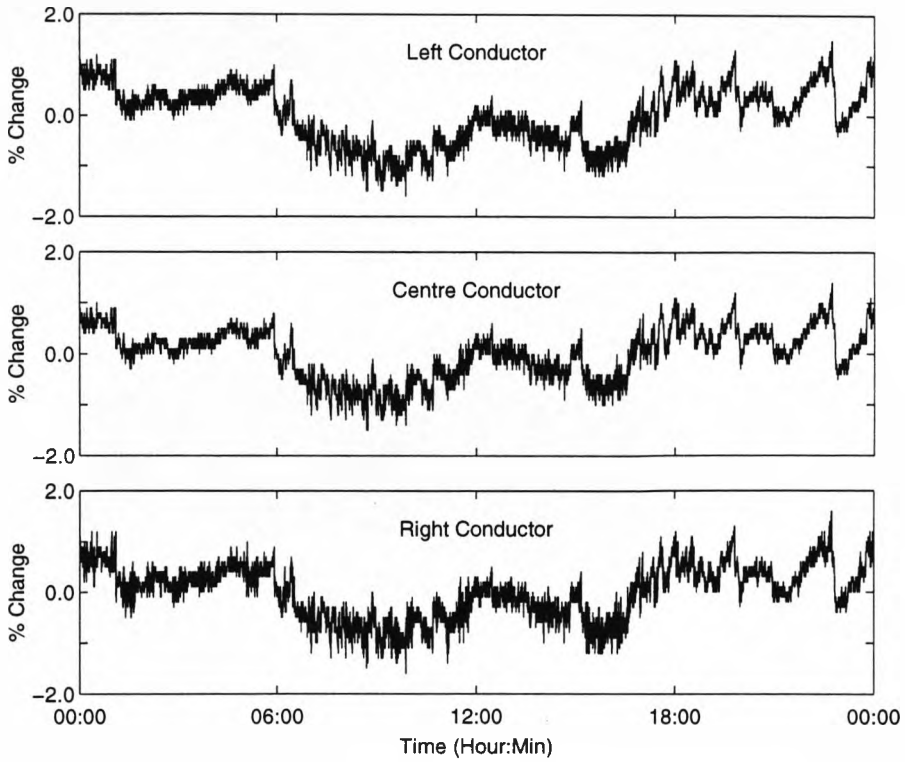

Figure 10.7 Typical Results, Change in Primary Conductor Voltages Determined by Non Contact System

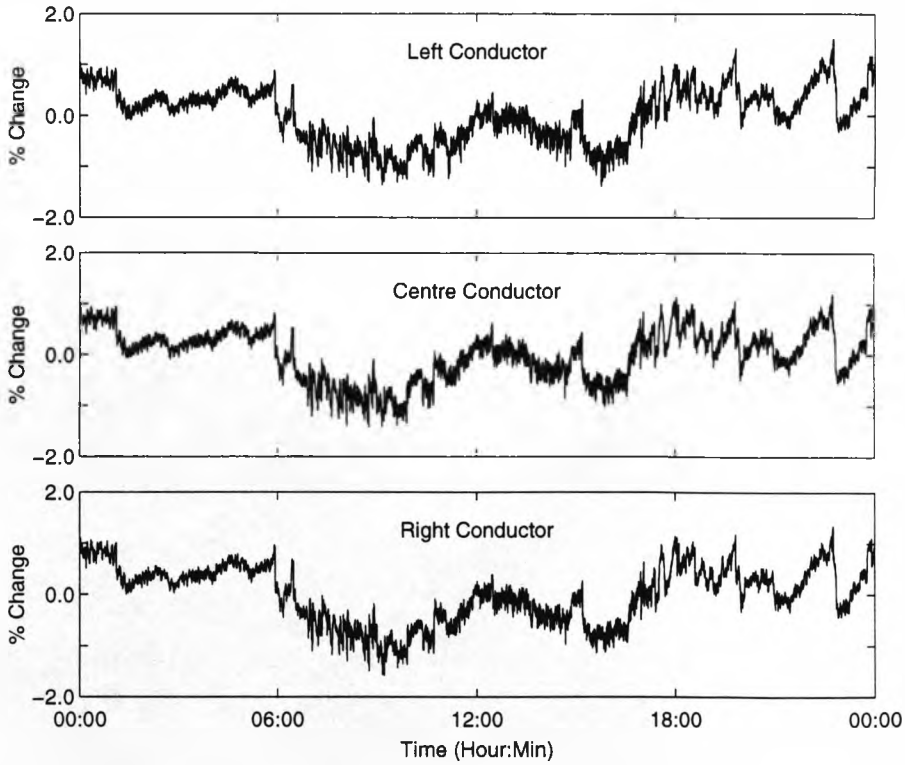

Figure 10.8 Typical Results, Change in Primary Conductor Voltages Determined by Contact System

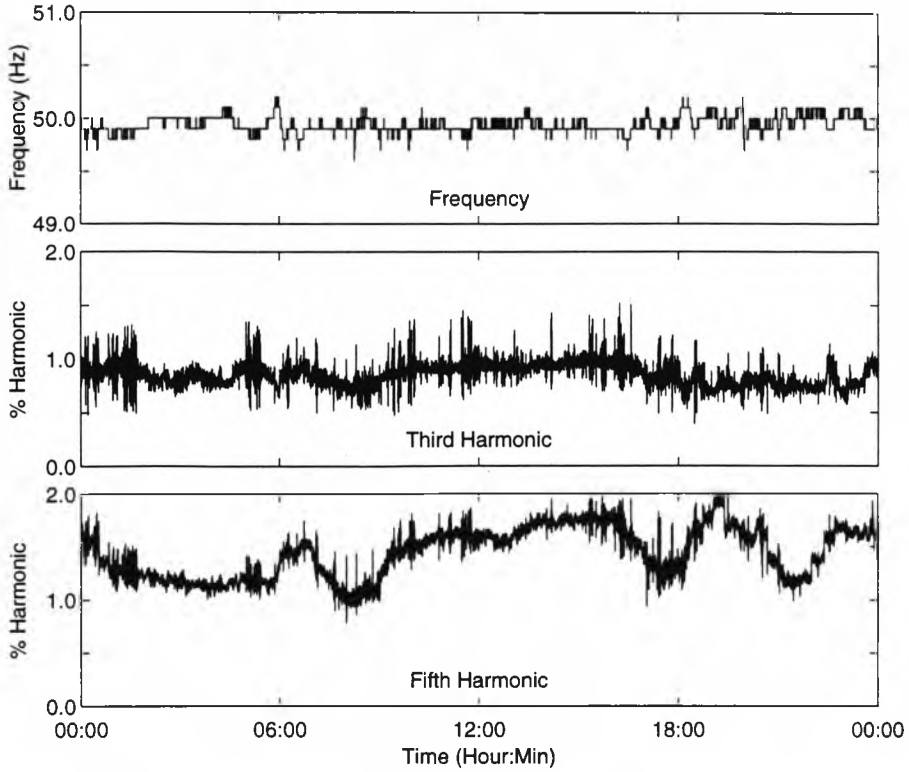

Figure 10.9 Typical Results, Frequency and Average Odd Harmonics Determined by Non Contact System

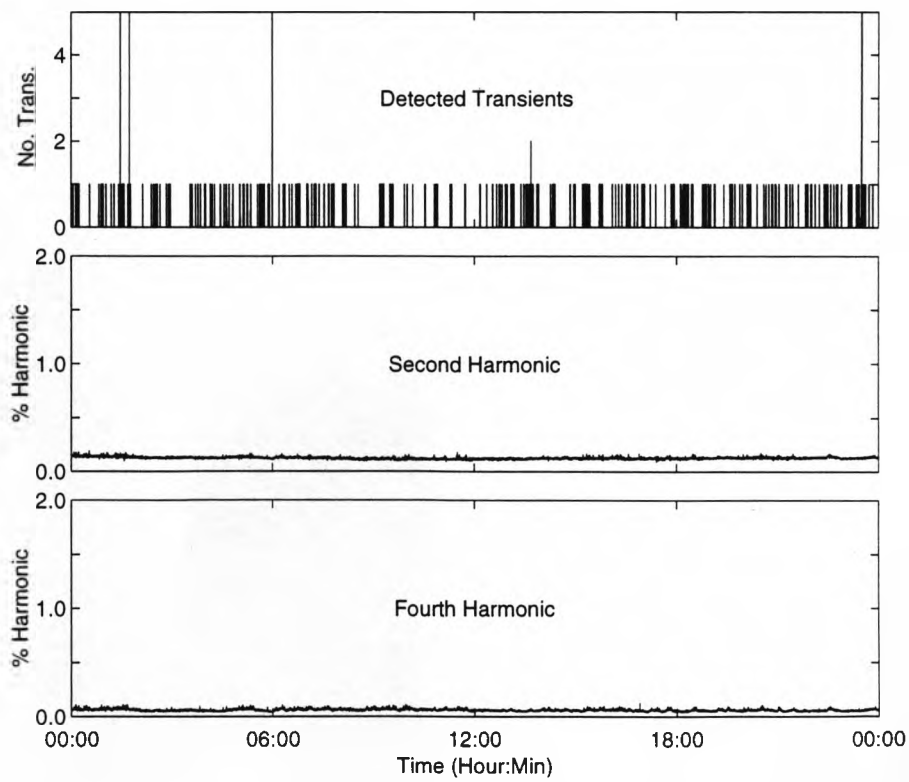

Figure 10.10 Typical Results, Average Even Harmonics and Detected Transients Determined by Non Contact System

Sets of 256 samples of the conductor voltages were stored by the contact system at five minute intervals for 24 hours, these samples were processed off line using commercial signal processing software, Matlab by the Mathworks Co. The harmonic content of the individual conductor voltages was determined and compared to the average value determined by the non contact system.

Transients occurring on the supply were detected by the fast processing system which was used to trigger the two digital storage oscilloscopes monitoring the conductor voltages.

In addition to monitoring the behaviour of the local power system, deliberate actions were taken to artificially create conditions corresponding to sags, swells, voltage imbalances, transients and supply failures. Results obtained with both systems were again compared.

10.4 Parameters for Comparison of Results

If the true change in a conductors primary voltage in the time period covered by data-set n is $\Delta V_A[n]$ and the changes measured and determined by the contact and non contact systems are $\Delta V_N[n]$ and $\Delta V_C[n]$ respectively, then if both systems were ideal

$$\Delta V_N[n] = \Delta V_A[n] \qquad [10.1]$$

$$\Delta V_C[n] = \Delta V_A[n] \qquad [10.2]$$

In any real measurement differences will exist between $\Delta V_A[n]$ and values from the two systems. **Piotrowski(1992)** describes the modelling of a measurement system

and indicates that the relationship between a measurand, $x(t)$, and a measured value, $y(t)$ may be approximated by

$$y(t) = k_0 + (1 + k_1)x(t) + k_2 x(t)^2 + k_3 x(t)^3 + \ldots\ldots + k_R(t) \qquad [10.3]$$

where k_0, k_1, k_2 etc. are constants and $k_R(t)$ represents random errors caused, for example, by noise on the signal.

During calibration the outputs of the analogue opto isolator were adjusted to remove any offsets, thus for the contact system k_0 was zero. When the contact system was calibrated it was shown, within measurement accuracy, to be linear, any differences due to the application of a signal were also assumed to be linear, thus k_2 and higher coefficients were assumed to be zero.

The sensor elements were tested and the outputs shown to be linear functions of the electric field with no offset. However the relationship between the changes in electric field sensor signals and changes in the conductor voltages is not linear, thus k_0 for the non contact system may not be assumed to be zero. Initial investigations showed that the non contact system gave similar results to the contact system and a first order approximation was assumed, that is k_2 and higher coefficients were neglected. Thus for the non contact system [10.1] is written as

$$\Delta V_N[n] = k_0 + (1 + k_1)\Delta V_A[n] + k_R[n] \qquad [10.4]$$

and for the contact system [10.2] is written as

$$\Delta V_C[n] = (1 + k_1^*)\Delta V_A[n] + k_R^*[n] \qquad [10.5]$$

An indication of the extent to which some of the different terms influence the results is obtained by determining particular average values. For N_V sets of results for each conductor the *mean difference*, D_A is

$$D_A = \frac{1}{N_V}\sum_{n=0}^{N_v-1}\left(\Delta V_N[n] - \Delta V_C[n]\right) \qquad [10.6]$$

Substituting [10.4] , [10.5] into [10.6] D_A is

$$D_A = \frac{1}{N_V}\sum_{n=0}^{N_V-1}\left[k_0 + \left(k_1 - k_1^*\right)\Delta V_A[n] + \left(k_R[n] - k_R^*[n]\right)\right] \qquad [10.7]$$

As the conductor voltages vary about the long term average value, differences due to $(k_1 - k_1^*)\Delta V_A[n]$ will be both positive and negative, for sufficiently large values of N_V the summation of these values will be zero. Random effects should also be symmetrical, thus as N_V increases the sum of the term $(k_R[n] - k_R^*[n])$ will also tend to zero, and D_A will tend to k_0.

For each conductor a measure of the difference between the measurements is the root mean square, rms, difference, D_B

$$D_B = \sqrt{\frac{1}{N_V}\sum_{n=0}^{N_V-1}\left(\Delta V_N[n] - \Delta V_C[n]\right)^2} \qquad [10.8]$$

Substituting [10.3] , [10.4] into [10.7] and squaring D_B^2 is

$$D_B^2 = \frac{1}{N_V}\sum_{n=0}^{N_v-1}\left[k_0^2 + \left(k_1 - k_1^*\right)^2\Delta V_A[n]^2 + \left(k_R[n] - k_R^*[n]\right)^2\right] + \\ + \frac{2}{N_V}\sum_{n=0}^{N_V-1}\left[k_0\left(k_1 - k_1^*\right) + \left(k_R[n] - k_R^*[n]\right)\left\{\left(k_1 - k_1^*\right) + k_0\right\}\right] \qquad [10.9]$$

If N_V is sufficiently large the cross product terms containing k_0 and ($k_R[n]$-$k_R^*[n]$) will sum to zero, thus D_B approximates to

$$D_B = \sqrt{k_0^2 + 2k_0\left(k_1 - k_1^*\right) + \frac{1}{N_V}\sum_{n=0}^{N_V-1}\left[\left(k_1 - k_1^*\right)^2 \Delta V_A^2[n] + \left(k_R[n] - k_R^*[n]\right)^2\right]} \quad [10.10]$$

As the square of the difference is taken random and proportional errors will not sum to zero, thus D_B indicates differences due to random noise, differences in the calibration factors of the two systems and the offset, k_0.

D_A and D_B provide estimates of the differences in the results produced by features of the two monitoring systems. A measure of the overall agreement between the primary voltage changes determined by each system may be found by calculating the correlation between them. For each conductor, **Porkless(1988)** describes the Parsons Product Moment Correlation Coefficient, r, as

$$r = \frac{S_{CN}}{S_C S_N} \quad [10.11]$$

where S_C and S_N are the standard deviations of primary voltage changes calculated by the contact and non contact systems and S_{CN} is the covariance to the two sets of voltage changes. If the mean value of voltage changes is μ_N for the non contact system and μ_C for the contact system S_{CN} is

$$S_{CN} = \frac{1}{N_V}\sum_{n=0}^{N_V-1}\left(\Delta V_N \Delta V_C\right) - \mu_C \mu_N \quad [10.12]$$

The coefficient r has values in the range $-1 \le r \le 1$; a value of 1 indicates a perfect correlation between the results, a value of 0, no correlation and a value of -1 perfect negative correlation. Constant differences between the two sets of results, k_0, and

differences proportional to the magnitude of the change, k_I,k_I^* do not influence the value of r, random differences, $k_R(t)$ and $k_R^*(t)$, do, **Wetherill(1986)**. **Wheldon(1962)** states that the value of r is also determined by the value of N_V, for small N_V a significant relationship between the two sets of results exists if

$$r > \frac{3}{\sqrt{N_V - 1}} \qquad [10.13]$$

For large values of N_V , as in tests of the non contact system, **Wheldon(1962)** states that $r > 0.9$ indicates a significant correlation.

10.5 Investigation of Long Term Average

The slow system software, section 8.1, assumes that, over a sufficiently long period the mean voltage of the conductors is equal to its normal operating value. By averaging the signals from the electric field sensors over this period the electric field corresponding to these normal voltages was found. If the period over which the average value is calculated is too short the value will not be a representation of the long term mean and the offset k_0 in equation [10.4] will be significant.

To test this assumption the conductor voltages were measured by the contact system for five days, table 10.2 shows the primary voltage of each conductor at four hour intervals throughout the first day, changes exceeding 1% were observed.

Time	00:00	04:00	08:00	12:00	16:00	20:00	00:00
Left (kV)	10.37	10.27	10.19	10.14	10.20	10.31	10.29
Centre (kV)	10.24	10.25	10.18	10.15	10.21	10.29	10.27
Right (kV)	10.25	10.24	10.20	10.13	10.20	10.32	10.29

Table 10.2 Conductor Primary Voltages at Four Hours Intervals - Day One

The local utility attempts to produce an average over twenty four hours that is equal to the nominal voltage, consequently a twenty four hour average period was selected for the non contact system, section 8.6.2. Table 10.3 shows the 24 hour average voltage of each conductor for five days and the cumulative average over the period.

The five day average values agree to within ±0.1% for the three conductors. Individual twenty four averages also agree to within ±0.3% of the five day values, hence the use of twenty four average values instead of the true normal values will only have a small effect on the results.

Day Number	1	2	3	4	5
Left : 24 Hour Avg. (kV)	10.24	10.24	10.27	10.23	10.24
Left : Cumulative Avg. (kV)	10.24	10.24	10.25	10.24	10.24
Centre : 24 Hour Avg. (kV)	10.23	10.22	10.26	10.23	10.23
Centre : Cumulative Avg. (kV)	10.23	10.23	10.23	10.23	10.23
Right : 24 Hour Avg. (kV)	10.24	10.25	10.24	10.23	10.24
Right : Cumulative Avg.(kV)	10.24	10.25	10.24	10.24	10.24

Table 10.3 Average Conductor Primary Voltages as Function of Average Period

10.6 Primary Voltage Changes

The scale model was monitored continuously for many days; the results for one week day are presented here, results obtained for the other days are contained in appendix 1. Figure 10.11 shows the individual conductor primary voltage changes determined by the non contact system, figure 10.12 shows the same changes measured by the contact system.

The conductor voltages changed throughout the day as loads changed on the power system. During the *working day* (typically 06:00 - 18:00hrs) loads were high and the voltage was below the average value, the voltage increased during the early evening as local and national loads decreased. During the remainder of the evening there was little change in local loads, known sudden national load changes, for example at the end of popular television programs were often detected during this period.

The differences between the two sets of results were investigated, table 10.4 shows the results parameters for the 24 hour period.

Conductor	Left	Centre	Right
D_A	0.0410	0.0384	0.0890
D_B	0.1392	0.1405	0.1524
r	0.9686	0.9419	0.9457

Table 10.4 Result Parameters for 24 Hour Monitoring of Laboratory Scale Model

D_A is below the measurement resolution of the non contact system, indicating the constant offset in the system, k_0, is small, this is thought to be due to difference between the long term average used by the system and the average of the twenty four hour period, section 10.4. D_B is larger indicating the major contribution to differences is random noise, $k_R[n]$ and $k_R^*[n]$. The value of the correlation coefficient is above the limit stated by **Weldon(1962)** indicating a significant agreement between the two sets of results.

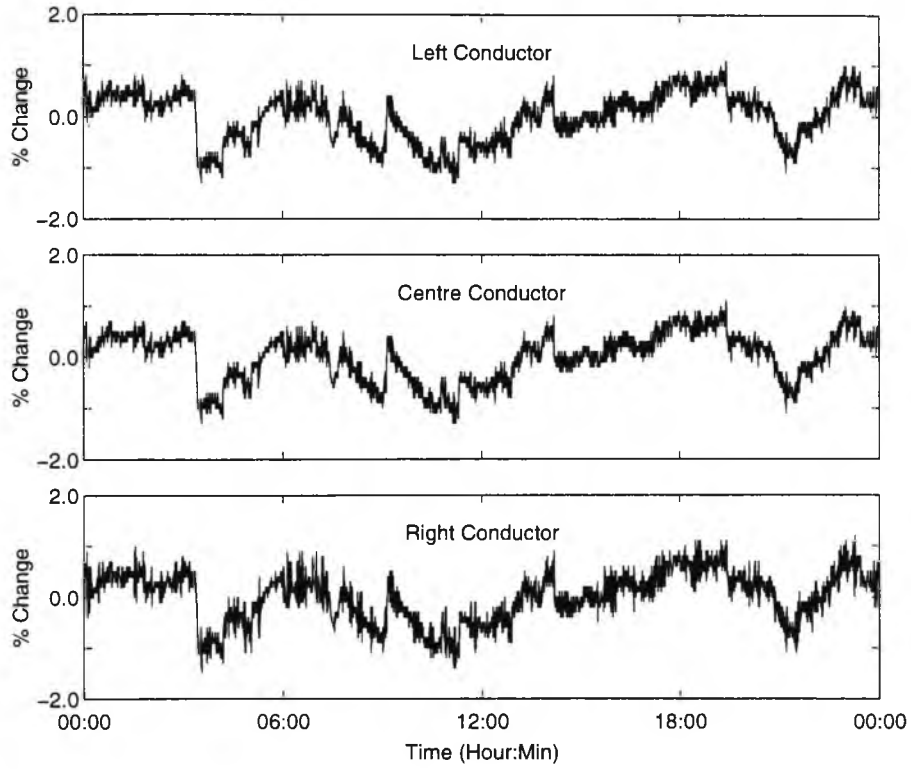

Figure 10.11 Change in Individual Conductor Primary Voltages Determined by Non Contact System

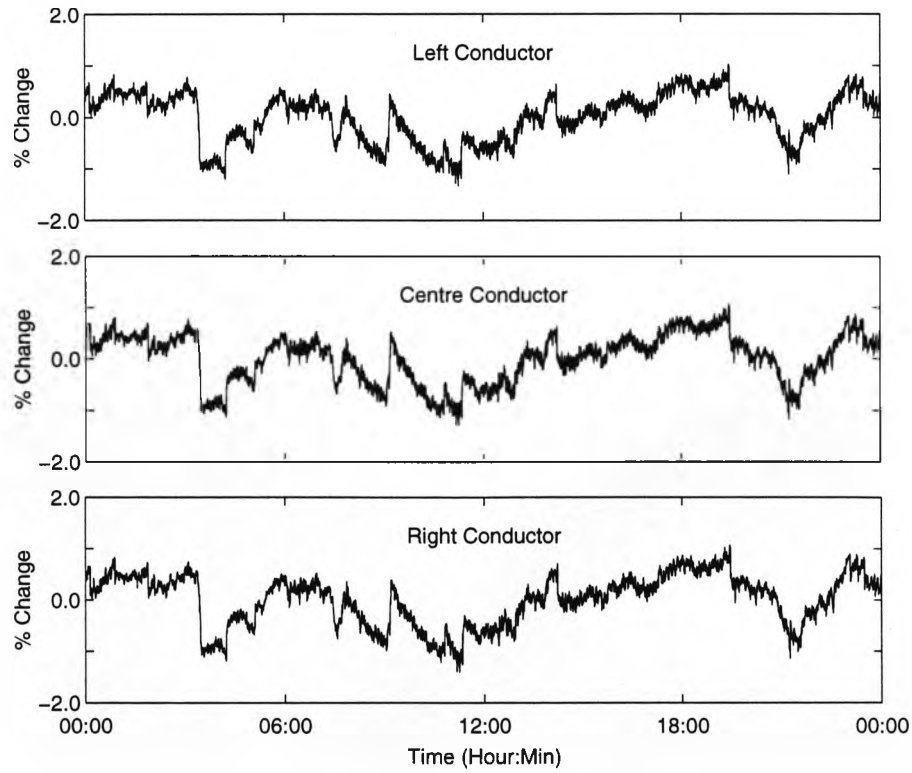

Figure 10.12 Change in Individual Conductor Primary Voltage Determined by Contact System

Monitoring of the conductors by the non contact system allowed the 'quality' of the supply to be measured, section 3.1.2, two features of interest to the supplier and users are the incidence of voltage imbalances and the stability of the supply.

For the calculation of the supply quality, imbalance was defined as a non identical voltage change in the three conductor primary voltages, the magnitude of the imbalance was defined as the maximum difference between any two of the three conductor values. Table 10.5 shows the number of hours during the day during which the voltage imbalance exceeded the indicated value, results are given for a weekday and a Sunday.

Imbalance Size (%) ≥	Total Duration (Hours)	
	Weekday	Sunday
0.1	11.37	6.09
0.2	1.57	1.05
0.3	0.37	0.09
0.4	0.07	0.00
0.5	0.00	0.00

Table 10.5 Voltage Imbalance Size and Duration Determined by Non Contact System

The stability of the supply was measured by the occurrence and size of sags and swells, from the normal voltages. Table 10.6 shows, for all conductors, the number of hours the sags and swells indicated were exceeded for a weekday and a Sunday.

For both imbalances and voltage variations the size and duration were larger on a weekday than on a Sunday when loads are lower.

10.7 Voltage Harmonic Content

The non contact system determined the average harmonic content of the three conductor voltages, as a percentage of the average of the three primary voltages, by averaging the harmonic component of each electric field sensor's signal, section 8.6.3.

Sag / Swell Magnitude (%) ≥	Duration (Hours)	
	Weekday	Sunday
0.2	21.53	19.44
0.4	15.38	12.48
0.6	9.62	6.60
0.8	21.9	2.90
1.0	1.99	0.91
1.2	0.43	0.10
1.4	0.05	0.00

Table 10.6 Voltage Variations, Size and Duration Determined by Non Contact System

The contact system was programmed to save 256 samples of each conductor voltage at five minute intervals, these samples were processed to determine the magnitude of each conductor's harmonic content, as a percentage of the primary voltage. Figures 10.13 to 10.17 show the results for the second to fifth harmonics.

The vector addition of the electric field produced by each conductor and the averaging of all sensor signals means that the results of the two systems could not easily be analytically compared, however changes in the harmonic content of individual conductor voltages resulted in changes in the non contact system average

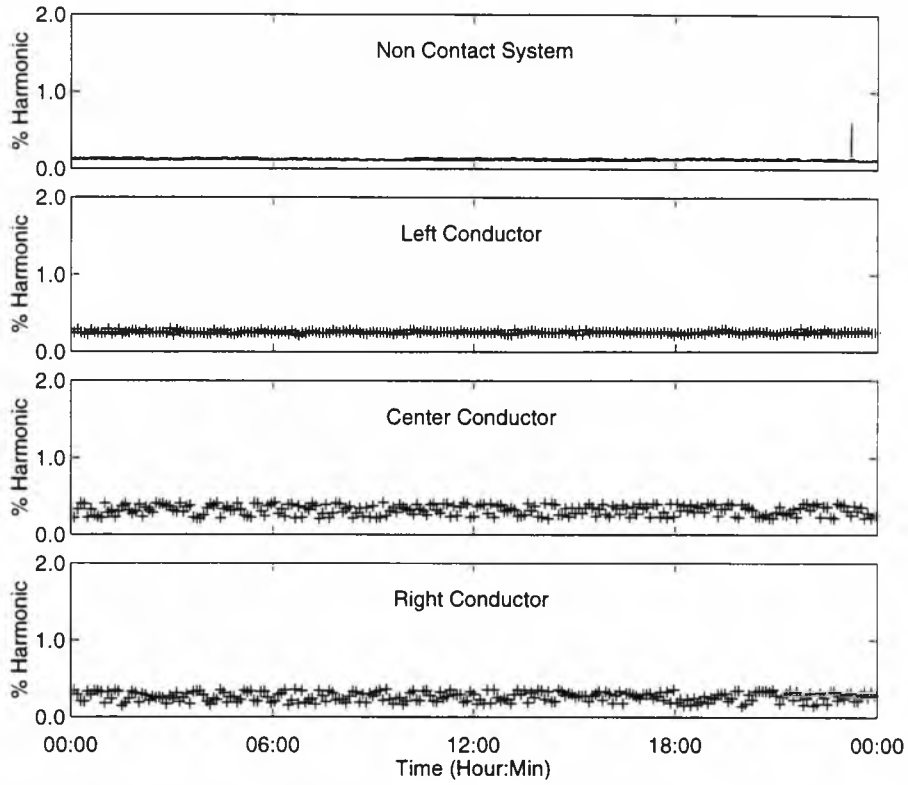

Figure 10.13 Second Harmonic - Average Determined by Non Contact System and Values for Individual Conductors Determined by Contact System

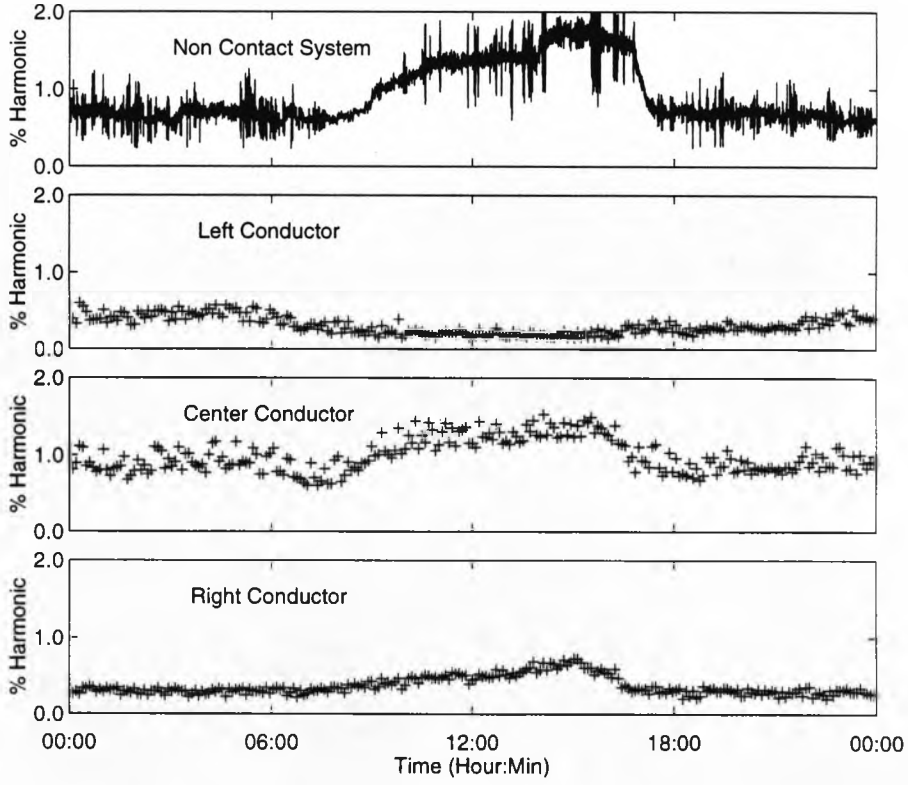

Figure 10.14 Third Harmonic - Average Determined by Non Contact System and Values for Individual Conductors Determined by Contact System

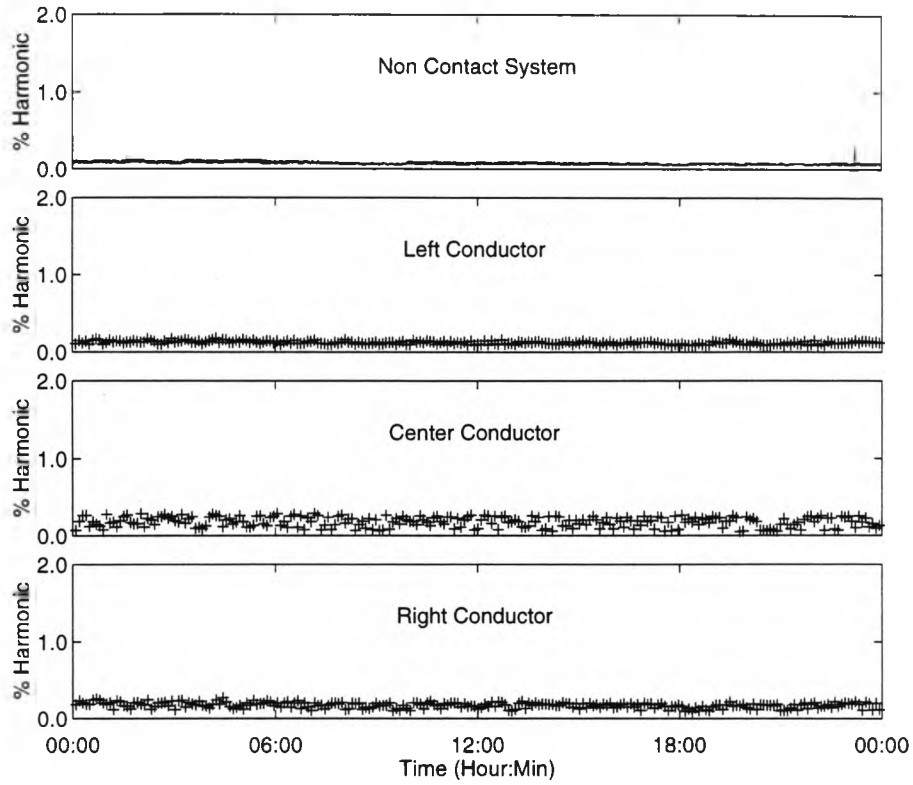

Figure 10.15 Fourth Harmonic - Average Determined By Non Contact System and Values for Individual Conductors Determined by Contact System

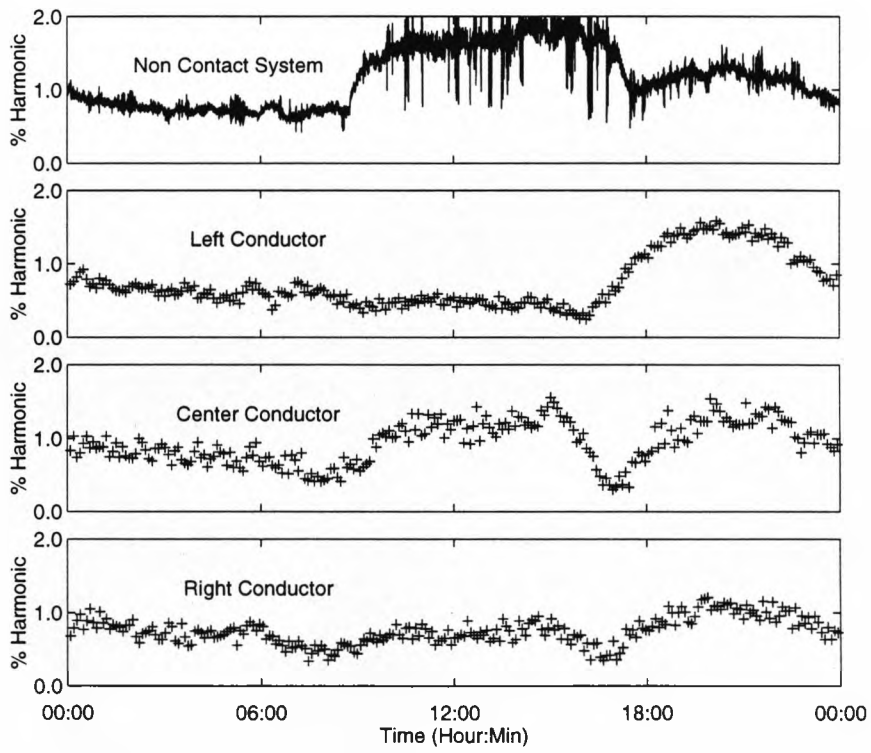

Figure 10.16 Fifth Harmonic - Average Determined by Non Contact System and Values for Individual Conductor Voltages Determined by Contact System

values. The amplitudes of even harmonics were very small, odd harmonics were present and were greater during the working day. A significant proportion of the fifth harmonic was found to be caused by the lighting system used within the laboratory.

10.8 Frequency Deviations

Figure 10.17 shows the frequency of the power system determined by the non contact system and the frequency of the centre conductor determined by the contact system. For all results the local supply frequency stayed within the limits 50 ± 0.3 Hz. The maximum difference between the results was 0.1Hz, the frequency resolution of both systems.

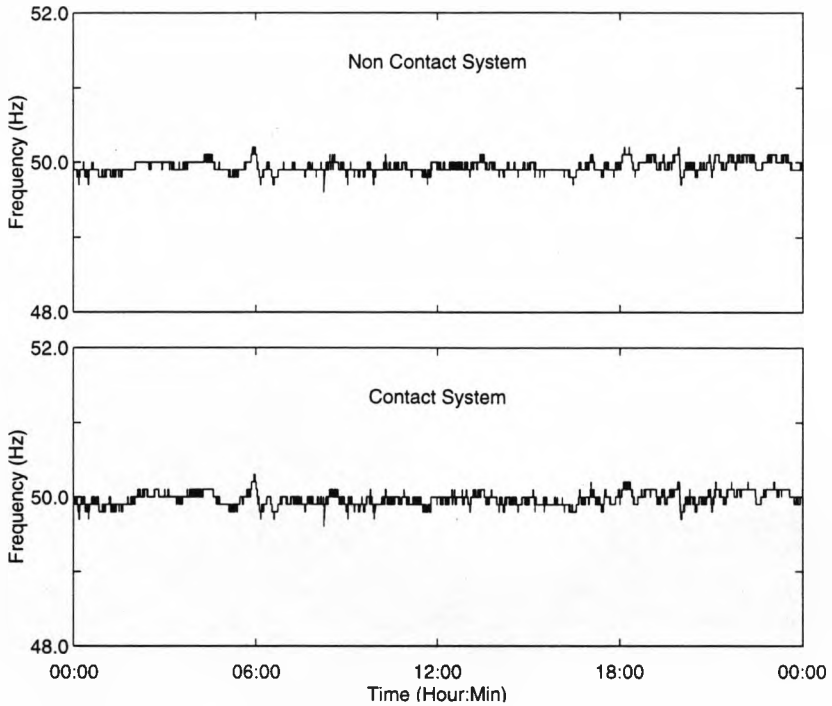

Figure 10.17 Frequency Deviations Measured by Both Systems

10.9 Transient Events

Two digital storage oscilloscopes with a pre-trigger display facility were used to monitor the individual conductor voltages, using the resistive dividers, and the signal from sensor element 0, the oscilloscopes were triggered by the 'transient detected' (TRAN) output of the non contact fast processing system.

Figures 10.18 and 10.19 are oscillograms of each conductor's voltage and the signal from sensor element 0 for a transient occurring on the local utility supply. The triggering point shows the time the transient on the left hand conductor was detected by the fast system.

Transients were also artificially created by momentarily disturbing the transformer supply, the ocsillograms in figures 10.20 and 10.21 show, for a transient created on all conductors, the conductor voltages, and signal from sensor element 0, the trigger point shows the time the transient was detected, the vertical scale on figure 10.20 has been reduced to allow the transient on the left conductor to be clearly seen

During the monitoring of the laboratory scale model transients occurred frequently on the supply, figure 10.22 shows the average number of transients detected per hour for five days monitoring.

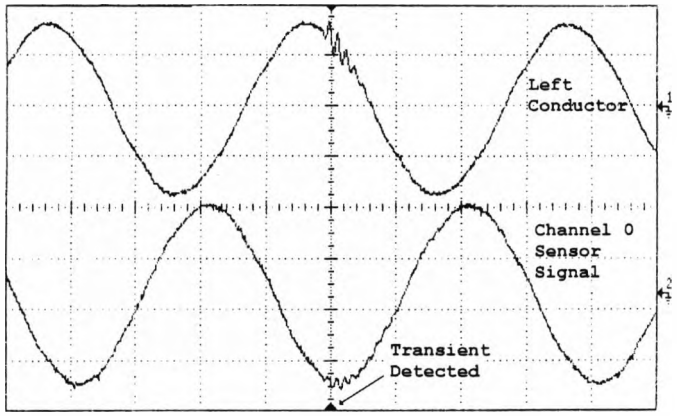

Figure 10.18 Voltage Transient Occurring on One Phase of Local Utility Supply, Left Conductor Voltage (5 kV/div) and Electric Ground Level (5kVm^{-1}/div) timebase 5ms/div

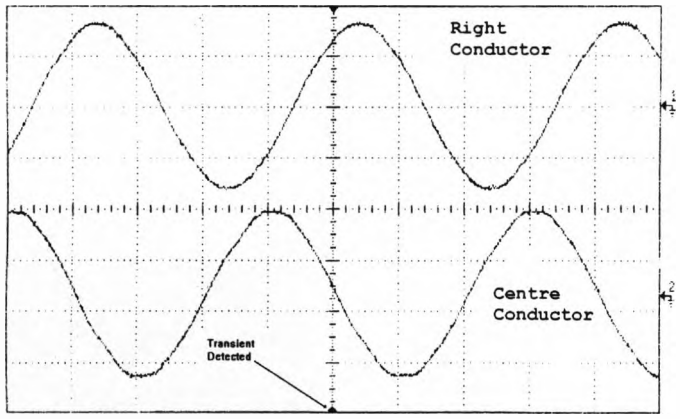

Figure 10.19 Voltage Transient Occurring on One Phase of Local Utility Supply, Left Conductor Voltage and Centre Conductor Voltage (5kV/div), Timebase (5ms/div)

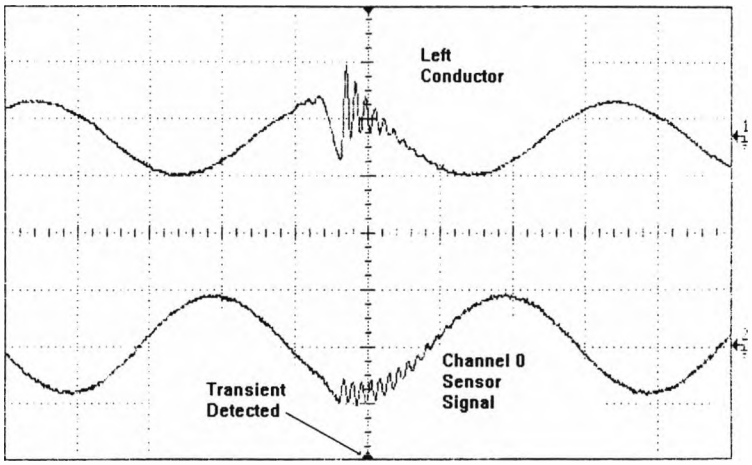

Figure 10.20 Voltage Transient Occurring on All Phases, Left Conductor Voltage (10kV/div) and Electric Field Sensor Signal (10kVm^{-1}/div), Timebase (5ms/div)

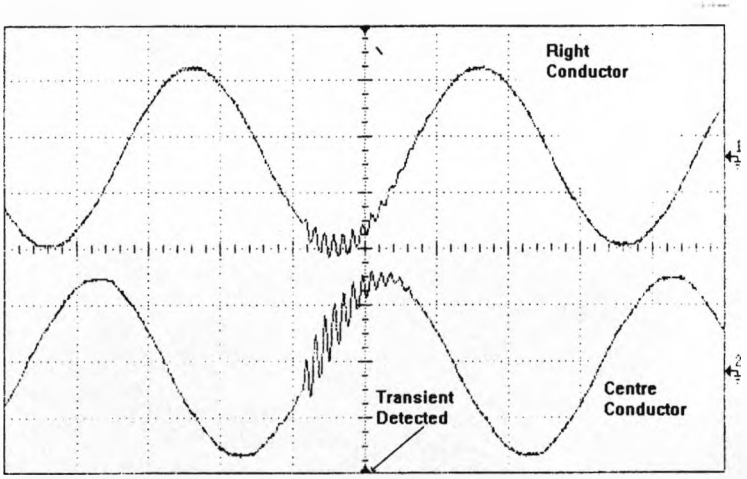

Figure 10.21 Voltage Transient Occurring on All Phases, Right Conductor Voltage and Centre Conductor Voltage (5V/div), timebase (5ms/div)

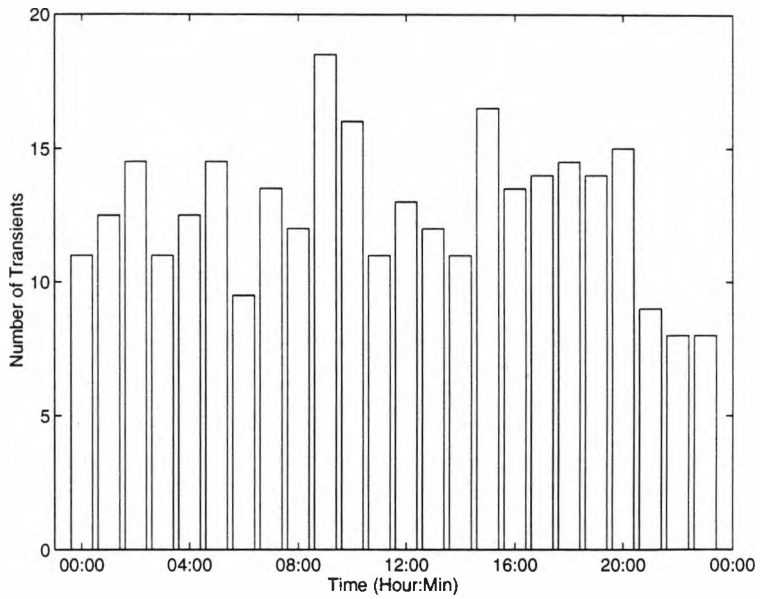

Figure 10.22 Average Number of Transients Per Hour for Five Day's Monitoring

Transients occurred throughout the day, and it is generally not possible to determine their cause, though the sudden increase in transient activity from 09:00 - 10:00 is probably due to local users turning on equipment at the start of the working day.

10.10 Abnormal local supply operation

During one monitoring period the local utility changed the source of supply to the local substation, figures 10.23 and 10.24 show the changes in primary voltage and odd harmonics determined by the non contact system for a 60 minute period which included this change. Investigation revealed that the sudden change in voltages and odd harmonics at 26 minutes from the start of the monitoring period occurred at the time at which the change was implemented, no detectable change occurred in the even harmonics.

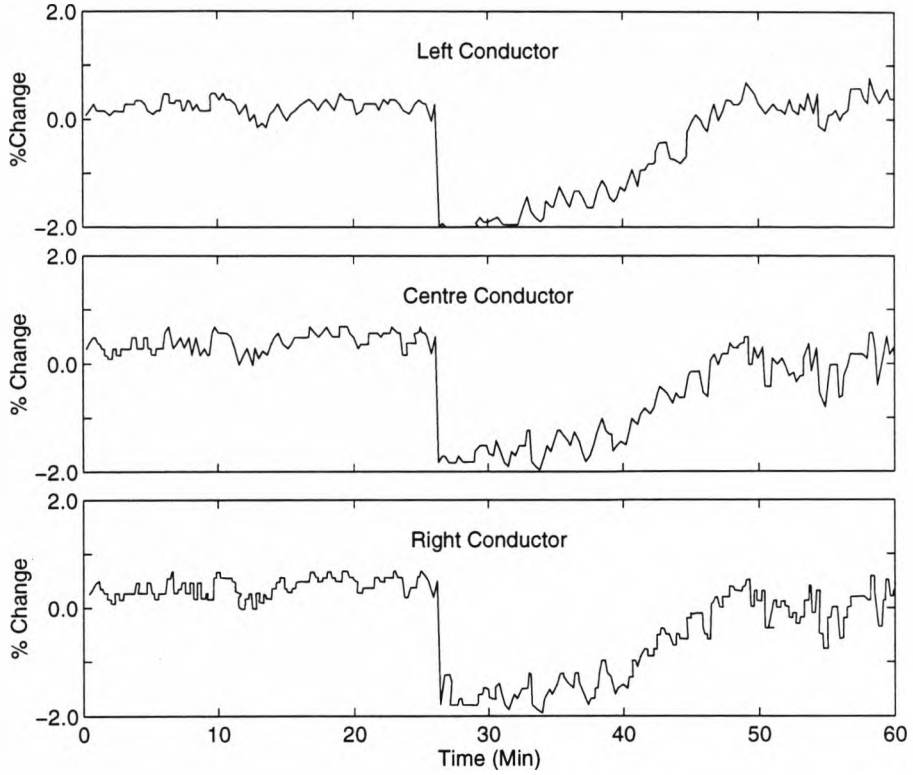

Figure 10.23 Change in Individual Conductor Primary Voltages Determined by Non Contact System for 60 Minute Period Including Switching of Local Utility Supply

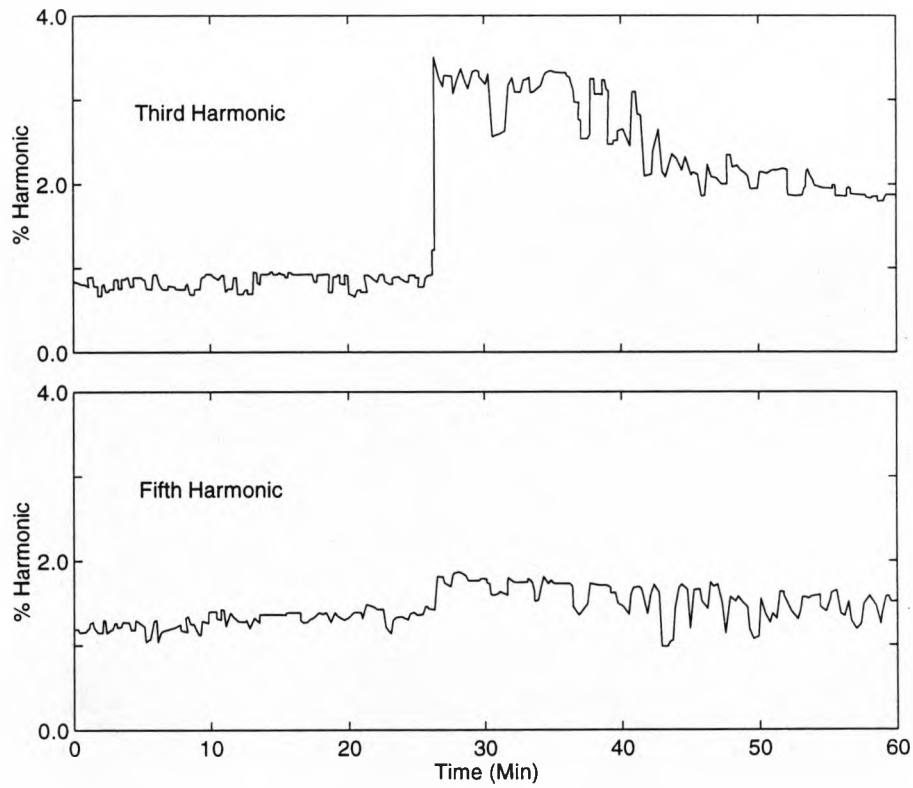

Figure 10.24 Change in Average Odd Harmonics Determined by Non Contact System for 60 Minute Period Including Switching of Local Utility Supply

10.11 Voltage Imbalances

Three individual auto transformers and resistive loads were configured to generate small gradually changing sags and swells in the conductor voltages, section 10.1.2, the tests were performed at a time the local supply was above its normal value. Initially the left and right conductors were loaded to generate a 0.5% sag in the voltages. Over a twenty minute period the load on the left and right conductors was gradually reduced to zero and the load on the centre conductor was increased. Figure 10.25 shows the changes in the primary conductor voltages determined by the non contact system, figure 10.26 the changes measured by the contact system.

A single load was connected suddenly onto the right hand conductor supply for three minutes to give a 'step' voltage imbalance. Figure 10.27 shows the change in primary voltage determined by the non contact system, figure 10.28 the changes measured by the contact system.

For both tests the value of D_A was similar to the value obtained from the twenty four hour monitoring, section 10.6. D_B was higher, approximately 0.2%, and r was lower, 0.91 for all conductors. This is probably due to the lower number of results, section 10.4. The value of r is still above that defined as a significant result.

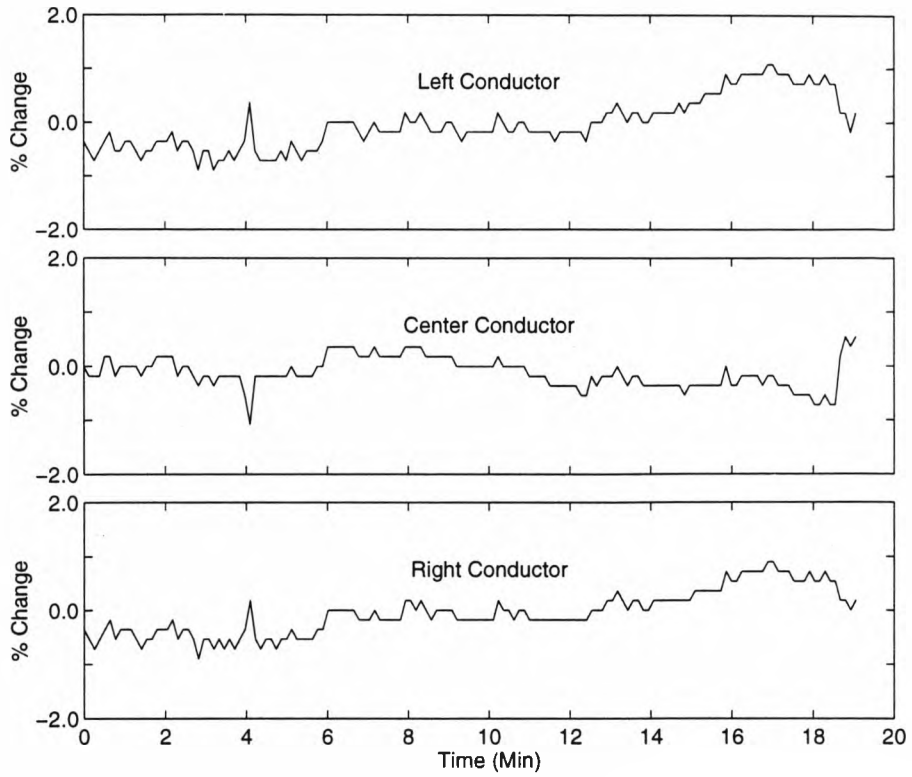

Figure 10.25 Change in Individual Conductor Primary Voltage Determined by Non Contact System During Gradually Changing Voltage Imbalance

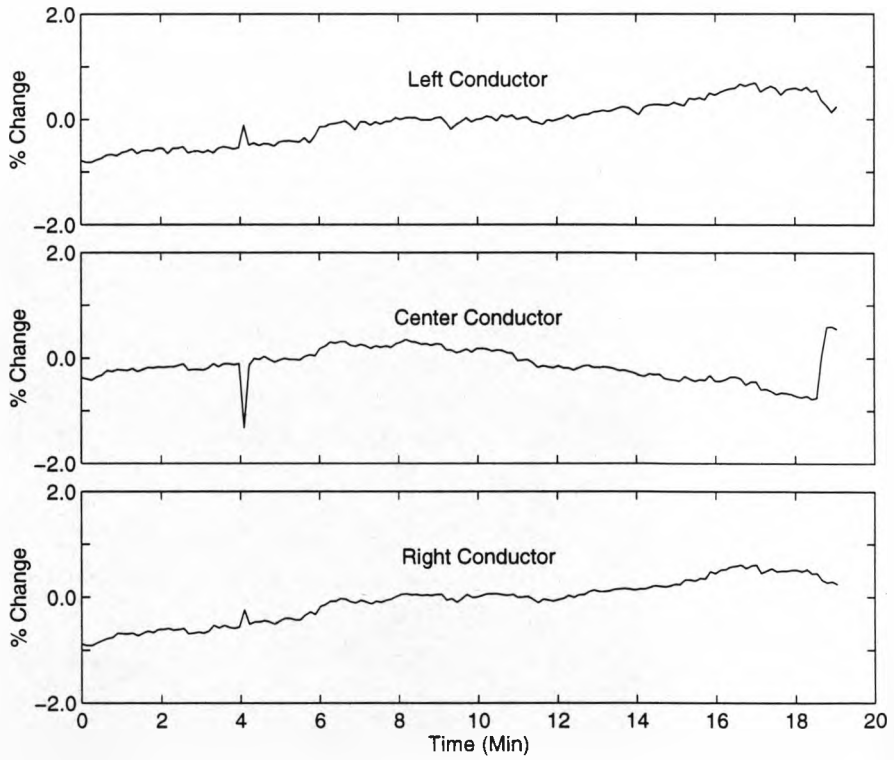

Figure 10.26 Change in Individual Conductor Primary Voltage Determined by Contact System During Gradually Changing Voltage Imbalance

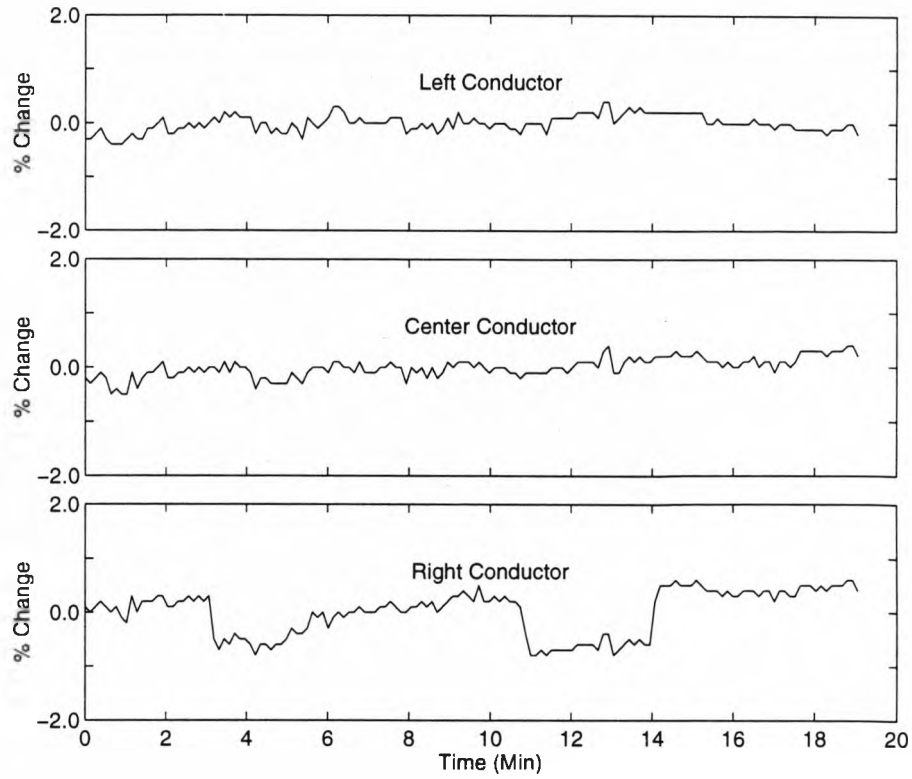

Figure 10.27 Change in Individual Conductor Primary Voltage Determined by Non Contact System During Step Voltage Imbalance

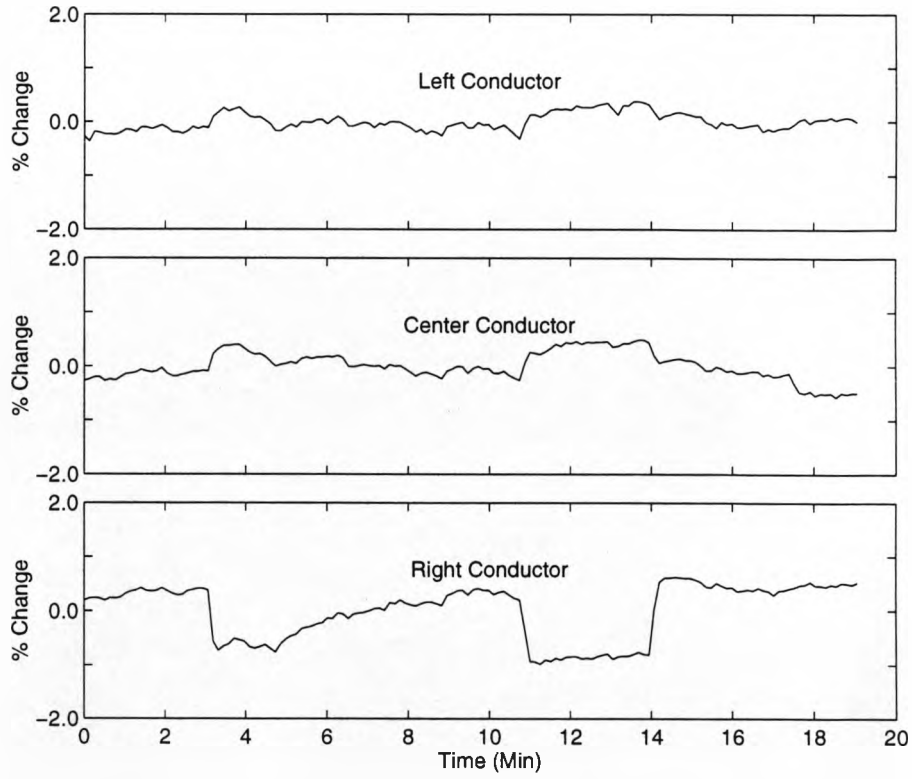

Figure 10.28 Change in Individual Conductor Primary Voltage Determined by Contact System During Step Voltage Imbalance

10.12 Information Redundancy

For a noiseless system three sensor elements, suitably positioned, will provide enough information to determine the changes in individual conductor voltages, section 5.3. As the use of an array of eight sensor elements provided more information than the theoretical minimum, the system should be able to operate with less than eight elements, this hypothesis was investigated.

10.12.1 Analysis Method

Using stored sets of voltage descriptors, *result sets*, a program was written to process the results sets, simulate the removal of a sensor element by removing its signal from the analysis, and determine the change in individual conductor primary voltages. These changes were compared with changes measured by the contact system.

In the analysis an individual sensor element may be either on or off, for eight sensor elements there are $8^2 = 256$ possible on / off combinations. A number of combinations had less than three active elements and were not considered. To further reduce the number of calculations combinations with two adjacent sensor elements in the off state were also not considered, this leaves 55 combinations.

Two result sets were analysed, set one was the results of the 24 hour monitoring, figure 10.11, set two was the "step" voltage imbalance, figure 10.28. The rms difference, D_B, between the primary voltage changes is used to indicate system performance, tabulated results for all sensor element combinations and all result parameters are contained in appendix 3.

10.12.2 Position of Removed Element

"Removal" of a sensor element changes the result parameters, however the effects depended both on the result set used for the analysis and the location of the sensor element. The result constant error D_A was again small, the correlation coefficient r remained approximately constant at 0.95, the largest change occurred in D_B.

Table 10.7 shows, for the 24 hour result set the rms difference, D_B, for the removal of one sensor element at each sensor position, the position of the removed element has little effect on the value of D_B. This is because the voltages remain approximately in balance, for each set of conductor voltage changes the field changes by approximately the same amount at each sensor position, thus when determining the voltage changes, section 8.5.5, no one sensor element is significantly more important than others.

Table 10.8 shows the same information for the "step" imbalance result set. D_B for the left and centre conductors remains approximately constant, however elements removed from the right hand side of the sensor array increase the left conductor value of D_B. Results in section 5.2 indicate that for imbalanced operation significant changes in the field distribution occur over a small range thus the signals from some sensor elements are more important than others.

Element Removed	Left	Centre	Right
0 (left)	0.1496	0.1529	0.1704
1	0.1491	0.1526	0.1696
2	0.1462	0.1518	0.1714
3	0.1433	0.1514	0.1703
4	0.1426	0.1553	0.1697
5	0.1426	0.1553	0.1697
6	0.1426	0.1553	0.1697
7 (right)	0.1426	0.1553	0.1697

Table 10.7 D_B Calculated For 24 Hour Result Set
Removal of One Sensor Element

Element Removed	Left	Centre	Right
0 (left)	0.1394	0.1627	0.1189
1	0.1394	0.1627	0.1189
2	0.1394	0.1627	0.1189
3	0.1394	0.1556	0.1189
4	0.1445	0.1640	0.1095
5	0.1509	0.1652	0.1212
6	0.1525	0.1667	0.1191
7 (right)	0.1555	0.1628	0.1136

Table 10.8 D_B For "Step" Imbalance Result Set
Removal of One Sensor Element

10.12.3 Number of Sensor Elements Removed

For each number of active sensor elements, n, $3 \leq n \leq 7$, there is more than one possible combination of on / off sensor arrangements in the array. For each value of n result parameters were calculated for all possible combinations and the mean value of each result parameter calculated. Again D_A, was less than the resolution of the non contact system and r remained approximately constant. Table 10.9 shows the mean value of D_B for each value of n for the 24 hour monitoring result set, table 10.10 shows the same information for the step imbalance result set.

No. Active Elements	D_B		
	Left	Centre	Right
4	0.1424	0.1828	0.1418
5	0.1428	0.1622	0.1141
6	0.1416	0.1627	0.1157
7	0.1448	0.1628	0.1165
8	0.1416	0.1602	0.1128

Table 10.9 Average Value of D_B For 24 Hour Monitoring Result Set

No. Active Elements	D_B		
	Left	Centre	Right
4	0.1464	0.1801	0.1592
5	0.1462	0.1565	0.1652
6	0.1450	0.1554	0.1675
7	0.1448	0.1537	0.1701
8	0.1455	0.1523	0.1724

Table 10.10 Average Value of D_B For Step Imbalance Result Set

For the twenty four hour result set the value of D_B increases for all channels as the number of active channels decrease, however there is no simple relationship and the change is not large. A similar result is seen for the left and centre conductors for the step imbalance result set, however for the right conductor, where the imbalance occurs, the reverse is true.

10.13 Summary

The non contact monitoring system was tested using a scale model of a power system, under normal and abnormal power system operation. Results were compared with those from a conventional contact system, in general there was good agreement between the two systems. The use of an array of eight sensor elements provides more information than the theoretical minimum necessary to determine the change in the conductor voltages, thus the system was shown to have an inherent redundancy.

11. Power System Investigations

In laboratory tests using a scale power system the non contact system produced values of changes in individual fundamental conductor voltages in good agreement with those from conventional contact measurements. Further tests were undertaken using a full size sensor array fitted below busbars in a 275kV substation operated by the UK National Grid Company (NGC).

11.1 Site Description

The NGC substation at Lister Drive is a 275kV to 132kV substation, it is one of the main connections from the national grid to a large area of Merseyside. The station supplies an area with a mixed load from industrial and domestic premises. The switchgear is enclosed within a large metal building and, in the region where the 275kV conductors enter the building, there are exposed bus bars suitable for monitoring by the non contact system. Figure 11.1 is a dimensioned plan and side view of part of the substation, the relevant dimensions are shown in table 11.1.

The conductors are not parallel to one another or to the ground. However they only deviate by small angles and in the cross section perpendicular to the ground and parallel to the switchgear fence, at a distance of 2m from the fence, the geometry is similar to that of the model described in section 4.1.

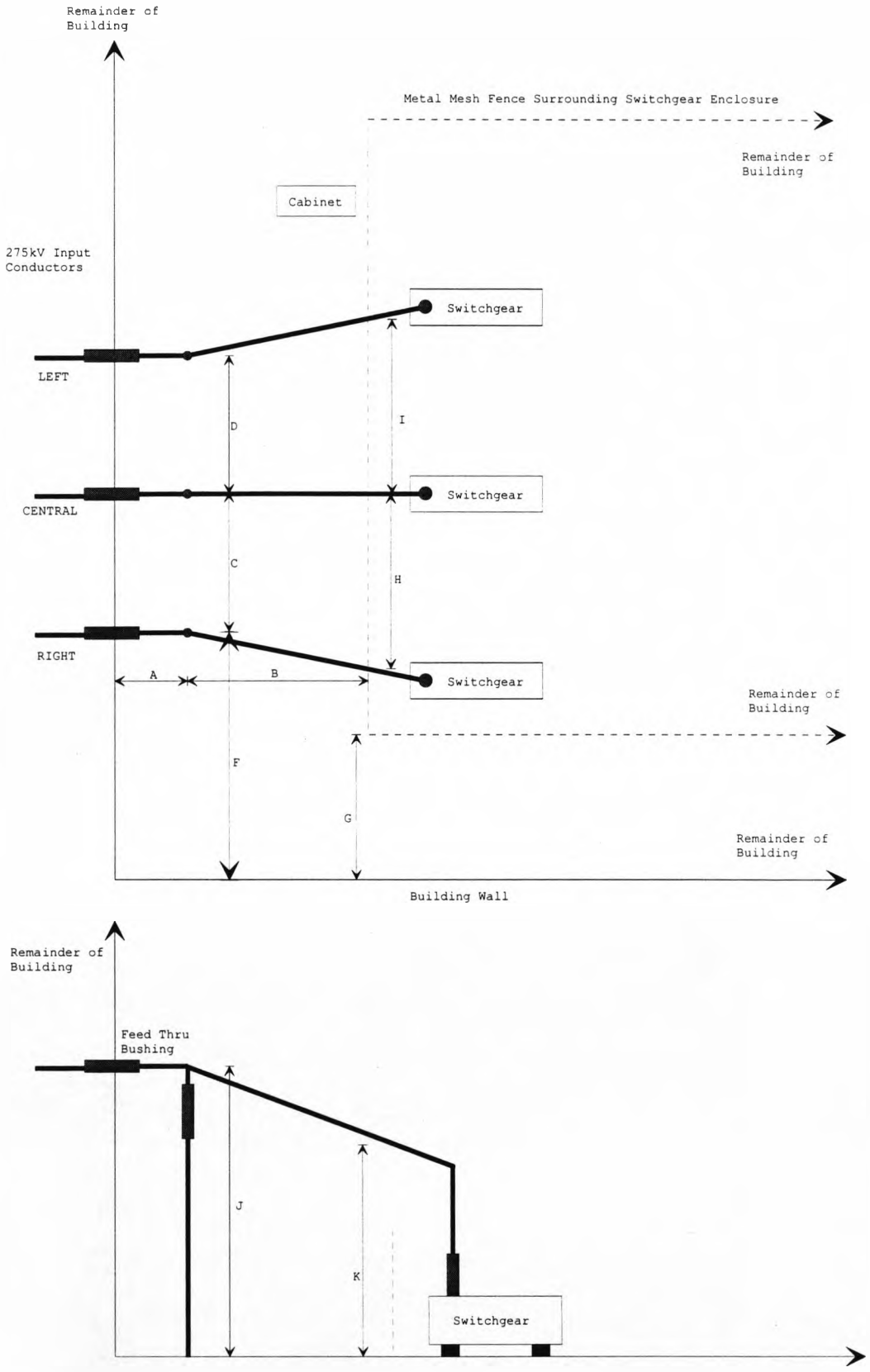

Figure 11.1 Plan and Side View of Substation Showing Conductor Entry

Dimension	Description	Value (m)
A	Support Poles to Outer Wall	3.7
B	Support Poles to Switchgear Enclosure	4.1
C	Right Hand Support Pole to Centre Support Pole	3.0
D	Left Hand Support Pole to Centre Support Pole	3.0
E	Left Hand Support Pole to Cabinet	2.4
F	Right Support Hand Pole to Inner Wall	12.0
G	Switchgear Enclosure to Inner Wall	7.8
H	Right to Centre Conductor at Switchgear Enclosure	3.7
I	Left to Centre Conductor Switchgear Enclosure	3.7
J	Conductor Height at Support Pole	6.0
K	Conductor Height at Switchgear Enclosure	4.3

Table 10.1 Lister Drive Sub Station Geometry

Initial investigation of the electric field was performed by moving a single sensor element along a line at ground level parallel to the fence at a distance of 2m from it, and recording the field at a number of equally spaced points. The analytical program, section 4.8, was used to calculate the ground level field distribution, figure 11.2 shows the calculated field distribution using the dimensions in table 11.1. The distribution that best fits the measured fields is also shown; this was obtained by making small modifications to the dimensions in table 11.1.

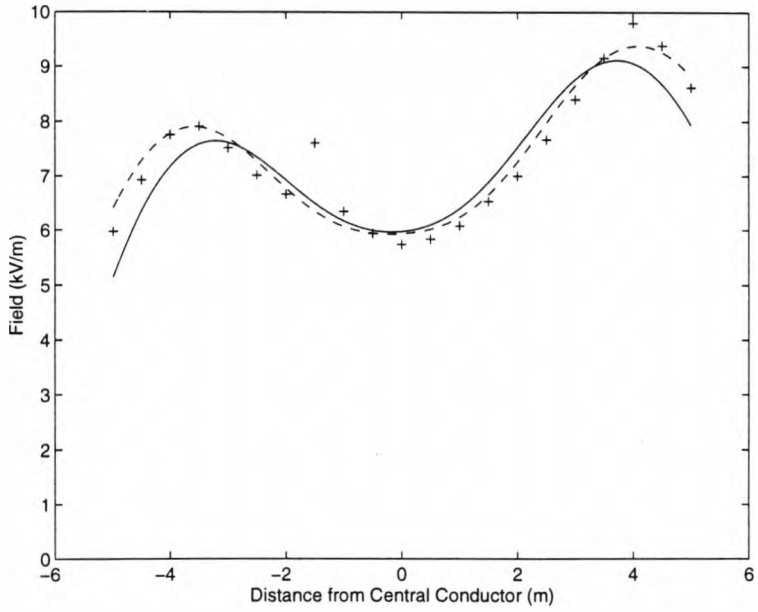

Figure 11.2 Ground Level Field Along a Line 2m From the Fence in Figure 11.1
+ = Measured Values *Solid Line* = Analytical Prog. *Dashed Line* = Best Fit

11.2 Modification of Laboratory Monitoring Systems

The field levels at ground level in the substation are the same magnitude as those in the laboratory scale model, section 4.7. However, as indicated in section 5.3, the spacing of the array sensor elements should be approximately half the conductor spacing, therefore a sensor array was constructed that was 9.8m long. It was constructed in sections, figure 11.3, with the sensor elements enclosed in individual boxes and mounted on 25mm square steel tubes, joined by bridge pieces. When assembled the array had eight sensor elements at 1.4m spacing. The non contact system data acquisition and processing systems, previously used for the laboratory investigations, were positioned behind the cabinet. Power for the non contact system was obtained from the local utility supply.

To check the results of the non contact system the 80286 PC and data acquisition card used in the laboratory contact monitoring system were also installed in the substation.

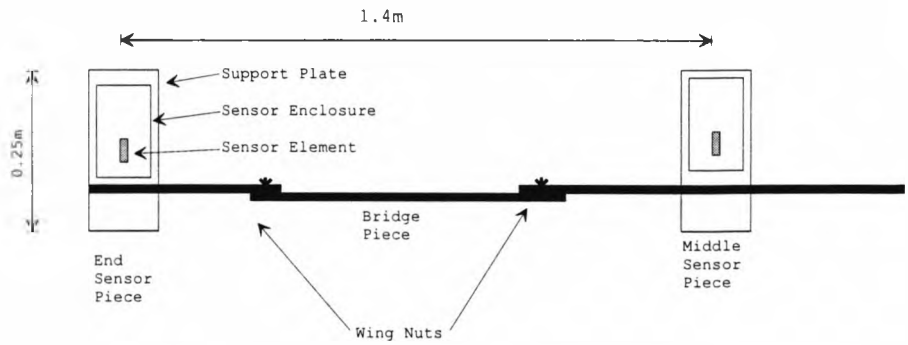

Figure 11.3 Section of Sensor Array Used in Substation

This could only monitor the voltage on one conductor because only one voltage transformer is installed in the substation. For the duration of these tests this voltage transformer was connected to the centre conductor. The ratio between input and output voltages was $1:231\times10^{-6}$, for a nominal conductor voltage of 275kV this gave a peak output voltage of 89.8V. This reference voltage signal was used for other functions within the substation, and the current that the contact system could draw was limited.

The data acquisition card used to record the voltages had a maximum input voltage of $\pm$ 5V and required a voltage source with impedance less than 100Ω. To meet these criteria the interface shown in figure 11.4 was constructed. The upper arm of the divider was 1 MΩ, the lower arm was 47 kΩ; these values gave a peak output voltage of 4.03V, the current drawn from the reference supply was less than 100μA. The output of the divider was buffered by the unity gain operational amplifier, type

CA 3140, to provide a low impedance source to the data acquisition card. Power for the amplifier was derived from the local utility supply.

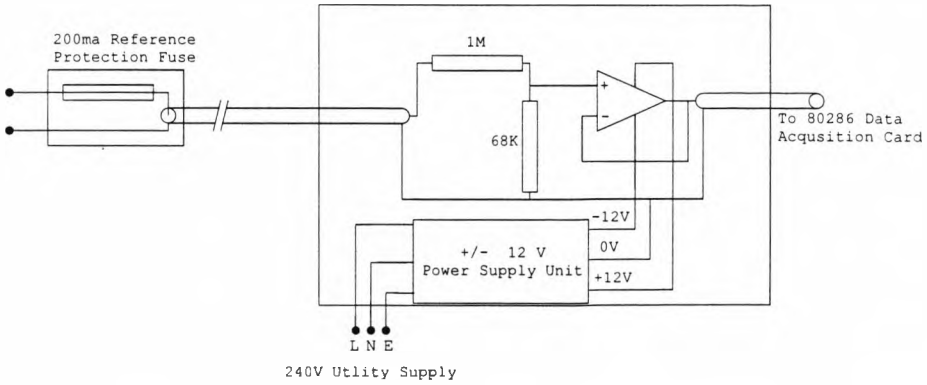

Figure 11.4 Interface Between Substation Reference Supply and 80286 PC Data Acquisition Card

The connection to the reference supply was a significant distance from the location of the non contact monitoring system and it was not possible to interlock the two systems by a physical connection therefore each system was programmed to operate independently. As the tests were to be unattended for several days it was necessary to save storage memory so the non contact system was programmed to save every tenth averaged descriptor set, this occurred at approximately 3.66s intervals. The contact system saved the value of the primary voltage at 2.2 second intervals. To allow the two sets of results to be compared the time, measured by each PC's internal clock, was saved as a part of each result. Before the test the drift of the clocks was measured in the laboratory, both systems were operated continuously for seven days and the results compared. The clocks drifted randomly, one did not systematically run at a slower rate than the other. The maximum difference observed was eight seconds and, as the duration of the tests was many days, this time difference was considered negligible.

11.3 Testing Process

As it was not possible to modify the conductor voltages, only long term monitoring, as for the laboratory system, section 10.6, was performed. The substation was monitored for 18 days, brief interruptions occurred on days 4 and 11 when the systems were inspected and the results downloaded from the slow system memory.

As the contact and non contact systems were not interlocked the stored results did not occur at the same time. To find the differences between the two sets of results linear interpolation was used to calculate the value using the contact system at the time at which the non contact system recorded a measurement. The result parameters described in section 10.4 were then computed.

11.4 Results

Figure 11.5 shows the changes in all conductor primary voltages determined by the non contact system and the changes in the centre conductor primary voltage determined by the contact system, on a typical weekday. Further results are contained in appendix 2.

For week days three distinct periods are observed; *night time*, from 00:00 to 07:00, the *working day*, from 07:00 to 18:00, and the *evening*, from 18:00 to 23:59. The power system loads affect the system voltage, section 10.1.2. During the night loads are low and the voltage remained approximately constant, although a rapid drop occurs at about 02:30, this drop was observed on all weekdays at approximately the same time. The voltage rapidly increases at approximately 06:30, this is thought to be

due to the actions of the supplier preparing to meet the increase in load caused by the working day. At the onset of the working day loads increase and the voltage decreases to an approximately constant level, towards the end of the working day there is a gradual increase in the voltage before a sudden decrease. The gradual increase is though to be due to the reduction of loads, while the decrease is probably due to actions of the supplier. These voltage changes are similar to those observed during the laboratory investigations, although in the laboratory larger changes occur during the working day due to changes in local loads.

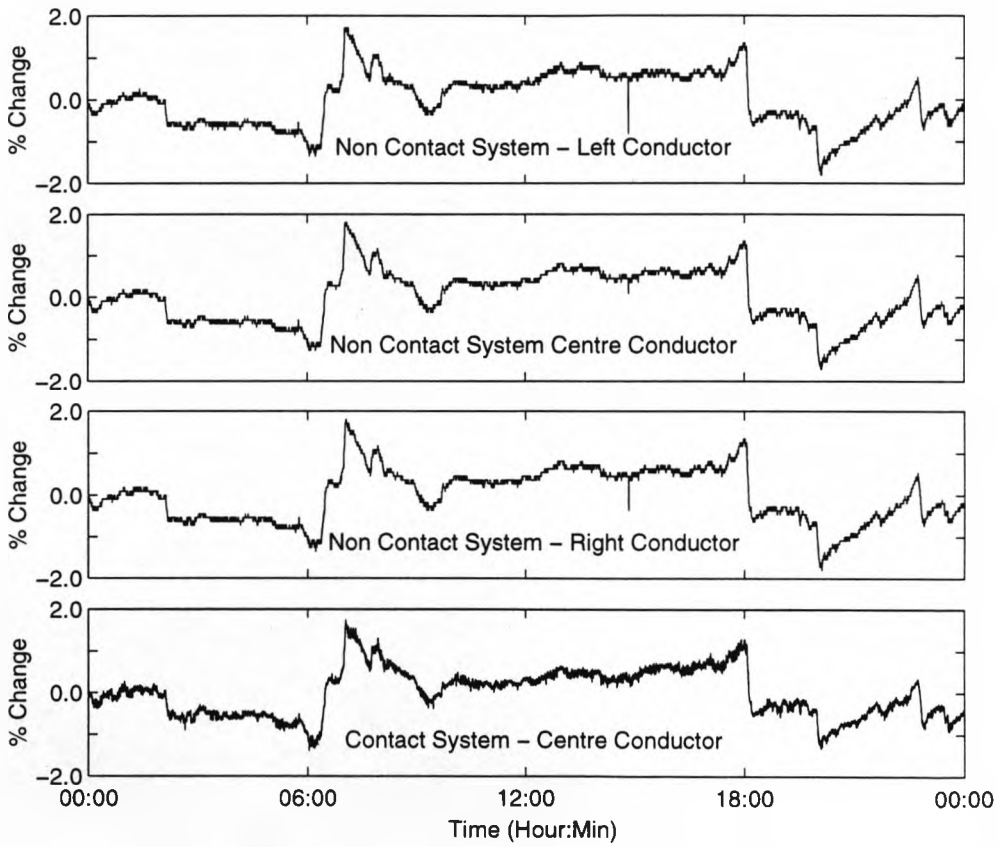

Figure 11.5 Change in All Conductors Primary Voltage Determined by Non Contact System and Change in Central Conductors Primary Voltage Determined by Contact System

No phase imbalance was detected during the tests. Table 11.2 shows the result parameters for the differences between the two systems for primary voltage changes on the central conductor during the 24 hour period in figure 11.5.

Metric	Value
D_A	-0.013
D_B	0.1819
r	0.9789

Table 11.2 Result Parameters for Centre Conductor Weekday Results

Values of D_A, D_B, and r are approximately the same as those obtained for twenty four hour monitoring in the laboratory. D_A is again less than the resolution of the non contact system indicating that the offset, k_0, is negligible; the value of r is above the level defined as significant by **Weldon(1962)**. The value of D_B is marginally higher than results in the laboratory, this is probably because the templates computed by the analytical program are less accurate than in the laboratory system. Further optimisation of the geometry entered into the analytical program would possibly reduce these errors.

Figure 11.6 shows the average harmonic content of the power system, as a percentage of the average conductor voltages, determined by the non contact system, for a typical weekday. The even harmonics are small, typically less than 0.1% and remain unchanged throughout the day, the third harmonic is also low, typically 0.3% with a slight reduction during the working day. The fifth harmonic is larger and increases to over 1% in the evening, this was possibly due to domestic loads and to

street lighting. Most street lighting uses discharge lamps, which are a well known source of harmonic distortion.

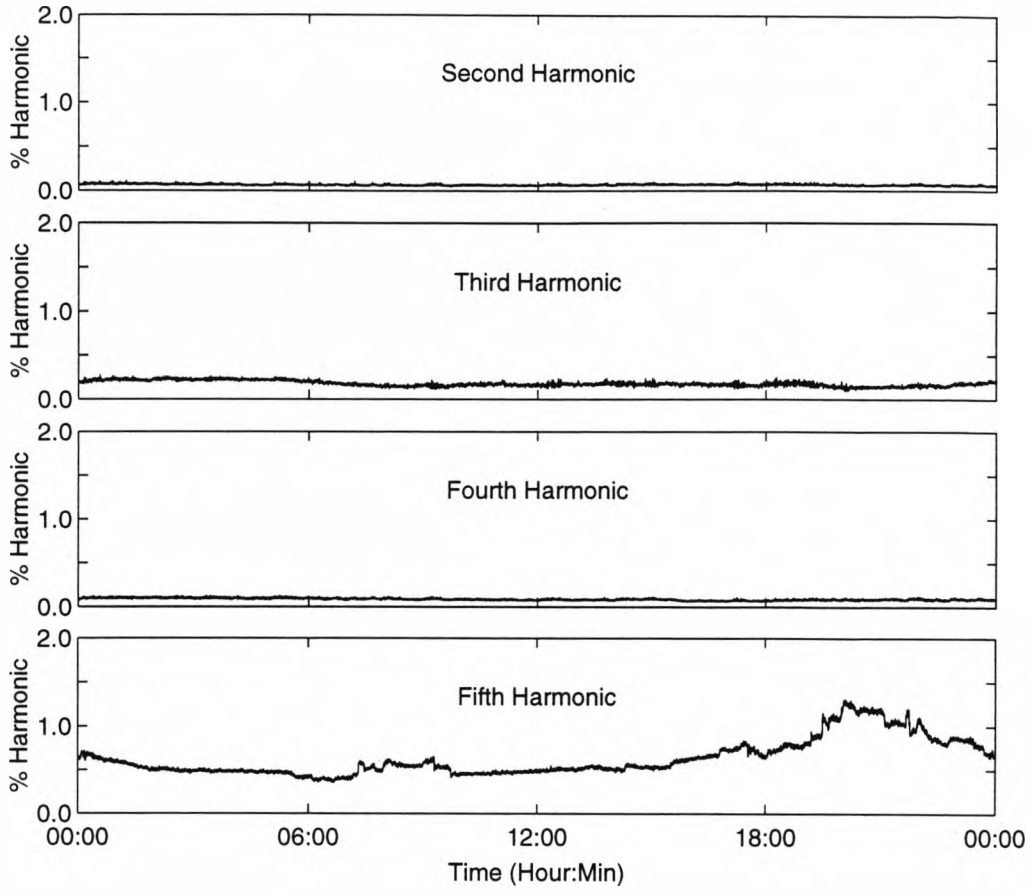

Figure 11.6 Average Harmonics as a Percentage of the Average Conductor Voltages Determined by the Non Contact System

The harmonic levels were lower than those monitored during the laboratory investigations indicating a large proportion of the harmonic content measured in the laboratory arose from the actions of local users.

Figure 11.7 shows the frequency of the power system determined by the contact and non contact systems. The frequency stayed within the limits 50±0.3Hz for the duration of the tests, the maximum difference between the results of the two systems was 0.1Hz, the resolution of both systems.

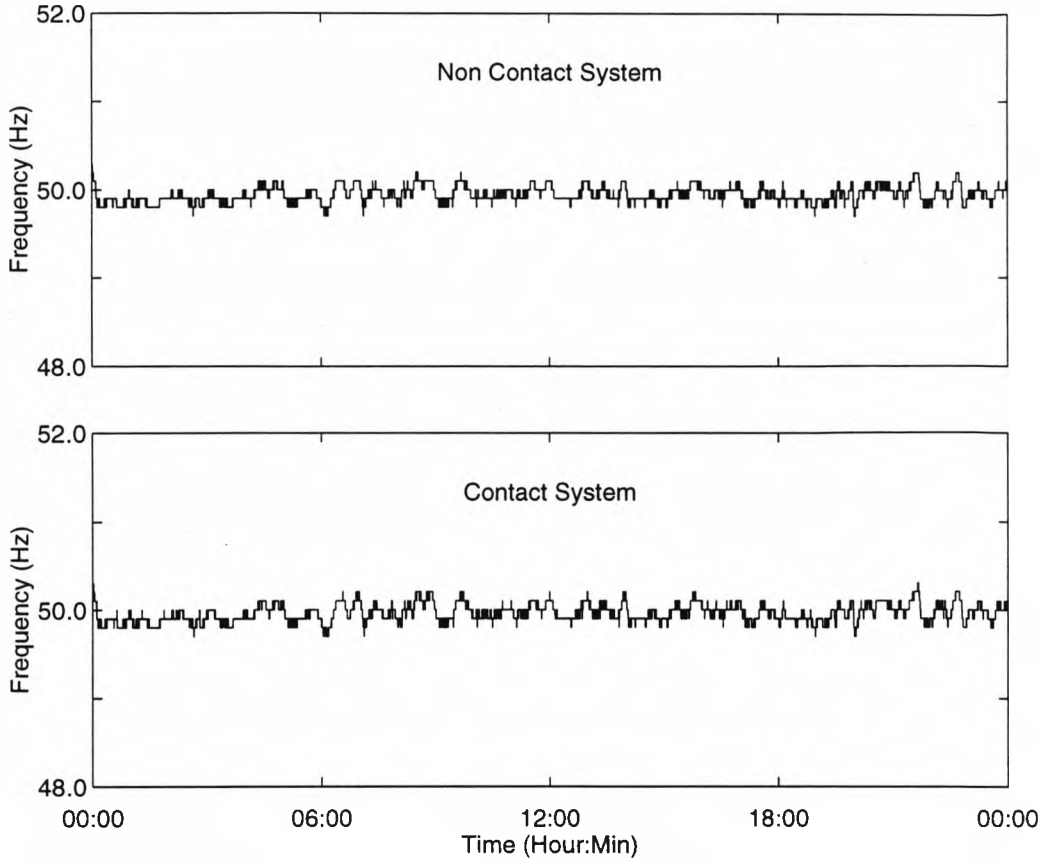

Figure 11.7 Frequency Measured by Both Systems

11.5 Element Failure (Redundancy)

It was shown, section 10.2, that the use of eight sensor elements provides more information than the minimum required to determine the change in the conductor voltages, if elements are removed from the analysis it is still possible to determine the changes in individual conductor voltage changes.

Figure 11.8 shows the determined and measured change in the system voltage for the last twelve hours of the third day of the test. At approximately 20:30hrs the non contact system started to produce erroneous results. Figure 11.9 shows the amplitude of the fundamental component of the signal descriptors from midnight to

09:00 for the next day. These traces suggest that sensor elements four and six are malfunctioning, voltage changes determined from this data were incorrect.

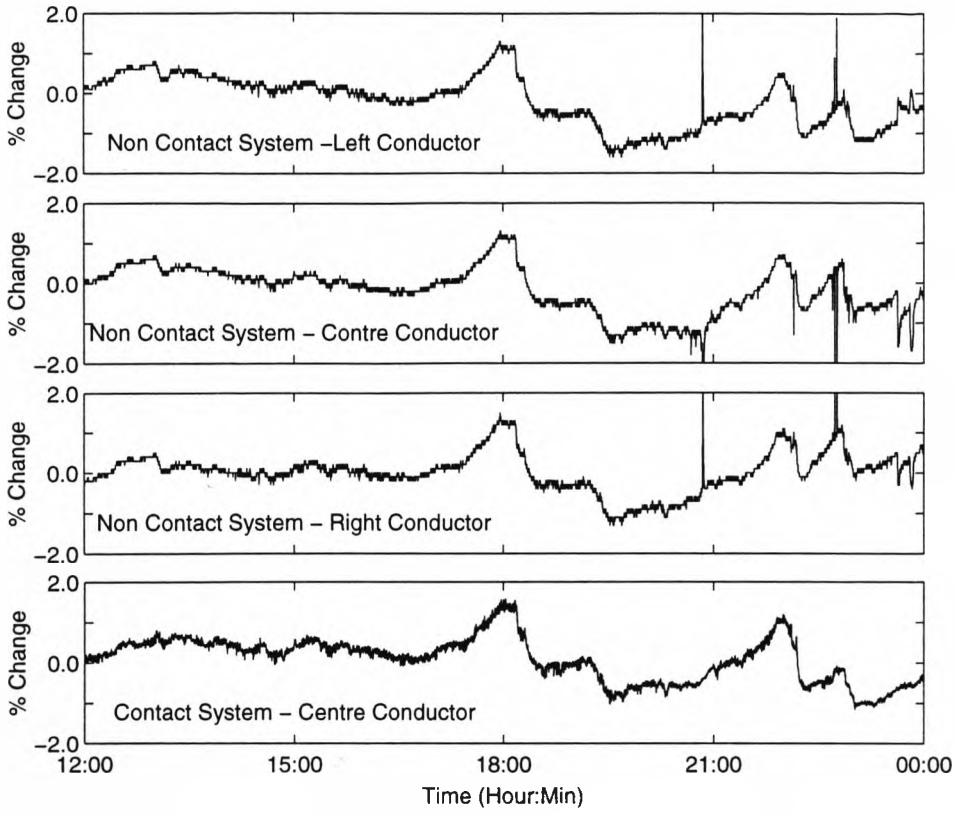

Figure 11.8 Changes in All Conductor Primary Voltages Determined by Non Contact System and Change in Central Conductor Voltage Determined by Contact System for Last Twelve Hours of Second Day of Tests

The processing of the signal descriptors was repeated with channels four and six ignored, figure 11.10 shows the changes in all conductor primary voltages determined by the non contact system and the changes in the central conductor voltage measured by the contact system. Removal of the signals from the two faulty elements still allowed the changes in conductor voltages to be determined.

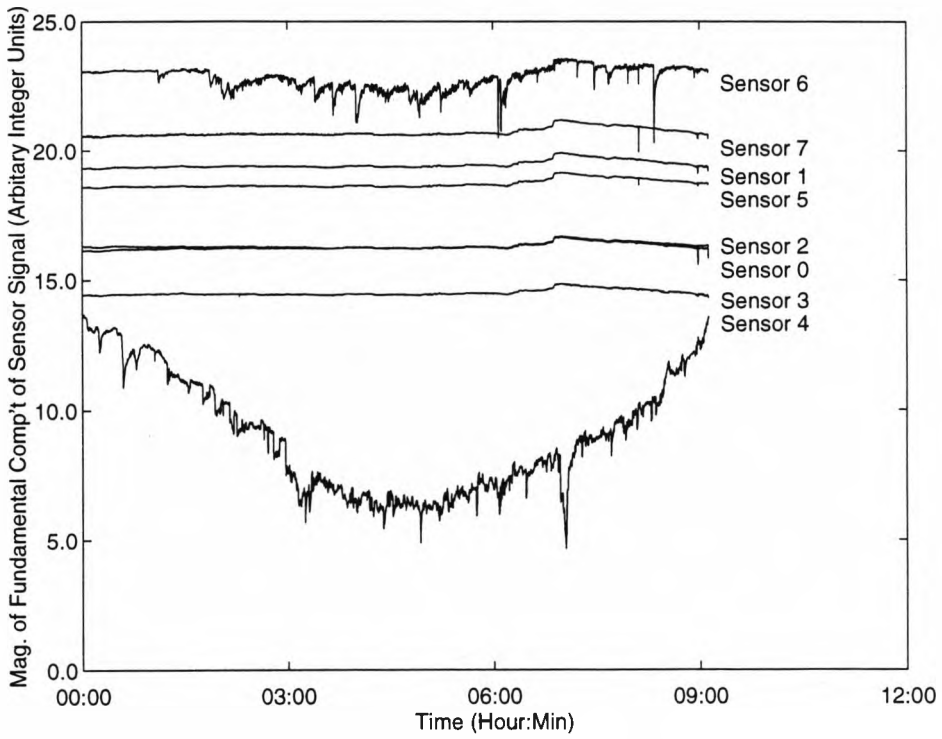

Figure 11.9 Fundamental Component of Signals from Sensors for First Nine Hours of Day Three of Tests

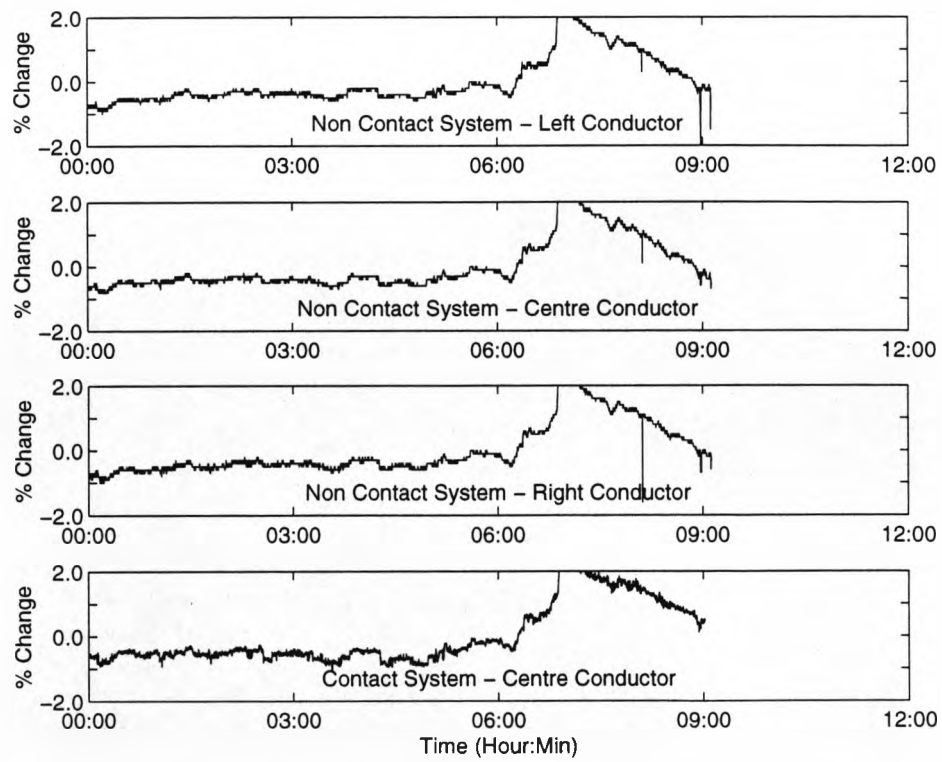

Figure 11.10 Change in All Conductor Voltages Determined by Non Contact System, Ignoring Signals From Sensor Elements Six and Four, and Change in Central Conductor Voltage Measured By Contact System for Day three of Tests

11.6 Summary

A full sized version of the non contact monitoring system was constructed and installed below an operating 275kV power system. A contact monitoring system was also connected to monitor the voltage of one conductor of the power system. The results using the non contact system agree with the results using the contact system. During the tests two sensor elements failed, due to the inherent redundancy in the non contact system if the signals from the failed elements are ignored it was still possible to determine the conductor voltages.

12. Conclusions and Suggested Developments

A non contact voltage monitoring system was developed. The principle of operation was that the electric field was measured at a number of positions underneath the conductors of a three phase power system and the measurements were used to determine information on the state of the power system. The system constructed determined, in real time, the change in the individual conductor primary voltages from their long term average values. The average harmonic content of all the conductors, the frequency of the power system and the number of transients were also monitored.

12.1 Performance of System Constructed

To test the non contact system it was positioned below a 10kV tenth scale model of a power system. To verify its behaviour a conventional contact measuring system was built to directly measure the conductor voltages. Extensive testing was undertaken for normal operating conditions. In addition faults and other abnormal operating conditions were generated on the power system. The changes in the individual conductor voltages determined by both systems were in good agreement, high levels of correlation were achieved. The non contact system correctly identified abnormal system operation and transient changes in the conductor voltages. Theoretical investigations showed that the non contact system measured the electric field at more points than the minimum number required to determine the change in the conductor voltages. Experiments showed that if the number of measurement positions was reduced the non contact system continued to operate reliably with a small decrease in accuracy, showing the system to have an inherent redundancy.

The system was also installed in on operating 275kV substation on the UK national grid, where it was only possible to directly monitor one conductor voltage. Again the results returned by the non contact system were in good agreement with those produced by the contact system. During the tests two electric field sensors failed; the inherent redundancy allowed the conductor voltages to be determined without the faulty sensors.

12.2 Non Contact System Hardware

As far as is known no similar voltage monitoring system exists, during development a large number of changes were made to the hardware to find the best design. For this reason a PC was used for the slow processing system, this was convenient for development purposes as both the hardware and software were easily modified. However the architecture of the PC was not optimised for real time operation, this is one of the reasons why the sampling frequency was limited to 699Hz. A processing system optimised for real time manipulation of measurements, for example a digital signal processor, would allow the sampling frequency of the system to be increased. Alternatively more sensors could be used or more sophisticated processing performed.

12.3 Software Algorithms

To determine the change in the individual conductor voltages the non contact system fitted pre-calculated templates to the measured change profiles. The two stage fitting algorithm was a compromise between accuracy and speed of operation. With further investigations and developments of the fitting process it may be possible to increase

the speed of operation. This would also allow improvements such as an increased sampling rate or the addition of more sensors.

The templates were calculated by the analytical program, the accuracy of the results is determined by the degree to which the analytical model can model the changes in the field distribution. Studies suggested that by making slight changes in the assumed power system geometry field distributions were obtained which were a better fit to the power system measurements. If a method of improving the analytical model was developed it may be possible to improve the accuracy of the system.

When two sensor elements failed it was still possible for the system to determine the changes in conductor voltages, however it was necessary for the user to determine which sensor elements failed. The signals from faulty sensors were distinctly different to those from a correctly functioning sensor. It may be possible to develop a sensor algorithm to automatically detect the failure of a sensor element and to ignore its signal.

12.3 Conclusion

The present study has shown that it is possible to monitor conductor voltages by the remote measurement of the electric field distribution. The instrumentation developed performed this task determining changes in individual conductor primary voltages to a resolution of ±0.1%. While this performance is lower than the requirements of some metering applications it exceeded the requirements necessary for many condition

monitoring tasks. Further, so far as is known, this is the first attempt to perform this type of monitoring and it should be possible to significantly improve the technique.

References

Ballik E.A. & Liu D.W. (1983)
Measurement of High-Voltage Pulses Employing a Quartz Pockels Cell.
IEEE Journal of Quantum Electronics. Vol 19, pp 1166-1168.

Banjaree P.P. & Poon T. (1991)
Principles of Applied Optics.
Asken Associates Inc, Boston USA.

Barker P., Burke J., Mancao T., Short T., Warren C., Burns C. & Siewierski J.(1994)
Power Quality Monitoring of a Distribution System.
IEEE Transactions on Power Delivery. Vol 9, pp1136-1142.

Bassen I.B. & Smith G.S. (1983)
Electric Field Probes - A Review.
IEEE Transactions on Antennal and Propagation. Vol 31, pp 710-718.

Bergen A.R. (1986)
Power Systems Analysis. pp 53 - 79.
Prentice Hall, USA.

Blalock T.J. , Bullock D.F. , Zaengl W.S. & Liao T. (1970)
A Capacitive Voltage Divider for UHV Outdoor Testing.
IEEE Transactions on Power Apparatus & Systems. Vol 89, pp 1404-1412.

Blatt D.W.E. (1991)
New Methods for Monitoring and Protection of High Voltage Switchyards.
IEE Proceedings-C. Vol 138, pp 228-232.

BSI (British Standards Institution) (1993)
British Standard BS 7625 - Voltage Transformers.

Buchanan D.J. , Jacobs M.L. & Travers F.A. (1994)
Using Hydrophones to Monitor Prestressed Concrete Pipe for Reinforcing Wire Failures.
Proceedings of International Conference on Hydraulics of Pipelines. pp212-225.

Cabral S.W. (1993)
A Survey of Commercially Available Electromagnetic Modelling Software.
IEEE Conference on Electro Magnetic Compatability. pp 284-287.

Carlson A.B.(1983)
Communication Systems, 3rd Ed.
Mc Graw Hill, London.

Carter C. (1994)
Personal Communication
FOCAS Inc, Atlanta, USA.

Caspers F. & Neuman E. (1980)
Optical Power Supply for Measuring or Communication Devices at High Voltage Levels.
IEEE Transactions on Instrumentation and Measurement. Vol 29, pp73-74.

Chartier V.L., Bracken T.D. & Capon A.S. (1985)
BPA Study of Occupational Exposure to 60Hz Electric Fields.
IEEE Transactions on Power Apparatus and Systems. Vol 104, pp 733-744.

Collins M. & Meek J.M.(1965)
Field Changes Preceding Impulse Breakdown of Rod / Plane Gaps.
Proc. 7th International Conference on Phenomena in Ionised Gases (ICPIG). Vol 7, pp581-585.

Cooley J.W. & Tukey J.W. (1965)
An Algorithm for the Machine Computation of Complex Fourier Series.
Mathematics of Computation. Vol 19, pp297-301.

Cosgrave J.A, Murphy N.M. , Jones G.R. , Spencer J.W. & Wilson A. (1992)
Non Invasive Optical Fibre Acoustic Monitoring of Potential Discharges within GIS
IEE 6th international conference on Dielectric Materials, Measurements and Applications. Manchester, England

Cui X., Liu J., Xie Y., He R., Zhang G. & Yang C. (1994)
Design of Insulated Structure for Load Ratio Voltage Power Transformer by Finite Element Method.
IEEE Transactions on Magnetics. Vol 30, pp2944-2947.

Davies A.J. & Turri R. (1990)
A composite probe for simultaneous electric field and conducted charge measurements.
Measurement Science Technology. Vol 1, pp 869-874.

Deno D.W. (1976)
Transmission Line Fields.
IEEE Transactions on Power Apparatus and Systems. PAS-95, pp 1600-1610.

Deno D.W. & Zaffanella L.E. (1987)
Transmission Line Reference Book - 345kV and above. pp340-358.
EPRI Publication EL-2500, EPRI 3412 Hillview Ave, Palo Alto, California USA.

Duhamel P. & Vetterli M. (1990)
Fast Fourier Transforms, A Tutorial Review and A state of the Art.
Signal Processing. Vol 19, pp259-299.

Eggebrecht L.C. (1994)
Interfacing to the IBM Personal Computer, 2nd Ed.
SAMS Publishers, USA

Feldman J.M., Reinhardt N. & Kuehn K. (1992)
A Hotstick Instrument for the Estimation of the Potential of an HVDC Conductor.
IEEE Transactions on Power Delivery. Vol 7, pp 1533-1541.

Feser K. & Pfaff W. (1984)
A Potential Free Spherical Sensor for the Measurement of Transient Electric Fields.
IEEE Transactions on Power Apparatus and Systems. Vol 103, pp 2904-2911.

Feser K., Pfaff W., Weyreter G. & Gockenback E. (1988)
Distortion Free Measurement of High Impulse Voltage.
IEEE Transactions on Power Delivery. Vol 3, pp 857-867.

FOCAS (1993)
Advertising Literature.
FOCAS Ltd, Swindon, Wiltshire SN2 2PJ, UK.

Friedlander G.D. (1976)
Matching Utility Output to Customer Demand.
IEEE Spectrum, September, pp50-52.

Hall W. (1993)
Personal Communication.
Reyrolle Switchgear, Newcastle Upon Tyne, NE31 1UP, UK.

Hayt W.H. (1989)
Engineering Electromagnetics, 5th Edn.
Mc Graw Hill International.

Hertz H.M. (1985)
Capacitively Coupled KD*P Pockels Cell for High Voltage Pulse Measurements.
Journal of Physics E, Scientific Instruments. Vol 18, pp 522-525.

Huang S.J., Erickson D.C. (1989)
The Potential Use of Optical Sensors for the Measurment of Electric Field Distribution.
IEEE Transactions on Power Delivery. Vol 4, pp 1579-1556.

IEC (International Electrotechnical Comission). (1960)
Recomendations for Voltage Measurement by Means of Sphere Gaps (One Sphere Earthed) 2nd Edition.

IEE (Institution of Electrical Engineers) (1991)
Report of a Working Group - The Possible Biological Effects of Low Frequency Electromagnetic Fields, July 1991

Jacobs P.D. & Dietrich F.M. (1984)
Measurement of Transmission Line Electric Fields in a Residential Environment.
IEEE Transactions on Power Apparatus and Systems. Vol 103, pp 2237-2241.

Jones G.R. (1994)
Chairman's Address
IEE Discussion Meeting on Fibre Optic Monitoring of Transmission and Distribution Plant. University of Liverpool May 1994

Kirkpatric P. & Miyake I. (1932)
A Generating Voltmeter for the Measurement of High Potentials.
Review of Scientific Instruments. Vol 3, pp 1-8.

Koo K.P. & Sigel G.H. (1982)
An Electric Field Sensor Utilizing a Piezoelectric Polyvinylidene Fluoride (PVF2) Film in an Single Mode Fiber Inferometer.
IEEE Journal of Quantum Electronics. Vol 18, pp 670-675.

Kuffel E. & Abdullah H. (1970)
High Voltage Engineering.
Pergamon Press, Oxford UK.

Kuffel E. & Zaengl W.S. (1984)
High Voltage Engineering - Fundamentals.
Pergamon Press, Oxford UK.

Kreyszig E. (1993)
Advanced Engineering Mathematics.
Wiley, New York, USA.

Lewis G. (1994)
Plant Condition Monitoring Using Optical Fibres
IEE Discussion Meeting on Fibre Optic Monitoring of Transmission and Distribution Plant. University of Liverpool May 1994

Leysop (1995)
17 Repton Court, Basilson, SS13 1LN, U.K.
Private Communication.

Licsko Z, Lenoard J & Koval D. (1992)
On Farm Monitoring of Electrical Power Quality.
Canadian Agricultural Engineering, Vol 34, pp239-245.

Lythall R.T. (1972).
The J & P Switchgear Book.
Newnes-Butterworth, London.

Moghsi, M. (1989)
Optical Fibre Voltage and Current Sensors.
PhD Thesis, University of Liverpool.

Moulton C. (1965)
Light Pulse System Shrinks High Voltage Protection Device.
Electronics. May 17, pp71-75.

Naidu M.S. & Kamaraju V. (1982)
High Voltage Engineering - 1st Edn.
Mc Graw Hill, New Delhi.

Neale (1987)
Trends in Maintenance & Condition Monitoring.
International Conference on Condition Monitoring, Swansea U.K. 1987

NGC (National Grid Company U.K.) (1992)
Doccument NGTS 1 - Overview National Grid System.
National Grid House, Kirby Corner Road, Coventry CV4 8JY, U.K.

NiTech. (1987)
Plus-1 The Portable Line Monitoring System That Lets You Read Between the Lines. Advertising Literature.
Nitec Inc., Fairfield CT, USA.

Ohnishi H., Yokoyama H., Yoneyama T., Aoyagi M., Akutsu Y., Kanoi M., Iwashita K., Haga H.& Nakamura M. (1994)
Insulation Deterioration Monitoring System for Underground Power Distribution Systems.
IEEE Transactions on Power Delivery. Vol 9, pp1028-1033.

Olsen R.G.(1994)
Power System Electromagnetics.
IEEE Antennas and Propagation Magazine, Vol 36, pp 7-16

Pilling N.A. (1992)
Optical Fibre Measurements in Power Systems.
PhD Thesis, University of Liverpool.

Piotrowski, J (1992)
Theory of Physical and Technical Measurment
Elsevier, Amsterdam

Porkless R. (1988)
Dictionary of Statistics.
Collins, Glasgow.

Ramirez R.W. (1985)
The FFT Fundamentals and Concepts.
Prentice Hall, New Jersey.

Rice J.A. & Wu S.M. (1993)
On the Feasibility of Catastrophic Cutting Tool Fracture Emission via Acoustic Emission Analaysis.
Journal of Engineering for Industry. Vol 115, pp390-397.

Ruiz J, Ortuondo J, Izquierdo J, Leturiondo L, Aramendi E & Amantegui J. (1995)
Real Time Power Supply Quality Measurement and Monitoring Multichannel System.
IEEE Transactions on Power Delivery. Vol 10, pp1191-1197.

Sarma-Maruvada P., Dallaire R.D. & Pedneault R. (1983)
Development of Field Level Instruments for Ground-Level and above Ground Level Electric Field Measurement under HVDC Transmission Lines.
IEEE Transactions on Power Apparatus and Systems. Vol 102, pp 738-744.

Say M.G. (1976)
Alternating Current Machines, 4th Edn.
Pitman, London.

Segerland L.J. (1976)
Applied Finite Element Analaysis.
John Whiley & Sons.

Shannon C. (1949)
Mathematical Theory of Communication.
Bell Systems Technical Journal, Vol 27.

Shibita K.(1983)
A Fibre Optic Electric Field Sensor Using the Electrooptic Effect of $Bi_4Ge_3O_{12}$.
IEE 1st International Conference on Fibre Optic Sensors.

SIBRE Power Research Institute. (1984)
Remote Voltage Measurement on Power Line Insulator- Using Electrode Inserted into Insulator Cap for Least Distortion of Local Electric Field.
Patent. SU1205-035-A.

Silvester P.P. & Ferrari (1990)
Finite Elements for Electrical Engineers.
Cambridge University Press, Cambridge.

Sollymar L. & Walsh D. (1993)
Lectures on Electrical Properties of Materials.
Oxford Science Publications.

Srinivasan K. & Jutras R. (1991)
Power System Disturbance Monitoring System.
Proceedings of the IEEE Power Engineering Society, Transmission & Distribution Conference. pp261-265.

Steed J.C. (1995)
Condition Monitoring Applied to Power Transformers - An REC View.
The reliability of Transmission & Distribution Equipment, IEE Conf. Pub 406. pp109-114.

Tardy A. & Derossis A. (1995)
A Current Sensor Remotely Powered and Monitored through an Optical Fibre Link.
Optical Fibre Technology. Vol 1, 181-185.

Tokoro K., Harumoto Y., Yamamoto H., Yoshida Y., Mukae H., Ohno Y., Shimada M. & Ida Y. (1982)
Develpment of Electronic Potential and Current Transducers suitable for Gas Insulated Switchgear and adequate for application to Substation Digital Control.
IEEE Transactions on Power Apparatus and Systems. Vol 101, pp 3967-3976.

Train D.& Dube R. (1983)
Measurements of Voltage distribution on suspension insulators for HVDC transmission lines.
IEEE Transactions on Power Apparatus and Systems. Vol 102, pp 2461-2475.

Turner M.J., Clough R.W., Martin H.C. & Lee C. (1956)
Stiffness and Deflection Analysis of Complex Structures.
Journal of Aeronautical Science, Vol 23 pp 805-824.

Wetherill G.B. (1986)
Regression Analysis With Applications.
Chapman & Hall, London.

Wheldon D. (1962)
Business Statistics and Statistical Methods, 4th Edn.
Mc Donald & Evans, London.

Wiggins C.M., Nickel F.S., Haney A.J. & Wright S.E. (1989)
Measurements of Switching Transients in a 115 kV Substation.
IEEE Transactions on Power Delivery. Vol 4, pp 756-769.

Wildi T. (1981)
Electrical Power Technology.
Wiley, New York.

Wolzak G.G., Bekkers J.A.G.& Van-der-Laan, P.C.T. (1981)
Capacitive Measurement of High DC Voltages.
Review of Scientific Instruments. Vol 52, pp 1571-1573.

Yamashita H., Shinozaki K. & Nakamae E. (1988)
A Boundary-Finite Element Method to Compute Directly Electric Field Intensity with High Accuracy.
IEEE Transactions on Power Delivery. Vol 4, pp 1754-1760.

Zaborsky J. & Rittenhouse W.H. (1954)
Electric Power Transmission. pp 138 - 171.
Thames & Hudson , London.

Z World (1995)
Advertising Literature
1724 Picasso Ave. Davis, California USA.

Appendix 1
Additional Results
Laboratory Investigations

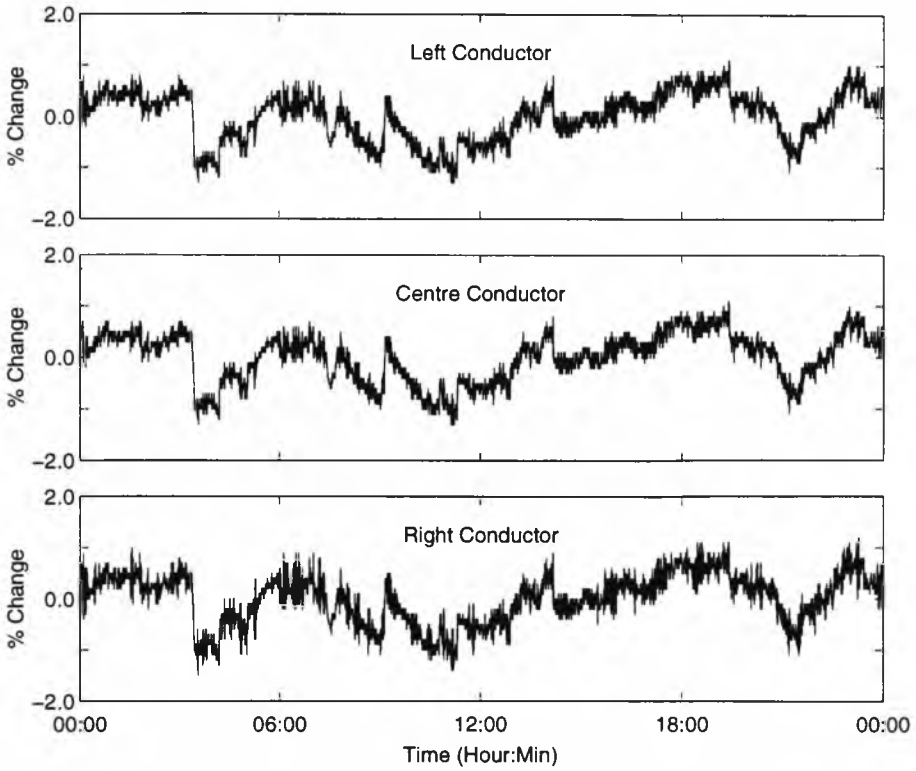

Figure A1.1 Change in Primary Conductor Voltages Determined by Non Contact System on Sunday 04/08/96

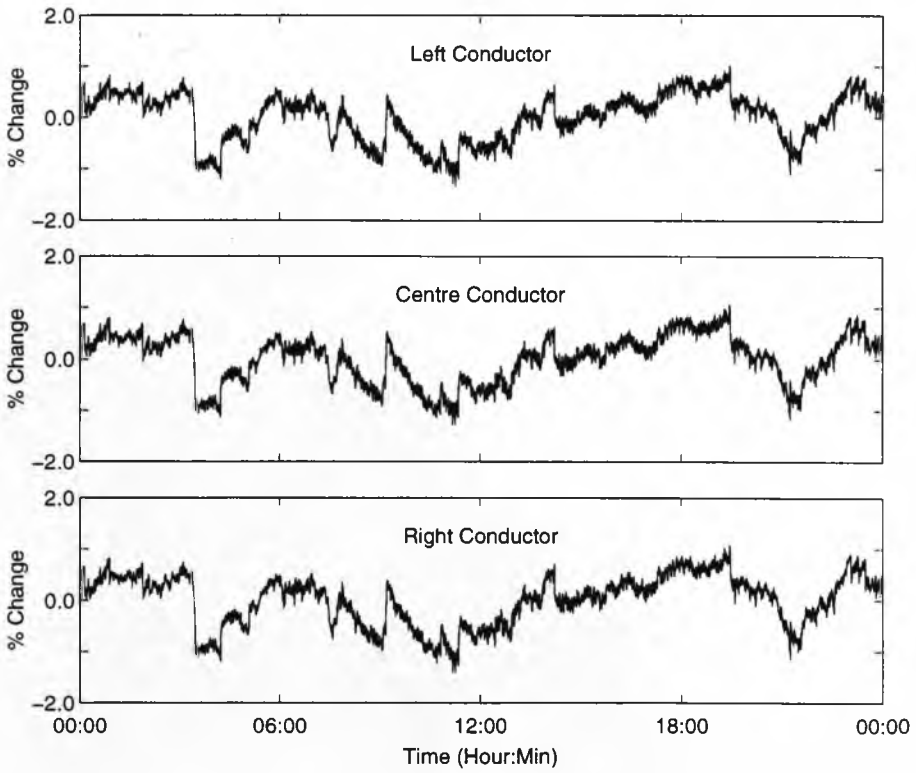

Figure A1.2 Changes in Primary Conductor Voltages Measured by Contact System on Sunday 04/08/96

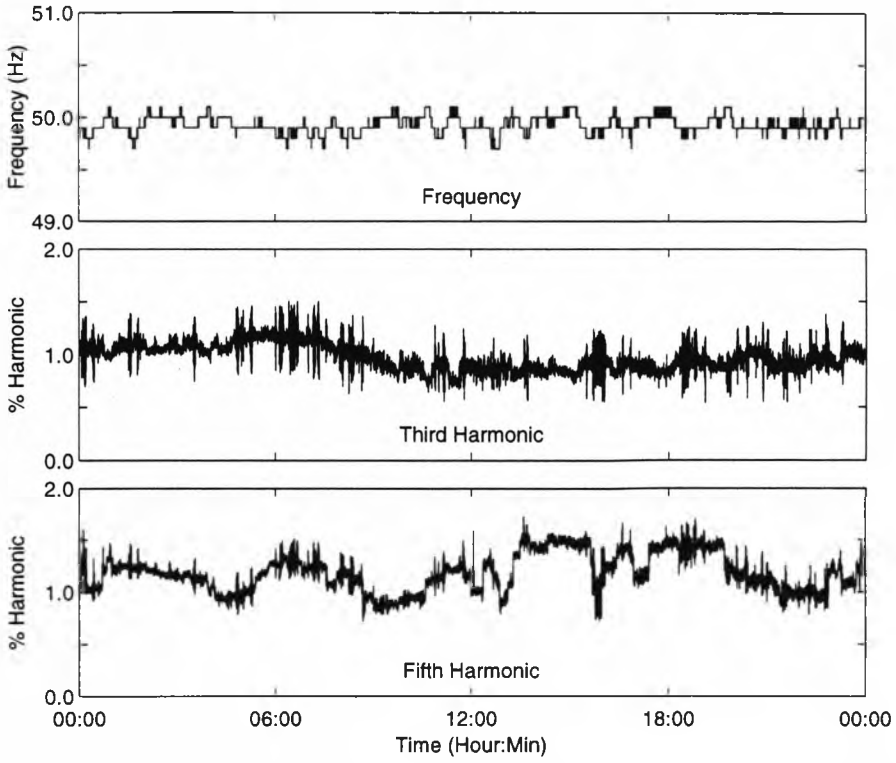

Figure A1.3 Odd Harmonics and Voltage Frequency Determined by Non Contact System on Sunday 04/08/96

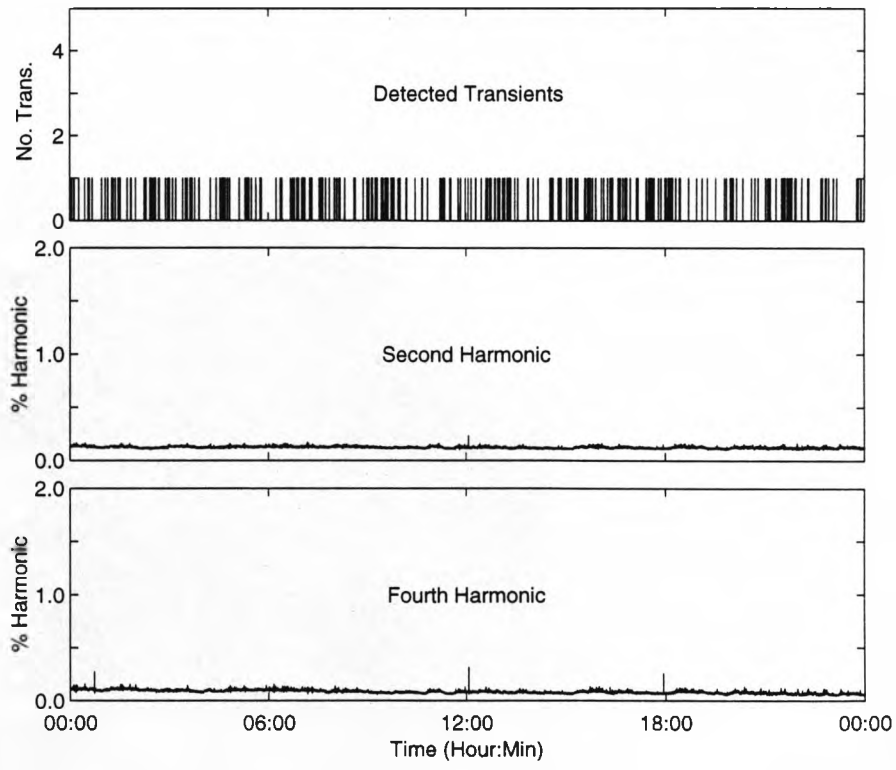

Figure A1.4 Even Harmonics and Detected Transients Determined by Non Contact System on Sunday 04/08/96

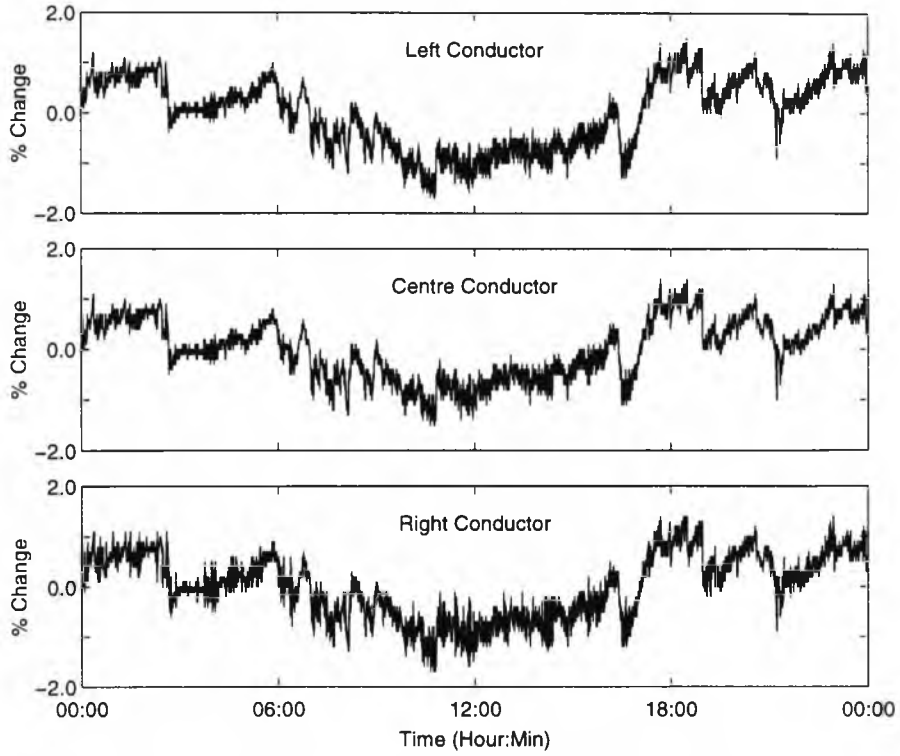

Figure A1.5 Change in Primary Conductor Voltages Determined by Non Contact System on Friday 02/08/96

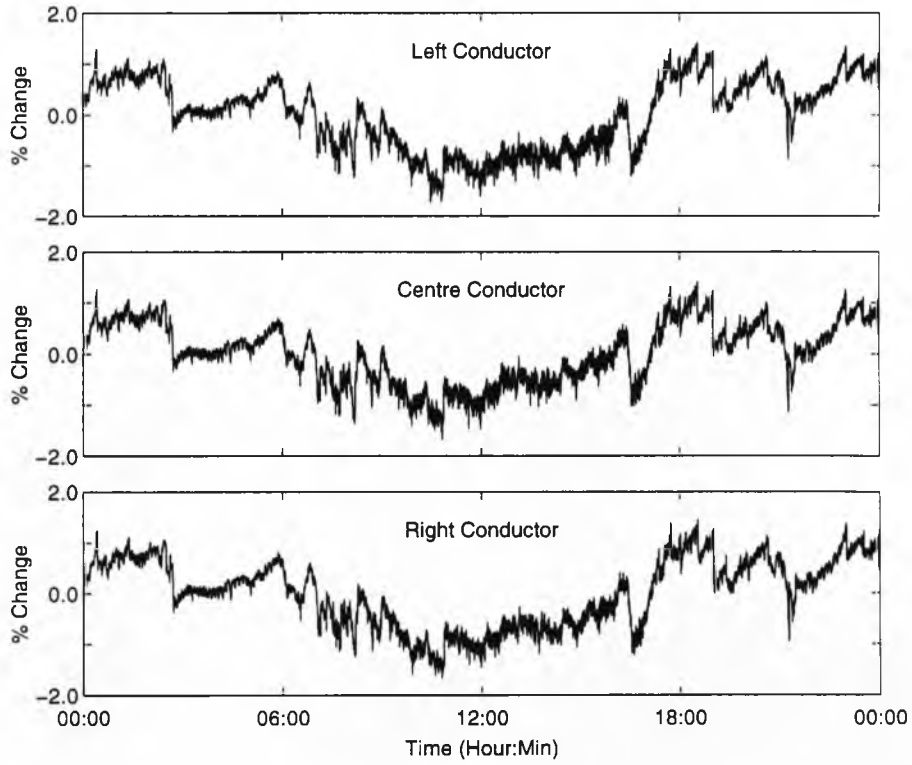

Figure A1.6 Changes in Fundamental Conductor Voltage Measured by Contact System on Friday 02/08/96

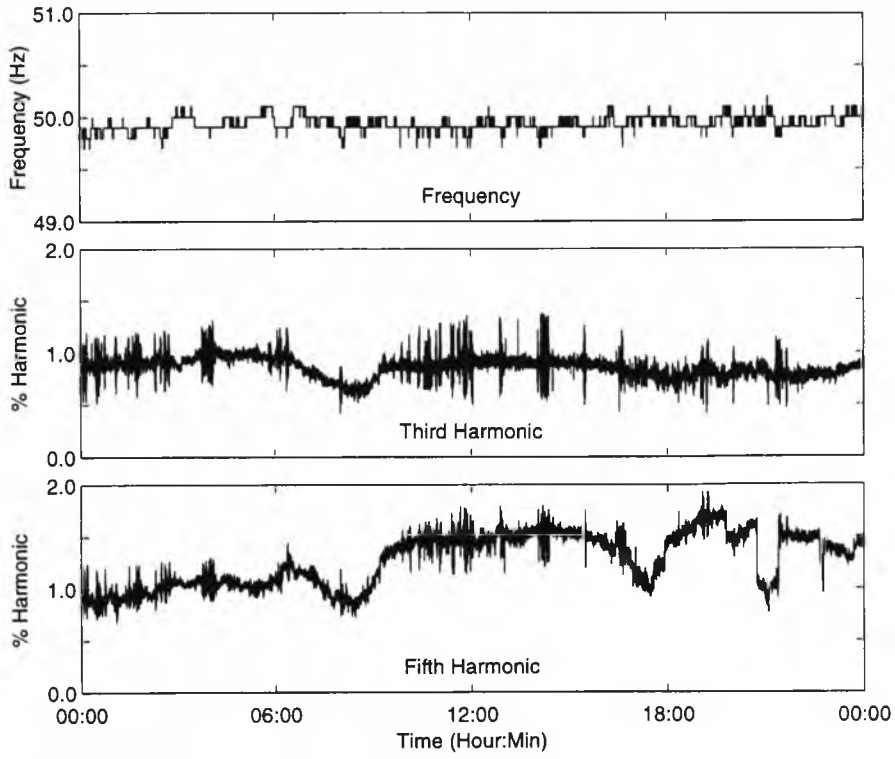

Figure A1.7 Odd Harmonics and Frequency Determined by Non Contact System on Friday 02/08/96

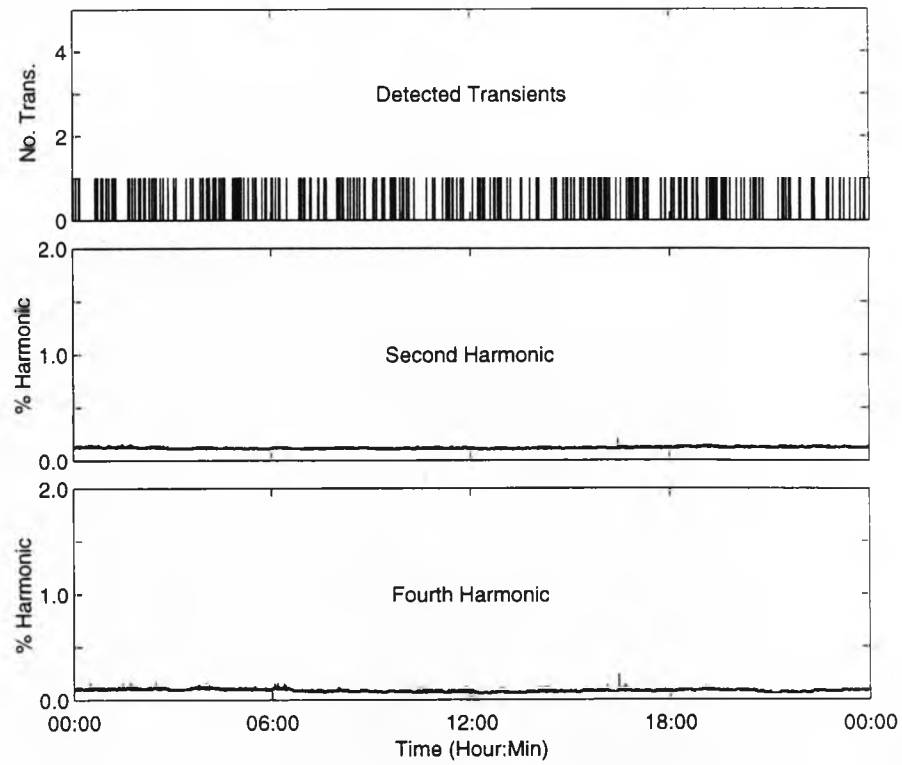

Figure A1.8 - Even Harmonics and Detected Transients Determined by Non Contact System on Friday 02/08/96

Appendix 2
Additional Results
Power System Investigations

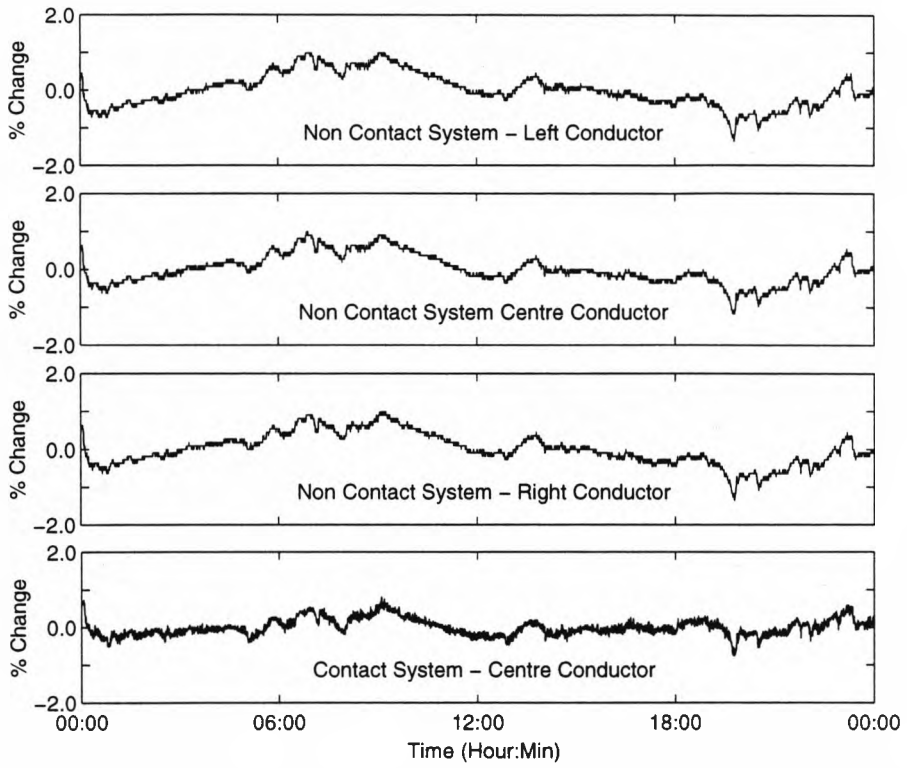

Figure A2.1 Change in All Primary Conductor Voltages Determined by Non Contact System and Change in Central Conductor Fundamental Voltage Determined by Contact System - Sunday 15/09/96

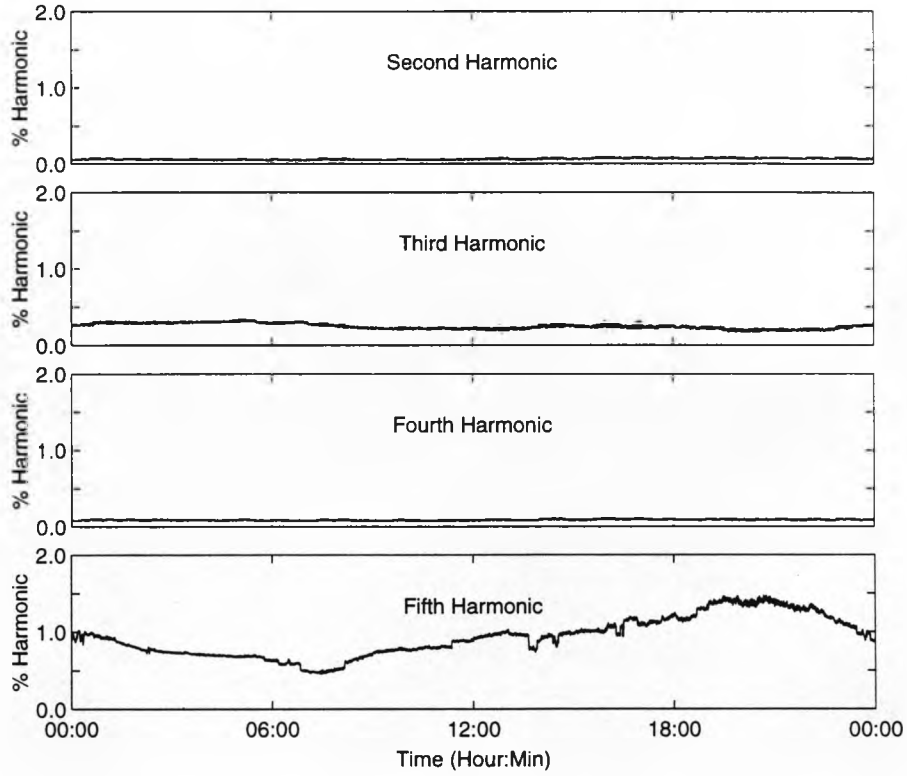

Figure A2.2 Average Harmonic Content as a Percentage of Average Primary Voltage Determined by Non Contact System - Sunday 15/09/96

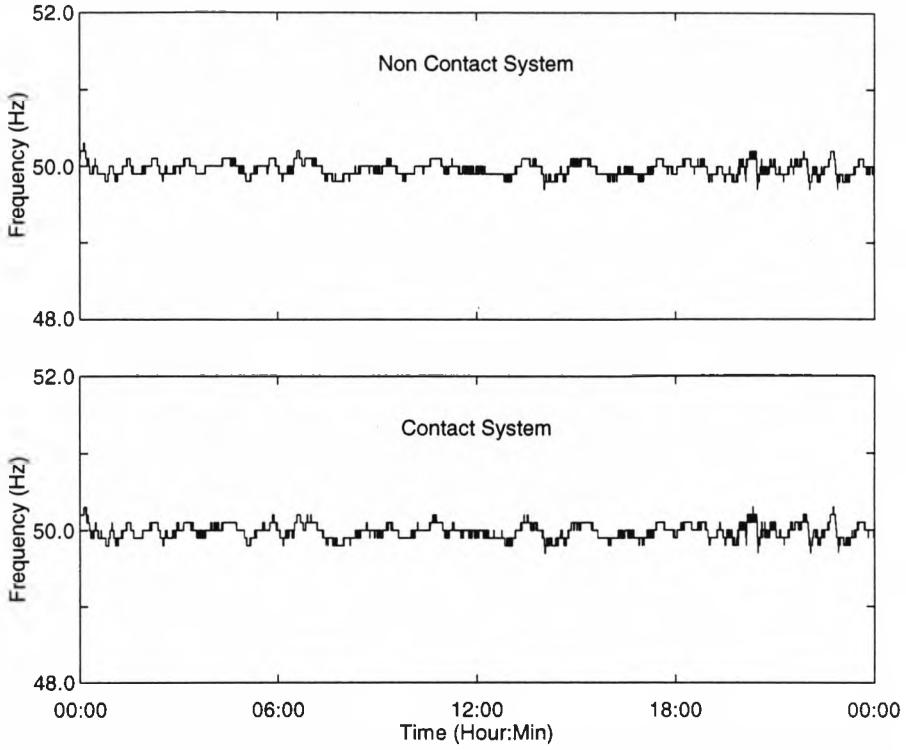

Figure A2.3 Frequency Determined by Both Systems - Sunday 15/09/96

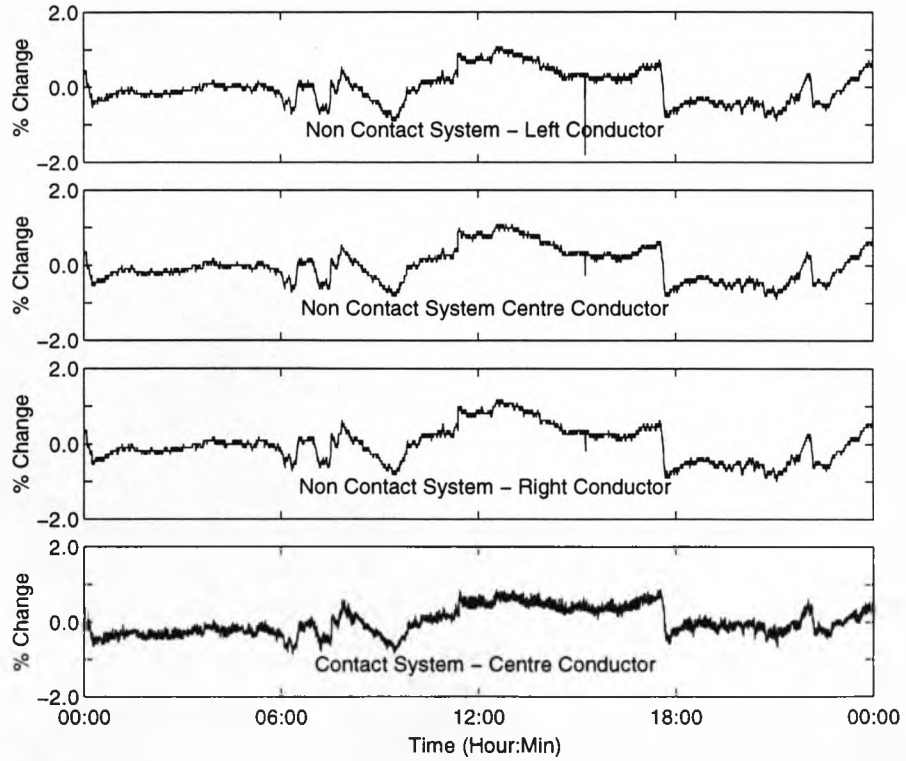

Figure A2.4 - Change in All Fundamental Conductor Voltage Determined by Non Contact System and Change in Central Conductor Voltage Determined by Contact System - Saturday 22/09/96

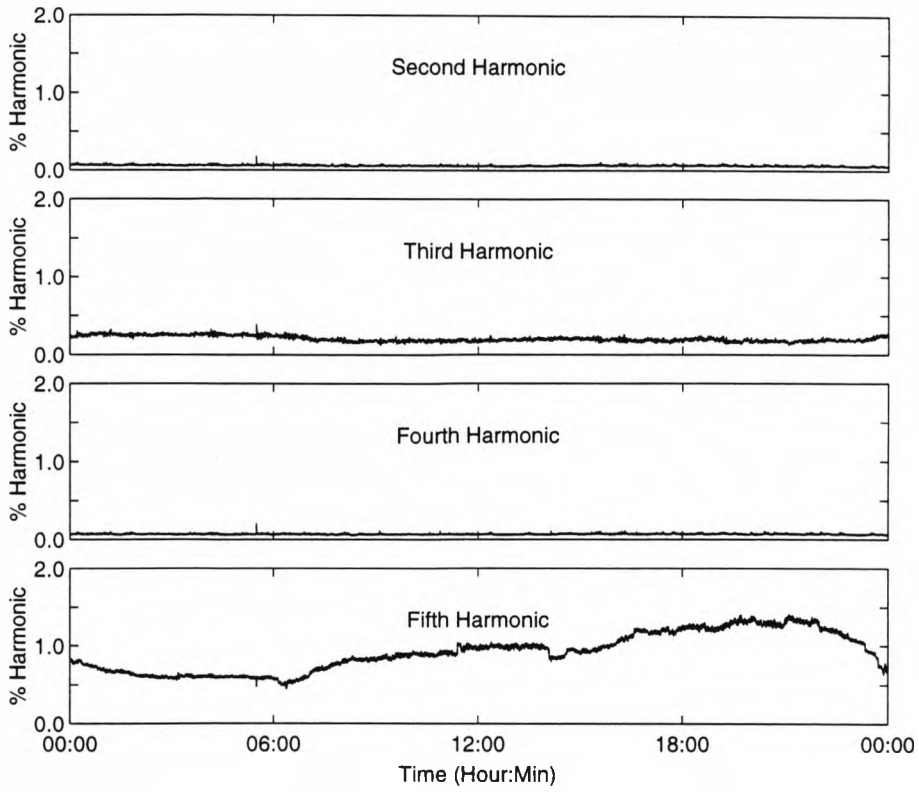

Figure A2.5 Average Harmonic Content as a Percentage of Average Primary Voltage Determined by Non Contact System - Saturday 22/09/96

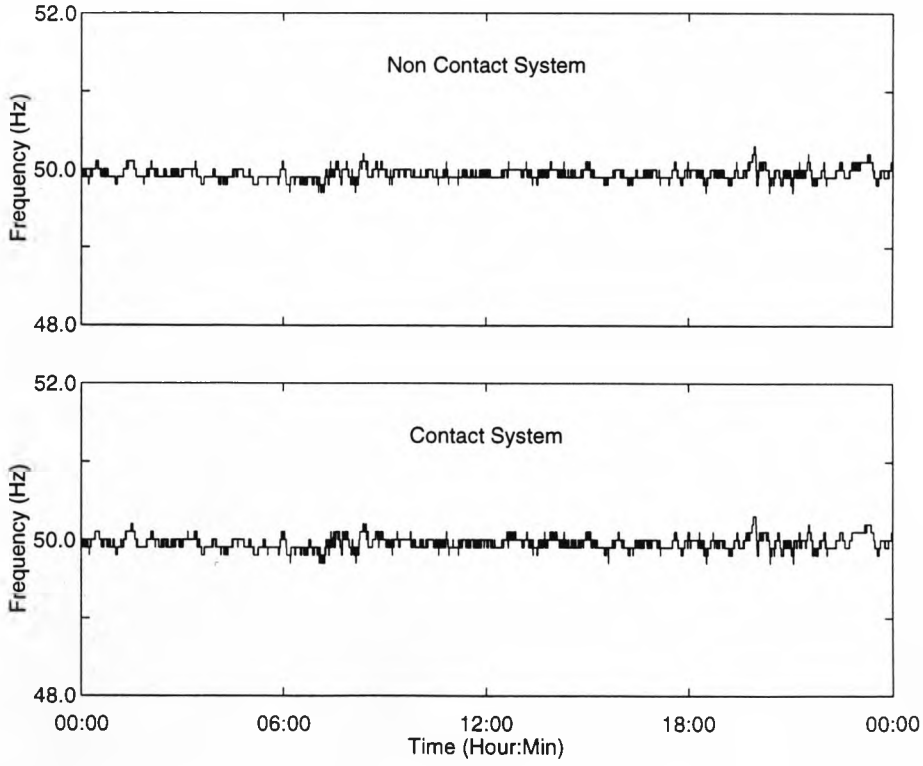

Figure A2.6 Frequency Determined by Both Systems - Saturday 22/09/96

Appendix 3
Redundancy Tests
Tabulated Results

Table A3.1 Redundancy Analaysis for Result Set 1 - 24 Hour Monitoring

Four Active Sensor Elements

Sensor States 0=On 1 =Off								Average Diference			RMS Diference			Correlation Coeficent		
L							R	Left	Centre	Right	Left	Centre	Right	Left	Centre	Right
1	0	1	0	1	0	1	0	0.0282	0.1194	-0.0257	0.1120	0.1824	0.1392	0.9592	0.9349	0.9543
0	1	1	0	1	0	1	0	0.0176	0.1406	-0.0357	0.1116	0.2039	0.1414	0.9592	0.9278	0.9532
0	1	0	1	1	0	1	0	0.0352	0.0429	-0.0139	0.1195	0.1271	0.1411	0.9584	0.9396	0.9540
0	1	0	1	0	1	1	0	0.0517	-0.0324	-0.0651	0.1249	0.1263	0.1636	0.9565	0.9421	0.9498
0	1	0	1	0	1	0	1	0.0546	-0.0289	-0.0622	0.1278	0.1290	0.1655	0.9570	0.9420	0.9488
Average Value								0.0375	0.0483	-0.0405	0.1191	0.1538	0.1502	0.9581	0.9373	0.9520

Five Active Sensor Elements

Sensor States 0=On 1 =Off								Average Diference			RMS Diference			Correlation Coeficent		
L							R	Left	Centre	Right	Left	Centre	Right	Left	Centre	Right
1	1	1	0	1	0	1	0	0.0311	-0.0883	-0.0592	0.1153	0.1608	0.1661	0.9595	0.9357	0.9494
1	1	0	1	1	0	1	0	0.0317	-0.0406	-0.0798	0.1173	0.1308	0.1726	0.9584	0.9416	0.9477
1	0	1	1	1	0	1	0	0.0452	-0.0347	-0.0710	0.1205	0.1315	0.1683	0.9582	0.9417	0.9487
0	1	1	1	1	0	1	0	0.0458	-0.0359	-0.0710	0.1221	0.1314	0.1695	0.9584	0.9418	0.9483
1	1	0	1	0	1	1	0	0.0317	-0.0406	-0.0798	0.1173	0.1308	0.1726	0.9584	0.9416	0.9477
1	0	1	1	0	1	1	0	0.0452	-0.0347	-0.0710	0.1205	0.1315	0.1683	0.9582	0.9417	0.9487
0	1	1	1	0	1	1	0	0.0458	-0.0359	-0.0710	0.1221	0.1314	0.1695	0.9584	0.9418	0.9483
1	0	1	0	1	1	1	0	0.0470	-0.0747	-0.0510	0.1181	0.1487	0.1570	0.9593	0.9360	0.9509
0	1	1	0	1	1	1	0	0.0529	-0.0759	-0.0451	0.1249	0.1507	0.1613	0.9593	0.9362	0.9507
0	1	0	1	1	1	1	0	0.0546	-0.0289	-0.0622	0.1278	0.1290	0.1655	0.9570	0.9420	0.9488
1	1	0	1	0	1	0	1	0.0317	-0.0406	-0.0798	0.1173	0.1308	0.1726	0.9584	0.9416	0.9477
1	0	1	1	0	1	0	1	0.0452	-0.0347	-0.0710	0.1205	0.1315	0.1683	0.9582	0.9417	0.9487
0	1	1	1	0	1	0	1	0.0458	-0.0359	-0.0710	0.1221	0.1314	0.1695	0.9584	0.9418	0.9483
1	0	1	0	1	1	0	1	0.0470	-0.0747	-0.0510	0.1181	0.1487	0.1570	0.9593	0.9360	0.9509
0	1	1	0	1	1	0	1	0.0529	-0.0759	-0.0451	0.1249	0.1507	0.1613	0.9593	0.9362	0.9507
0	1	0	1	1	1	0	1	0.0546	-0.0289	-0.0622	0.1278	0.1290	0.1655	0.9570	0.9420	0.9488
1	0	1	0	1	0	1	1	0.0470	-0.0747	-0.0510	0.1181	0.1487	0.1570	0.9593	0.9360	0.9509
0	1	1	0	1	0	1	1	0.0529	-0.0759	-0.0451	0.1249	0.1507	0.1613	0.9593	0.9362	0.9507
0	1	0	1	1	0	1	1	0.0546	-0.0289	-0.0622	0.1278	0.1290	0.1655	0.9570	0.9420	0.9488
0	1	0	1	0	1	1	1	0.0546	-0.0289	-0.0622	0.1278	0.1290	0.1655	0.9570	0.9420	0.9488
Average Value								0.0459	-0.0495	-0.0631	0.1218	0.1378	0.1657	0.9584	0.9398	0.9492

Six Active Sensor Elements

Sensor States 0=On 1 =Off								Average Diference			RMS Diference			Correlation Coeficent		
L							R	Left	Centre	Right	Left	Centre	Right	Left	Centre	Right
1	1	1	1	1	0	1	0	0.0305	-0.0453	-0.0834	0.1180	0.1354	0.1755	0.9590	0.9414	0.9472
1	1	1	1	0	1	1	0	0.0305	-0.0453	-0.0834	0.1180	0.1354	0.1755	0.9590	0.9414	0.9472
1	1	1	0	1	1	1	0	0.0311	-0.0883	-0.0592	0.1153	0.1608	0.1661	0.9595	0.9357	0.9494
1	1	0	1	1	1	1	0	0.0317	-0.0406	-0.0798	0.1173	0.1308	0.1726	0.9584	0.9416	0.9477
1	0	1	1	1	1	1	0	0.0452	-0.0347	-0.0710	0.1205	0.1315	0.1683	0.9582	0.9417	0.9487
0	1	1	1	1	1	1	0	0.0458	-0.0359	-0.0710	0.1221	0.1314	0.1695	0.9584	0.9418	0.9483
1	1	1	1	0	1	0	1	0.0305	-0.0453	-0.0834	0.1180	0.1354	0.1755	0.9590	0.9414	0.9472
1	1	1	0	1	1	0	1	0.0311	-0.0883	-0.0592	0.1153	0.1608	0.1661	0.9595	0.9357	0.9494
1	1	0	1	1	1	0	1	0.0317	-0.0406	-0.0798	0.1173	0.1308	0.1726	0.9584	0.9416	0.9477
1	0	1	1	1	1	0	1	0.0452	-0.0347	-0.0710	0.1205	0.1315	0.1683	0.9582	0.9417	0.9487
0	1	1	1	1	1	0	1	0.0458	-0.0359	-0.0710	0.1221	0.1314	0.1695	0.9584	0.9418	0.9483
1	1	1	0	1	0	1	1	0.0311	-0.0883	-0.0592	0.1153	0.1608	0.1661	0.9595	0.9357	0.9494
1	1	0	1	1	0	1	1	0.0317	-0.0406	-0.0798	0.1173	0.1308	0.1726	0.9584	0.9416	0.9477
1	0	1	1	1	0	1	1	0.0452	-0.0347	-0.0710	0.1205	0.1315	0.1683	0.9582	0.9417	0.9487
0	1	1	1	1	0	1	1	0.0458	-0.0359	-0.0710	0.1221	0.1314	0.1695	0.9584	0.9418	0.9483
1	1	0	1	0	1	1	1	0.0317	-0.0406	-0.0798	0.1173	0.1308	0.1726	0.9584	0.9416	0.9477
1	0	1	1	0	1	1	1	0.0452	-0.0347	-0.0710	0.1205	0.1315	0.1683	0.9582	0.9417	0.9487
0	1	1	1	0	1	1	1	0.0458	-0.0359	-0.0710	0.1221	0.1314	0.1695	0.9584	0.9418	0.9483
1	0	1	0	1	1	1	1	0.0246	-0.0589	-0.0692	0.1233	0.1370	0.1754	0.9581	0.9417	0.9474
0	1	1	0	1	1	1	1	0.0246	-0.0589	-0.0716	0.1246	0.1381	0.1756	0.9582	0.9419	0.9470
0	1	0	1	1	1	1	1	0.0370	-0.0471	-0.0763	0.1342	0.1365	0.1845	0.9568	0.9418	0.9467
Average Value								0.0363	-0.0481	-0.0730	0.1201	0.1369	0.1715	0.9585	0.9408	0.9481

Seven Active Sensor Elements

Sensor States 0=On 1 =Off								Average Diference			RMS Diference			Correlation Coeficent		
L							R	Left	Centre	Right	Left	Centre	Right	Left	Centre	Right
1	1	1	1	1	1	1	0	0.0305	-0.0453	-0.0834	0.1180	0.1354	0.1755	0.9590	0.9414	0.9472
1	1	1	1	1	1	0	1	0.0305	-0.0453	-0.0834	0.1180	0.1354	0.1755	0.9590	0.9414	0.9472
1	1	1	1	1	0	1	1	0.0305	-0.0453	-0.0834	0.1180	0.1354	0.1755	0.9590	0.9414	0.9472
1	1	1	1	0	1	1	1	0.0305	-0.0453	-0.0834	0.1180	0.1354	0.1755	0.9590	0.9414	0.9472
1	1	1	0	1	1	1	1	0.0170	-0.0659	-0.0757	0.1160	0.1360	0.1762	0.9587	0.9416	0.9469
1	1	0	1	1	1	1	1	0.0288	-0.0547	-0.0839	0.1261	0.1359	0.1842	0.9582	0.9421	0.9464
1	0	1	1	1	1	1	1	0.0346	-0.0489	-0.0792	0.1297	0.1345	0.1831	0.9580	0.9422	0.9469
0	1	1	1	1	1	1	1	0.0358	-0.0483	-0.0775	0.1340	0.1365	0.1872	0.9578	0.9421	0.9464
Average Value								0.0298	-0.0499	-0.0812	0.1222	0.1356	0.1791	0.9586	0.9417	0.9469

Table A3.2 Redundancy Analaysis for Result Set 2 - Step Voltage Imbalance

Four Active Sensor Elements

Sensor States 0=On 1 =Off								Average Diference			RMS Diference			Correlation Coeficent		
L							R	Left	Centre	Right	Left	Centre	Right	Left	Centre	Right
1	0	1	0	1	0	1	0	-0.0039	0.0039	0.0034	0.1569	0.2627	0.1940	0.9592	0.9349	0.9477
0	1	1	0	1	0	1	0	0.0121	-0.0675	0.0187	0.1805	0.2976	0.1941	0.9592	0.9278	0.9392
0	1	0	1	1	0	1	0	-0.0079	-0.0008	-0.0019	0.1660	0.1959	0.1892	0.9584	0.9396	0.9487
0	1	0	1	0	1	1	0	0.0034	-0.0001	0.0067	0.1897	0.2011	0.1856	0.9565	0.9421	0.9386
0	1	0	1	0	1	0	1	-0.0006	-0.0015	0.0021	0.1881	0.2062	0.1529	0.9570	0.9420	0.9617
Average Value								0.0006	-0.0132	0.0058	0.1762	0.2327	0.1832	0.9581	0.9373	0.9472

Five Active Sensor Elements

Sensor States 0=On 1 =Off								Average Diference			RMS Diference			Correlation Coeficent		
L							R	Left	Centre	Right	Left	Centre	Right	Left	Centre	Right
1	1	1	0	1	0	1	0	-0.0019	-0.0121	0.0007	0.1679	0.1929	0.1444	0.9595	0.9357	0.9709
1	1	0	1	1	0	1	0	0.0001	-0.0021	-0.0006	0.1654	0.2016	0.1543	0.9584	0.9416	0.9668
1	0	1	1	1	0	1	0	0.0001	-0.0001	0.0027	0.1680	0.2027	0.1498	0.9582	0.9417	0.9688
0	1	1	1	1	0	1	0	-0.0026	-0.0008	0.0001	0.1726	0.2056	0.1458	0.9584	0.9418	0.9697
1	1	0	1	0	1	1	0	0.0001	-0.0021	-0.0006	0.1654	0.2016	0.1543	0.9584	0.9416	0.9668
1	0	1	1	0	1	1	0	0.0001	-0.0001	0.0027	0.1680	0.2027	0.1498	0.9582	0.9417	0.9688
0	1	1	1	0	1	1	0	-0.0026	-0.0008	0.0001	0.1726	0.2056	0.1458	0.9584	0.9418	0.9697
1	0	1	0	1	1	1	0	-0.0033	-0.0101	-0.0013	0.1664	0.1947	0.1443	0.9593	0.9360	0.9715
0	1	1	0	1	1	1	0	-0.0066	-0.0128	-0.0033	0.1714	0.1963	0.1367	0.9593	0.9362	0.9743
0	1	0	1	1	1	1	0	-0.0006	-0.0015	0.0021	0.1881	0.2062	0.1529	0.9570	0.9420	0.9617
1	1	0	1	0	1	0	1	0.0001	-0.0021	-0.0006	0.1654	0.2016	0.1543	0.9584	0.9416	0.9668
1	0	1	1	0	1	0	1	0.0001	-0.0001	0.0027	0.1680	0.2027	0.1498	0.9582	0.9417	0.9688
0	1	1	1	0	1	0	1	-0.0026	-0.0008	0.0001	0.1726	0.2056	0.1458	0.9584	0.9418	0.9697
1	0	1	0	1	1	0	1	-0.0033	-0.0101	-0.0013	0.1664	0.1947	0.1443	0.9593	0.9360	0.9715
0	1	1	0	1	1	0	1	-0.0066	-0.0128	-0.0033	0.1714	0.1963	0.1367	0.9593	0.9362	0.9743
0	1	0	1	1	1	0	1	-0.0006	-0.0015	0.0021	0.1881	0.2062	0.1529	0.9570	0.9420	0.9617
1	0	1	0	1	0	1	1	-0.0033	-0.0101	-0.0013	0.1664	0.1947	0.1443	0.9593	0.9360	0.9715
0	1	1	0	1	0	1	1	-0.0066	-0.0128	-0.0033	0.1714	0.1963	0.1367	0.9593	0.9362	0.9743
0	1	0	1	1	0	1	1	-0.0006	-0.0015	0.0021	0.1881	0.2062	0.1529	0.9570	0.9420	0.9617
0	1	0	1	0	1	1	1	-0.0006	-0.0015	0.0021	0.1881	0.2062	0.1529	0.9570	0.9420	0.9617
Average Value								-0.0021	-0.0048	0.0001	0.1726	0.2010	0.1474	0.9584	0.9398	0.9686

Six Active Sensor Elements

Sensor States 0=On 1 =Off								Average Diference			RMS Diference			Correlation Coeficent		
L							R	Left	Centre	Right	Left	Centre	Right	Left	Centre	Right
1	1	1	1	1	0	1	0	-0.0006	-0.0008	0.0001	0.1674	0.2027	0.1542	0.9590	0.9414	0.9664
1	1	1	1	0	1	1	0	-0.0006	-0.0008	0.0001	0.1674	0.2027	0.1542	0.9590	0.9414	0.9664
1	1	1	0	1	1	1	0	-0.0019	-0.0121	0.0007	0.1679	0.1929	0.1444	0.9595	0.9357	0.9709
1	1	0	1	1	1	1	0	0.0001	-0.0021	-0.0006	0.1654	0.2016	0.1543	0.9584	0.9416	0.9668
1	0	1	1	1	1	1	0	0.0001	-0.0001	0.0027	0.1680	0.2027	0.1498	0.9582	0.9417	0.9688
0	1	1	1	1	1	1	0	-0.0026	-0.0008	0.0001	0.1726	0.2056	0.1458	0.9584	0.9418	0.9697
1	1	1	1	0	1	0	1	-0.0006	-0.0008	0.0001	0.1674	0.2027	0.1542	0.9590	0.9414	0.9664
1	1	1	0	1	1	0	1	-0.0019	-0.0121	0.0007	0.1679	0.1929	0.1444	0.9595	0.9357	0.9709
1	1	0	1	1	1	0	1	0.0001	-0.0021	-0.0006	0.1654	0.2016	0.1543	0.9584	0.9416	0.9668
1	0	1	1	1	1	0	1	0.0001	-0.0001	0.0027	0.1680	0.2027	0.1498	0.9582	0.9417	0.9688
0	1	1	1	1	1	0	1	-0.0026	-0.0008	0.0001	0.1726	0.2056	0.1458	0.9584	0.9418	0.9697
1	1	1	0	1	0	1	1	-0.0019	-0.0121	0.0007	0.1679	0.1929	0.1444	0.9595	0.9357	0.9709
1	1	0	1	1	0	1	1	0.0001	-0.0021	-0.0006	0.1654	0.2016	0.1543	0.9584	0.9416	0.9668
1	0	1	1	1	0	1	1	0.0001	-0.0001	0.0027	0.1680	0.2027	0.1498	0.9582	0.9417	0.9688
0	1	1	1	1	0	1	1	-0.0026	-0.0008	0.0001	0.1726	0.2056	0.1458	0.9584	0.9418	0.9697
1	1	0	1	0	1	1	1	0.0001	-0.0021	-0.0006	0.1654	0.2016	0.1543	0.9584	0.9416	0.9668
1	0	1	1	0	1	1	1	0.0001	-0.0001	0.0027	0.1680	0.2027	0.1498	0.9582	0.9417	0.9688
0	1	1	1	0	1	1	1	-0.0026	-0.0008	0.0001	0.1726	0.2056	0.1458	0.9584	0.9418	0.9697
1	0	1	0	1	1	1	1	0.0067	-0.0028	0.0067	0.1922	0.2136	0.1466	0.9581	0.9417	0.9646
0	1	1	0	1	1	1	1	0.0021	-0.0068	0.0027	0.1911	0.2137	0.1426	0.9582	0.9419	0.9665
0	1	0	1	1	1	1	1	0.0034	-0.0021	0.0061	0.1913	0.2158	0.1491	0.9568	0.9418	0.9618
Average Value								-0.0003	-0.0030	0.0013	0.1716	0.2033	0.1492	0.9585	0.9408	0.9679

Seven Active Sensor Elements

Sensor States 0=On 1 =Off								Average Diference			RMS Diference			Correlation Coeficent		
L							R	Left	Centre	Right	Left	Centre	Right	Left	Centre	Right
1	1	1	1	1	1	1	0	-0.0006	-0.0008	0.0001	0.1674	0.2027	0.1542	0.9590	0.9414	0.9664
1	1	1	1	1	1	0	1	-0.0006	-0.0008	0.0001	0.1674	0.2027	0.1542	0.9590	0.9414	0.9664
1	1	1	1	1	0	1	1	-0.0006	-0.0008	0.0001	0.1674	0.2027	0.1542	0.9590	0.9414	0.9664
1	1	1	1	0	1	1	1	-0.0006	-0.0008	0.0001	0.1674	0.2027	0.1542	0.9590	0.9414	0.9664
1	1	1	0	1	1	1	1	-0.0019	-0.0115	0.0001	0.1738	0.1945	0.1413	0.9587	0.9416	0.9719
1	1	0	1	1	1	1	1	0.0021	-0.0055	0.0021	0.1867	0.2129	0.1518	0.9582	0.9421	0.9615
1	0	1	1	1	1	1	1	0.0027	-0.0035	0.0047	0.1857	0.2122	0.1417	0.9580	0.9422	0.9671
0	1	1	1	1	1	1	1	0.0021	-0.0041	0.0041	0.1892	0.2160	0.1435	0.9578	0.9421	0.9652
Average Value								0.0003	-0.0035	0.0014	0.1756	0.2058	0.1494	0.9586	0.9417	0.9664

Appendix 4
Circuit Diagrams

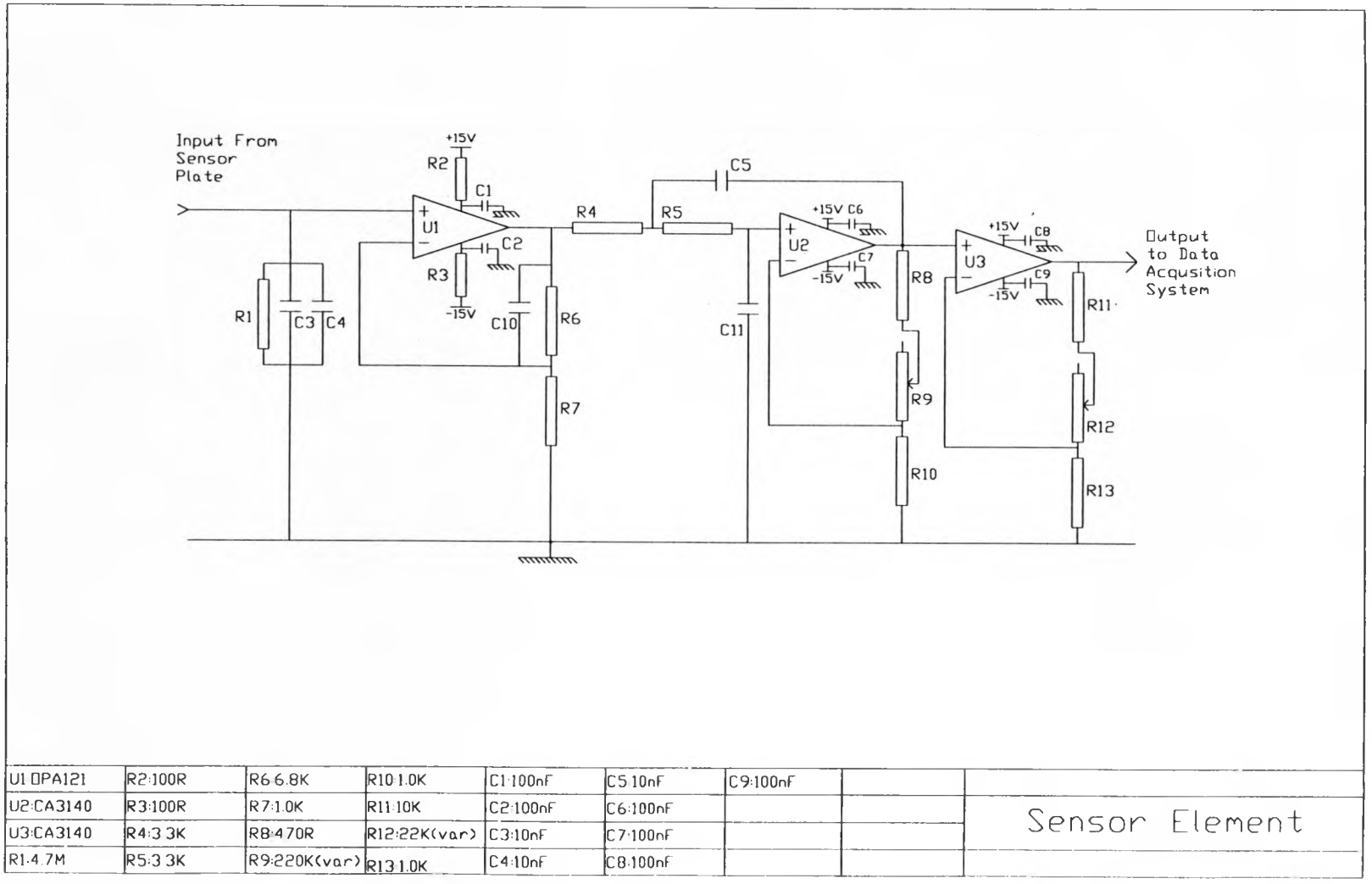

Figure A4.1 Sensor Circuit Diagram

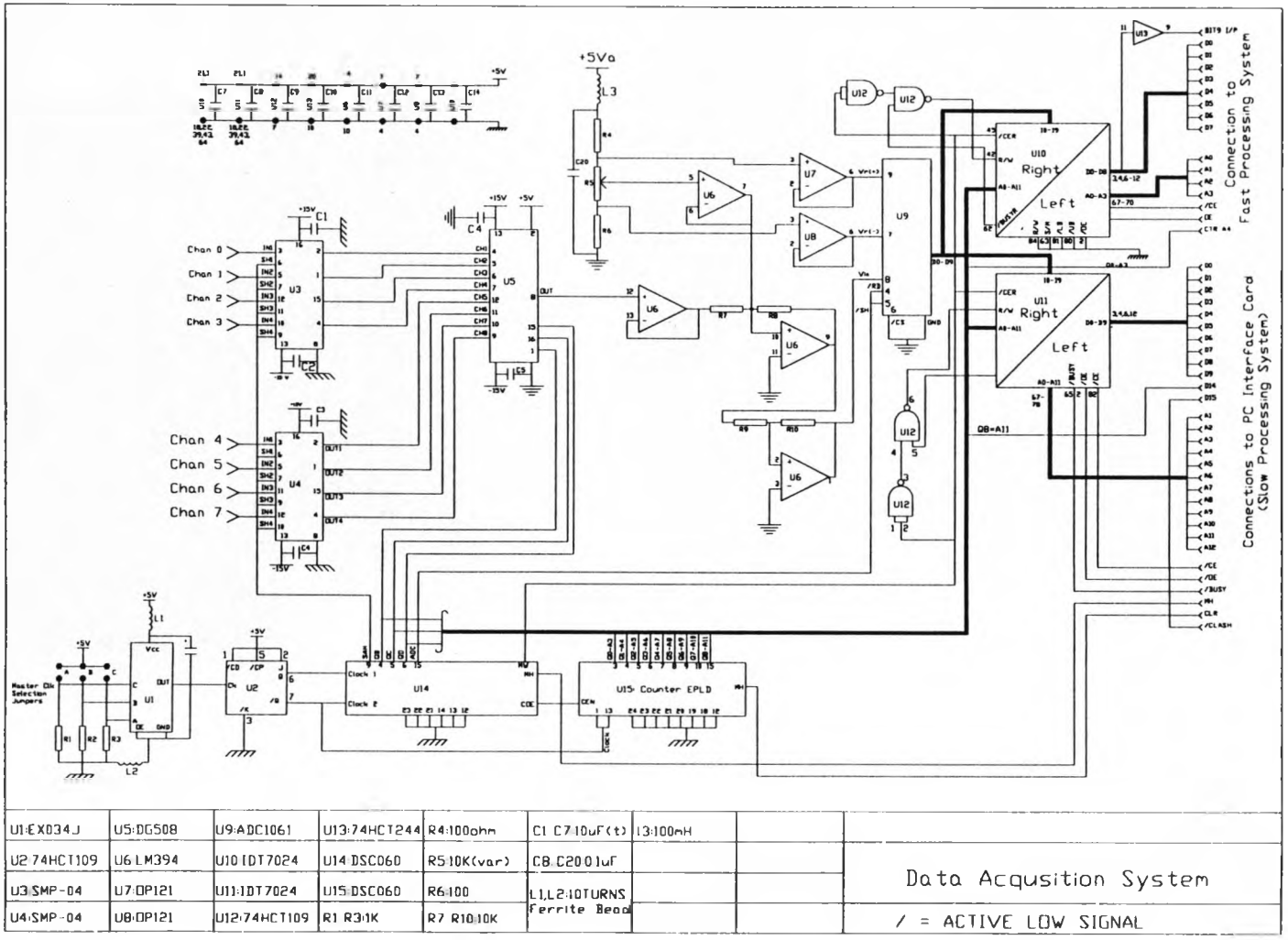

U1:EX034J	U5:DG508	U9:ADC1061	U13:74HCT244	R4:100ohm	C1 C7:10uF(t)	L3:100mH	
U2:74HCT109	U6:LM394	U10:IDT7024	U14:DSC060	R5:10K(var)	C8 C20:0.1uF		Data Acqusition System
U3:SMP-04	U7:OP121	U11:IDT7024	U15:DSC060	R6:100	L1,L2:10TURNS Ferrite Bead		/ = ACTIVE LOW SIGNAL
U4:SMP-04	U8:OP121	U12:74HCT109	R1 R3:1K	R7 R10:10K			

Figure A4.2 Data Acqusition System Circuit Diagram

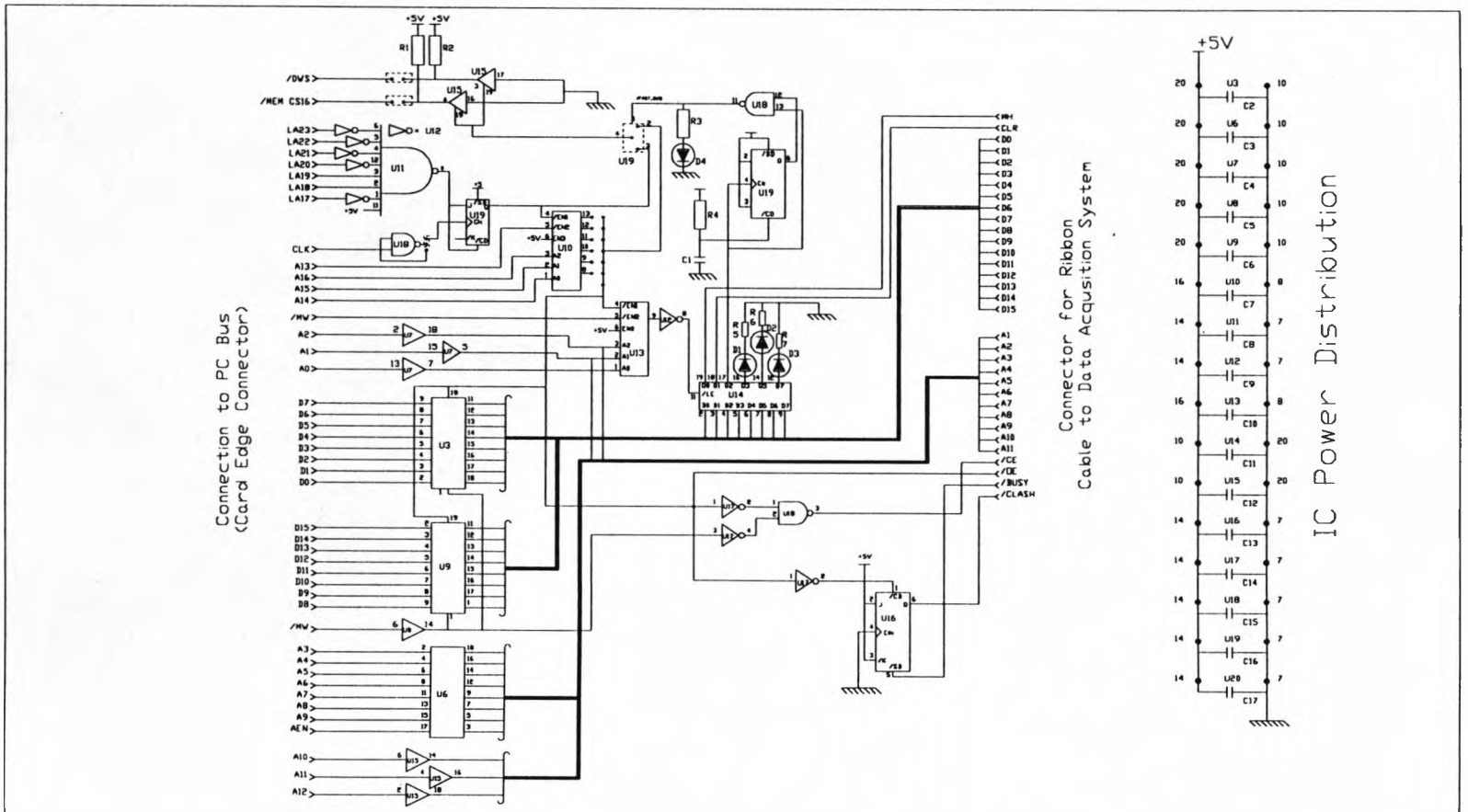

U3:74HCT245	U9:74HCT245	U13:74HCT138	U17:74HCT04	R1:10K	C1:21uF	/=Active Low Signal	
U6:74HCT244	U10:74HCT138	U14:74HCT573	U18:74HCT00	R2..R3:10K	C2..C17:100nF		Slow System Interface
U7:74HCT244	U11:74LS30	U15:74HCT244	U19:74HCT109	R4:100K			
U8:74HCT244	U12:74HCT04	U16:74HCT109	U20:74HCT157	R5..R7:100R			

Figure A4.3 Slow System PC Interface Circuit Diagram

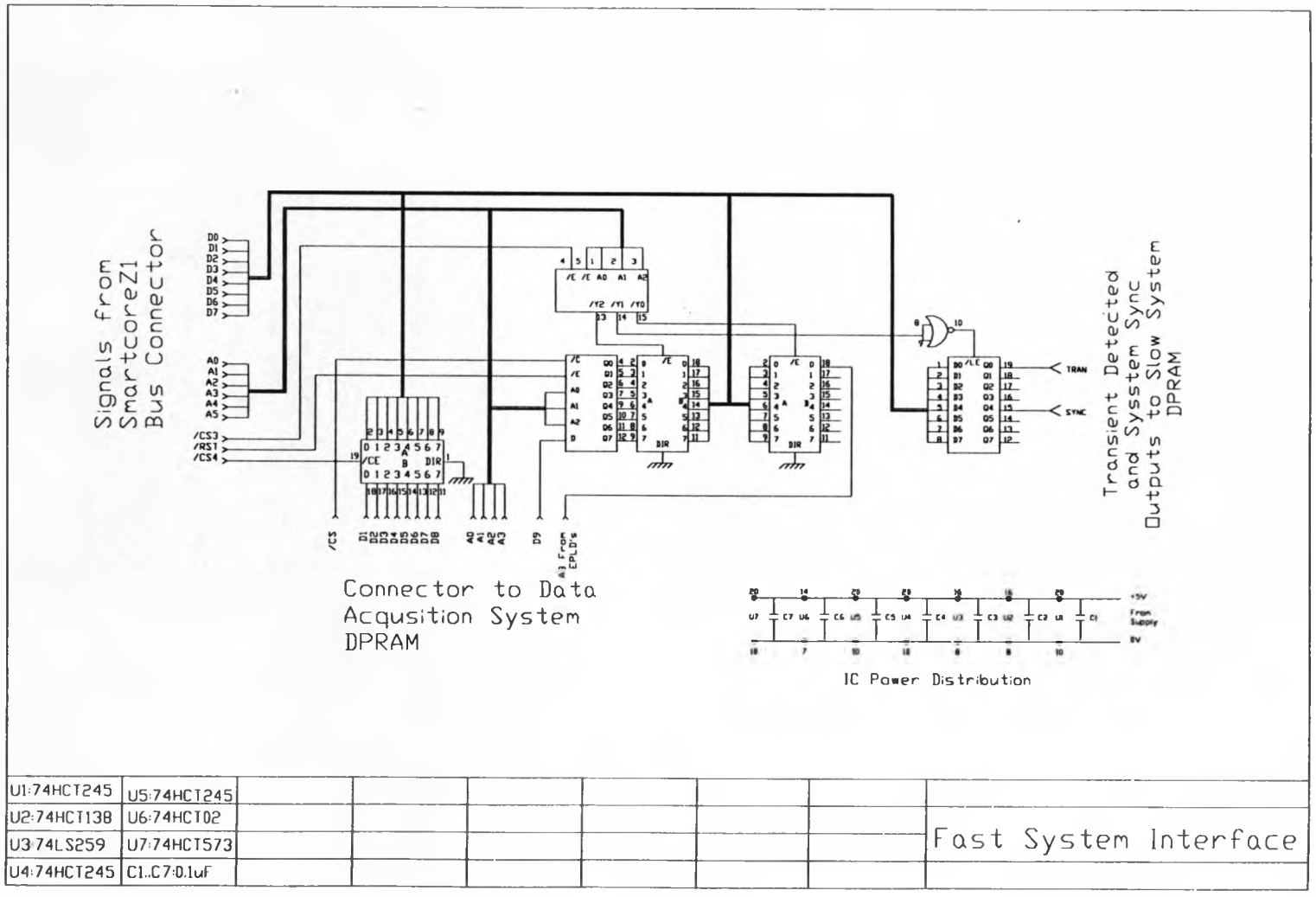

Figure A4.4 Fast System Interface Circuit Diagram

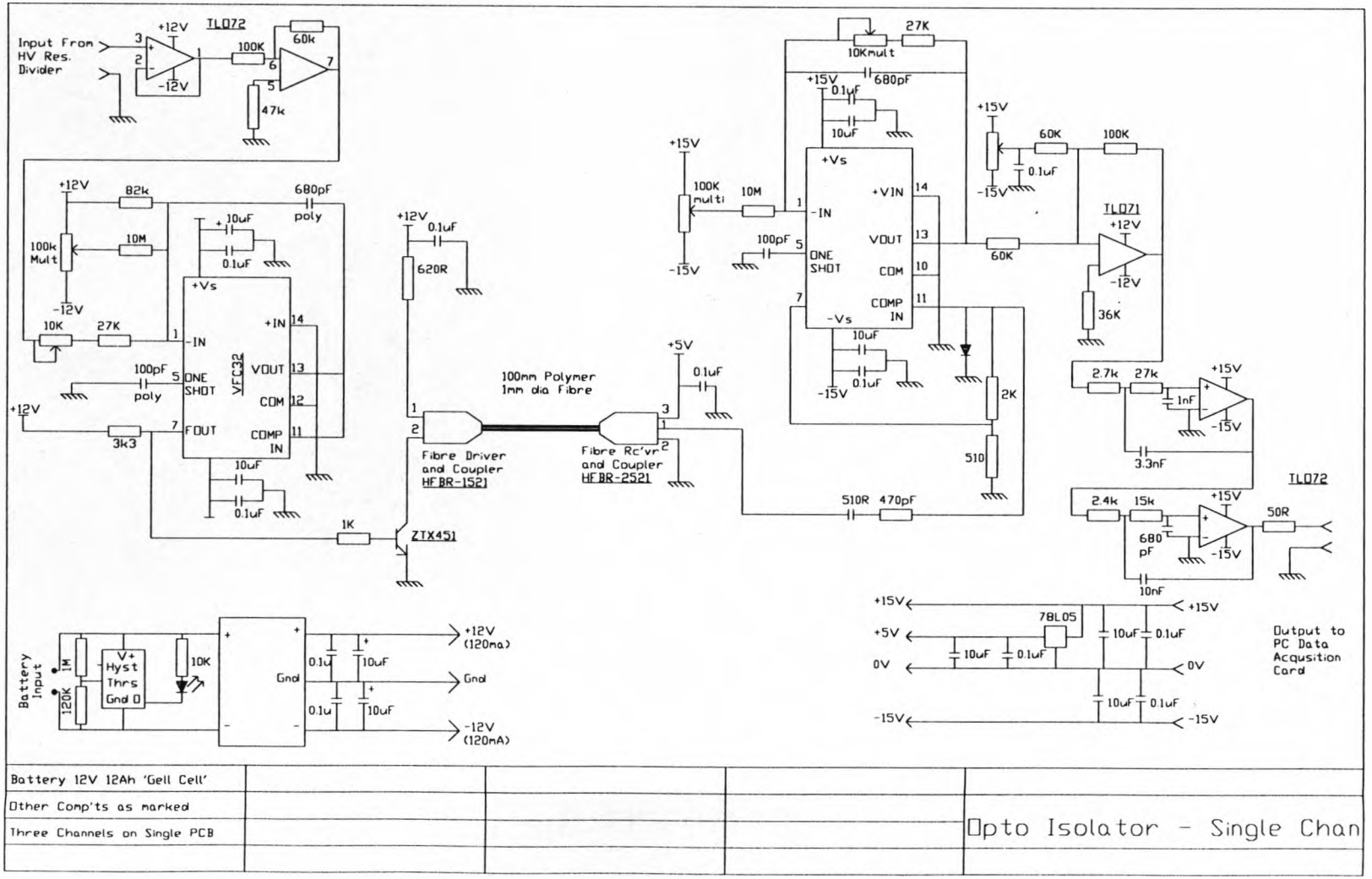

Figure A4.5 Contact System Opto Isolator Circuit Diagram

Appendix 5 - Pascal Program for Real Time Monitoring

```
(*RTP_PRG 2 - Program with both fast and slow systems - Real Time Voltage Fitting*)
(*THIS VERSION FITS VOLTAGE TEMPLATES IN REAL TIME*)
(*****************************************************************************************************************)
{$N+}   (*Numeric Co Processing*)
{$G+}   (*286 Instructions*)
{$Q-}   (*Overflow Checking off for speed*)
{$R-}   (*Range Checking off for speed*)
{$S-}   (*Stack Overflow Checking off for speed*)
program rtp_prg2;

uses ncv_data,ncv_ctrl,ncv_disp,ncv_proc,ncv_test,
     dos,crt,printer,ncv_dp,ncv_mon,ncv_io,ncv_file,ncv_fit,ncv_anal;

const s ='  ,  ';                          (*delimiter in ascii log file*)

    data_file_path = 'c:\tmp';            (*path to save result files to*)
    log_file_name  = 'c:\tmp\test.log';    (*filename to log messages to*)

    samples_file   = 118000;              (*number of samples per file*)
    samples_lta    = 236000;              (*number of samples per long term average*)
                                          (*118,000 = ca 12 hours*)

(*//////////////////////////Program Data ////////////////////////////////////////////////////////////////////////*)
var dp_mirror   : mem_type;               (*mirror of half of DP ram (data set)*)

    current_his,                          (*current value of history counter*)
    tran_ctr    : integer;                (*number of transients counted in current data set*)

    cap_ctr     : longint;                (*control counter incremented for each data set read*)
    cap_ctr_str : string;                 (*string representation of cap_ctr for screen display*)

    to_do       : mem_area;               (*token = UPPER / LOWER for next area of memory to read*)

    class_dat_sum10,                      (*sum of last ten descriptor sets*)
    sta_dat_10,                           (*short term average of last 10 descriptor sets*)
    lta_class,                            (*long term average descriptor sets*)
    class_dat_inst : class_type;          (*descriptors of current data set*)

    data_summary: summary_type;           (*summary of current data set*)

    lta_mag1,                             (*long term average of fundamental field*)
    lts_mag1,                             (*long term sum used to calculate average*)
    dif_mag1 : dft_type;                  (*percentage difference between current short term av and long term av.*)
```

```
    class_dat_hist: array [0..9] of class_type;  (*rolling buffer of sums averages*)

    file_no:integer;                    (*number of current file*)
    sum_save_name,
    class_save_name:string;             (*filename of current file*)

    key_in : char;                      (*key pressed by user to interupt system*)

begin                                   (*Start of Program*)

(*//////////////////////////Commands to Initialise Both Systems/////////////////////////////////////////////////////////////////////*)
  key_in :=' ';                          (*Clear Input Character Buffer*)
  clrscr;                               (*Clear Display Screen*)
  io_open_log(log_file_name);            (*open log file*)
                                         (*log file stays open for all data files*)

  io_write_log('');
  io_write_log('*******COMMENCING RUN!*******************************');
  io_write_log('');

  io_write_log('PROG - Starting Data Acqusition System');

  ctrl_out(hold,off,go);               (*start DATA ACQ system running*)
  io_write_log('PROG - Reseting & Starting Fast System ');

  ctrl_out(rst,on,go);                 (*reset & start FAST system*)
  delay(100);
  ctrl_out(rst,off,go);

  io_write_log('PROG - Loading Twiddle Factors');

  mon_init;                             (*Initialise System - Load Twiddle Factors*)

  cap_ctr :=1;                          (*Initialise Counter*)


  io_write_log('PROG - Calculating and Loading Initial Average');

  anal_avg_class_file(lta_filename,lta_class);   (*Calculate average of file of stored descriptor sets*)
                                                 (*to form initial long term avaerage*)

  lta_mag1 := lta_class.mag1;                    (*extract magnitude from descriptor set*)


  io_write_log('PROG - Loading Voltage Templates');

  fit_load_templates(temp_filename);              (*load templates*)
```

```
  mon_clr_class(class_dat_sum10);                (*clear classifiers average*)

  io_write_log('PROG - Waiting for Fast System to complete Initialisation');

  ctrl_wait_for_fast;                              (*wait for fast system to initialise*)

  io_write_log('PROG - Running !');

  (*START OF MULTIPLE FILES LOOP*)
  repeat
    (*GENERATE FILENAME TO SAVE DATA UNDER*)

    (*DESCRIPTOR SET FILE*)
    file_no := file_next_number(data_file_path,'CLA');              (*find number of next descriptor set file*)
    class_save_name := file_data_name(data_file_path,'CLA',file_no); (*create filename of permanent store*)
    io_write_log('PROG - Next Classifier Filename : '+class_save_name);

    (*SUMMARY FILE*)
    file_no := file_next_number(data_file_path,'SUM');              (*find number of next summary file*)
    sum_save_name := file_data_name(data_file_path,'SUM',file_no);   (*create filename of permanent store*)
    io_write_log('PROG - Next Summary Filename : '+sum_save_name);

    (*OPEN TEMPOARY RESULTS FILES*)
    io_open_av(class_filename);
    io_open_sum(sum_filename);

    (*SET UP DISPLAY*)
    clrscr;                          (*clear screen for display*)
    disp_class_screen_head;          (*display headers for descriptor sets*)
    disp_summary_head;               (*display headers for summary*)

    dp_clr_dft(lts_mag1);            (*clear long term sum*)

    (*PREPARE TO ENTER SINGLE FILE LOOP*)
    to_do := upper;             (*start with upper area*)

    ctrl_wait_for_upper;        (*wait until starting writing to upper*)
    ctrl_wait_for_lower;

    (*START OF SINGLE FILES LOOP*)
    repeat
(*////////////////////////////Commands to Read a Data Set from DPRAM/////////////////////////////////////////////////////////////*)
      if (to_do = lower) then                    (*Read Lower Memory*)
      begin
        ctrl_wait_for_upper;                     (*wait until controler writing to UPPER*)
        ctrl_read_DP(lower,dp_mirror,tran_ctr); (*read Lower Memory + Transiets*)
```

```
        to_do := upper;                          (*change token to read upper next time*)
      end
      else                                       (*Read Upper Memory*)
      begin
        ctrl_wait_for_lower;                     (*wait until controll writing to LOWER*)
        ctrl_read_DP(upper,dp_mirror,tran_ctr); (*Read Upper Memory + Transient*)
        to_do := lower;                          (*change token to read lower next time*)
      end;

(*////////////////////////////Commands to Calculate Signal Descriptors//////////////////////////////////////////////////////////////*)
      (*Calculate Descriptor Set*)
      mon_calc_class(dp_mirror,tran_ctr,class_dat_inst);

      (*get current value of history counter*)
      current_his := cap_ctr mod 10;

      (*subtract 10th classifier back from sum*)
      mon_sub_class(class_dat_sum10,class_dat_hist[current_his],class_dat_sum10);

      (*add current classifier on to short term sum*)
      mon_add_class(class_dat_inst,class_dat_sum10);

      (*calculate average value of classifiers*)
      mon_div_class(class_dat_sum10,10,sta_dat_10);

      (*save current value to the history list*)
      class_dat_hist[current_his] := class_dat_inst;

      (*Summarise Short Term Average*)
      mon_calc_summary(sta_dat_10,data_summary);

(*////////////////////////////Commands to Fit the Voltage Templates//////////////////////////////////////////////////////////////*)

      (*find percentage difference of fundamental from LTA*)
      dp_sub_dft(sta_dat_10.mag1,lta_mag1,dif_mag1);
      mon_calc_p_diff_small(dif_mag1,lta_mag1,dif_mag1);

      (*write voltages into data_summary record*)
      with data_summary do
      begin
        fit_two_stage(dif_mag1,two_stg_crude,V_lhs,V_cen,V_rhs);
      end;

      io_write_av(sta_dat_10,dp_pack_time);     (*write current descriptor sets & time to memory*)
      io_write_sum(data_summary,dp_pack_time); (*write current summary to memory*)

      (*display classifers*)
```

```
      disp_class_screen_data(sta_dat_10,disp_date_time_str(dp_pack_time)+' DS No : '+cap_ctr_str
      +' Filename : '+class_save_name);

      (*display summary*)
      disp_summary_data(data_summary);


  (*the adding to the long term average is only done ever 10 samples otherwise over 24 hours*)
  (*a longint would not be big enough to hold the sum! *)

      if current_his = 0 then
      begin
        (*add current mag1 sta to long term sum (lts)*)
        dp_add_dft(lts_mag1,sta_dat_10.mag1,lts_mag1);
      end;

      (*calculate new long term average LTA approx every 24 hours*)
      if (cap_ctr mod samples_lta) = 0 then
      begin
        dp_div_big_dft(lts_mag1,(cap_ctr div 10),lta_mag1);
      end;
      str(cap_ctr,cap_ctr_str);

      (*INCREMENT CONTROL COUNTER*)
      {$R-}
        inc(cap_ctr);                                  (*increment control counter*)
      {$R+}                                            (*range checking turned off*)
                                                       (*to allow overflow*)

      if keypressed then key_in := upcase(readkey);    (*check for user abort*)

      (*end of single file loop*)
      until (((cap_ctr MOD samples_file) = 0) OR (key_in ='Q'));  (*repeat until all samples read or 'Q' or 'q' pressed*)

      io_close_av;                                      (*close current descriptor set memory file*)
      io_close_sum;                                     (*close current summary memory file*)

      (*copy classifier file to permanent (disk) filename*)
      file_copy(class_filename,class_save_name);
      io_write_log('PROG - classifier file saved to '+class_save_name);

      (*copy summary file to permanent filename*)
      file_copy(sum_filename,sum_save_name);


    (*end of multiple files loop*)
    until key_in = 'Q';              (*repeat until user presses 'Q' or 'q'*)
```

```
    io_close_log;                    (*close log file*)
end.    (*end of program rtp_prg2*)
```

Appendix 6
Publications

Gerrard C.A. & Gibson J.R. (1996)
Remote detection of conditions on high voltage systems
IEE Colloquia on Applications of Field Modelling to Power Systems,
London, January 1996

Gerrard C.A. , Gibson J.R. , Jones G.R. , Holt L. , Simkin D.
Deduction of conductor voltages from remote electric field distributions
Submitted to IEE Proceedings - Generation, Transmission & Distribution
London, February 1997

Gerrard C.A. , Gibson J.R. , Jones G.R. , Holt L. , Simkin D.
Measurements of power system voltages using remote electric field monitoring
Submitted to IEE Proceedings - Generation, Transmission & Distribution
London, February 1997